The Effect of Solidification Variables on the Microstructure of Hypereutectic Al-Si alloys.

Masoumeh Faraji

January 2007

Submitted in partial fulfilment for the degree of

Doctor of Philosophy

Department of Engineering Materials

The University of Sheffield

Table of Contents

		Page No.
1	**Introduction**	1
2	**Literature review**	4
2.1	**Fundamentals of nucleation of solid from the melt**	4
	2.1.1 Homogeneous nucleation	5
	2.1.2 Heterogeneous nucleation	6
	2.1.3 Nucleation kinetics	7
	2.1.4 Grain refinement mechanism by inoculation	13
2.2	**Solidification of hypereutectic Al-Si alloys**	16
	2.2.1 The microstructure and properties of hypereutectic Al-Si alloys	16
	2.2.2 Refinement of the primary silicon	18
	i. Level and type of refiners	20
	ii. Effect of refiner on the formation temperature of primary silicon	22
	iii. Effect of refiner on size of primary silicon	23
	2.2.3 Modification of the eutectic silicon	23
	i. Eutectic modification theories	23
	ii. Quench modification	27
	2.2.4 Simultaneous modification and refinement of eutectic and primary silicon	27
3	**Experimental procedure**	**31**
3.1	**Materials**	**31**
	3.1.1 Aluminium-silicon alloy	31

3.1.2 Al-Fe-P refining inoculant 31

3.1.3 Al-Cu-P refining inoculant 32

3.1.4 Al-Sr modifying agent 32

3.2 Casting processes 33

3.3 Heat treatment 35

3.4 X-ray diffraction 35

3.5 Metallographic preparation for optical microscopy 35

3.6 Quantitative metallography 36

3.7 Differential Thermal Analysis (DTA) 37

3.8 Electron Back Scatter Diffraction (EBSD) 38

4 Results 39

4.1 Microstructural characterisation 39

4.2 Cooling curves 39

4.3 Quantitative metallography 43

4.3.1 Eutectic modification 43

4.3.2 Volume fraction of silicon 43

4.3.3 Morphological observations 43

4.3.4 Numbers of primary silicon particles 45

4.4 X-ray diffraction 47

4.5 Differential Thermal Analysis (DTA) 47

4.6 EBSD 48

5 Discussion 51

5.1 The effect of different parameters on the Perepezko nucleation model 51

5.1.1 Surface-dependent heterogeneous nucleation 51

i. Effect of number of particles 52

ii. Effect of undercooling 53

iii. Effect of phosphorus addition level 54

5.1.2 Volume-dependent heterogeneous nucleation 55

i. Effect of phosphorus addition level 55

5.2 Effect of phosphorus and strontium additions individually and simultaneously on microstructure and cooling curves **56**

5.2.1 Effect of phosphorus on microstructure and cooling curve 56

5.2.2 Effect of strontium on microstructure and cooling curve 62

5.2.3 Effect of strontium and phosphorus together on microstructure and cooling curve 63

5.3 DTA **64**

5.4 EBSD **65**

6 Conclusions **68**

7 Suggestions for further work **71**

8 References **72**

Appendix A 81

Appendix B 83

Appendix C 85

Tables

Figures

Summary

In this work, the effect of phosphorus, as a primary silicon refiner, and of strontium, as a eutectic silicon modifier, individually and simultaneously, on the microstructure of hypereutectic Al-Si alloys was studied.

Al-18.6Si-0.35Fe-0.02Cu-0.0014P (wt%) alloy was used for casting and phosphorus was added in a range of 0.015-0.08 wt% mainly by means of Al-6.75Fe-4.91P (wt %), and in a few cases by Al-17.1Cu-0.89P (wt%), master alloys. Eutectic silicon was modified using Al-5.93 wt% Sr over a range of 0.04-0.3 wt% Sr. Two different casting methods were used: bottom casting into sand moulds and chamber casting into steel moulds. The melt temperature was 800°C and holding time for each addition was 15 min.

Adding 0.02 wt% P led to an increase in the number of primary silicon particles per unit volume (N_V) by 1.5 times. N_V was trebled by adding 0.08 wt% phosphorus during chamber casting into steel moulds. N_V was decreased by about 20 times by adding 0.2 wt% Sr and 0.02 wt% Sr+0.02 wt% P to untreated alloy during bottom casting into a sand mould. Adding strontium increased primary silicon undercooling from 7.1±1.0 to 46.6±6.5 K, though phosphorus addition of 0.02, 0.04 and 0.08 wt% (for ingots chamber cast into steel moulds) gave a primary silicon undercooling of 18.7±10.4, 8.5±1.2 and 9.1±0.9 K respectively (compared to 9.0±5.0 K for untreated ingots).

The nucleation models (one surface-dependent and the other volume-dependent) of Perepezko were applied to the observed nucleation behaviour of primary silicon. It was found that the nucleation temperature was the most crucial variable in both models. Applying the models to our results showed that contact angle

from the surface-dependent model varied over the range of 24.3 to 30 degrees, compared with 17.7 to 23.5 degrees from the volume-dependent model.

Additionally, Electron Back Scatter Diffraction (EBSD) was used to determine possible crystallographic relationships between neighbouring primary silicons in untreated and P-inoculated ingots. Between two connected primary silicon particles, the outermost layers of each silicon particle were often found to be twin-related by a 60° rotation around axis <111>.

ACKNOWLEDGMENTS

I would like to gratefully acknowledge the Government of the Islamic Republic of Iran for funding.

I wish to express my sincere gratitude to my supervisors, Professor Howard Jones and Dr Iain Todd, for their guidance and support throughout my research and during the completion of this thesis.

I am grateful to Dr Hajime Kinoshita for his constructive advice and help with some thermomechanical concepts and calculations used in the nucleation modelling section.

I would like to thank all my friends, fellow post-graduate students, especially I.A. Figueroa for his help with producing the DTA samples, and the technical staff in the Department of Engineering Materials at the University of Sheffield.

Special thanks to my parents, sister and brothers for the continuous encouragement and support they provided me through my entire life. I am particularly thankful to my husband and best friend, Masoud, without whose love, support, understanding and patience, I could not have finished this thesis.

1. Introduction

Hypereutectic aluminium–silicon alloys are well known for their lightness and good wear resistance and thus are widely used in the automotive industry. Fine primary silicon particles distributed evenly in these alloys improve their strength and machinability. Hardness, tensile strength, yield strength and fatigue strength are comparable to other aluminium casting alloys. These alloys have low ductility that is improved by eutectic modification. Their high thermal conductivity, good wear resistance and excellent strength to weight ratio have made them suitable for uses such as engine blocks. Also these alloys have very good fluidity, resistance to hot cracking and very good corrosion resistance.

Hypereutectic Al-Si alloys without any addition can have very large primary silicon particles, as large as even several millimetres, and flake-like eutectic silicon. Since both types of silicon are stress-raisers, they impair mechanical properties. Refinement in hypereutectic Al-Si alloys (either by adding inoculants, such as phosphorus or increasing the cooling rate) reduces the size of primary silicon particles, which accompanies an increase in the number of primary silicon particles and also morphological changes (from irregular plate-like or star-like to polyhedral) and consequently the mechanical properties are improved (Tenekedjiev and Gruzleski 1990).

Additionally, adding strontium alone, as a eutectic modifier, can modify the eutectic silicon and enhance the tensile strength of the alloy by changing its morphology from flake-like to fibrous (Sigworth 1983). Strontium suppresses primary silicon formation (Jenkinson and Hogan 1975).

Some experiments have been carried out to investigate the effect of simultaneous addition of strontium and phosphorus. These show that strontium tends to eliminate the refining effect of phosphorus by introducing Sr_3P_2 to the melt, although some researchers have claimed that simultaneous refinement and modification of primary and eutectic silicon can be achieved (Cissé et al 1975, and Park et al 1995).

In the present work the effect of phosphorus (by means of Al-6.75Fe-4.91P (wt %) and in a few cases by Al-17.1Cu-0.89P (wt%) master alloys), as a primary silicon refiner, and strontium (by means of Al-5.93 wt% Sr master alloy), as a eutectic silicon modifier, individually and simultaneously, on the microstructure and solidification behaviour of Al-18.6 wt% Si alloy was studied using cooling curves acquired during solidification and quantitative metallography. Two different casting methods (bottom casting into sand moulds and chamber casting into steel moulds) were used, giving different cooling conditions. The casting variables included the amount of phosphorus addition (from 0.015 wt% to 0.08 wt%), the amount of strontium addition (from 0.04 wt% to 0.3 wt%), and the imposed cooling rate below the peak temperature (T_p) and above the formation temperature (T_f) of primary silicon (from ~1.7 K/s for chamber cast into alumina mould to ~2.6 K/s for chamber casting into steel mould). In the present work, possibility of any systematic relation between number per unit volume (N_V) and T_f is investigated under different solidification conditions. Therefore, using optical microscopy the number of primary silicon particles per unit volume was determined and solidification parameters such as T_f, eutectic arrest temperature (T'_{Eu}) and the formation temperature of eutectic silicon

(T''_{Eu}), cooling rate between T_P and T_f ($\dot{T}_1$) and cooling rate between T_f and T'_{Eu} ($\dot{T}_2$) were measured using acquired cooling curves.

By applying the published data for the liquidus temperature (T_L), T_f, cooling rate, between T_P and T_f for the present work, and N_v from Liang et al (1995), Ohmi et al (1991, 1994, and 1997), Kaneko et al (1979) and the results of the present work in Perepezko's surface-dependant nucleation and volume-dependant nucleation models, the effects of number of primary silicon particles, the formation temperature of primary silicon, and phosphorus addition on the contact angle between primary silicon nucleus and the nucleant, calculated by these models, were investigated.

Finally, to study the nucleation behaviour of primary silicon and formation of primary silicon clusters in uninoculated and P-inoculated ingots, Electron Back Scatter Diffraction (EBSD) was used. There was no previously documented study of possible crystallographic relationships between primary silicon particles. In this work the main focus specifically was on the evidently connected primary silicon particles. However, this method (EBSD) has been used by other workers to study the possible relationship between eutectic silicon particles in unmodified and modified hypoeutectic and hypereutectic alloys.

2. Literature review

2.1 Fundamentals of nucleation of solid from the melt

Many transformations (e.g. solidification) can occur by nucleation and growth. To nucleate a new phase, based on the initial theory proposed by Volmer (1929) and by Becker and Doring (1935), which was developed later by Turnbull (1948), there should be sufficient molecules or atoms gathered from the mother phase to surmount a nucleation barrier. This barrier is determined by the volume free energy change and interfacial energy associated with the formation of the new phase.

During the nucleation process, a particle of the new phase that reaches a critical size (r*) needed for continued growth, is called a nucleus and those below this size are named as embryos. The embryo is unstable because of its high surface-to-volume ratio. Meanwhile there are some attachments and detachments of atoms from the parent phase to the embryo and vice versa that cause fluctuations. Therefore nuclei are formed through these statistical fluctuations. The formation of a nucleus alters the bulk free energy of the mother phase embedded in, in addition to a change in the interface energy by creating a new interface (Turnbull 1948, Fisher et al 1948).

There is eventually a constant rate of nucleus formation at a constant temperature. The time during which the formation rate of nuclei becomes steady state is called the transient period. This period is very short in vapour-to-liquid systems, though is longer and observable in condensed systems (Kelton et al 1983).

In solidification, the cooling of a molten metal below its equilibrium melting temperature (T_m) provides a driving force for the start of the transformation. For almost all studied systems, homogeneous nucleation is observed at around 0.8 of the equilibrium temperature (Jackson 1965). However, in practice, this homogeneous

nucleation at high undercooling is not seen because some agencies such as the melt container walls or impurities within the melt facilitate the formation of the new phase and promote heterogeneous nucleation at low undercooling (Turnbull 1952).

2.1.1 Homogeneous nucleation

The free energy of formation of small sphere of solid, ΔG_{Total}, can be written (Turnbull 1948) as:

$$\Delta G_{Total} = - V_S \Delta G_V + A_{SL} \sigma_{SL} \qquad \text{Eq. 2.1}$$

$$\text{with } \Delta G_V = G_V^L - G_V^S \qquad \text{Eq. 2.2}$$

where V_S is the volume of the solid sphere, A_{SL} is the solid/liquid interfacial area; σ_{SL}, the solid/liquid interfacial free energy per unit area, and G_V^L and G_V^S are the Gibbs free energies per unit volume of the melt and crystal. The maximum value of ΔG_V for nucleation from liquid can be expressed as:

$$\Delta G_V = L_V.\Delta T/T_m \qquad \text{Eq. 2.3}$$

where L_V is the latent heat of fusion per unit volume and ΔT is undercooling. For an isotropic particle shape (a sphere of radius r), ΔG_{Total} for solidification from the liquid is:

$$\Delta G_{Total} = -(4\pi/3)\, r^3 \Delta G_V + 4\pi r^2 \sigma_{SL} \qquad \text{Eq. 2.4}$$

Fig 2.1 shows that there is a critical radius r* for any given undercooling which has the maximum free energy ΔG^*, and particles with larger radius than r* remain solid (Turnbull 1952). By differentiation of Eq. 2.4, r* and ΔG^* are obtained as:

$$r^*=2\,\sigma_{SL}/\Delta G_V \qquad \text{Eq. 2.5}$$

and $$\Delta G^* = 16\pi\,\sigma_{SL}^{\,3}/3\Delta G_V^{\,2} \qquad \text{Eq. 2.6}$$

Using Eq. 2.3, Eqns. 2.5 and 2.6 may be written as:

$$r^*=(2\,\sigma_{SL}.T_M)/(L_V.\Delta T) \qquad \text{Eq. 2.7}$$

and $$\Delta G^* = \frac{16\pi}{3}\sigma_{SL}^{\,3}.\left(\frac{T_M^2}{L_V^2.\Delta T^2}\right) \qquad \text{Eq. 2.8}$$

2.1.2 Heterogeneous nucleation

For nucleation at low undercooling, the σ_{SL} term needs to be reduced by nucleation on the wall of a mould or on impurities or inoculants in the melt. The heterogeneous nucleus is usually modelled as a spherical cap on a flat substrate with a contact angle θ (Fig.2.2) (Turnbull 1950 a). Then:

$$\sigma_{NL} = \sigma_{SL}.\cos\theta + \sigma_{SN} \qquad \text{Eq. 2.9}$$

where σ_{NL}, σ_{SN} and σ_{SL} are the nucleant/liquid, solid/nucleant and solid/liquid interfacial energies per unit area respectively and θ is the contact angle. The formation of the above mentioned nucleus has a free energy as follows:

$$\Delta G_{het} = \{-4\pi/3\, r^3\Delta G_V + 4\pi r^2\,\sigma_{SL}\}\, f(\theta) \qquad \text{Eq. 2.10}$$

where $f(\theta) = \left[2-3\cos\theta+(\cos\theta)^3\right]/4$ Eq. 2.11

By differentiation of Eq. 2.10, r* and ΔG* are obtained as:

$$r^*=2\,\sigma_{SL}/\Delta G_V \qquad \text{Eq. 2.12}$$

and $\Delta G^* = 16\pi \sigma_{SL}{}^3/(3\Delta G_V{}^2)f(\theta)$ Eq. 2.13

When $f(\theta) \leq 1$, the activation energy barrier to heterogeneous nucleation is smaller than for homogeneous nucleation because:

$$\Delta G^*_{het} = f(\theta)\, \Delta G^*_{hom} \quad \text{Eq. 2.14}$$

2.1.3 Nucleation kinetics

The principal purpose of a nucleant is to increase the nucleation frequency (Turnbull and Vonnegut 1952). The nucleation behaviour of alloys in steady state has been modelled by many researchers including Perepezko (1988). According to the model of Perepezko, a description of the rate of nucleation of clusters requires that the cluster population distribution should be calculated. With very little solute in solution in an undercooled melt, the entropy can be calculated on the basis of an ideal solution. The metastable equilibrium concentration, $C_{(n)}$ of clusters of a given size is given by:

$$C_{(n)} = C_a \exp\left(\frac{-\Delta G^*}{kT}\right) \quad \text{Eq. 2.15}$$

where C_a is the number of atoms per unit volume in the liquid and ΔG^* is given by Eq. 2.6. It should be added that n^* is the number of atoms in a nucleus, and it is expressed as $n^* V_a = (4/3\,\pi.r^{*3})/3$ where V_a is the atomic volume.

If solid nucleation is regarded as the growth of clusters past the critical size, then the resulting cluster flux or the nucleation rate I (e.g. in $m^{-3}.s^{-1}$) can be given kinetically by:

$$I = \upsilon_{SL}.S_{cr}.C(n^*) \quad \text{Eq. 2.16}$$

where υ_{SL} is the jump frequency associated with atom jumps from the liquid to join the cluster and can be estimated from the liquid diffusivity, D_L, and jump distance, a, as (D_L/a^2); S_{cr} is the number of atoms surrounding a nucleus that is estimated as $2\pi.r^{*2}(1-\cos\theta)/a^2$ for a spherical cap geometry; and C(n*) is the concentration of critical clusters given by Equation 2.15. The full expression for the steady-state nucleation rate for heterogeneous nucleation then becomes:

$$I_{het} = \left(\frac{D_L}{a^2}\right)\left(\frac{2\pi r^{*2}(1-\cos\theta)}{a^2}\right)N_0 \exp\left[\left(\frac{-\Delta G^*(\text{hom})}{kT}\right)f(\theta)\right] \qquad \text{Eq. 2.17}$$

where k is Boltzmann's constant (1.3806×10^{-23} J/atom K) and N_0 is the concentration of critical clusters in terms of the number of surface atoms of the nucleation site per unit volume of liquid.

Taking r* and $\Delta G^*(\text{hom})$ from equations 2.5 and 2.8, equation 2.16 can be rewritten for the steady-state heterogeneous nucleation frequency from bulk melts to give:

$$Iss = \frac{8\pi D_L \sigma_{SL}{}^2(1-\cos\theta)N_\circ}{a^4(\Delta Gv)^2}\exp\left(\frac{b\sigma^3 f(\theta)}{kT(\Delta Gv)^2}\right) \qquad \text{Eq. 2.18}$$

where I_{ss} is the nucleation frequency for the steady state condition and D_L is diffusivity of solute in the melt which can be gained from an Arrhenius relationship such as:

$$D_L = D_\circ \exp(-Q/kT) \qquad \text{Eq. 2.19}$$

where D_o is a material constant and Q is the activation energy for diffusion of solute in the melt, a_o is jump distance for attachment of an atom to the nucleus, and b is a geometric factor (-16π/3 for spherical nuclei).

In general, nucleation rate may be written (Turnbull 1952) as:

$$I_i = \Omega_i \exp\left(\frac{-\Delta G^*}{kT}\right) \qquad \text{Eq. 2.20}$$

where I_i corresponds to either heterogeneous surface nucleation, I_a, homogenous nucleation I_s or heterogeneous nucleation on volume distributed nucleant sites, I_v (Boettinger and Perepezko 1993). Then, for volume-dependent heterogeneous nucleation (e.g. in rapid solidification processing, spray deposition and surface melting), I_i and the prefactor are expressed (Turnbull 1952, Gremaud et al. 1996, etc.) as:

$$I_v = \Omega_v \exp\left(\frac{-\Delta G^*}{kT}\right) \qquad \text{Eq. 2.21}$$

$$\text{with } \Omega_V = \left[\frac{2D_L}{V_L}\left(\frac{\sigma_{SL}}{kT}\right)^{1/2}\left[f(\theta)\right]^{1/6}\right]\left[A_P N_v'\right] Z\left(1 - f_s\right) \qquad \text{Eq. 2.22}$$

where V_L is the atomic volume of an atom in the liquid, A_p is the surface area per mote, f_s is solid fraction, and Z is the Zeldovich factor (which corrects the equilibrium nucleation rate for nuclei that grow beyond the critical size). Z is calculated (Vekhamäki et al 2006) via:

$$Z = \sqrt{\frac{-1}{2\pi kT}\left(\frac{\partial^2 \Delta G}{\partial n^2}\right)_{n^*}} \qquad \text{Eq. 2.23}$$

where n is the number of atoms in an embryo, n* is the number of atoms in the nucleus. $N_v^{'}$ in Eq. 2.22 is the number of catalytic motes per unit volume which is given (Turnbull 1953) by:

$$N_v^{'} = N_V^0 \exp(\beta \Delta T) \qquad \text{Eq. 2.24}$$

where N_v^0 is a base level of nucleants estimated to be to 10^{13} m^{-3} and β is a positive constant (Boettinger and Perepezko 1985). The catalytic behaviour of these nucleants can be classified into one of the following forms: first, those that can activate at discrete undercooling and second, those that can activate with increasing undercooling (Perepezko at al 2002). The reason for the second type could be a different size of nucleant. Perepezko (1988) estimated (by using parameters for some metallic alloys in Eq. 2.22) Ω_i to be near to 10^{40} $s^{-1}m^{-3}$ for homogenous nucleation and $10^{35}s^{-1}m^{-3}$ for heterogeneous nucleation. By considering Eqns. 2.3, 2.6 and 2.20, Perepezko and Paik (1984) discovered that, regardless of σ_{SL} and L_V, I_V increases with increasing $\Delta T/T_m$ and reaches a maximum at $\Delta T/T_m$=2/3 which is recognised as the utmost limit for liquid undercooling. Fig. 2.3 shows the variation of I_V with ΔT for different values of θ in heterogeneous nucleation (McCartney 1989), as I (I_V) may be rewritten (Turnbull 1981) as:

$$I = \Omega \exp\left(\frac{b.\sigma_{SL}^{\ 3}}{kT.(\Delta T)^2.(\Delta S_v)^2}\right) \qquad \text{Eq. 2.25}$$

where ΔS_V is the entropy of crystallization per unit volume. For surface-dependent heterogeneous nucleation, I_a is defined (Turnbull 1950 b) by:

$$I_a = \Omega_a \exp\left(\frac{-\Delta G^*}{kT}\right) \qquad \text{Eq. 2.26}$$

where the prefactor is expressed (Perepezko 1988, Perepezko and Tong 2003) as:

$$\Omega_a = \rho\left(\frac{D_L}{a^2}\right)\left(\frac{2\pi r^{*2}(1-\cos(\theta))}{a^2}\right)\exp\left(\frac{b\sigma_{SL}{}^3 f(\theta)}{\Delta G_V^2 kT}\right) \qquad \text{Eq. 2.27}$$

where, ρ is the heterogeneous site density. Using calculations for nucleation of Bi-40 at% Cd, Perepezko and Tong (2003) determined ρ as 5.7×10^{19} m^{-2}. Using Eq. 2.20, the number of nuclei per unit area/volume (depending on I) (Hirth 1978) is:

$$N = \frac{1}{\dot{T}}\int_{T_f}^{T_L} I dT \qquad \text{Eq. 2.28}$$

where $\dot{T}$ is the cooling rate, T_L is the equilibrium liquidus temperature and T_f is the formation temperature of the new phase.

To study the effect of solidification parameters, such as temperature gradient G and growth velocity V, on the number of primary silicon particles and T_f, Liang et al (1995) applied the steady-state heterogeneous surface-dependent model (embodied in Eq. 2.18) to their results for nucleation of primary silicon in Bridgman solidified Al-18.3 wt% Si. Based on these results shown in Table 2.1, they concluded that increasing $\Delta T_P = T_L - T_f$ from 35 to 52 K over the range $1 < \dot{T} < 20 K/s$, was associated with an increasing θ from 26 to 36°.

Gremaud et al (1996) conducted a study on nucleation and growth kinetics of a laser-produced uninoculated Al-26 wt% Si alloy. Based on their solidification conditions, they applied the heterogeneous volume-dependent approach for the nucleation process (Eqns. 2.21, 2.22). Their reason for choosing this approach was

observed particle density (4.5×10^6 Si particles/m^3) too low for homogenous nucleation. Their analysis predicted 71.3° for the value of θ on the spherical cap model with 215 K undercooling at a temperature gradient of 2×10^6 K/m.

It should be stated that the spherical cap model is not applicable for potent nucleation as for θ≤10° the nucleus reduces to a monolayer thick (Greer 2004). Applying the entrained droplet technique, which is based on the action of a solid matrix as a heterogeneous nucleation site for very fine entrained droplets (~20nm), this model failed (Greer 2004). As an example, Ho and Cantor (1993) recorded a value of 43° for θ and a nucleation density of 2×10^{-11} per droplet for nucleation of silicon in Al-3wt%Si alloy with an undercooling of 60 K, at cooling rate over the range 4-15K/min. The nucleation model they used was based on the classical heterogeneous nucleation theory proposed by Turnbull (1952) and developed by Perepezko (1988). This nucleation density of 2×10^{-11} per droplet was unphysical, however, as each droplet must have more than one available nucleation site. Kim and Cantor (1992), by analysing the nucleation kinetics of lead particles, in copper matrix, showed that, when there is a very potent nucleation, the values for θ, f (θ) and ΔG* approach zero because, when θ is under 20°, the nucleus is only a few atoms thick and it becomes less than a monolayer thick when θ is under 10°, consequently indicating a breakdown of the classical spherical cap model of heterogeneous nucleation (Cantor 2003). However, a review by Cantor (1994) and the results of Kim and Cantor (1991) conclude that this model fits for nucleation at higher undercooling (ΔT>50 K) which gives higher θ (θ>40°).

Plotting number per unit volume (N_v) versus $\dot{T}$, using collected data for hypereutectic Al-Si alloys, Faraji et al (2005) showed empirically that there is a power

relationship between N_V (for primary silicon in hypereutectic Al-Si alloys) and cooling rate:

$$N_v = A.\ \dot{T}^n \qquad \text{Eq. 2.29}$$

where, typically, n~1 and A≈130 $mm^{-3}(K/s)^{-1}$ for uninoculated samples and A≈720 $mm^{-3}(K/s)^{-1}$ for phosphorus inoculated samples.

2.1.4 Grain refinement mechanism by inoculation

Metals and alloys tend to solidify in coarse columnar structures under normal casting conditions (Flemings 1974). One of the ways to produce finer grains is to increase the number of nucleants (McCartney 1989) via inoculation. By increasing undercooling, the grain size decreases due to the increase in nucleation rate. Thus, high cooling rate results in finer grains (McCartney 1989). For a potent nucleant to promote heterogeneous nucleation, there are some requirements (Murty et al 2002):

i. Higher melting point is required compared to the solidifying alloy.

ii. It should be able to nucleate solid from melt at very low undercooling.

iii. An adequate number of the nucleants should be distributed evenly in the melt.

iv. Their size should exceed the critical size (r*) which, based on Eq. 2.7, depends on ΔT.

In potent inoculation, the grain initiation is restricted by inoculant particle size and it starts on the largest particles (Greer 2003).

To be classified as an effective nucleant it should wet the nucleating solid showing as low θ as possible. Considering Eq. 2.9 therefore, a low σ_{SL} and/or σ_{SN} and/or high $\sigma_{NL}$is required. It should be added that σ_{SL} and σ_{NL} are highly dependant on the

alloying elements present (Murty et al 2002). In addition, Turnbull and Vonnegut (1952) claimed that effective nucleants have low index planes with very similar atomic arrangements to the low index planes of the newly solidified nuclei.

To study the grain refinement mechanism, Maxwell and Hellawell (1975) investigated the effect of cooling rate, contact angle and phase diagram parameters on relationship between the grain densities and the nucleant particle densities in Al-Ti as a model system. They introduced a model to predict the density of grains based on the density of nucleant particles which was further developed by Greer et al (2000). Maxwell and Hellawell (1975) showed that the effect of nucleant particle size was rather small compared with the influence of other parameters. Considering Eq. 2.20, they argued that the maximum nucleation rate occurs with the nucleus composition that minimises ΔG^* i.e. $\sigma^3.f(\theta)/\Delta G_V^2$. Since σ and θ are difficult to determine, they kept them constant and the only variable parameter was $\Delta G_V = \Delta S_V.\Delta T$. In their model, the growth restriction (caused by curvature undercooling and solute diffusion) of already nucleated grains was the reason for the new nucleation. This nucleation continued until all the latent heat was released, resulting in a decrease of undercooling. The rate of growth was calculated (Maxwell and Hellawell 1975 and developed by Greer et al (2000)) from:

$$r = \lambda_s (D_s t)^{1/2} \qquad \text{Eq. 2.30}$$

where $\lambda_s = \left[\frac{-S}{2\pi^{1/2}}\right] + \left[\frac{S^2}{4\pi} - S\right]$ Eq. 2.31

and $S = \frac{2(C_{IL} - C_A)}{(C_{IS} - C_{IL})}$ Eq. 2.32

where r is the radius of the crystal, D_s is solute diffusion coefficient, t is time, C_A is the bulk liquid concentration, and C_{IL}, C_{IS} are equilibrium interface compositions in the liquid and solid, respectively. Maxwell and Hellawell (1975) showed that the number of grains increased with the number of nucleants up to a critical value and reaches saturation beyond this value.

Johnson et al (1993) concluded that both nucleants and solute elements influence the grain refinement. The extent of solute segregation was governed by the Growth Restriction Factor (Q), equal to $mC_0(k-1)$, where m is the slope of the liquidus, C_0 is the concentration of the solute in the melt and k is the equilibrium partition ratio (C_{IS}/C_{IL}). Greer et al (2000) adopted Q as controlling the effectiveness of the refiner (Al-Ti-B) and showed that grain diameters reduced with increasing Q. Greer (2004) suggested that, when nucleation is potent, grain refinement can be quantified by the free-growth model. This model can predict the grain size using the distribution of nucleant particles as input. Greer et al (2000, 2006) showed that if the size of nucleant particle is small enough (such that $d<2r^*$, where d is nucleant particle diameter), then the nucleus cannot reach the spherical shape beyond which free growth of the crystal from the melt is possible. Free growth of the nucleus is possible just when the undercooling rises to decrease r^*. Free growth undercooling is calculated (Greer et al, 2000) as:

$$\Delta T_{fg} = \frac{4\sigma_{SL}}{\Delta S_V . d} \qquad \text{Eq. 2.33}$$

In this model, a key feature is ΔT_{fg} which is determinable compared to 0 which is not directly measurable (Greer et al 2003).

2.2 Solidification of hypereutectic Al-Si alloys

The Al-Si diagram has been presented by Murray and McAlister (1984) (Fig. 2.4). This system is a simple binary eutectic with the eutectic reaction at 577.1°C and 12.6 wt% Si, so, all alloys containing more than 12.6 wt% Si can have a hypereutectic microstructure, although, in commercial practice, silicon levels in these alloys vary between 14 and 25 wt%.

2.2.1 The microstructure and properties of hypereutectic Al-Si alloys

The solidification microstructure of commercial hypereutectic Al-Si alloys consists of three phases, primary aluminium solid solution, primary silicon and the aluminium-silicon eutectic. It should be noted that, in these alloys, the eutectic is between aluminium solid solution (in fact with mainly silicon, copper and magnesium as solutes) and silicon. Usually, solidification conditions, such as cooling rate, presence of impurities and nucleation sites during solidification, change the morphology, size and distribution of the primary and eutectic silicons (Tenekedjiev and Gruzleski 1990).

The silicon morphologies depend strongly on growth rate, temperature gradient and composition during solidification. Tenekedjiev and Gruzleski (1990) classified silicon morphology into nine categories as follows:

1. Star-like primary silicon (Fig 2.5a) observed in untreated alloys at very low cooling rate. Weiss and Loper (1987) classified this type of silicon into three subcategories as, solid star, radial star and lamellar star.

2. Polyhedral primary silicon (Fig 2.5b) resulting from phosphorus additions (Tenekedjiev and Gruzleski 1990) or high cooling rate (Zhou et al. 1991). Kim

and Heine (1963-64) noted that, in unmodified alloys, polyhedral silicon is produced at higher formation temperature.

3. Plate-like silicon, as observed eg by Fredriksson et al (1973).

4. Dendritic primary silicon (Fig. 2.5c) observed in alloys chemically modified by Na or Sr.

5. Spheroidal primary silicon (Fig. 2.5d) associated with sodium modification and high cooling rates.

6. Feathery (or skeleton, lamellar or web) silicon (Fig. 2.5e) as a result of high undercoolings with a decrease in silicon levels.

7. Y-like or angular primary silicon (Y in Fig. 2.6a), although Atasoy et al. (1984), for example, considered this as a eutectic silicon.

8. Flake-like (E in Fig. 2.6a) silicon that refers to eutectic silicon in unmodified alloys and P-treated alloys.

9. Fibrous eutectic silicon (Fig. 2.6b) observed in modified alloys.

Of the above-mentioned morphologies just the dendritic primary silicon and fibrous eutectic silicon caused by quench modification are usually considered to be non-faceted. However, some studies (Fredriksson 1973, Kobayashi and Hogan 1985 and Lu and Hellawell 1987a) have revealed that such chemically modified eutectic silicon is microfaceted.

Hypereutectic Al-Si alloys without any addition can have very large primary silicon crystals, as large as even several millimetres, with flake-like eutectic silicon. Since both types of silicon are stress-raisers, they are detrimental to mechanical properties (Bell and Winegard 1966, and Day 1969). However, with increasing

undercooling (using the droplet emulsion technique), Kang et al (2004, 2005) showed that primary silicon morphology changed from star-like to plate-like. Kang et al (2005) also observed a morphological change from flake to fibrous for eutectic silicon in hypereutectic alloys from increasing undercooling as it was recorded by Steen and Hellawell (1972) and Lu and Hellawell (1987a). They suggested a change in growth kinetics from layered growth to radial growth with increased undercooling as a reason for this transition. They added that the critical undercooling level needed for this morphological transition increased with silicon alloying content.

According to Mandal et al. (1991), the size of primary silicon is the most important parameter that controls the tensile strength of these alloys. With modification, the structure becomes finer and the silicon more rounded, so the tensile strength and ductility increase (Fig. 2.7). Thus, the reason for the improved mechanical properties in modified alloys is directly because of changing the microstructure (Gruzleski and Closset 1990).

In comparing the effect of refinement of primary silicon and modification of eutectic silicon on the mechanical properties of hypereutectic Al-Si alloys, it should be noted that the improvements in tensile properties from modification are better than those obtained by primary silicon refinement (Tenekedjiev et al. 1989). Also impact strength can be improved by modification of the eutectic silicon (Tenekedjiev et al. 1989). Tables 2.2 and 2.3 show tensile properties of two hypereutectic alloys after refinement and modification compared with their untreated conditions.

2.2.2 Refinement of the primary silicon

Refinement in hypereutectic Al-Si alloys refers to any treatment that reduces the size of primary silicon crystals. Refinement accompanies an increase in the

number of primary silicon particles and also morphological change from irregular plate or star-like to polyhedral (Tenekedjiev and Gruzleski 1990) and, as a result, the mechanical properties are improved (Fig 2.8).

There are a few ways to achieve refinement of primary silicon, such as rapid solidification (Zhou et al. 1991), use of a low casting temperature (Rooy 1972) and adding some elements e.g. arsenic, sulphide, elemental sulphur or phosphorus-bearing compounds as a refiner (Telang 1963, Bates and Calvert 1966 and Sigworth 1987). However, since the addition of a refiner is usually simpler, it is the most accepted method in this case.

For nucleation of primary silicon in hypereutectic Al-Si alloys, a level of undercooling is required. At a low level of undercooling, normally just a few particles are nucleated, so they will be large. Also, since the primary silicon is lighter than liquid aluminium, it travels upwards under buoyancy forces and causes segregation. Both of these results have negative effects on mechanical properties, such as machinability. By addition of a refiner to promote nucleation of primary silicon, such properties can be improved.

Different studies (Arnold and Prestley 1961, Telang 1963, Crosley and Mondolfo 1966, Sigworth 1987 and Gruzleski and Closset 1990), found that phosphorus is one of the best refiners for these alloys. After addition, phosphorus forms AlP which precipitates in the melt and twinned silicon crystals are considered to nucleate on AlP. The orientation relationship between silicon and AlP, also Al and Si is cube-cube (Ho and Cantor 1995a). AlP is an effective heterogeneous nucleant for silicon because it has the same crystal structure (diamond cubic) and similar lattice parameter to silicon. The lattice parameter for silicon is 0.542 nm and for AlP it is 0.545 nm (Sigworth 1987) and the melting point of AlP (2530°C) is higher than the

Al-Si hypereutectic liquidus temperature (Weiss and Loper 1987). Ho and Cantor (1995a,b) claimed that they could trace phosphorus in the primary silicon particles using STEM X-ray elemental mapping and TEM. Nogita et al (2004a) reported the presence of P, Al and oxygen (O) in the eutectic silicon formed in a hypoeutectic Al-Si alloy, applying conventional energy-dispersive spectroscopy (EDS). Because AlP has a similar structure and lattice parameter to silicon, they assumed the nucleus was AlP and not $AlPO_4$.

i. Level and type of refiners

There are different suggested levels for phosphorus addition, such as 0.005 to 0.03 wt% (Weiss and Loper 1987) and 0.001-0.01 wt% (Tenekedjiev et al. 1989). Kyffin et al (2001a) recorded that the highest level of primary silicon refinement was achieved for their conditions by adding 0.02 wt% P in an Al-20 wt% Si alloy. However, the amount of additive depends on the levels of other process variables such as superheat, cooling rate, holding time, or temperature of addition (Weiss and Loper 1987). Phosphorus has been added elementally or as different salts, phosphorus bearing alloys or compounds. Examples include phosphorus pentachloride (PCl_5), copper-15 wt% phosphorus, copper-8 wt% phosphorus, specially designed commercial additives (Alphosit, Nucleant 11, 120), red phosphorus, aluminium phosphide (AlP), manganese phosphide (Mn_3P) (Telang 1963, McAlister 1985, Poirier 1987, Liu et al. 1989 and Long et al 1994 and Acosta et al. 1995), or as an Al-Cu-P refiner made by cold die compacting of Cu-P alloy with Al powder (Schneider 1993). Another recently used refiner is Al-Fe-P (Vogel and Schneider 1991, Schneider 1993, Mason 1995). It is produced by blending Fe-P alloy and Al powders but then cold isostatically consolidating into a billet. Wang et al (1994)

applied both cast ingot routes and P/M routes to produce Al-Cu-P refiner. According to them, Al-Cu-P is more effective than conventional Cu-14 wt% P alloy. Schneider (1993) used the P/M route; he blended Al 99.7 wt% and Cu-7 wt% P powders, cold compacted, then extruded to a rod 10 mm diameter and heat treated. Another refiner is the Cu-8 wt% P alloy that is very convenient to use and is available as a brazing alloy in rod or shot form (Gruzleski and Closset 1990). It should be added that one important restriction for its usage is the limited tolerance for copper in some commercial Al-Si alloys.

Rooy (1972), Mandal et al. (1991), Jorstad (1968 and 1984) and Schneider (1960) concluded that the main parameters that may alter the effectiveness of refinement are: casting method, cooling rate, type of refiner, form and method of addition, addition temperature, holding time, degassing sequence, type of degassing agent, pouring superheat, fluxing, remelting cycles, fineness of the additive, if a powder, and consideration of the negative effects of interaction between some additives. It is very important to add phosphorus after removing Sr, Na or Ca from the melt as they can nullify the inoculating effect of phosphorus by chemical interaction (Schneider 1960, Crosley and Mondolfo 1966, Hellawell 1970, Mondolfo 1976, Sigworth 1983 and Weiss and Loper 1987). The refinement has no significant effect on the eutectic phase, whereas strontium or sodium can modify it (Tenekedjiev et al. 1989).

Recently, some researchers have studied the effect of calcium as a primary silicon refiner. Usually calcium is present within the alloy as an impurity. According to studies by Kobayashi et al. (1997), Kim (2003) and Kim et al (2004), calcium can change the morphology of the eutectic silicon and modify it, while also refining the primary silicon.

In addition, Chang and Moon (1998) studied the effect of rare earth (RE) metals on the primary silicon. They reported that adding 3 wt% rare earth metals changed the star-shape of primary silicon in an Al-21 wt% Si alloy into fine polyhedral particles, regardless of cooling rate (between primary reaction and eutectic reaction temperature) over the range of 33 to 130 K/s.

ii. Effect of refiner on the formation temperature of primary silicon

In addition to the refinement, phosphorus changes both the primary silicon and eutectic silicon growth temperatures. Zhang et al (2001) recorded an increase of 17.3 K (from 739.7 to 757°C) and 4 K (from 565.4 to 569.4°C) in these, respectively, in Al-25 wt% Si alloy on adding 0.1 wt% phosphorus, for a cooling rate of ~0.33 K/s. Kyffin et al (2001b) reported an increase of about 45 K (from ~635 to ~680°C) in the formation temperature of primary silicon in Al-20 wt% Si alloy as a result of adding 0.01 wt% phosphorus, for a cooling rate of ~1 K/s. Song et al (2004) recorded an increase of 6.4 K in T_f from 594.1 to 600.5°C on adding 0.02 wt% P to a near eutectic Al-Si alloy. Colligan and Gunes (1973), in contrast, concluded that in phosphorus-refined Al-17 wt% Si alloy, primary silicon nucleates at lower temperature (627°C) compared to the unrefined alloys (665°C). They concurred, however, that phosphorus inoculation caused a 2 to 8 K increase in eutectic arrest temperature in hypereutectic alloys, though phosphorus addition lowered it by 3 to 10 K in eutectic alloys, while Sigworth (1987) found no direct relation between T_f and phosphorus addition in an Al-17 wt% Si alloy as it was varying randomly from 612 to 638°C regardless of size or structure of primary silicon. Additionally, Chang et. al. (1998) showed that inoculation by 3 wt% rare earth (RE) metals depressed T_f by 12-17 K in an Al-21

wt% Si alloy, so concluding that adding a rare earth bearing compound (mainly Al-Ce) refines primary silicon by suppressing its formation temperature.

iii. Effect of refiner on size of primary silicon

Kyffin et al (2001a) reported that adding 0.01 wt% phosphorus (using Al-Fe-P master alloy) to an untreated Al-20 wt% Si, decreased the diameter of primary silicon particles from 120 μm to 56 μm. Also, Jiang et al (2005) reported that by adding 0.5 and 1.5 wt% of a combined inoculant (Al-P-Ti-TiC-Y), the size of primary silicon in Al-20 wt% Si and Al-29 wt% Si decreased from 100 and 250 μm to 20 and 35 μm, respectively. Song et al (2004) reported a primary silicon size reduction from 65 μm to 15 μm on adding 0.02 wt% phosphorus, using an Al-P master alloy, for an untreated near eutectic alloy.

2.2.3 Modification of the eutectic silicon

To change the eutectic silicon morphology from flake-like to fibrous, a chemical additive, as a modifier, or a high cooling rate, is needed (Hellawell 1970).

i. Eutectic modification theories

In order to understand the effect of modifiers on the morphology of eutectic silicon, numerous studies have been carried out that are presented in historical order as follows:

Thall and Chalmers (1949) suggested that the modifier reduces the interfacial energy of the molten Al-Si/solid Si interface which was confirmed by Nakae and Kanamori (1997) by the sessile drop method. In addition, Davies and West (1963-64) suggested that sodium absorbed on the solid eutectic silicon/melt surface and thus retarded its growth, a result from poisoning of the growth sites of the eutectic silicon

by the modifier. According to Thall and Chalmers (1949), aluminium was the 'leading' phase, but later the opposite was revealed (Flood and Hunt 1981). Kim and Heine (1963-64) studied the effect of modifier on primary silicon and detected a change in growth shape of primary silicon from coarse plate to spheroidal silicon. They explained this as a consequence of lowering the nucleation temperature of the primary silicon although this was not verified experimentally.

Hamilton and Seidensticker (1960) introduced a mechanism for silicon growth by twinning known as the twin plane re-entrant edge (TPRE) mechanism later developed by Kobayashi et al (1975) and Lu and Hellawell (1987a). Twins form easily in silicon crystallization on the <111> planes, causing a 141 degree groove at the S/L interface, making a re-entrant corner. There is another external angle, 219 degrees that makes a ridge. The preferential site is the re-entrant corner, so, more corners lead to rapid growth along the [211] direction. If there are two twins, there will be more sites for nucleation, due to the existence of six re-entrant corners, as shown in Fig. 2.9, and this makes more re-entrant corners and so on.

There was another suggestion for a growth mechanism by Kitamura et al. (1979), based on screw dislocations. As indicated in Fig. 2.10, there are four preferential growth sites in a specific faceted crystal: kinks, steps, re-entrant corners and surface. It should be said that the most effective sites are kinks and the weakest one is the surface. When screw dislocations are on the surface, the TPRE mechanism is not responsible for growth and also when there are more screw dislocations on the surface than at the twin junctions. It should be added that further studies by Sungawa and Yasuda (1983) revealed that, for a quartz crystal, growth occurred at the re-entrant corner of a twin junction that had a high density of screw dislocations, so, it was concluded that the TPRE mechanism is not the only one.

Lu and Hellawell (1985) and also Shamsuzzoha et al. (1992) did detailed TEM studies on impurity modified eutectic silicon fibres to record their growth mechanism. According to them, the growth of silicon is in a zigzag mode similar to the branching mode observed for flake silicon and depicted in Figs. 2.11 and 2.12. Also they observed a lot of twinning in both chemically modified and unmodified silicon, although there was none in the quench-modified fibres. Regarding their observations of more twinning in impurity modified compared to unmodified silicon, they concluded that the responsible mechanism for flake morphology, rather than TPRE, is by a layer mechanism as shown in Fig. 2.13. So to explain the change of eutectic silicon morphology caused by additives they introduced an impurity induced twinning theory in which additives like strontium or sodium increase the incidence of twinning. According to this theory, chemical modifiers are impurities which, by attaching to preferential nucleation sites on the growing layer of silicon at the S/L interface, such as at steps and kinks, poison the layer growth and prevent the attachment of further silicon atoms onto the crystal.

Also, Lu and Hellawell (1987a) calculated that a growth twin was formed at the interface when the ratio of modifier atom radius to silicon atom radius was 1.6457 or slightly above that, which is consistent with the radius ratios of elements used for modification, including Na, Sr, Sb, Ba, Ca, Y and Yb (Nogita et al 2004b).

Flood and Hunt (1981) found that, in unmodified alloys, the eutectic silicon nucleates on the α-Al, whereas in modified alloys that was not observed. It was confirmed by Dahle et al. (1997, 2001), Nogita and Dahle (2001,a,b), and Nogita and Dahle (2001a), that modification does not just change the morphology of the eutectic silicon, but also changes the nucleation behaviour. The work of Nogita and Dahle (2001a) showed that chemical modification by strontium and sodium causes a

transition in the eutectic silicon morphology and also reduced the number of nucleated eutectic grains. However, McDonald et al (2004) concluded that the flake-to-fibre transition as a result of impurity modification did not change the eutectic nucleation mode or frequency.

Nogita et al (2004 c) reported that the eutectic solidification mode is strongly dependent on the content of modifier. They also suggested that the silicon morphology was not controlled only by the TPRE mechanism, but was also strongly controlled by the growth rate of the eutectic grains, and by the alloy composition.

Nogita et al. (2003, 2004 d) have recorded that nucleation of primary silicon is suppressed by additions of strontium, which therefore results in supersaturation of the liquid before nucleation and also an increase in the growth rate. They have noted that, with increasing strontium addition, silicon crystals become less faceted and more dendritic. Also it has been found by them that twinning in primary silicon crystals did not increase with added strontium.

There have been some works (Nogita et al 2004 b, Nogita and Dahle 2001 a,b, and Heiberg and Arnberg 2001) on eutectic silicon using Electron Back Scatter Diffraction method (EBSD) to determine crystallographic relationships between neighbouring silicon particles before and after adding strontium. However, there was no equivalent study on the primary silicon using EBSD so far. Heiberg and Arnberg (2001) claimed that, in both modified and unmodified hypoeutectic alloy, neighbouring eutectic silicons have a twin relationship with each other by a rotation of 60 degrees around <111>. Nogita et al (2004d) reported that there was no relationship between neighbouring primary and eutectic silicon in unmodified hypereutectic alloy. In contrast, in the Sr-modified alloy, they did find a twin relationship. It is worth noting that Nogita et al (2004a) recorded that AlP particles and the surrounding

eutectic silicon have the same orientation in unmodified hypoeutectic alloys consistent with nucleation of eutectic silicon by AlP.

ii. Quench modification

Experiments revealed that a fibrous eutectic phase can be achieved without using chemical additives as a modifier. This process, known as quench modification, is done by cooling rapidly to give a 400 to 1000 μm per second growth velocity (Gruzleski and Closset 1990). Although optical micrographs show a similar microstructure to chemically modified alloys, there is a significant difference between them (Gruzleski and Closset 1990). The Sr- or Na-modified alloys have considerable amounts of twinning in the silicon, whereas there is none, or a very low amount, in quenched modified microstructures. Also, quenching causes a transition from anisotropic to isotropic growth, but sodium creates a multifaceted silicon by multiple and repetitive twinning (Lu and Hellawell 1986). The chemical modification could be even more effective at very high cooling rates in that a finer microstructure could be reached by increasing the twinning frequency and the angle of branching simultaneously (Gruzleski and Closset 1990).

2.2.4 Simultaneous modification and refinement of eutectic and primary silicon

As mentioned before, addition of phosphorus to hypereutectic alloys refines the primary silicon but the eutectic silicon remains unmodified. With addition of phosphorus and strontium simultaneously, both primary and eutectic silicons should be refined and improved mechanical properties could be achieved. Unfortunately, however, eutectic modifying elements are incompatible with phosphorus and react with it so that strontium phosphide or sodium phosphide is formed. Since these

compounds are more stable than aluminium phosphide, AlP dissolves and so primary silicon becomes coarser.

Tensile properties are not reduced, however, when just strontium is added, despite the coarse primary silicon, for such as the A390 alloy (17 wt% Si, 4.5 wt% Cu, 0.55 wt% Mg, and max. 0.5 wt% Fe). With phosphorus refinement, its UTS and elongation to fracture on standard samples are 198 MPa and 0.8 % respectively, but by adding just 0.16 wt% Sr instead, the UTS reached 212 MPa while keeping the elongation to fracture the same (Tenekedjiev et al. 1989 and Gruzleski and Closset 1990).

Considering that the equilibrium weight fraction of eutectic in binary Al-17 wt% Si alloy is about 95%, it is not surprising that the modification of the eutectic can make more improvement of the overall properties of the alloy than just the 5% of primary silicon. So, where tensile properties are concerned, eutectic modification is the first priority (Tenekedjiev et al. 1989, Gruzleski and Closset 1990).

In order to study the combined effects of refiner and modifier, Mondolfo (1965) used sodium and phosphorus together. He did this at first without sodium and then with sodium. Fig. 2.14 shows his results schematically. He argued that AlP particles are good nucleation sites for both primary and eutectic silicons. He used a hypoeutectic alloy and found that with AlP in the melt, the undercooling needed for the nucleation of eutectic silicon on it (Line 2 in Fig. 2.14) was lower than the undercooling needed for nucleation on the α-Al phase (line 5 in Fig 2.14), when there was no AlP. So he concluded that, at first, the eutectic nucleated on AlP then, when the temperature reaches point H, eutectic will form on α-Al. But after adding sodium, he found that sodium nullified the nucleating effect of AlP by forming sodium phosphide. Bercovici (1980) confirmed Mondolfo's findings and showed that, with

increasing phosphorus in the alloy, the amount of sodium (or strontium) required for modification of the eutectic is increased.

Although a few workers (Lee and Kang 1995, Park et al. 1997 and Wu et al 2003, Xu et al 2006) claimed to obtain a simultaneous refinement of primary and eutectic silicons, they presented no convincing evidence. It should be noted that, if they added a phosphorus-containing refiner, such as Cu-P alloy, and strontium (or sodium), then according to the following equation the formation of Sr_3P_2 (or Na_3P) compounds is anticipated, so, as a result, both refinement and modification are weakened (Park et al. 1995).

$$3Sr + 2P \rightarrow Sr_3P_2 \qquad \text{Eq. 2.34}$$

Park et al. (1995), however, added Al-Cu-P alloy that was fabricated by the extrusion of compacted mixed powders and heat treatment. They also used Al-Sr alloy to modify the eutectic silicon too. Due to heat treatment of the refiner before its addition, AlP is formed in it and then when it was added to the melt they thought that this AlP might be decomposed to Al and P to form Sr_3P_2 after reaction between AlP and Sr. Also, the formation of undesirable Sr_3P_2 compound was retarded because at first AlP has to be decomposed and then take part into the reaction. Thus, if the casting and solidification was completed before this decomposition of AlP occurred, it would be possible to achieve refinement of both primary and eutectic silicon. They claimed to have confirmed the effects of these agents by thermal analysis. Fig. 2.15 shows the cooling curves of Al-20 wt% Si, without addition (a) and with a combined Al-Sr and Al-Cu-P addition (b). The liquidus temperature for this alloy taken from the equilibrium phase diagram was about 680°C. As Figure 2.15 shows, the 35 K undercooling reduced to a few degrees from the curve (a) to (b), making nucleation

easier after addition of 0.01 wt% P+0.05 wt% Sr and both primary and eutectic silicon were refined in the treated melt.

Wu et al (2003) claimed that using P-Na compound refines both primary and eutectic silicon. They concluded that, by adding sodium, viscosity of the melt increased and therefore the diffusion coefficient of phosphorus in it decreased, so remaining attached to the silicon growth front and retarding its growth so causing refinement. Their evidence was the presence of phosphorus within refined primary silicon particle revealed by X-ray diffraction patterns. They did not present enough evidence though on both refinement and modification. Recently, Xu et al (2006) claimed that use of Al-P-Ti-TiC-Nd modifier refined the size of primary and eutectic silicon in Al-20 wt% Si alloy from 60 μm and 40 μm in length to 22 μm and 18 μm, respectively. They suggested that by absorbing on silicon, neodymium increased the twin frequency in eutectic silicon and also changed the primary silicon growth mode from anisotropic to isotropic.

There was an older attempt to achieve the desirable double refinement of primary and eutectic silicon by Cissé et al. (1975). They claimed that, to minimize the reaction between sodium and phosphorus, a two stage process should be used. They added phosphorus first, before solidification started and then sodium was added very close to the eutectic temperature. But in this case, again, no clear evidence of the claimed double refinement was presented.

3. Experimental procedure

3.1 Materials

3.1.1. Aluminium-silicon alloy

An Al-20 wt% Si alloy supplied by Norton Aluminium Products Ltd was used to study the nucleation and refinement behaviour of primary silicon and modification of eutectic silicon. The chemical analysis provided by the supplier is given in Table 3.1. Table 3.2 shows the results of chemical analysis of the supplied ingot for different positions in the ingot, carried out at Sheffield.

3.1.2 Al-Fe-P refining inoculant

An Al-Fe-P alloy inoculant has been utilised as a primary silicon refiner in this study. The chemical composition of a sample of this additive is given in Table 3.3. The process of preparing a 30 mm diameter billet-shape inoculant by KB Alloys, which was provided in a cold isostatically pressed (CIPped) condition, was as follows:

Commercial purity aluminium and Fe-P alloy powders were first blended as 80 to 20 wt% proportionally. Then in order to produce a billet 150 g in weight, 120 mm in length and 30 mm in diameter, a pressure between 25000 and 30000 psi (172 to 207 MPa) was applied in a wet bag.

The holding time after its addition to the Al-Si alloy melt was set at 15 min at 800°C (compared with 10 min in Kyffin et al's (2001c) work and 15 min in Park et al's (1995) work for the same alloy). The amount added varied from 0.02 to 0.08 wt% retained P (the effective amount of phosphorus for good refinement was reported to be 0.005 to 0.5 wt% (Rooy, 1972, Weiss and Loper, 1987). Kyffin et al (2001c),

however, claimed the optimum amount for Al-20 wt% Si was 0.02 wt%, therefore the range 0.02 to 0.08 wt% added phosphorus was chosen for the present study. The melt temperature at addition was set at 800°C, as the optimum temperature for the best result of refinement by phosphorus for Al-20 wt% Si alloy recommended by Kattoh et al (2002).

3.1.3 Al-Cu-P refining inoculant

Extruded rod of Al-Cu-P alloy has been utilised as the other type of primary silicon refiner in this study. The chemical composition of this additive is given in Table 3.4. Like Al-Fe-P inoculant, the holding time after addition to the Al-Si melt was set at 15 min. The amount of this additive was 0.02 wt% added phosphorus and the addition temperature was 800°C.

3.1.4 Al-Sr modifying agent

In order to modify the eutectic silicon, Al-5.93 wt%Sr supplied by LSM Ltd was applied as small lumps (nearly 10 mm in dimensions). The chemical analysis of this agent is given in Table 3.5. In this case, holding time and temperature were set constant at 15 min and 800 °C respectively. However, two different methods were used. First, the Al-Sr master alloy was added 15 min after adding the phosphorus inoculant and then the melt was held for 15 min before degassing with NITRAL tablets (supplied by FOSECO) and pouring into the mould. The second method was to add it into the mould, and then pour the melt immediately. For this, two different melts were investigated, uninoculated and phosphorus-inoculated. In both cases, 0.05 wt% Sr was added, because it was found by Park et al. (1995) that this amount is the optimum percentage. It should be noted that different additive amounts, and ways of addition were investigated in the present work.

3.2 Casting processes

Fig. 3.1 shows schematically the bottom casting apparatus used. The dimensions of the furnace cavity were 320 mm in length and 90 mm in diameter with an alumina crucible in it. There was a ceramic stand as a platform for the crucible. Usually 150 g of hypereutectic aluminium-silicon ingot was charged in every batch. The alumina crucible was 220 mm in height and 80 mm bore. There was a 16 mm diameter orifice at the bottom of the crucible that had a graphite nozzle placed in it. The dimensions of the nozzle are shown in Fig. 3.2. This was closed by an alumina stopper rod until teeming was required. The tubular stopper rod was held by a tight clamp on a fixed stand. For teeming, the stopper was withdrawn allowing the melt to teem into the sand mould (Fig. 3.3) which was placed underneath the apparatus. As a routine, after every three runs, the nozzle was replaced. The sand mould incorporated a type K thermocouple with output fed to a data logger to collect cooling curve information. Fig. 3.4 shows the whole procedure of casting using this apparatus. It should be noted that there was an additional alumina sheath inside the crucible for use as a stirring rod after every addition. The temperature of the melt was determined by another K-type thermocouple that was inserted in the hollow stopper rod.

Four types of experiment were done; untreated, adding phosphorus, adding strontium and adding both phosphorus and strontium. For this alloy, the casting temperature was 800°C and 0.015-0.08 wt% P was used as a primary silicon refiner and 0.04-0.2 wt% Sr for eutectic silicon modification. The holding time for melt homogenising after reaching to 800°C was 15 min. To minimize phosphorus loss, the additive was placed in aluminium foil and then quickly plunged below the melt. After 20 seconds of stirring to promote homogeneity, it was held for 15 minutes and then 0.05 wt% Sr was added as Al-Sr master alloy. In simultaneous primary silicon

0.05 wt% Sr was added as Al-Sr master alloy. In simultaneous primary silicon refinement and eutectic modification there was an extra procedure for casting. Strontium was added into the mould then the melt was teemed on to it immediately. This was done in order to minimize the interaction between AlP and strontium and as a result, possibly, achieve both primary silicon refinement and eutectic silicon modification simultaneously. The conditions studied are specified in Table 3.6.

In addition to bottom casting, another method was used to reduce the effect of melt turbulence during casting and to produce more temperature-controlled samples, as a result. In this method, a crucible mould with a cold charge of metal (90 g) was put into a chamber furnace which was set to 800°C. Inoculation was done outside the furnace by plunging (0.02, 0.04 and 0.08 wt% P) AlFeP wrapped with aluminium foil into the melt using an alumina plunger. Following this, the mould was returned into the furnace for 15 minutes. Then it was taken out and placed onto a copper block (thickness, 35 mm: diameter, 75 mm). For the whole time, there was a ceramic-fibre lid (thickness, 13 mm) on the mould. A hole was drilled through this to allow a sheathed thermocouple to be inserted into the melt so as to monitor temperatures during solidification.

To have different cooling conditions, two types of moulds were used in this method of casting. One was an alumina crucible (bore, 40 mm: height, 45 mm: wall thickness, 2 mm) and the other one was a stainless steel cup (bore, 30 mm: height, 30 mm: wall thickness, 1 mm). The steel mould was coated internally with HOLCOTE 110 made by FOSECO.

3.3 Heat treatment

To be able to determine the total volume fraction of silicon in the very fine microstructure of modified ingots, samples numbers B2, B3, B4, B5, B6 (analyses shown in Table 3.6) were spheroidized via heat treatment in a Lenton chamber furnace at 500°C for 145 h and then cooled in air.

3.4 X-ray diffraction

To study and identify the phases within the Al-Cu-P, Al-Fe-P and Al-Sr inoculants and modifier, XRD was done for each sample separately. Except for Al-Fe-P examined as powder (obtained by grinding and sieving pieces of supplied billet), others were cut into small pieces (10×10×5 mm) to be examined after polishing with grinding papers, 120 and 400 grades.

To produce Co Kα radiation, a Philips X-ray tube was used at 40 kV and 30 mA. The divergence angle of the slits was: 1° between the tube and the sample; and 0.2° between the sample and the detector. Scanning was carried out over a range of 10° to 70° 2θ.

3.5 Metallographic preparation for optical microscopy

In order to ascertain the microstructure of Al-Cu-P and Al-Sr additives by optical microscopy, a piece of each was cut and then preliminary metallographic preparation was done by rotary wet grinding on SiC grinding papers, with 120, 400, 800 and 1200 grades. Then, polishing was done by standard diamond polishing techniques with 6 and 1 micron diamond paste. Finish polishing used a suspension of colloidal silica (particle size smaller than 0.06 μm). There was no etching at the end.

Also, after completion of solidification, the cast samples were removed from the mould and cut with an abrasive disc in two stages. Firstly, the sample was cut in a half longitudinally and then this longitudinal section was polished (as shown in Fig. 3.5). It should be noted that the microstructure of the whole section was studied. The preliminary metallographic preparation, as mentioned above, was done for all of these samples as well.

Then microstructures were observed at different magnifications and recorded by a Reichert Polyvar Metallurgical Microscope, connected to an Iiyama computer with an image grabber and KSRun 3 image analysis software.

3.6 Quantitative metallography

Measurements of the volume fraction of silicon were carried out by means of image analysis software (SigmaScan Pro, version five). To acquire each measurement, five areas through each heat-treated sample were selected, and after taking micrographs, were analysed by the software.

In order to check the microstructure of ingots by optical microscopy, each ingot was halved longitudinally (as shown in Fig. 3.5) and a preliminary metallographic preparation was carried out. Then microstructures were observed at different magnifications and recorded by means of an Olympus VANOX-T Microscope, connected to an Iiyama computer with an image grabber and KSRun 3 image analysis software. Following this, photomicrographs were taken from the bottom to the top of the ingots on the longitudinal axis down the centre line (Fig. 3.6). In order to measure the number of particles per unit area (N_A), all micrographs for each ingot (15 on average) were considered and point counted by hand. It was not

possible to count by image analysis software because it could not distinguish reliably between primary silicon particles and eutectic silicon.

By measuring N_A and volume fraction f, number of primary silicon particles per unit volume (N_V) is obtainable based on the following:

$\overline{N_V} = \overline{N_A} / \overline{D_V}$ and, for equalized spheres of radius r (Martin 1980):

$$f = \frac{4}{3}\pi r^3 . N_v \text{ (Martin, 1980)}$$

$$\text{Here } r = \overline{D_V}/2 \text{ so } \overline{N_V} = \left(\frac{\pi}{6f}\right)^{1/2} \overline{N_A}^{3/2}$$

where $\overline{D_V}$ is true mean volume diameter and r is the volume radius of particles.

3.7 Differential Thermal Analysis (DTA)

To study the effect of phosphorus on the liquidus temperature of the alloy, samples A1, A2 and S10 (Table 3.6), were selected and Copper Die Suction Casting was used to produce 2 mm diameter rods. In this process, pre-alloyed ingot is melted in an argon arc furnace and the melted alloy is sucked into a water-cooled copper die under the influence of a negative pressure differential between the copper die and the melting chamber. The melt temperature for this alloy was set at around 1000 °C and the cooling rate was 700 K/s. For each DTA sample, 50 mg of material was taken from each rod. The DTA process was carried out as follows:

Heating up to 800 °C at 10 K/min, holding at 800 °C for 15 minutes, cooling down to 50 °C at 10 K/min, using alumina crucibles in an argon atmosphere. To assess the

reproducibility of the result, this procedure was performed three times for each sample.

After thermal analysis using Perkin Elmer DTA 7 hardware and Pyris software, the number per unit volume of primary silicon particles (N_V) was determined by quantitative metallography on the same samples which were then sent for chemical analysis to determine the content of silicon and phosphorus.

3.8 Electron Back Scatter Diffraction (EBSD)

In order to find out whether there was a relationship between neighbouring, interconnected or attached primary silicon particles, Electron Back Scatter Diffraction (EBSD) was used. It can detect the crystallographic orientation at the point where the electron beam is positioned. The equipment used was a JEOL SEM, JSM 6400 which was equipped with Oxford Instruments EBSD (EBSD hardware) and with HKL Channel 5 software. Sample preparation for EBSD consisted of two parts. First, the usual preparation for optical microscopy was done; then, the sample was polished on a vibratory polisher with 0.05 μm colloidal silica for about two and a half hours. Specimens were prepared from uninoculated and phosphorus inoculated ingots under different solidification conditions (C4, A2, S1, S2 and S5: specified in Table 3.6). The orientation measurements were performed on neighbouring primary silicon particles and some clusters in each sample.

4. Results

4.1 Microstructural characterisation

Fig. 4.1 shows the distribution of the phases in ingots produced using bottom casting with different additives. Typical microstructures are shown in Fig. 4.2.

4.2 Cooling curves

Figs. 4.3, 4.4, 4.5 and 4.6 show the cooling curves for ingots in different states; untreated, inoculated by P, modified by Sr and simultaneously modified and inoculated, respectively, all produced via bottom casting. Formation temperature of primary silicon phase (T_f) was determined for each sample from the first derivative of cooling curves. The liquidus temperature (T_L) of the alloy was calculated as the assessed equilibrium value (Murray and McAlister 1984) given by the following equation (Liang et al 1995):

$$T_L = T_{EU} + 14.93(C-C_{EU}) - 9.28\times10^{-2}(C-C_{EU})^2 + 3.59\times10^{-4}(C-C_{EU})^3 \qquad \text{Eq. 4.1}$$

where T_L: liquidus temperature (°C); T_{EU}: equilibrium eutectic temperature, 577.1°C; C, alloy composition (at%) and C_{EU}: equilibrium eutectic composition, 12.2 at.% Si. For this alloy (18.6 wt%≡18 at%: the average value for silicon composition using Table 3.2), Eq. 4.1 gives T_L as 660.7°C. Then, the undercooling for primary silicon formation (ΔT_P) was obtained as $T_L - T_f$ for each sample.

In addition, the cooling curves were used to determine the cooling rate of cast ingots using two slopes in two different ranges; one ($\dot{T}_1$) from the peak temperature to T_f and the other ($\dot{T}_2$) from T_f to the eutectic arrest temperature (T'_{Eu}). Also the minimum formation temperature of the eutectic (T''_{Eu}) and undercooling for the eutectic ($\Delta T_{Eu} = T'_{Eu} - T''_{Eu}$) were determined from the cooling data. ΔT_{Eu} was

measured as the difference between T'_{Eu} and the lowest temperature T''_{Eu} on the cooling curve before the increase in temperature to the arrest at T'_{Eu} due to recalescence. These results; T_f, ΔT_P, $\dot{T}_1$, $\dot{T}_2$, T'_{Eu}, T''_{Eu} and ΔT_{Eu} are shown in Table 4.1. Temperatures T_P , T_L, T_f, T_{Eu}, T'_{Eu} and T''_{Eu} are defined on the schematic cooling curve shown in Fig. 4.7.a.

For untreated samples, Fig. 4.3 shows that reproducibility of cooling curve is ~ ± 15 K between 650 and 577°C (T_f and T'_{Eu}) but with different slopes above and below T_f, $\dot{T}_1$ and $\dot{T}_2$ in Table 4.1. The other reproducible feature is T'_{Eu} at around 576°C, and the duration of this arrest temperature (t_{Eu}), 459±9 seconds on average. However, ΔT_{Eu} for C2 (0.98K) is not in agreement with that for the other samples of its group (2.2 to 2.9K). Another feature for untreated samples from Fig 4.3 and Table 4.1 is that, for these samples, values of T_f are close to each other (±1 K).

On adding phosphorus, Table 4.1 shows that ΔT_P increases slightly from 7.1±1.0 K for untreated samples to 9.1±2.3 K. In addition, t_{Eu} increases from slightly 459±9 s for untreated samples to 471±16 s for this group.

For added strontium, the main result from Fig. 4.5 and Table 4.1 is the depression of T_f from 652 to 654°C for untreated samples to 606 to 620°C. Also, Table 4.1 shows that T'_{Eu} was reduced by about one degree, from 576.3±0.1 to 574.9±0.2°C, though T''_{Eu} increases just by 0.5 K from 574.1±0.9 to 574.6±0.5°C and ΔT_{Eu} becomes 0.4±0.3 K compared with 2.2±0.9 K and 2.1±1.0 K for untreated and P-added samples. In this group of curves, t_{Eu} is not so reproducible and ranges from 448 to 501 s. Another feature in Table 4.1 for this group of samples (C9 to C12) is a varying slope above T_f from 1.94 to 6.56 K/s.

For combined phosphorus and strontium additions, Table 4.1 and Fig. 4.6 show similar depression of T_f to that for added strontium, but with more reproducibility in slope giving values of cooling rate above T_f of 2.58±0.15 K/s.

The cooling curves of untreated Al-Si alloy for samples melted and solidified in alumina crucibles produced via chamber furnace casting are shown in Fig. 4.7. Fig. 4.7 and Table 4.1 show that t_{Eu} differed between two uninoculated samples (D3 and D5) while their cooling rate ($\dot{T}_1$) is similar over the range of T_P to 650°C. On adding phosphorus, D4 shows higher T_f, while its slope is similar. T'_{Eu} for D4 is 6 K lower than for D3 and D5 (570.6 compared to 576.5°C) and t_{Eu} is similar to those for D3.

The cooling curves for uninoculated and 0.02 wt% P-inoculated samples cast into steel cups are illustrated in Figs. 4.8 and 4.9. Fig. 4.8 and Table 4.1 show that, among untreated samples, S1, S2 and S3, there are slight differences in cooling rates and differences in T_f span 9K, while T'_{Eu} and t_{Eu} are more consistent. Table 4.1 shows that 0.02 wt% P decreases T_f from 652±5°C for untreated to 642±10°C and T'_{Eu} from 575.5±0.6 to 574.5±1.3°C. Also, among the values of t_{Eu} in this group, S5 has the highest value.

Finally, Fig. 4.10 and Fig. 4.11 show the cooling curves for 0.04 wt% and 0.08 wt% P-inoculated samples, melted and solidified in steel cups (quantitative data in Table 4.1). For 0.04 wt% P, Fig. 4.10 and Table 4.1 show very reproducible results for the cooling rates, for T_f (652.2±1.2°C) and for T'_{Eu} (574.7±1.0°C). For 0.08 wt% P, Fig. 4.11 and Table 4.1 show that the cooling rates ($\dot{T}_2$) vary more, though the curves show similar values of T_f (651.6±0.9°C). S12 gives a slightly higher T'_{Eu}

(574.0°C) and shorter t_{Eu} (177.1s) than S10 and S11 (T'_{Eu} : 573.5, 573.4°C and t_{Eu}: 229.3, 207.3s). Comparing results for 0.04 wt% P and 0.08 wt% P shows the same T_f (652±1°C) for both groups.

To observe any possible relationship between the formation temperature (T_f) of primary silicon phase and the quantity of added phosphorus, the results for all untreated cast ingots and P-inoculated ingots (Table 4.1) are illustrated in Figs. 4.12a and their average values are shown in Fig. 4.12b with overall averages in Fig. 4.12c. Fig. 4.12c shows that by increasing the amount of phosphorus from almost 0 to 0.08 wt% maximum, the overall average value of T_f reduces by no more than 2 K (from up to ~654°C to ~652°C). Notably, 0.02 wt% P addition gave a very broad range of T_f, including a maximum of 660°C and a minimum of 631°C (Fig. 4.17a).

In conclusion, Table 4.1 shows that, in a sand cast condition, adding 0.2 wt% strontium alone increased primary silicon undercooling (ΔT_p) by a factor of 6.7 (from 7.1±1.0 to 46.6±6.5 K) and adding also 0.02 wt% phosphorus does not change this significantly. In comparison, Table 4.1 shows that by changing the casting process from sand mould bottom casting to steel mould chamber casting, the cooling rate between T_f and T'_{Eu} increases by up to 3 times (from ~ 0.3K/s to 0.9 K/s). Figs. 4.12a and 4.12c show that adding 0.04 or 0.08 wt% phosphorus does not change T_f of untreated primary silicon produced via chamber casting into a steel mould, detectably, while adding 0.02 wt% phosphorus lowers it on average by 10 K. Figs. 4.12a, 4.12b and 4.12c show that adding 0.02 wt% phosphorus gives the biggest scatter in T_f. Table 4.1 however, shows a significant effect of strontium on T_f.

4.3 Quantitative metallography

4.3.1 Eutectic modification

Efficiency of the modification of as-cast ingots was assessed on the basis of percentage of well-modified microstructure from micrographs. Fig. 4.13 shows that the amount of modified eutectic structure rises to a maximum of 70% with increasing strontium addition at 0.1 wt% Sr then declines slowly with further addition to a small (40×35×40 mm) Sr-modified ingot.

4.3.2 Volume fraction of silicon

In order to confirm the total volume fraction of silicon in parts of the ingots which were modified very well, five micrographs of each heat treated sample (microstructures shown in Fig. 4.14 which shows that spheroidisation heat treatment results in the formation of nodular, rounded tips and bigger eutectic fibres) were measured by means of SigmaScan Pro, version five image analysis software. It should be noted that the calculated equilibrium total silicon volume fraction for the used alloy (Al-18.6 wt% Si) at 500°C is about 19.6%. While, based on image analysis, total silicon volume fraction determines 20.0±3.7%.

4.3.3 Morphological observations

Table 4.2.a shows the distribution of silicon morphologies for untreated and P-treated ingots produced via bottom casting (samples C1-8 specified in Table 3.6). These microstructural observations were taken from the bottom to the top of the ingots on the longitudinal axis along the centre line (Fig. 4.15). From Table 4.2.a it can be concluded that:

- In the bottom of all ingots C1-C8, coarse primary silicon (Zone A) appears for about 1-2 mm height only.

- Eutectic phase without any primary silicon (Zone B) forms in a wide position range from -20 to -10 mm, regardless of whether the ingot was inoculated or not.

- In samples C3, C4, C7 and C8 around the thermocouple position (just above the thermocouple), a pore of size 11×2.5, 6×2.5, 18×1 and 17×5 mm^2 respectively was observed which could have affected the cooling curves, although this pore was narrow (1 mm width) in sample C7. Samples C7 and C8 show a higher T_f than of that for C5 and C6 (Table 4.1).

- In almost all ingots (even those in which pores surrounded the thermocouple), above and below the thermocouple position there are polyhedral primary silicons (Zone C). Further towards the thermocouple they become coarse primary silicon (Zone A). Comparing inoculated and uninoculated samples indicates that inoculation increases the possibility of polyhedral primary silicon formation by tending to increase the incidence of Zone C.

Table 4.2.b gives the average lengths of different phase zones for samples C1 to C8. Its results are demonstrated as a bar chart in Fig. 4.16 to show the morphological changes, in consequence of inoculation. The chart confirms that inoculation with 0.02 wt% phosphorus nearly halves the length of Zone A (coarse primary silicon) from 23±6 to 13±3 mm and, on average, doubles the length of Zone C (polyhedral primary silicon) from 7±3 to 14±8 mm.

4.3.4 Numbers of primary silicon particles

Tables 4.3 and 4.4 show the results of quantitative metallography for bottom casting experiments whereas Tables 4.5 and 4.6 show the results for ingots produced in the chamber furnace.

For each sample, numbers of primary silicon particles per unit volume (N_V) were determined from N_A using $\overline{N_V} = \left(\frac{\pi}{6f}\right)^{1/2} \overline{N_A}^{3/2}$ [Martin, 1980] where f is the volume fraction of primary silicon phase. To observe the effect of morphological changes, in consequence of inoculation, on the numbers of primary silicon particles per unit area (N_A), Table 4.3 summaries the values of N_A and N_V for uninoculated and inoculated ingots. Table 4.3 shows that inoculation with 0.02 wt% phosphorus increases N_A from 30 to 40 mm^{-2}. The increased number of primary silicon particles per unit area (N_A) occurs in parallel with the decreased area of the plate/star like primary silicon particles and increased area of polyhedral particles for each group of untreated and P-inoculated samples given in Tables 4.2.b and 4.3.

In addition, Table 4.3 reports a rise of 1.5 times in N_V as a consequence of inoculation by 0.02 wt% phosphorus in the sand mould/bottom cast condition. According to Table 4.4, there is about the same value for N_V for modification by 0.2 wt% Sr alone or applying strontium and 0.02 wt% phosphorus simultaneously which give N_V relatively 25 times lower than for the untreated ingot (Table 4.3). It can be concluded again from Table 4.5, that N_V is doubled by adding 0.02 wt% phosphorus.

Table 4.6 displays the increasing values of N_V for steel mould chamber cast ingots resulting from increased phosphorus addition from almost 0 to 0.08 wt%. It

shows a rise (by 1.5 times) on adding 0.02 wt% phosphorus to untreated ingots. As inoculant quantity increases to 0.04 wt%, the rise becomes nearly 2.5 times. Eventually, it is increased nearly 3 times by 0.08 wt% phosphorus addition.

Quantitative measurements for all of the cast samples are summarised in Table 4.7 by giving the average value for each individual casting condition. Table 4.7 indicates that 0.02 wt% P increased N_V by a factor of ~2, while 0.2 wt% Sr and 0.2 wt% Sr+0.02 wt% P decreased its value by 20 times in the bottom casting process.

To correlate the number of primary silicon particles per unit volume (N_V) to the addition of phosphorus, the results for all untreated cast ingots and those refined by phosphorus (Tables 4.3, 4.5 and 4.6) are illustrated in Fig. 4.17. (The results are averaged over polyhedral primary silicon zone and areas with a mixture of both polyhedral and non-polyhedral primary silicon, especially for untreated samples.) Fig. 4.17 shows that increasing the amount of phosphorus from almost 0 to 0.02 wt% increases N_V, then above 0.04 wt% the curve tends to plateau off at 0.08 wt%. In order to compare the same casting and cooling condition, Fig. 4.18 illustrates N_V versus amount of added phosphorus only for ingots chamber cast in steel moulds. It also shows that by increasing the amount of inoculant from 0.02 wt% to 0.08 wt% P, N_V is approximately tripled, using steel moulds and the chamber casting process.

To study the possibility of primary silicon migration inside the melt, after being nucleated, Stokes' Law was applied (Appendix B) and it is shown that there is no enough time for them to transport from one part of the ingot to the another part.

4.4 X-ray diffraction

Figure 4.19 shows an XRD trace of the Al-Fe-P powder confirming the presence of both Fe_2P and FeP phases. Fig. 4.20 shows that the main phase within the Al-Sr modifier is Al_4Sr, while Fig. 4.21 shows Al_2Cu and Cu_3P in the Al-Cu-P inoculant.

4.5 Differential Thermal Analysis (DTA)

The results of subsequent chemical analysis for three selected differential thermal analysis (DTA) samples A1, A2 and S10 (Table 3.6) are given in Table 4.8. The DTA curves for each sample are illustrated in Figs. 4.22, 4.23 and 4.24. It should be mentioned that each sample was heated, cooled and its data recorded three times to check for reproducibility and Figs. 4.22 to 4.24 show that reproducibility was good.

Table 4.9 compares the DTA results for the liquidus temperature (T_L) with the assessed equilibrium value given by equation 4.1.

Table 4.8 shows that, while the phosphorus level after DTA was not detected, the detected level of silicon was higher than for the externally-supplied of ingot provided for the casting process of A1, A2 and S10. It should be mentioned that samples A1, A2 and S10, as the ingots for DTA sampling, were not chemically analysed. However, both the DTA sample compositions and initial ingot source composition are used in the calculations and the results are shown in Table 4.9. Table 4.9 shows that the measured results for T_L give values closer to the calculated T_L for 18.6 wt% Si.

Additionally the measured values for T_L are 40-60 K lower than the calculated values for the compositions detected on the chemical analysis after DTA. This

discrepancy may be related to the presence of elements like Fe, Cu which are not considered in the equation (Eq. 4.1) used for the calculations. In addition, producing DTA samples by suction casting caused possibly a loss of aluminium.

While it is notable that the phosphorus level was different in each DTA sample and that equation 4.1 does not include an effect of phosphorus level, any effect is expected to be small.

4.6 EBSD

Table 4.10 summarises the samples in which the possible crystallographic relationship between their primary silicon particles were investigated using EBSD. Fig. 4.25 shows the microstructure of Al-18.6 wt% Si, uninoculated and bottom cast.

In comparison, Figs. 4.26, 4.27, 4.28, and 4.29 show different parts of the microstructure of Al-18.6 wt% Si inoculated by 0.015 wt% P from AlCuP and bottom cast. In order to detect the crystallographic orientation of polyhedral primary silicon particles, a part of the microstructure was randomly selected and some primary silicon particles were numbered. Some specific interconnected and neighbouring particles were among those selected, then EBSD data were collected by HKL Channel 5 software. For analysing the results, the objective was to find the nearest zone axis and angle which would relate one silicon particle to another. It should be added that this was based on the crystallographic specification of the relative orientation between two chosen silicon particles rather than the entirety of these particles. This means that even if there was no clear contact between the two neighbouring particles, the outermost layer of each was chosen for the orientation determination. Table 4.11 shows the orientation/angle pairs for silicon particles specified in Fig. 4.25 and Tables 4.12 to 4.16 shows the same parameters respectively for Figs. 4.26 to 4.30.

Figs. 4.26 to 4.30 show polyhedral primary silicons produced with inoculation via bottom casting with different cooling rates. Tables 4.12 to 4.16 represent the orientation/angle pairs for silicon particles specified in Figs. 4.26 to 4.30. Rotation of 60° around <111> axis is characteristic of twinning for silicon particles (Heiberg and Arnberg, 2001). Tables 4.12 to 4.16 show this specific twinning relationship between interconnected or neighbouring polyhedral silicon particles in both inoculated and uninoculated ingots with different cooling rates.

In addition, in order to assess the relationship among a cluster of polyhedral primary silicon particles, pole figures were drawn for two different parts of sample EBSD-No2 (description in Table 4.10, microstructures shown in Figs 4.31 and 4.32) in Figs 4.33 and 4.34. Tables 4.17 and 4.18 represent the orientation/angle pairs for their silicon particles.

Fig. 4.33 represents the pole figures drawn for 15 selective silicon particles specified in Fig. 4.31 (No. 1 through to 15). Fig. 4.33 shows that neighbouring particles have their own individual zone axis, whereas a twinning relationship (60° rotation around <111> axis) between Nos. 7 and 8, 9 and 10, 11 and 12; and 13 and 14 is displayed in Table 4.17.

Similar to that, despite the twinning relationship revealed in Table 4.18 between particles 1 and 2, 3 and 4, and 6 and 7, five pole figures of the silicon particles shown in Fig. 4.32, (pole figures drawn in Fig. 4.40) show dissimilar zone axes, nevertheless, particles specified as 6 and 7 show very similar zone axes. It is notable that particles 6 and 7 show a 60° rotation nearly around <111> axis, recognised as a twinning relationship.

Results for stainless steel moulds, cast chamber, uninoculated and inoculated by 0.02 wt% P from AlFeP are shown in Figs 4.35 to 4.39 as described in Table 4.10. Their orientation/angle pairs are given in Tables 4.19 to 4.23. Tables 4.19 to 4.23 again show that some neighbouring particles exhibit the twin relationship (near to 60° rotation around <111> axis) regardless of being inoculated or not for the chamber cast condition.

Fig. 4.40-a shows a specific cluster of polyhedral silicon particles from Fig. 4.38 (uninoculated and chamber cast). Fig. 4.40-b illustrates pole figures drawn for polyhedral primary silicon particles specified as Nos 8 through to 16 in Fig. 4.40-a. It can be seen that each particle has its own crystallographic orientation which proves that each one probably nucleated separately. However, many of them have a twinning relationship (60° rotation around <111> axis) with an interconnected neighbouring particle.

In order to study statistically the possible effect of phosphorus on the formation of interconnected polyhedral primary silicon particles, the numbers of interconnected particles were counted for selected inoculated/ uninoculated EBSD samples, as well as the numbers of particles per unit area, N_A. The results are represented in Table 4.24. Table 4.24 reports the occurrence of interconnected primary silicon as the ratio of interconnected N_A to the total N_A in the sample. Data presented in this Table shows that inoculation increases the frequency of interconnected particles only slightly, regardless of the type of casting process.

5. Discussion

5.1 The effect of different parameters on the Perepezko nucleation model

As described in section 2.1.3, there are two different heterogeneous nucleation models proposed for the nucleation kinetics in metallic alloys; one for surface-dependent nucleation, the other for volume-dependent nucleation. Our cooling conditions gave ΔT_P = 7.1-18.7 K and $\dot{T}_1$ = 1.6-2.9 K/s, hence, it was assumed that the surface-dependent model was more applicable to our conditions. However, as a comparison, the application of the second model to our results and to those of some other workers was studied and is given in the following sections.

Tables 5.1 and 5.2 give the values of parameters used in this model to determine the operative nucleation contact angle.

5.1.1 Surface-dependent heterogeneous nucleation

By using the published data for T_L, T_f, $\dot{T}$ and N_v from Liang et al (1995), Ohmi et al (1991, 1994, and 1997), and Kaneko et al (1979) in Perepezko's surface-dependant nucleation model (Eq. 2.17), the effects of number of particles and undercooling on the contact angle calculated by this model were investigated. In addition, by applying the results of the present work presented in Tables 4.1, 4.3, 4.5 and 4.6 to this model, the effect on contact angle (θ) (between primary silicon nucleus and nucleant) of phosphorus addition level was obtained. To distinguish the contact angles between the surface-dependent and the volume-dependent model, θ_1 refers to the value of θ calculated using the former model and θ_2 to the latter.

Liang et al (1995) used a general equation for binary metallic alloys, introduced by Thompson and Spaepen (1983), to calculate Gibbs free energy (ΔG_V) per unit volume for formation of primary silicon from liquid Al-Si in which they assumed a constant entropy of fusion (ΔS_V) of the melt, although ΔS_V varies with temperature (Yao et al 2006), whereas, Murray and McAlister (1984) introduced thermodynamic parameters to calculate ΔG_V for binary Al-Si alloys. Therefore, in this work the thermodynamic parameters of Al-Si alloy given in Murray and McAlister (1984), and used by Gremaud et al (1996), were used to calculate ΔG_V. The results amended values of θ_1 for Liang et al's (1995) published work are given in Table 5.3.

(i.) Effect of number of particles

Table 5.4 shows the calculated contact angles (θ_1 and θ_2) (method for calculation is given in Appendix A) for different cooling conditions for Al-22 wt% Si and Al-32 wt% Si. Cooling conditions are taken from the graphs shown by Ohmi et al (1991, 1994, and 1997). The number of particles per unit volume for these data are acquired from $N_V = \frac{4}{\pi}\left(\frac{2}{3}\right)^{1/2}\left(\frac{f}{D_A^3}\right)$ (Faraji et al 2005), based on the 'size' of primary silicon particles given in the papers (D_A) and calculated volume fraction (f). It is assumed that 'size' here is mean diameter of silicon particles, although Ohmi has since indicated that maximum dimension was measured.

In order to study the effect of number of particles on contact angle the numbers of particles was multiplied by 10 and the new Thetas acquired for the new conditions. These data are shown in Table 5.5. As can be seen, multiplying N_V by ten reduced the contact angle negligibly by only 0.4-1.0 degrees. Therefore, the measured number of particles per unit volume is not a very important factor in changing the value of the applicable contact angle.

(ii.) Effect of undercooling

Another set of data from the results of Kaneko et al (1979) is shown in Table 5.6. The data for use in the programme are taken from a graph showing the measured number of primary silicon crystals after solidification at various cooling rates for an Al-19 wt% Si alloy. The temperatures were from thermal analysis, from which, solidification of the alloy was observed to start at 949 K on the average, which was 6 K less than the liquidus temperature derived from the phase diagram.

Comparing Table 5.4 and Table 5.6 shows the importance of the formation temperature of primary silicon (T_f) in this model. With a very low undercooling a smaller contact angle is expected to be consistent with heterogeneous nucleation. By putting the Liang et al (1995) results in increasing order of undercooling as shown in Table 5.3, it is clear that the smallest contact angle is indeed for the lowest undercooling.

Figs. 5.1 and 5.2 show the effect of undercooling (ΔT_p) and temperature (T_f) for the formation of primary silicon on resulting surface-dependant contact angle for our results. Fig. 5.3 plots the calculated contact angles versus undercooling of primary silicon for the present work and that of other workers. There are two groups of results, one represents Theta1: the contact angle calculated by surface-dependant nucleation model and the second represents: Theta2: the contact angle from the volume-dependant model. Their conditions were; Liang et al (1995): Al-18.3 wt% Si, no P addition, $\dot{T}$: 0.6-18.9 K/s, Kaneko et al (1979): Al-19 wt% Si, 0.02 wt% P addition, $\dot{T}$: 0.017-1.67 K/s, Ohmi et al (1991, 1994): Al- 32 wt% Si, Al- 22 wt% Si, uninoculated, $\dot{T}$: 10.7-198 and 13.1-221 K/s, respectively.

Figs. 5.1 to 5.3 confirm that the value of theta from Perepezko's model is very sensitive to T_f.

(iii.) Effect of phosphorus addition level

The calculated contact angles (θ_1) (surface-dependant model) for the ingots produced in this work using different additives for different cooling conditions are presented in Table 5.7. Fig. 5.4 shows the effect of amount of added phosphorus on the contact angle for ingots cast into steel moulds. Since the results given in Fig. 4.12c show that added phosphorus does not change T_f considerably, Table 5.7 and Fig.5.4 show that phosphorus also has no significant effect on contact angle, though adding 0.02 wt% phosphorus gives a broad scatter in the contact angle values due to creating a broad range in T_f (Fig. 4.12c). However, a potent nucleant is expected to decrease the operative nucleation contact angle (e.g. Ho and Cantor 1995a), but that evidently was not the case for our conditions.

It is worth noting that in all different cooling conditions, solid Si/liquid Al-Si interfacial energy (σ_{SL}) was assumed constant even if the phosphorus level or formation temperature was changed, because it was shown by Körber and Löhberg (1971) using the sessile drop method, that adding phosphorus up to 1wt% did not change the solid/liquid interfacial energy for Al-12 to 15 wt %Si alloys. Fujii et al (2006) showed that the solid/liquid interfacial energy (σ'_{SL}) of solid silicon in molten silicon is dependant on temperature according to:

$$\sigma'_{SL} = 733 - 0.062(T - 1687) \quad (\sigma'_{SL}: \text{in mJ/m}^2) \qquad \text{Eq. 5.1}$$

where T is temperature in K. The applicable temperature range for this equation was 1357 to 1890 K. They made their measurements by both the oscillating

drop method and an improved sessile drop method. Although there is some uncertainty concerning the effect of additives and temperature on the interfacial energy of solid silicon in Al-Si alloy, their effects on values of theta would seem to be small.

5.1.2 Volume-dependent heterogeneous nucleation

The volume-dependent heterogeneous nucleation model (exemplified by Eqns. 2.21 and 2.22) was set up to compare results of the present work with those of Gremaud et al (1996). They used this model to interpret the nucleation behaviour of laser treated Al-26 wt%Si alloy undercooled by up to 215 K. They calculated θ_2 as 71.3 degrees.

(i.) Effect of phosphorus addition level

The acquired θ_2 values for the present work are given in Table 5.8. Comparing Table 5.7 and Table 5.8 shows that the contact angle from the volume-dependent model is lower than from the surface-dependent model for the same casting and cooling conditions (both values for theta are compared in Table 5.9). Fig. 5.5 plots the theta values (θ_1 and θ_2) against the formation temperature of primary silicon (T_f). A decreasing trend of theta value as T_f increases is evident from both models. Fig. 5.6 shows the effect of adding phosphorus on θ_2 .Likewise from the surface-dependent model, Table 5.8 and Fig.5.6 show phosphorus has no significant effect on contact angle, except on adding 0.02 wt% phosphorus that gives a big scatter in theta values by about 5 degrees (a summary is given in Table 5.9). Therefore, as Table 4.7 shows, phosphorus does not seem to act as a very potent as ΔT_p is not changed by significantly adding phosphorus and varies from 7 to 18.7 K for untreated and P-inoculated samples (wide range of ΔT_p can be related to the different observed

microstructure, e.g. S4, S5, S6, S14 and S15 contain branched/star-like primary silicon: Appendix C). It can be concluded that both models are very sensitive to ΔT_P and, since phosphorus did not decease ΔT_P appreciably in the present work, hence, it could not decrease the derived contact angle detectibly.

5.2 Effect of phosphorus and strontium addition individually and simultaneously on microstructure and cooling curves

As has been explained in detail in Chapter 2, as well as primary and eutectic α-aluminium there are two main features in the microstructure of a hypereutectic Al-Si alloy, primary and eutectic silicon. By changing their shape, size and distribution, better properties can be reached. There are two main different chemical additives for obtaining improvement in their microstructure individually, phosphorus and strontium (or sodium) for primary and eutectic silicon, respectively. When added together, however, their effects tend to be neutralised. The effect of added phosphorus and strontium on size refinement of primary silicon and modification of eutectic silicon of hypereutectic Al-18.6 wt% Si, separately and simultaneously, has been investigated under different casting conditions.

5.2.1 Effect of phosphorus on microstructure and cooling curve

As expected (Sigworth 1987, Wang et al 1994 and Kyffin et al 2001 a), after adding phosphorus most of the primary silicon became polyhedral, although there were already some polyhedral particles in untreated samples, possibly because of the presence already of 0.0014 wt% P in the ingot supplied to us by Norton Aluminium. Furthermore, the inoculated microstructure became almost free of star-shaped and very large plate-like primary silicons. One noticeable fact was the size of polyhedral primary silicon particles with and without phosphorus. They became finer after

adding phosphorus, as reported or found by Tenekedjiev and Gruzleski (1990), Wang et al (1994), Kyffin et al (2001 b) and others. While no possible size measurements were made in the present work, Tables 4.2.a and 4.2.b show that adding 0.02 wt% phosphorus reduced the length of the coarse primary silicon zone (from 23±6 mm for uninoculated to 13±3 mm for 0.02 wt% P-inoculated) in favour of an increase in the length of the polyhedral silicon zone (from 7±3 mm for uninoculated to 14±8 mm for 0.02 wt% P-inoculated). Additionally, Table 4.3 shows that adding 0.02 wt% phosphorus increased the number per unit volume (N_V) of primary silicon particles from 255±52 /mm^3 for untreated ingots to 382±100 /mm^3. Fig. 4.16 and Table 4.2.b show that there is a direct relation between the number per unit area (N_A) of primary silicon particles and the length of zone C (polyhedral silicon), in that the increased length of zone C is associated with higher values of N_A. For instance, among untreated samples (C1 to C4), the largest value of N_A belongs to C3 which has the largest length of zone C. Among P-treated samples (C5 to C8), C7 with the largest area of polyhedral primary silicon also has the largest value of N_A.

The refinement of primary silicon after the addition of phosphorus is attributed to the formation of AlP, which is considered to become the nucleant for primary silicon (Rooy 1972, Colligan and Gunes 1973, Tenekedjiev et al 1989) and to increase the nucleation rate of primary silicon.

Fig. 4.17 shows that number of primary silicon particles per unit volume (N_V) was increased by 1.5 times by inoculating the alloy initially containing 0.0014 wt% phosphorus with 0.02 wt% phosphorus during bottom casting. N_V is trebled by adding 0.08 wt% phosphorus, the slower increase in N_V between 0.04 wt% and 0.08 wt% P is consistent with the conclusion of Bates and Calvert (1966) that there is a

phosphorus level for any casting/alloy condition beyond which no additional refinement can be obtained. This level was obtained experimentally as 0.02 wt% (10 min holding time) in the previous study of Kyffin et al (2001 a). It was explained as due to agglomeration of AlP particles at excessive levels of phosphorus addition. Also Bates and Calvert (1966) noted that some AlP particles floated into the dross on adding phosphorus beyond its optimum level.

Fig 5.7.a summarises the effect of ΔT_p on the number of primary silicon particles for uninoculated ingots from our results and from the results of Liang et al (1995), Kyffin et al (2001 a, b), under different process conditions, but with about the same cooling rate from 0.91 to 2 K/s. Similarly Fig 5.7.b summarises the effect of ΔT_p on the number of primary silicon particles for P-inoculated ingots from our results and those of Kaneko et al (1979), and Kyffin et al (2001 a, b), with about the same cooling rate from 0.89 to 1.67 K/s.

Fig. 5.7.a shows for the results of Liang et al (1995) for uninoculated Al-18.3 wt% Si produced via Bridgman solidification with a cooling rate ($\dot{T}$) of 1.0 to 2.0 K/s, no change of N_V as the value of ΔT_p changes.

Kyffin at al (2001 a, b) measured T_f and calculated liquidus temperature (T_L) using the polynominal equation approximated by Liang et al (1995) for 0.01 wt% P-inoculated Al-20 wt% Si ingot, bottom cast into sand mould, to give ΔT_p as approximately 0.5 K and T_L as 680°C respectively, while, ΔT_p of uninoculated ingot was measured as 45 K. Kyffin et al (2001 b) found that the best refinement effect of primary silicon was obtained by adding 0.02 wt% P. Additionally, they recorded only one value for ΔT_p in uninoculated and one for 0.01 wt% P-inoculated samples which

makes their results for T_f and ΔT_p less reliable. Comparing with Kyffin et al (2001 b), the results of Kaneko et al (1979) and ours in Fig. 5.7.b shows no systematic relation between ΔT_p and N_V.

It should be added that there was some variation in T_f of untreated/P-treated ingots in our condition because in these experiments it was difficult to control sufficiently some important parameters, such as the volume fraction of silicon present (as it was variable on a different area of supplied ingot) and the cooling conditions, especially in bottom casting. In chamber casting, the thermocouple was inserted by hand, making it difficult to ensure that it was in exactly the same position for all samples.

Tenekedjiev et al (1989) reported an increase in T_f for an Al-17 wt% Si alloy from 622 to 642°C as a result of inoculation by 0.003 wt% phosphorus. Song et al (2004) reported that added phosphorus can decrease or even eliminate undercooling for the formation of primary silicon (ΔT_p) by shifting its formation to a higher temperature. They recorded an increase of 6.4 K in T_f from 594.1 to 600.5°C on adding 0.02 wt% P to a near eutectic Al-Si alloy. On the contrary, Colligan and Gunes (1973) showed a decrease of 38 K in an Al-17 wt% Si alloy from 665 to 627°C on inoculating and Weiss and Loper (1987) claimed that adding phosphorus nucleated primary silicon at lower formation temperature with no data presented. Sigworth (1987), on the other hand, reported that there was no relation between the formation temperature - which refers to the formation temperature of primary silicon (T_f) - in the cooling curve and the mean size of the primary silicon particles. He recorded a variation of 26 K in T_f, from 612 to 638°C in a random fashion for an Al-17 wt% Si alloy containing 0.004 wt% P on adding sulphur, strontium and lanthanum and

different cooling condition. He claimed that ΔT_p did not appear to relate directly to the structure of silicon. In addition, he believed that phosphorus lowered the growth rate of silicon when it was present in the melt, although he did not present convincing evidence for this.

In our condition, as it can be seen in Figs. 5.7a and 5.7b, no simple relation was found between ΔT_p and N_V. As Figs. 4.12a and 4.12b also show, no link between level of P-inoculation and T_f was found due to no significant change of T_f, however, resulted from adding 0.04 or 0.08 wt% P (651.7±5.0°C, 652.2±1.2°C and 651.6±0.9°C for untreated, 0.04 and 0.08 wt% P-inoculated, chamber cast into steel moulds respectively) though it became significant by adding 0.02 wt% phosphorus (642±10.4°C).

One possible explanation for the increased value of N_V by adding P could be its effect in delaying or restricting growth of silicon, as suggested by Sigworth (1987). Maxwell and Hellawell (1975) introduced a model based on growth restriction for describing the grain-refinement of aluminium alloys using an inoculant. In their model, growth restriction of already nucleated α–Al grains permits further nucleation in the undercooled melt until release of latent heat causes recalescence and increases the melt temperature. Our results (Table 4.1, ingots S1 to S15), show a slight increase in the cooling rate below T_f ($\dot{T}_2$) from 0.91±0.15 K/s for untreated to 1.05±0.20 K/s for 0.08 wt% P-inoculated ingots, as a result of preventing recalescence and preventing the release of latent heat resulting by adding phosphorus.

There has been recent research on the effect of growth restriction resulting from adding grain refiner in aluminium alloys (Greer et al 2002, 2003) and in titanium alloys (Tamirisakandala et al 2005). Their work identified a parameter called growth

restriction factor Q= $mC_0(k-1)$, where m is the slope of the liquidus, C_0 is the concentration of the solute in the melt and k is the equilibrium partition ratio (C_{IS}/C_{IL}) and C_{IL}, C_{IS} are equilibrium interface compositions in the liquid and solid respectively) as crucial in refinement, each element present or added into the alloy contributing to Q. Greer et al (2000) showed that grain diameters reduced with increasing Q (as a result of adding Al-Ti-B as inoculant), due to increasing restriction of the growth of nucleated primary phase. Consequently, the refinement of primary silicon by adding phosphorus can possibly be attributed to growth restriction rather than to nucleation.

As regards the effect of cooling rate on the number of particles, it is significant that ingots solidified at higher cooling rate for the same additive conditions have more primary silicon particles. As an example N_v for C7 in Table 4.3 with $\dot{T}_2$=0.37 K/s is 508 mm^{-3}, compared to C6 which is 372 mm^{-3} with $\dot{T}_2$=0.31 K/s (both inoculated by 0.02 wt% P). The refinement of primary silicon by increased cooling rate is attributed to an increase in nucleation rate. Therefore more particles are nucleated (Mondolfo 1982). However, as Table 4.7 shows by increasing cooling rate (below T_f) from 0.35±0.06 K/s for untreated ingots produced via bottom casting into the sand moulds to 0.91±0.15 K/s for untreated ingots produced via chamber casting into the steel moulds there is no significant increase in N_V (255±52 /mm^3 for former and 257±66 /mm^3 for latter), despite a small increase of 2 K in ΔT_p from 7.1±1.0 to 9.0±5.0 K, respectively.

5.2.2 Effect of strontium on microstructure and cooling curve

As Table 4.4 shows adding 0.02 wt% strontium alone, decreases the number of primary silicon particles per unit volume (N_V) from 255±52 /mm^3 for an untreated sample to 12.6±1.1 /mm^3. This is an evidence for nuclei poisoning as suggested by Jenkinson and Hogan (1975). They believed when strontium is added individually as a modifier, it is considered to have absorbed at the re-entrant twin grooves and therefore the rate of attachment of silicon will be reduced. At the nucleation stage of primary silicon, the addition of strontium could deactivate or poison nuclei and so tend to suppress formation of primary silicon. The real mechanism of such poisoning is unclear (Nogita et al 2004d) but strontium is known to react with phosphorus to form Sr_3P_2 (Park et al 1995).

The cooling curves show (Fig. 4.5, tabulated in Table 4.1) that the other main role of strontium is to increase the undercooling required to form primary silicon (46.6±6.5 K, compared to 7.1±1.0 K for untreated), consistent with the conclusion by Jenkinson and Hogan (1975) and Yilmaz et al (1992) that the main action of strontium is poisoning of the growth layer rather than preventing nucleation.

Table 4.1 shows a small decrease in eutectic arrest temperature from 576.3±0.1°C to 574.9±0.2°C as a result of adding 0.2 wt% Sr to untreated samples. This is in agreement with the findings of Djurdjevic et al (2001), that this depression is controlled by the level of strontium addition, though they recorded a larger decrease in eutectic arrest temperature (T'_{Eu}) from 563.5°C to 552°C by adding 96 ppm strontium to a 319 alloy (7.5 wt% Si) with a cooling rate of 1.0 K/s. They attributed the effect to the poisoning of the growth layer on eutectic silicon.

Microstructurally, as illustrated in Fig. 4.2.b, strontium changes the morphology of primary silicon from highly-faceted to dendritic as was shown also by Nogita et al (2004d), who considered that strontium caused roughening of the primary silicon, so that crystal tips become less stable so promoting branching of the crystals.

Addition of strontium alone (B1 through B6: conditions given in Table 3.6) resulted in an increasing area of the ingot in which primary silicon was suppressed and in which the eutectic was fully modified; 70% of a small ingot (40×35 mm) produced by bottom casting became modified eutectic on adding 0.1 wt% strontium (Fig. 4.13). This is in agreement with the results of Jenkinson and Hogan (1975) who showed that there is an optimum amount of modifier which can suppress the formation of primary silicon. They recorded, for instance, by adding 0.02 wt% strontium (freezing rate in the range 10-1000 μm/s) that the microstructure of an Al-17 wt% Si alloy became fully modified eutectic and free of primary silicon.

5.2.3 Effect of strontium and phosphorus together on microstructure and cooling curve

Simultaneous addition of 0.015 wt% P and 0.04 wt% Sr refined some of the primary silicon but the eutectic modifying effect of strontium was limited to a very small part of the ingot (less than 2% by area of a 43×35 mm ingot). However, on increasing this addition of modifier to 0.2 wt% Sr with 0.015 wt% P, primary silicon refinement disappeared while modification of the eutectic was complete. This conclusion is in agreement with the reports of other workers (Mondolfo 1965, Cissé et al. 1975, Ho and Cantor 1995 b). Cissé at al (1975) suggested that, to reduce the reaction between strontium and phosphorus, the addition of phosphorus should be done before the solidification starts and then modifier should be added just above the

eutectic temperature. The subsequent adding of strontium in the mould, however, was not successful in our study.

The results of quantitative metallography, presented in Table 4.4 as N_V, for Sr-treated ingots (C9 to C12) and for Sr+P-treated ingots (C13 to C15) show that N_V is similar in both cases (12.6±1.1 /mm^3 and 10.7±2.9 /mm^3). Comparing N_V for Sr+P-treated ingots (C13 to C15) and Sr-treated ingots (C9 to C12) with those of untreated ingots (C1 to C4) (Table 4.3 and 4.4) show complete nullifying of the effect of phosphorus in ingots C13 to C15 as the addition of strontium alone or with phosphorus reduce N_V of an untreated sample produced by bottom casting by a factor of 20.

In addition, the formation temperature for the primary silicon (T_f) in Sr+P treated ingots (621.5±2.4°C) was a few degrees higher than for the Sr-only added samples (614.1±6.6°C) whereas it was much lower than for P-only added untreated samples (651.6±2.3°C) (Table 4.1). This decreased T_f is explained by the nullification of phosphorus by strontium. Considering the eutectic arrest temperature (T'_{Eu} in Table 4.1), it is revealed that the addition of 0.2 wt% Sr + 0.02 wt% P decreases T'_{Eu} of an untreated sample produced via bottom casting by 1.5 K compared to a decrease of 1.4 K for only 0.2 wt% Sr addition. As mentioned previously, this effect is attributed to the growth layer poisoning of silicon and neutralisation of AlP nucleants present in the melt.

5.3 DTA

To detect T_L in uninoculated and P-inoculated samples three different samples (A1, A2, S10) were prepared and sent for Differential Thermal Analysis (DTA) (see Table

3.6 for casting conditions). Unfortunately, the subsequent chemical analysis could not detect any phosphorus in the small samples though it found higher silicon content than expected (Table 4.8). However, the measured values of T_L show closer results to the analysed content of silicon in the as-supplied ingots (Table 4.9). Without considering the chemical analysis of DTA samples, the results in Table 4.9 appear to show that with increasing phosphorus, T_L decreases. Nafisi et al (2004) recorded for Al-17 wt% Si alloy that adding phosphorus from 0.05 to 0.15 wt% increased T_L (by up to 55K) and then, on adding more phosphorus (0.2%), it began to decrease.

Recently there have been some other attempts to determine the effect of further additions on T_L for Al-Si alloys (Vijayaraghavan et al 1996, Hernandez et al 2005). They recorded an increase on T_L on adding some alloying elements, e.g. Cu, Mg, Fe and a decrease on adding Ti and B. However, they did not establish any result for phosphorus.

5.4 EBSD

There have been some studies (Nogita et al 2004 d, Nogita and Dahle 2001 a, and b, and Heigberg and Arnberg 2001) on eutectic silicon using EBSD to determine crystallographic relationships between the neighbouring silicon particles before and after adding strontium. However, it seems that there was no equivalent study on the primary silicon in Al-Si alloys using EBSD so far. In the present research some preliminary work has done on polyhedral primary silicon particles produced by inoculating with 0.015 wt% phosphorus and without phosphorus addition for different solidification conditions. Considering Figs. 4.26 through 4.30 and Tables 4.12 through 4.16, it was found that there is a specific twinning relationship between

interconnected or attached silicon particles: the outermost layer of each such particle is related by a rotation around <111> of 60 degrees with the neighbouring connected particle.

Table 4.24 gives the statistics of incidence of interconnection among primary silicon for five different samples. It can be seen that adding 0.015-0.02 wt% phosphorus increases the incidence of interconnection by only 3%. With regard to the high standard deviation of up to 8% for the incidence of interconnection, however, it is hard to conclude that addition of phosphorus increases the occurrence of connected particles numbers and therefore, increases the incidence of twinning. This evidently needs more results and also to find a way to image the contact interface by means of three dimensional microscopic facilities.

In theory, there are two different mechanisms for clustering of primary silicon particles; one is attachment of individually formed particles to each other and the other is the development of new particles from the edge of formed particles (Liang et al 1995).

In the present work, in order to investigate the mechanism of clustering in primary silicon particles, three different clusters (Figs. 4.31, 4.32 and 4.40-a) were chosen and their pole figures were plotted (Figs. 4.33, 4.34 and 4.40-b). It can be seen in Figs. 4.33, 4.34 and 4.40-b that every particle which is connected to its neighbouring particle has its own crystallographic orientation which proves that they nucleated individually. Only particles no 6 and 7 in Fig. 4.32 (their pole figures are given in Fig. 4.34) show a similar crystallographic orientation. In addition, Tables 4.17, 4.18 and 4.22 show the twin relationship between some of the interconnected neighbouring particles. Therefore, it can be concluded that in interconnected neighbouring particles, one particle originated separately and then, typically, a new

particle nucleated on the edge of already nucleated one by a twinning relationship (60° rotation around <111> axis). Thus, the second mechanism, the development of new particles from the edge of formed particles, is applicable in clustering of primary silicon particles as recorded by Liang et al (1995) via microstructural observations.

6. Conclusions

1. The number per unit volume of primary silicon particles (N_V) was increased by 1.5 times, from 250±50 to 382±100 /mm^3, by inoculating (at 800°C) Al-18.6 wt% Si alloy containing 0.0014 wt% phosphorus with 0.02 wt% phosphorus during bottom casting into sand moulds.

2. Adding 0.02 wt% phosphorus reduced the length of the coarse primary silicon zone from 23±6 mm to 13±3 mm in favour of an increase in the length of the polyhedral silicon zone from 7±3 mm to 14±8 mm.

3. The number of primary silicon particles per unit volume (N_V) was increased from 260±70 /mm^3, for untreated ingots initially containing 0.0014 wt% phosphorus, by 1.5 times 390±90 /mm^3 on inoculating (at 800°C) with 0.02 wt% phosphorus, and was trebled to 690±130 /mm^3 by adding 0.08 wt% phosphorus during chamber casting into steel moulds.

4. The number per unit volume of primary silicon particles decreased from 260±50, for untreated ingots, by 20 times to 12.6±1.1 /mm^3, on adding 0.2 wt% strontium (at 800°C) via bottom casting into sand moulds. This is evidence for the poisoning of primary silicon nucleation by strontium.

5. The number per unit volume of primary silicon particles decreased from 260±50 /mm^3, for untreated ingots, by about 24 times to 10.7±2.9 /mm^3, on adding 0.2% wt strontium and 0.02 wt% phosphorus simultaneously (at 800°C) via bottom

casting into sand moulds, indicating that the inoculating effect of phosphorus was nullified by strontium.

6. Addition of 0.1 wt% strontium, via bottom casting into sand moulds resulted in 70% of a small ingot (40×35 mm) becoming modified eutectic in which the formation of primary silicon was suppressed.

7. Simultaneous addition of 0.015 wt% P and 0.04 wt% Sr refined some of the primary silicon but the eutectic modifying effect of strontium was limited to a very small part of an ingot produced via bottom casting into a sand mould (less than 2% of a 43×35 mm ingot). However, on increasing this addition of modifier to 0.2 wt% Sr with 0.015 wt% P, primary silicon refinement disappeared while modification of the eutectic was complete. This elimination of the refining effect of phosphorus on primary silicon on addition of strontium along with phosphorus has been attributed to the formation of a new compound Sr_3P_2 as a result of decomposition of AlP as a consequence of adding strontium

8. Eutectic arrest temperature (T'_{Eu}) of an untreated sample produced via bottom casting into sand moulds was decreased by 1.4 K from 576.3±0.1°C to 574.9±0.2°C as a result of adding 0.2 wt% Sr. Similarly the addition of 0.2 wt% Sr + 0.02 wt% P decreases T'_{Eu} of an untreated sample by 1.5 K.

9. Inoculation by 0.02 wt% phosphorus did not change the formation temperature for the primary silicon (T_f) of untreated ingots produced via bottom casting, significantly (from 653.6±1.1 to 651.6±2.3°C).

10. Adding 0.2 wt% Sr to untreated ingots produced via bottom casting into sand moulds increased undercooling for the formation of primary silicon (ΔT_P) from 7.1±1.1 K to 46.6±6.5 K. Adding 0.2 wt% Sr+0.02 wt% P gave this undercooling as 39.2±2.4 K.

11. Adding 0.04 and 0.08 wt% P to ingots produced via chamber casting into sand moulds had no significant effect on the value of T_f (from 651.7±5.0 to 652.2±1.2, 651.6±0.9°C, respectively) whereas adding 0.02 wt% P gave a large scatter from 631 to 652°C.

12. The formation temperature is the most crucial variable in both the surface-dependent and the volume-dependant nucleation models applied to the formation of primary silicon in hypereutectic Al-Si alloys.

13. Assuming spherical-cap model, the contact angle changes only by the interfacial energy. However, the data applied to Perepezko's model showed it changes by undercooling. Therefore, it is suggested that the Perepezko's nucleation model is not applicable for analysing data in inoculated hypereutectic Al-Si alloy.

14. Between two connected primary silicon particles, the outermost layers of each silicon particle are often related by a 60° rotation around axis <111>. However, plotting pole figures of a few clusters of primary silicon particles, showed that every particle which was connected to its neighbouring particle had its own crystallographic orientation which proves that they nucleated individually.

7. Suggestions for further work

1. TEM observations and energy-dispersive X-ray analysis to investigate the presence of AlP as a nucleant within the primary silicon nucleus.

2. To measure the liquidus temperature by DTA in further samples with and without phosphorus to allow the nucleation undercooling of primary silicons to be evaluated more reliably from the formation temperature.

3. More EBSD study and orientation measurements on primary silicon particles in inoculated and uninoculated samples to elucidate the effect of phosphorus on the nucleation/growth mechanism of primary silicon.

4. To study the possible applicability to the inoculation of hypereutectic alloys by phosphorus of Greer's grain refinement/nucleation model based on the growth restriction mechanism.

References

- Acosta G., F.A.; Castillejos E., A.H.; Almaza R., J.M.; Flores V., A., 1995, *Metal. Mater. Trans.* **B 26**, 159-171.
- Arnold F.L., Prestley J.S., 1961, *AFS Trans.* **69**, 129.
- Atasoy O.A., Yilmaz F., Elliott R., 1984, *J. Cryst. Growth*, **66**, 137-146.
- Bates A.P., Calvert D.S., 1966, *Br. Foundryman*, **59**, 119-133.
- Becker R., Doring W., 1935, *Ann. Phys.* **24**, 719.
- Bell J.A.E., Winegard W.C., 1966, *J. Inst. Metals* **94**, 226-227.
- Bercovici S., 1980, *Giesserei* **67** (17) 522-532.
- Boettinger W.J., Perepezko J.H., 1985, in Rapidly Solidified Crystalline Alloys, ed. by S.K. Das, B.H. Kear, C.M. Adam, TMS, Warrendale, PA, p.24.
- Boettinger W.J., Perepezko J.H., 1993, in Rapidly Solidified Alloys, ed. by H.H. Liebermann, Marcel Dekker, Inc., 17-78.
- Cantor B., 1994, *Mater. Sci. Eng.*, A **178**, 225-231.
- Cantor B., 2003, *Phil. Trans. R. Soc. Lond.* A **361**, 409-417.
- Chalmers B., 1964, "Principles of Solidification", John Wiley and Sons, P.66.
- Chang J., Moon I., Choi C., 1998, *J. Mater. Sci.* **33** (20), 5015-5023.
- Cissé J., Bolling G.F., Kerr H.W., 1975, *Met. Trans.* B **68**, 195-97.
- Colligan G.A., Gunes M.A., 1973, *AFS Trans.* **78**, 359-365.
- Crosley P.B., Mondolfo L.F., 1966, *Mod. Cast.* **49**, 53-64.
- Dahle A.K., Hjelen J., Arnberg L., 1997, : Proc. 4th Decennial Int. Conf. on Solidification Processing, ed. by J. Beech and H. Jones, University of Sheffield, Sheffield, UK, pp. 527-530.
- Dahle A.K., Nogita K., Zindel J.W., MacDonald S.D., Hogan L.M., 2001, *Metall. Mater. Trans. A* **32**, 949-960.

- Davies V.deL., West J.M., 1963-64, *J. Inst. Met.*, **92**, 175-180.
- Day M.G., 1969, *J. Metals*, April, 31-34.
- Djurdjevic M., Jiang H., Sokolowski J., 2001, *Material Characterization*, **46**, 31-38.
- Elliott R., 1984, *Mater. Sci. Eng.*, **65**, 85-92.
- Evans P.V., Stiffler S.R., 1991, *Acta Metall. Mater.*, **39**, (11), 2727-2731.
- Faraji M., Todd I., Jones H., 2005, *J. Mater. Sci.*, **40**, (24), 6363-6365.
- Fisher J. C., Hollomon J.H., and Turnbull D., 1948, *J. Appli. Phys.*, **19**, 775-784.
- Flemings M.C., 1974, 'Solidification Processing' New York, McGraw-Hill, 341-344.
- Flood S.C., Hunt J.D., 1981, *Met. Sci.* **15**, 287-294.
- Fredriksson H., Hillert M., Lange N., 1973, *J. Inst. Metals* **101**, 285-299.
- Fujii H., Matsumoto T., Izutani S., Kiguchi S., Nogi K., 2006, *Acta Mater.*, **54**, 1221-1225.
- Fujii K., Waseda A., Tanaka M., 2001, *IEEE Transactions on Instrumentation and Measurement*, **50** (2), 616-621.
- Geiger G.H., Poirier D.R., 1973, 'Transport Phenomena in Metallurgy', London, Addison-Wesley.
- Greer A.L., Bunn A.M., Tronche A., Evans P.V., Bristov D.J., 2000, *Acta Mater.*, **48**, 2823-2835.
- Greer A.L., Quested T.E., Spalding J.E., 2002, in Light Metals 2002 as held at the 2002 TMS Annual Meeting ed. by W.A. Schneider (TMS, Warrendale, PA), 687-694.
- Greer A.L., 2003, *Phil. Trans. R. Soc. Lond.* A, **361**, 479-495.

- Greer A.L., Cooper P.S., Meredith M.W., Schneider W., Schumacher P. Spittle J.A., Tronche A., 2003, *Adv. Eng. Mater.*, **5**, (1-2), 81-91.
- Greer A.L., 2004, in Solidification of Aluminum Alloys as held at the 2004 TMS Annual Meeting; Charlotte, NC; USA; 14-18 Mar. 2004, ed. by M.G. Chu, D.A. Granger and Q. Han, 131-146.
- Greer A.L., Quested T.E., 2006, *Philosophical Magazine*, **86**, (24), 3665-3680.
- Gremaud M., Allen D.R., Rappaz M., Perepezko J.H., 1996, *Acta Mater.*, **44**, 7, 2669-2681.
- Gruzleski J.E., Closset B.M., 1990, "The Treatment of Liquid Aluminium-Silicon Alloys", American Foundryman's Society.
- Gündüz M., Hunt J.D., 1985, *Acta Metall.*, **33** (9), 1651-1672.
- Hamilton D.R., Seidensticker. R.G., 1960, *J. Appl. Phys.* **31**, 1165-1168.
- Heiberg G., Arnberg L., 2001, *J. Light Metals*, **1**, 43-49.
- Hellawell A., 1970, *Progress in Mater. Sci.* **15** (1) 76.
- Hernandez F.C.R., Djurdjevic M.B., Kierkus W.T., Sokolowski J.H., 2005, *Mat. Sci. Eng.*, A **396**, 271-276.
- Hirth J.P., 1978, *Met. Trans. A*, **9**, 401-404.
- Ho C.R., Cantor B., 1993, *Mater. Sci. Eng* A **173**, 37-40.
- Ho C.R., Cantor B., 1995 a, *Acta Metall. Mater.* **43**, 3231-3246.
- Ho C.R., Cantor B., 1995 b, *J. Mater. Sci.*, **30**, 1912-1920.
- Iida T., Guther R.I.L, 1993, 'The Physical Properties of Liquid Metals', Oxford, Clarendon Press, 71.
- Jackson K.A., 1965, *Ind. Eng. Chem.* 57, 12, 29-32.
- Jenkinson D.C., Hogan L.M., 1975, *J. Cryst. Growth*, **28**, 171-187.
- Jiang Q.C., Xu C.L., Lu M., Wang H.Y., 2005, *Mater. Letters*, **59**, 6, 624-628.

- Johnson M., Bäckerud L., Sigworth G.K., 1993, *Metall. Trans.* A, **24**, 481-491.
- Jorstad J.L., 1968, *Trans. Metall. Soc. AIME* **242**, 1217-22.
- Jorstad J.L., 1984, *AFS. Trans.* **92**, 573-578.
- Kaneko J., Sugamata M., Aoki K., 1979, *Trans. Jpn. Inst. Met.* **20**, 734-741.
- Kang H.S., Yoon W.Y., Kim K.H., Kim M.H., Yoon E.P., 2004, *Mater. Sci. Forum,* **449-452**, 169-172.
- Kang H.S., Yoon W.Y., Kim K.H., Kim M.H., Yoon Y.P., 2005, *Mater. Sci. Eng.*, A **404**, 117-123.
- Kattoh H., Hashimoto A., Kitaoka S., Sayashi M., Shioda M., 2002, *J. Jap. Inst. Light Metals*, **52** (1), 18-23.
- Kelton K.F., Greer A.L., Thompson C.V., 1983, *J. Chem. Phys*, **79**, 6261-6276.
- Kim C.B., Heine R.W., 1963-64, *J. Inst. Met.*, **92**, 367-376.
- Kim H.J., 2003, *Mater. Sci. Tech.* **19**, 915-18.
- Kim W.T., Cantor B., 1991, *J. Mater. Sci.*, **26**, 2868-2878.
- Kim W.T., Cantor B., 1992, *Acta Metall. Mater.*, **40**, 3339-3347.
- Kim H.J., Yoon E.P., Kobayashi T., 2004, *Mater. Sci. Forum*, **449-452**, 165-168.
- Kitamura M., Hosoya S., Sunagawa I., 1979, *J. Cryst. Growth* **47**, 93.
- Kobayashi K., Shingu P.H., Ozaki R., 1975, *J. Mater. Sci.* **10**, 290-299.
- Kobayashi K.F., Hogan L.M., 1985, *J. Mater. Sci.* **20**, 1961-1975.
- Kobayashi T., Kim H.J., Ninom M., 1997, *Mater. Sci. Tech.*, **13**, 497-502.
- Körber K., Löhberg K., 1971, *Giessereiforschung* (in English), **23** (4), 157-161.
- Kyffin W.J., Rainforth W.M., H. Jones, 2001 a, *Mater. Sci. Tech.* **17**, 901-905.

- Kyffin W.J., Rainforth W.M., H. Jones, 2001 b, *Mater. Trans.* **42** (10), 2098-2101.
- Kyffin W.J., Rainforth W.M., H. Jones, 2001 c, *Z. Metallkd.*, **92** (4), 396-398.
- Lee J.M., Kang S.B., 1995, *J. Korean Inst. Met. Mater.* **33** (11), 1406-1413.
- Liang D., Bayraktar Y., Jones H., 1995, *Acta Metall. Mater.* Vol. **43**, No. 2, 579-585.
- Liu C.Y., Murakami K., Okamoto T., 1989, *Mater. Sci. Tech.* **5**, 1148.
- Long S., Zhang Z., Flower H.M., 1994, *Acta Metal. Mater.* **42** (4), 1389.
- Lu S., Hellawell A., 1985, *J. Cryst. Growth* **73**, 316.
- Lu S.Z., Hellawell A., 1986: in Aluminum Alloys: Their Physical and Mechanical Properties. Vol. I; ed. by E.A. Starke and T.H. Sanders, Charlottesville, Virginia; USA; 15-20 June 1986, pp. 81-94.
- Lu S.Z., Hellawell A., 1987 a, *Met. Trans. A 18*, 1721-1733.
- Lu S.Z., Hellawell A., 1987 b: in Solidification Processing, Institute of Metals, London, p131.
- Mandal P., Saha A., Chakraborty M., 1991, *AFS Trans.*, **99**, 643-651.
- Martin J.W., 1980, "Micromechanisms in particle-hardened alloys", Cambridge University Press, Cambridge, UK, p142.
- Mason D.W., 1995, in "Light Metals 1995", ed. by James W. Evans, The Minerals, Metals and Materials Society, pp. 1019-1023.
- Maxwell I., and Hellawell A., 1975, *Acta Metall.* **23**, 229-237.
- McAlister A.J., 1985, *Bulletin of Alloy Phase Diagrams*, **6**, 222.
- McCartney D.G., 1989, *Int. Mater. Rev.*, **34**, 5, 247-260.
- McDonald S.D., Nogita K., Dahle A.K., 2004, *Acta Mater.* **52**, 4273-80.
- Mondolfo L.F., 1965, *J. Austral. Met.* **10**, 169.

- Mondolfo L.F., 1976, "Aluminium Alloys: Structure and Properties", Butterworth, London.
- Mondolfo L.F., 1982, in Grain Refinement in Castings and Welds, ed. by G.J. Abbaschian and S.A. David, Conf. Proc. 25-26 October 1982, The Metallurgical Society of AIME, St. Lousie, Missouri, USA, 3-50.
- Murray J.L., McAlister A.J., 1984, *Bull. Alloy Phase Diagrams* **5**, 74-84.
- Murty B.S., Kori S.A., and Chakraborty M., 2002, Int., Mater. Rev., **47**, 1, 3-29.
- Nafisi S., Hedjazi J., Boutorabi S.M.A., Ghomashchi R., 2004, in Light Metals 2004 as held at the 133rd TMS Annual Meeting; Charlotte, NC; USA; 14-18 Mar. 2004, ed. by Alton T. Tabereaux, TMS (The Minerals, Metals and Materials Society), 851-856.
- Nakae H., Kanamori H., 1997, in Solidification Processing, ed. by J. Beech and H. Jones, proceedings of the 4th Decennial International Conference on Solidification Processing, Sheffield, UK, July 1997, pp. 477-480.
- Nogita K., Dahle A.K., 2001a, *Mater. Trans.* **42** (2), 207-214.
- Nogita K., Dahle A.K., 2001b, *Mater. Trans.* **42** (3), 393-396.
- Nogita K., Drennan J., Dahle A.K., 2003, *Mater. Trans.* **44**, 625-628.
- Nogita K., McDonald S.D., Tsujimoto K., Yasuda K., Dahle A.K., 2004 a, *J. Electron Microscopy,* **53** (4), 361-369.
- Nogita K., McDonald S.D., Dahle A.K., 2004b, *Mater. Trans.* **45** (2), 323-326.
- Nogita K., McDonald S.D., Dinnis C., Lu L., Dahle A.K., 2004c, in Solidification of Aluminium Alloys, ed. By M.G. Chu, D.A. Granger and Q. Han, TMS (The Minerals, Metals and Materials Society), 93-102.
- Nogita K., McDonald S.D., Dahle A.K., 2004d, *Phil. Mag.* **84**(17), 1683-1696.

- Ohmi T., Tanaka Y., Kudoh M., 1991, *Bull. Fac. Eng. Hokkaido Univ.*, **156,** 1-10.
- Ohmi T., Kudoh M., Ohsasa K., Itoh Y., Matsuura K., Ishii K., 1994, *J. Jap. Inst. Light Metals*, **44**, (2), 91-96.
- Ohmi T., Matsuura K., Kudoh M., Itoh Y., 1997, *Jap. Inst. Light Metals*, **47,** (2), 71-77.
- Park H.S., Kim J.H., Kim K.M., Yoon E.P., 1997, *J. Korean Inst. Met. Mater.* **35** (10), 1332-1340.
- Park J.Y, Lee J.S, Ra H.Y, 1995, Proc. 3rd Asian Foundry Congress Nov. 8-10, (1995), ed. by Z.H. Lee, C.P. Hong, M.H. Kim, The Korean Foundrymen's Society, pp. 167-174.
- Perepezko J.H., and Paik J.S., 1984, *J. Non-Crystalline Solids*, **61/62,** 113.
- Perepezko J.H., 1988, in Metals Handbook, 9th edn, Vol. **15,** P. 101, ASM Metals Park, Ohio.
- Perepezko J.H., Sebright J.L., Höckel P.G., Wilde G., 2002, *Mater. Sci. Eng.*, A **326**, 144-153.
- Perepezko J.H., and Tong W.S., 2003, *Phil. Trans. R. Soc. Lond.* A **361,** 447-461.
- Petrescu M., 1970, *Z. Metallk.* **61,** 14.
- Poirier D.R., 1987, *Metal. Trans. B* **18,** 245.
- Rooy E.L., 1972, *AFS Trans.* **80,** 421-426.
- Schneider K., 1960, *AFS Trans.* **68,** 176-181.
- Schneider W., 1993, in "Light Metals 1993", ed. by S.K. Das, The Minerals, Metals and Materials Society, pp. 815-820.
- Shamsuzzoha M., Hogan L.M., 1986, *J. Cryst. Growth*, **76,** 429-439.

- Shamsuzzoha M., Hogan L.M., Berry J.T., 1992, *AFS Trans.*, **100**, 619-629.
- Sigworth G.K., 1983, *AFS Trans.* **91**, 7-16.
- Sigworth G.K., 1987, *AFS Trans.* **95**, 303-314.
- Smithells, C.J., 1983, "Smithells Metals Reference Book", London, Butterworths.
- Song X., Bian X., Qi X., Liu X., Zhang J., Wang B., Zhu L., 2004, *Journal of University of Science and Technology Beijing*, **11** (1), 81-84.
- Steen H.A.H., Hellawell A., 1972, *Acta Met.*, **20**, 363-370.
- Sunagawa I., Yasuda T., 1983, *J. Cryst. Growth*, **65**, 43.
- Tamirisakandala S., Bhat R.B., Tiley J.S., Miracle D.B., 2005, *Scripta Mater.*, **53**, 1421-1426.
- Telang Y., 1963, *AFS Trans.* **71**, 232-40.
- Tenekedjiev N., Argo D., Gruzleski J.E., 1989, *AFS Trans.* **97**, 127-136.
- Tenekedjiev N., 1989, M. Eng. Thesis, McGill University.
- Tenekedjiev N., Gruzleski J.E., 1990, *Cast Metals*, **3** (2), 96-105.
- Thall B.M., Chalmers B., 1949, *J. Inst. Met.* **78**, 79.
- Thompson C.V., Spaepen F., 1983, *Acta Metall.* **31**, 2021-2027.
- Turnbull D., 1948, Trans. AIME, **175**, 774-783.
- Turnbull D., 1950 a, *J. Chem. Phys.* **18**, 2, 198-203.
- Turnbull D., 1950 b, *J. App. Phys.* **21**, 1022-1028.
- Turnbull D., 1952, *J. Chem. Phys.*, **20** (3) 1952, 411.
- Turnbull D., Vonnegut B., 1952, *Industr. Eng. Chem.*, **44**, 6, 1292-1298.
- Turnbull D., 1953, *Acta Metall.*, **1**, 8.

- Turnbull D., 1981, Progress in Materials Science: Chalmers Anniversary Volume, ed., by J.W. Christian, P. Haasen and T.B. Massalski, Pregamon Press. pp. 269-275.
- Vekhamäki, H., Määttänen A., Lauri A., Napari I., Kulmala M., 2006, Atmos. Chem. Phys. Discuss., **6**, 9069–9083.
- Vijayaraghavan N., Pelle J., Boileau J., Zindel J., Beals R., 1996, *Scripta Mater.*, **35** (7), 861-867.
- Vogel W., Schneider W., 1991, *Giesserei*, **78** (23), 848-853.
- Volmer M., 1929, *Z. Phys. Chem.*, **25**, 555.
- Wang D.M., Zheng Z,Q., Chen Z.G., 1994, Proc. 4th International Conference on Aluminium Alloys (ICAA4), Atlanta, September 11-16, 1994, Vol **1**, pp. 123-126.
- Weiss J.C., J.C. Loper Jr. J.C., 1987, *AFS Trans.* **95**, 51-62.
- Wu S.S., TU X.L., Fukuda Y., Kanno T., Nakae H., 2003, *Trans. Nonferrous Met. Soc. China*, **13** (6), 1285-89.
- Xu C.L., Jiang Q.C., Yang Y.F., Wang H.Y., Wang J.G., 2006, *J. Alloys Compounds*, **422**, L1-L4.
- Yao X., Dahle A.K., Davidson C.J., StJohn D.H., 2006, *J. Mater. Res.*, **21** (10), 2470-2479.
- Yilmaz F., Atasoy O.A., Elliott R., 1992, *J. Cryst. Grwoth*, **118**, 377-384.
- Zhang Z.H., Bian X.F., Wang Y., Liu X.F., 2001, *Trans. Nonferrous Met. Soc. China*, **11** (3), 374-377.
- Zhou J., Duszczyk J., Korevaar B.M., 1991, *J. Mater. Sci.*, **26**, 3041-50.

Appendix A

Using Eqns. 2.18 and 2.19 from section 2.1.3, with the following assumptions after Liang et al 1995, the contact angle (θ_1) from the surface-dependant nucleation model was calculated:

Assuming a constant cooling rate $\dot{T}$, the number of nuclei per unit volume N_V may be expressed as:

$$N_V = \frac{1}{\dot{T}} \int_{T_f}^{T_L} I_V(T).dT \qquad \text{Eq. A1}$$

where

$$I_V = \Omega \exp\left(\frac{b\sigma^3 f(\theta)}{kT(\Delta Gv)^2}\right) \qquad \text{Eq. A2}$$

$$\text{and } \Omega = \frac{8\pi D_L {\sigma_{SL}}^2 (1-\cos\theta) N_\circ}{a^4 (\Delta Gv)^2} \qquad \text{Eq. A3}$$

By assuming that σ_{SL} and Ω are independent of temperature over the temperature range of interest, the integral was evaluated. The required data for the calculations is given in Tables 5.1 and 5.2.

Using Eqns. 2.21 to 2.24 from section 2.1.3, with the following simplifications after Gremaud et al 1996, the contact angle (θ_2) from the volume-dependant nucleation model was calculated:

Although the integral in Eq. A1 may be evaluated numerically, it can be approximated by:

$$\int_{T_f}^{T_L} I_V(T).dT \cong (T' - T_f) I_V(T_f) \qquad \text{Eq. A4}$$

where T′ is the intersection between the tangent of $I_V(T)$ at T_f and the temperature axis. This approximation implicitly neglects the contribution of nuclei between T_L and T′. Assuming that σ_{SL} and Ω_V are independent of temperature over the temperature range of interest, differentiation of Eq. A4 gives:

$$I_V(T_f)V.t = -\frac{b.(\sigma_{SL}^3).f(\theta).\Delta T\left[2T_f\frac{d\Delta G_V}{dT}+\Delta G_V\right]}{k(\Delta G_V^3)T_f^2} \qquad \text{Eq. A5}$$

The required data for completing the calculation are given in Tables 5.1 and 5.2.

Appendix B

Using Stokes' Law (Geiger and Poirier 1973), the required time for the transporting of primary silicon particle nucleated in the molten alloy from the bottom of an ingot to the top is calculated:

$$\eta = \frac{2R^2.(\Delta\rho).g}{9.V} \qquad \text{Eq. B1}$$

where, η is the viscosity of the molten alloy, R the radius of the moving particle, $\Delta\rho$ is the difference between the density of the liquid phase and the density of solid particle, g is the gravitational acceleration which is equal to 9.81 m/s^2 and V is the velocity of moving particle. Considering the velocity of movement calculated via Eq. B1 and measuring the height of each ingot (Table 4.1), the required time can be calculated.

Ingot S10 is used as an example to calculate the time. Its height is measured as 25 mm. By applying its quantitative results from Table 4.6 to the following equation (Faraji et al 2005):

$$N_V = \frac{N_A}{D_V} \qquad \text{Eq. B2}$$

where D_V is the true mean volume diameter, the mean radius of primary silicon is calculated as 40 μm.

Table 1 gives the physical parameters used for the velocity calculation and Table 2 gives the values for time which varies by the variation of primary silicon particles size.

Table B.1. Parameters used for Al-Si alloy

Parameter	Symbol	Value	Reference
Viscosity of liquid aluminium	η	1.30 $mNsm^{-2}$	Smithells 1983
Liquid density for aluminium	ρ_{Al}	2380 Kg/m^3	Iida and Guthrie 1993
Solid density for silicon	ρ_{Si}	2329.1 Kg/m^3	Fujii et al 2001

Table B.2. The variations of calculated time with the variations of primary silicon particle size for the movement of primary silicon particles from the bottom of ingot to the top for sample S10 (specification is given in Table 3.6).

Primary silicon particle radius (m)	Calculated time (hr)
20×10^{-6}	203.4
40×10^{-6}	50.8
50×10^{-6}	32.5

It should be noted that using cooling curves depicted in Fig.4.11 gives an estimated time of 125 seconds for the completion of primary silicon solidification and as mentioned in Table 4.1, it gives an estimation of 229.3 seconds to complete solidification of the ingot.

Appendix C

Table C.1: The microstructure description as morphology distribution from bottom to top of uninoculated and inoculated ingots; melt temperature 800°C (Description Table 3.6).
The position of thermocouple has been considered as zero in Cartesian coordinates (Fig 4.14), so negative y is for the points below the thermocouple. A: coarse primary Si, B: coarse eutectic Si, C: polyhedral primary Si. A+C: partly refined primary silicon accompanied by unrefined Si, P: plate-like primary Si, S: star-like primary Si, A (small): primary silicon formed in the bottom of ingot, Eu: eutectic phase.

	Position for	S1	S2	S3	S4	S5	S6	S13	S14	S15
	Y=..mm	**Uninoculated**			**Inoculated by 0.02 wt% P**					
	17							A+C		
	15						•	A+C		
	13.75							C+Pore	A+C	A+S
Upper part of ingot	12.5	A+C						A+C	A	A+C
	11.25	A+C			A+C	A+S+C	A	Pore		A+S
	10			A	A+C	A	A	A+C	A+S+C	S+Pore
	8.25	C	A+C	A+Pore	A+C	A+C	A+S+C	A+C	A+S+C	A+C
	7.5	C	A+C	A	A+C	A+C	A+S+C	A+C	A+C	Pore
	6.25	A+C+pore	C+Pore	A+C+P	A	A+S+C	A+S+C	A+Pore	S+C	C
	5	A+C	C+Pore	A+P	A	A+S	A+S+C	A+C	Pore	C
	3.75	Pore	C+Pore	C+Pore	S	C	A+S+C	A+P+C	Pore	C
	2.5	C	A+C	A+P	S+C	A+Pore	A+S+C	A+C	Pore	Eu+C
	1.25	A+P+C	A+P+C	A+C	S	Eu+C	A+C	A+C	A+Pore	Eu
	0	**Thermocouple position**								
Lower part of ingot	-1.25	A+C	C	Eu+C	S+Pore	C	A+C	A+C	S+C	Pore
	-2.5	C	C	C	S	C	C	Eu+C	S+C	A+S
	-3.75	C	C	C+Pore	A+S	C	Eu+C	Eu+C	S+C	A+C
	-5	A	C	Eu+C+Pore	C+S	C	Eu	Eu+C	S+C	C
	-6.25	A	C	C	C	C	Eu+C	Eu	S+C	C
	-7.5	A	Eu	C	Eu+C	C	Eu+C	Eu	S+C	Eu
	-8.25	A	Eu	Eu	Eu+C	Eu+C	Eu+C		S+C	Eu
	-10	A	Eu		Eu	Eu+C	A(small)	Eu	S+P+C	A(small)
	-11.25	A(small)			Eu			A(small)		
	-12.5				S			A(small)		
	-13.8				S				S	

Note: Based on microstructural observations, no branched/star-like primary silicon was formed in the samples inoculated by 0.04 and 0.08 wt% P (S7 through S12).

Table 2.1 Nucleation parameters for primary silicon in Bridgman solidified Al-18.3 wt% Si (Liang et al. 1995).

Conditions				*Constituent particle size*		*Number density*		*Formation temperature*	*Local concentration*	*Liquidus temp.*	*Undercooling*	*Effective wetting parameters*	
No	V (mm/s)	G (K/mm)	$\dot{T}$ (K/s)	L (μm)	d (μm)	N_A mm^{-2}	N_v mm^{-3}	T_f (K)	C_f (wt% Si)	T_L (K)	ΔT (K)	f(θ)	θ (deg)
1	0.06	10	0.6					867.5	16.8	909.10	41.6		
2	0.10	10	1.0	98±6	147±9	10±3	68	881.1	17.3	915.90	34.8	0.0086	27.0
3	0.12	10	1.2					886.2	17.3	915.90	29.7		
4	0.06	25	1.5	93±9	140±15	11±2	79	858.0	16.8	909.10	51.1	0.0182	33.0
5	0.17	10	1.7	92±7	138±1	10±2	73	886.5	17.8	922.80	36.3	0.0092	27.5
6	0.05	37	1.9					859.3	16.7	907.70	48.4		
7	0.08	25	2.0	95±8	143±12	12±1	84	862.7	17.1	913.20	50.5	0.0175	29.6
8	0.20	10	2.0					896.8	17.9	924.20	27.4		
9	0.10	25	2.5	83±7	125±11	11±1	88	869.2	17.3	915.90	46.7	0.0149	31.3
10	0.12	25	3.0	72±9	108±15	18±4	167	877.1	17.5	918.50	41.4	0.0116	29.2
11	0.34	10	3.4					897.1	18.4	931.00	33.9		
12	0.20	25	5.0	48±7	72±11	26±3	361	885.7	17.9	924.20	38.5	0.0098	28.0
13	0.51	10	5.1	52±4	78±6	29±3	372	898.8	18.4	931.00	32.2	0.0068	25.5
14	0.24	25	6.0	47±8	71±12	34±4	479	881.4	18.1	926.80	45.4	0.0133	30.4
15	1.00	10	10.0	38±6	57±9	54±4	947	896.8	18.4	931.00	34.2	0.0074	25.9
16	0.34	12.6	12.6					877.0	18.4	931.00	54.0		
17	0.51	12.8	12.8	33±3	50±5	58±5	1160	888.0	18.4	931.00	43.0	0.021	34.0
18	0.51	18.9	18.9	34±8	51±12	56±5	1098	866.1	18.4	931.00	64.9	0.024	35.5
19	0.71	26.3	26.3					878.1	18.4	931.00	52.9		

Table 2.2 Tensile properties of Sr-treated and P-treated Al-17 wt% Si alloy (Tenekedjiev et al. 1989).

Sr, wt%	P, wt%	UTS (MPa)	YS, 0.2% (MPa)	Elongation in 50 mm (%)	E (GPa)
0	0	120	102	0.5	80
0.02	0	150	102	1.4	72
0.04	0	148	101	1.7	71
0.06	0	150	112	1.9	78
0	0.003	145	93	1.3	73

Table 2.3 Tensile properties of untreated and Sr-treated A390 alloy (17 wt% Si, 4.5 wt% Cu, 0.55 wt% Mg, and max. 0.5 wt% Fe), (Tenekedjiev et al. 1989).

Sr, wt%	UTS (MPa)	YS 0.2% (MPa)	Elongation in 50 mm (%)
0	198	189	0.6
0.16	212	170	0.8
0.17	218	172	0.8

Table 3.1 The nominal chemical composition in wt% of Al-20 wt% Si alloy ingot supplied by Norton Aluminium Products Ltd.

Composition Percentage by Analysis (where .00 quoted actual < .01).											
Cu	Mg	Si	Fe	Mn	Ni	Zn	Pb	Sn	Ti	P	Al
.02	.00	19.70	.347	.01	.00	.00	.00	.00	.02	.0014	80

Table 3.2 Results of top to bottom chemical analysis (ICP method) of a sample of hypereutectic Al-20 wt% Si alloy ingot supplied by Norton Aluminium.

	Composition, wt%			
Element	Top of ingot	Middle of ingot	Bottom of ingot	Accuracy %
Si	18.9%	18.4%	18.6%	±0.3%
Cu	<0.02%	<0.02%	<0.02%	/
P	<0.005%	<0.005%	<0.005%	/

Table 3.3 Results for Fe and P content (ICP method) of the CIPped Al-Fe-P inoculant, supplied by KB Alloys.

Element	Composition, wt%	Accuracy, %
Fe	6.75	± 0.05
P	4.41	± 0.05

Table 3.4 Results for Cu and P content (ICP method) of the Al-Cu-P inoculant

Element	Composition, wt%	Accuracy, %
Cu	17.1	± 0.02
P	0.89	± 0.02

Table 3.5 Results for Sr content (ICP method) of the Al-Sr alloy modifier supplied by London and Scandinavian Metallurgical Co Ltd.

Element	Composition, wt%	Accuracy, %
Sr	5.93	± 0.05

Table 3.6 The conditions investigated (melt at 800°C), (* melting temperature: 730 °C).

Samples	Additive	Type	Casting Method	Mould
A1	None		Bottom Casting	Sand
A2	0.015 wt% P	Al-Cu-P	Bottom Casting	Sand
A3	0.015 wt%P+0.04wt% Sr	Al-Cu-P+ Al-Sr	Bottom Casting	Sand
A4*	0.02 wt% P+0.04 wt% Sr	Al-Fe-P + Al-Sr	Bottom Casting	Sand
A5*	0.02 wt% P+0.04 wt% Sr	Al-Fe-P, adding Sr in the mould	Bottom Casting	Sand
B1	0.04 wt% Sr	Al-Sr	Bottom Casting	Sand
B2	0.1 wt% Sr	Al-Sr	Bottom Casting	Sand
B3	0.15 wt% Sr	Al-Sr	Bottom Casting	Sand
B4	0.2 wt% Sr	Al-Sr	Bottom Casting	Sand
B5	0.25 wt% Sr	Al-Sr	Bottom Casting	Sand
B6	0.3 wt% Sr	Al-Sr	Bottom Casting	Sand
C1	None		Bottom Casting	Sand
C2	None		Bottom Casting	Sand
C3	None		Bottom Casting	Sand
C4	None		Bottom Casting	Sand
C5	0.02 wt% P	Al-Fe-P	Bottom Casting	Sand
C6	0.02 wt% P	Al-Fe-P	Bottom Casting	Sand
C7	0.02 wt% P	Al-Fe-P	Bottom Casting	Sand
C8	0.02 wt% P	Al-Fe-P	Bottom Casting	Sand
C9	0.2 wt% Sr	Al-Sr	Bottom Casting	Sand
C10	0.2 wt% Sr	Al-Sr	Bottom Casting	Sand
C11	0.2 wt% Sr	Al-Sr	Bottom Casting	Sand
C12	0.2 wt% Sr	Al-Sr	Bottom Casting	Sand
C13	0.02 wt %P+0.2 wt %Sr	Al-Fe-P + Al-Sr	Bottom Casting	Sand
C14	0.02 wt %P+0.2 wt %Sr	Al-Fe-P + Al-Sr	Bottom Casting	Sand
C15	0.02 wt %P+0.2 wt %Sr	Al-Fe-P + Al-Sr	Bottom Casting	Sand
D1	None		Chamber Casting	Alumina
D3	None		Chamber Casting	Alumina
D5	None		Chamber Casting	Alumina
D2	0.02 wt% P	Al-Fe-P	Chamber Casting	Alumina
D4	0.02 wt% P	Al-Fe-P	Chamber Casting	Alumina
S1	None		Chamber Casting	Steel
S2	None		Chamber Casting	Steel
S3	None		Chamber Casting	Steel
S4	0.02 wt% P	Al-Fe-P	Chamber Casting	Steel
S5	0.02 wt% P	Al-Fe-P	Chamber Casting	Steel
S6	0.02 wt% P	Al-Fe-P	Chamber Casting	Steel
S7	0.04 wt% P	Al-Fe-P	Chamber Casting	Steel
S8	0.04 wt% P	Al-Fe-P	Chamber Casting	Steel
S9	0.04 wt% P	Al-Fe-P	Chamber Casting	Steel
S10	0.08 wt% P	Al-Fe-P	Chamber Casting	Steel
S11	0.08 wt% P	Al-Fe-P	Chamber Casting	Steel
S12	0.08 wt% P	Al-Fe-P	Chamber Casting	Steel
S13	0.02 wt% P	Al-Fe-P	Chamber Casting	Steel
S14	0.02 wt% P	Al-Fe-P	Chamber Casting	Steel
S15	0.02 wt% P	Al-Fe-P	Chamber Casting	Steel

Table 4.1 The quantitative results obtained from cooling curves

No	Sample	Mould	Addition	Process	Total Ingot Height (mm)	T_f (°C)	Tdot_1 (K/s)	Tdot_2 (K/s)	ΔT_P (K) $=T_L - T_f$	T'_{Eu} (°C)	T''_{Eu} (°C)	ΔT_{Eu} (K) $=T'_{Eu}$-	t_{Eu}(s)
1	C1	Sand	.....	Bottom casting	40	654.8	2.92	0.31	5.9	576.2	573.3	2.93	472.8
2	C2	Sand	.....		40	654.0	2.02	0.28	6.7	576.3	575.3	0.98	453.1
3	C3	Sand	.....		43	652.5	2.50	0.36	8.2	576.4	574.2	2.20	454.7
4	C4	Sand	.....		39	653.3	2.42	0.43	7.4	576.5	573.6	2.86	454.7
Average:					**40.5±1.7**	**653.6±1.1**	**2.46±0.37**	**0.35±0.06**	**7.1±1.0**	**576.3±0.1**	**574.1±0.9**	**2.24±0.90**	**458.8±9.3**
5	C5	Sand	0.02 wt% P		42	648.6	2.70	0.32	12.1	576.4	574.7	1.66	471.4
6	C6	Sand	0.02 wt% P		41	651.7	2.10	0.31	9.0	575.3	573.8	1.49	490.8
7	C7	Sand	0.02 wt% P		43	654.2	2.87	0.37	6.5	576.0	574.3	1.71	471.4
8	C8	Sand	0.02 wt% P		37.5	652.0	2.81	0.40	8.7	576.4	572.8	3.58	452.0
Average:					**40.9±2.4**	**651.6±2.3**	**2.62±0.35**	**0.35±0.04**	**9.1±2.3**	**576.0±0.5**	**573.9±0.8**	**2.11±0.98**	**471.4±15.8**
9	C9	Sand	0.2 wt% Sr		43	618.4	1.94	0.26	42.3	575.1	575.1	0.02	481.4
10	C10	Sand	0.2 wt% Sr		44	620.4	4.37	0.23	40.3	574.9	574.6	0.28	501.4
11	C11	Sand	0.2 wt% Sr		43	611.5	2.90	0.38	49.2	574.7	574	0.73	474.7
12	C12	Sand	0.2 wt% Sr		43	606.1	6.56	0.32	54.6	575.1	574.6	0.52	448.0
Average:					**43.2±0.5**	**614.1±6.6**	**3.94±2.01**	**0.30±0.07**	**46.6±6.5**	**574.9±0.2**	**574.6±0.5**	**0.39±0.31**	**476.4±22.1**
13	C13	Sand	0.2wt%Sr+0.02wt%P		44	618.9	2.75	0.28	41.8	574.1	573.9	0.15	487.1
14	C14	Sand	0.2wt%Sr+0.02wt%P		42	623.5	2.46	0.26	37.2	575.2	575.1	0.12	463.9
15	C15	Sand	0.2wt%Sr+0.02wt%P		44	622.1	2.52	0.28	38.6	575.0	574.8	0.23	490.0
Average:					**43.3±1.1**	**621.5±2.4**	**2.58±0.15**	**0.27±0.01**	**39.2±2.4**	**574.8±0.6**	**574.6±0.6**	**0.17±0.06**	**480.3±14.3**
16	D1	Alumina	.....	Chamber furnace	35								
17	D3	Alumina	.....		42	653.9	1.59	0.78	6.8	576.9	571.9	4.95	222.1
18	D5	Alumina	.....		37	647.1	1.71	1.11	13.6	576.1	576.1	0.00	150.9
Average:					**38.0±3.6**	**650.5±4.8**	**1.65±0.08**	**0.94±0.23**	**10.2±4.8**	**576.5±0.6**	**574.0±3.0**	**2.47±3.50**	**186.5±50.3**
19	D2	Alumina	0.02 wt% P		36								
20	D4	Alumina	0.02 wt% P		**41**	**659.8**	**1.73**	**0.82**	**0.9**	**570.6**	**570.6**	**0.04**	**204.7**
21	S1	Steel	.....	Chamber furnace	25	646.0	1.98	0.78	14.7	575.3	574.2	1.09	223.3
22	S2	Steel	.....		21	653.9	2.24	1.09	6.8	576.1	575.7	0.43	190.7
23	S3	Steel	.....		20	655.3	2.08	0.91	5.4	575.0	574.2	0.80	225.6
Average:					**22.0±2.6**	**651.7±5.0**	**2.10±0.13**	**0.91±0.15**	**9.0±5.0**	**575.5±0.6**	**574.7±0.9**	**0.77±0.33**	**213.2±19.5**
24	S4	Steel	0.02 wt% P		25	642.0	2.60	1.00	18.7	576.3	576	0.3	185.9
25	S5	Steel	0.02 wt% P		25	630.8	1.95	0.88	29.9	572.5	571.9	0.6	235.7
26	S6	Steel	0.02 wt% P		23	638.6	2.63	1.04	22.1	575.1	574.7	0.4	180.3
27	S13	Steel	0.02 wt% P		28	655.5	2.20	0.74	5.2	575.0	574	1.0	214.0
28	S14	Steel	0.02 wt% P		27	632.0	2.39	0.80	28.7	573.9	573.5	0.4	211.2
29	S15	Steel	0.02 wt% P		25	653.0	1.97	0.89	7.7	574.4	573.7	0.7	203.3
Average:					**25.5±1.8**	**642±10.4**	**2.29±0.30**	**0.89±0.11**	**18.7±10.4**	**574.5±1.3**	**574.0±1.3**	**0.6±0.3**	**205.1±20.2**
30	S7	Steel	0.04 wt% P		23	650.8	2.57	1.09	9.9	574.6	573.6	1.02	181.1
31	S8	Steel	0.04 wt% P		20.5	652.5	2.46	1.09	8.2	575.7	574.1	1.63	189.0
32	S9	Steel	0.04 wt% P		24	653.2	2.60	1.11	7.5	573.7	572.6	1.14	187.0
Average:					**22.5±1.8**	**652.2±1.2**	**2.54±0.07**	**1.10±0.01**	**8.5±1.2**	**574.7±1.0**	**573.4±0.8**	**1.26±0.32**	**185.7±4.1**
33	S10	Steel	0.08wt% P		25	652.7	2.17	0.90	8.0	573.5	572.7	0.77	229.3
34	S11	Steel	0.08wt% P		22	651.0	2.28	0.97	9.7	573.4	571.1	2.32	207.3
35	S12	Steel	0.08wt% P		24	651.1	3.26	1.28	9.6	574.0	573	0.98	177.1
Average:					**23.7±1.7**	**651.6±0.9**	**2.57±0.60**	**1.05±0.20**	**9.1±0.9**	**573.6±0.3**	**572.3±1.0**	**1.36±0.84**	**204.6±26.2**

T_f: formation temperature of Pri Si, Tdot_1: cooling rate from peak temp. to T_f, Tdot_2: cooling rate from T_f to eutectic arrest, ΔT_P Undercooling for Pri Si, T'_{Eu}: eutectic arrest, T''_{Eu}: minimum formation temperature of eutectic phase, ΔT_{Eu} Eu undercooling, t_{Eu} Eu arrest duration.

Table 4.2.a The microstructure description as morphology distribution from bottom to top of uninoculated and inoculated ingots; melt temperature 800°C, bottom cast into Quikcup sand moulds.

The position of thermocouple has been considered as zero in Cartesian coordinates (Fig 4.15), so negative y is for the points below the thermocouple. A: coarse primary Si, B: coarse eutectic Si, C: polyhedral primary Si. A+C: partly refined primary silicon accompanied by unrefined Si, A* very coarse (bulky) primary Si, A": plate-like primary Si, A``: star-like primary Si.

Position for	C 1	C 2	C 3	C 4	C 5	C 6	C 7	C 8
y=..(mm)	Uninoculated				Inoculated by 200ppm AlFeP			
22.5	.....	.....	A	.....	.....	.....	A	.....
21.25	.....	.....		.....	A	C	A	.....
20	.....	A	A	A	A			.....
19.25	A	A						.....
18.75	A+C	A		A	C		A+C	.....
17.5	A+C	A+C	A	A	C			.....
15.5					C	A``		
15	A+C	A	A	A	A+C		A+C	
13.75	A+C	A*+B	A	C	A		A+C	A+C
12.5	A	A*	A	A+C	A		A	A+C
11.25	A	A*	A+C	A	A	A"	A+C	A+C
10	A+C	A	C	Pore	A		A+C	A+B
8.25	Pore	A	C			A	A+C	A+C
7.5	A	A	C	Pore	A	A+C	A+C	A``
6.25	A+C		C	A+C		C	A+C	C
5	A+C	A	C	A+C	A+C	C	C	Pore
3.75				A+C	C	C	C	Pore
2.5	C	C	Pore	Pore	C	C	C	Pore
1.25		B	Pore	Pore	C	B	Pore	Pore
0	Thermocouple position							
-1.25	A	A	A	A	A"+C	A	C	A
-2.5	A+C,	A	A	A,	A+C	A+C	A+C	A
-3.75	A,	A``	A	A+C	A	C	A+C	A
-5	A,	A	A	A+C	A		C	A
-6.25		C	A+C	A+C	A+C	C	C	
-8.25	A	C	C		C	C	C	C
-10	C	A	C	C	C	C+B	C	C
-11.25	C	C+B	C	C	B+C	B	C	C
-12.5	C	Pore	B+ Pore	B	Pore	B	C	C
-13.25	A+C	B	B	B	B	B	B	B
-18.75	B	B	B	A(very small)&B	B	B		B
-19.25	B	B	A(very small)&B	.....	B	A(very small)&B	A(very small)&B	B
-20	B	A	.....	.....	A(very small)&B	.....	.....	B
-20.75	A(very small)&B	.....	.....	.....	.....	.....	.....	A(very small)&B

Upper part of ingot

Lower part of ingot

Table 4.2.b The length of zones A, B, C and A in the bottom of ingots for samples bottom cast into Quikcup sand moulds (Table 4.2.a); A: primary Si, B: coarse eutectic Si, C: polyhedral primary Si.

	Zones / Samples	A (mm)	B (mm)	C (mm)	A (Bottom) (mm)	Height (mm)
Uninoculated	C1	30	6.5	3	0.5	40
	C2	17±8	13±8	7.5±3.5	1	40
	C3	21±10	12±3.5	9.5±6	0.5	43
	C4	25±7	8.5±1	7±3	0.5	39
	Average	**23±6**	**10±3**	**7±3**	**0.6±0.2**	**40±2**
0.02 wt% P added	C5	17.5±6	15±7	6±1	1	42
	C6	13.5±5	18.5±3.5	12.5±5	1	41
	C7	10	7.5	25	0.5	43
	C8	12±7	12±3.5	14±3	0.5	37.5
	Average	**13±3**	**13±5**	**14±8**	**0.7±0.3**	**41±2**

Table 4.3 Number of primary silicon particles per unit area for uninoculated and inoculated ingots produced via bottom casting into sand moulds.

	No	Code	Degassing	N_A(/mm^2)	N_V(/mm^3)
Uninoculated	1	C1	Yes	28±15	226
	2	C2	No	27±18	215
	3	C3	No	36±28	330
	4	C4	No	30±22	251
	Average± STD			**30±4**	**255±52**
0.02 wt% P added	5	C5	Yes	31±28	263
	6	C6	Yes	39±20	372
	7	C7	No	48±31	508
	8	C8	No	40±19	386
	Average± STD			**40±7**	**382±100**

Table 4.4 Number of primary silicon particles per unit area for Sr-modified and simultaneously Sr-modified and P-inoculated ingots produced via bottom casting.

	No	Code	N_A(/mm^2)	N_V(/mm^3)
0.2 wt% Sr added	1	C9	4.0±2.4	13.6±11.1
	2	C10	3.8±2.0	12.5±10.1
	3	C11	3.8±2.7	13.0±13.6
	4	C12	3.5±2.1	11.1±8.8
	Average± STD		**3.8±0.2**	**12.6±1.1**
0.2 wt% Sr + 0.02 wt% P added	5	C13	3.9±1.9	12.8±9.3
	6	C14	3.7±1.7	11.8±8.1
	7	C15	2.7±1.2	7.4±4.2
	Average± STD		**3.4±0.6**	**10.7±2.9**

Table 4.5 The quantitative results for ingots melted, (some refined by Al-Fe-P) and solidified in alumina crucibles and chamber cast.

	No	Code	Having thermocouple	N_A(/mm^2)	N_V(/mm^3)
Uninoculated	1	D1	No	42±24	415
	2	D3	Yes	31±19	263
	3	D5	Yes	32±17	276
	Average± STD			**35±6**	**318±84**
0.02 wt% P added	4	D2	No	65±28	800
	5	D4	Yes	54±19	606
	Average± STD			**60±8**	**703±137**

Table 4.6 The quantitative results for ingots melted, (some refined by Al-Fe-P) and solidified in stainless steel cups and chamber cast.

	No	Code	N_A(/mm^2)	N_V(/mm^3)
Uninoculated	1	S1	29±17	238
	2	S2	36±18	330
	3	S3	26±17	202
	Average		**30±5**	**257±66**
0.02 wt% P added	4	S4	35±20	316
	5	S5	49±20	524
	6	S6	41±23	401
	7	S13	45±17	461
	8	S14	35±15	276
	9	S15	40±24	386
	Average		**40±6**	**394±91**
0.04 wt% P added	10	S7	56±21	640
	11	S8	55±20	623
	12	S9	61±12	727
	Average		**57±3**	**663±56**
0.08 wt% P added	13	S10	65±24	800
	14	S11	61±14	727
	15	S12	51±10	556
	Average		**59±7**	**694±125**

Table 4.7 Summary of quantitative results and cooling/casting conditions for the untreated and P-inoculated samples.

Casting Condition	AVERAGE±STD DEVIATION				
	N_A(/mm^2)	N_V(/mm^3)	T_f (°C)	Tdot_2 (K/s)	ΔT_P (°C)
Sand, ...	30±4	255±52	653.3±5	0.35±0.06	7.1±1.0
Sand, 0.02 wt% P	40±7	382±100	651.6±2	0.35±0.04	9.1±2.3
Sand, 0.2 wt% Sr	3±1	10±2	614.1±7	0.30±0.07	46.6±6.5
Sand, 0.2 wt% Sr+0.02 wt% P	4±1	11±2	621.5±2	0.27±0.01	39.2±2.4
Alumina, ...	35±6	318±84	650.5±4	0.94±0.23	10.2±4.8
Alumina, 0.02 wt% P	60±8	703±137	659.8	0.82	0.9
Steel, ...	30±5	257±66	651.7±5	0.91±0.15	9.0±5.0
Steel, 0.02 wt% P	40±6	394±91	642±10	0.89±0.11	18.7±10.4
Steel, 0.04 wt% P	57±3	663±56	652.2±1	1.10±0.01	8.5±1.2
Steel, 0.08 wt% P	59±7	694±125	651.6±1	1.05±0.20	9.1±0.9

Table 4.8 Results of chemical analysis (ICP-OES method) of DTA samples.

Sample		Composition (wt%)	
		Chemical composition of ingots provided for DTA sampling	Chemical analysis of DTA samples
A1	Si	18.6	23.7
	P	0.0014	<0.01
A2	Si	18.6	24.2
	P	0.015	<0.01
S10	Si	18.6	24.2
	P	0.08	<0.01

Table 4.9 Results for T_L values of DTA samples by calculation and measurement using Equation 4.1 and DTA curves.

Sample	Liquidus Temperature (°C)			
	Calculation (Si content in wt%)		Measurement	
A1	Si: 18.6%, 660.7	Si: 23.7%, 727.8	No 1: 702.7 No 2: 673.2 No 3: 673.7 No 4: 700.0	**687.4±16.1 ≡20.6±1.2%Si**
A2	Si: 18.6%, 660.7	Si: 24.2%, 734.1	No 1: 695.2 No 2: 681.7 No 3: 680.0	**685.6±8.3 ≡20.5±0.6%Si**
S10	Si: 18.6%, 660.7	Si: 24.2%, 734.1	No 1: 677.5 No 2: 668.7 No 3: 677.0	**674.4±10.2 ≡19.6±0.4%Si**

Table 4.10 Samples used for EBSD tests.

No	Code of sample	Cast specification
1	C3	Bottom cast, sand mould, uninoculated.
2 (1-7)	A2	Bottom cast, sand mould, inoculated by 0.015 wt% P from Al-Cu-P, (sample without any cooling data detection, however, the casting condition was very close to C5-8).
3 (1-3)	S1	Chamber cast, stainless steel mould, uninoculated.
4	S2	Chamber cast, stainless steel mould, uninoculated.
5	S5	Chamber cast, stainless steel mould, inoculated by 0.02 wt% P from Al-Fe-P.

Table 4.11 The orientation/angle pairs for polyhedral particles specified in Fig. 4.25 sample C3.

Particles		Angle [°]	Indices
No 1	No 2	±1	(Axis)
1	**2**	**56**	**-433**
3	4	42	120
4	5	34	-11-2
6	**7**	**56**	**-212**
6	**8**	**59**	**-332**
7	8	38	141
7	10	21	2-3-2
7	**11**	**59**	**1-1-1**
10	11	21	0-23
10	12	52	2-34
12	**13**	**59**	**-3-3-4**
13	**14**	**60**	**3-3-4**
14	**15**	**55**	**323**
15	**16**	**59**	**111**
17	18	44	234
18	**19**	**55**	**-4-43**
20	21	44	-1-23
21	22	31	01-1
22	**23**	60	111
24	25	46	431
26	**27**	**60**	**-1-1-1**
26	**28**	**60**	**-1-1-1**
28	29	54	33-4
29	**30**	**56**	**1-33**
27	**29**	**58**	**-44-1**
30	**31**	**59**	**21-2**
31	**32**	**60**	**3-22**
33	11	43	0-14

Table 4.12 The orientation/angle pairs for polyhedral particles specified in Fig. 4.26 (A2-1).

Particles No 1	Particles No 2	Angle [°] ±1	Indices (Axis)
1	**2**	**60**	**-3-44**
1	3	44	-3-2-3
4	**5**	**60**	**-1-11**
5	6	31	-4-2-3
8	**7**	**60**	**11-1**
7	**9**	**59**	**11-1**
9	**10**	**60**	**11-1**
10	*11*	*37*	*011*
12	13	35	102
Mapping for No12, 13 was not clear enough, so the offset was too much.			
13	**14**	**60**	**-111**
14	15	30	-130
15	**16**	**54**	**-4-3-3**
16	**17**	**54**	**-4-3-3**
17	**18**	**55**	**-4-33**
18	**19**	**58**	**334**
18	20	43	4-41
18	20	28	01-3
13	21	38	-1-43
22	23	43	-2-31
23	26	39	40-1
24	**25**	**60**	**-1-1-1**
27	**28**	**60**	**-443**
28	29	49	-3-2-2
27	**29**	**55**	**-4-3-3**
30	31	52	-34-1

Table 4.13 The orientation/angle pairs for polyhedral particles specified in Fig 4.27 (A2-2).

Particles No 1	Particles No 2	Angle [°] ±1	Indices (Axis)
1	**2**	**55**	**-2-23**
2	**3**	**60**	**-111**
3	4	53	3-42
4	**5**	**56**	**21-2**
5	**6**	**59**	**323**
7	8	51	-13-3
8	**10**	**60**	**3-3-4**
7	9	26	-32-1
10	11	54	-4-3-4
11	**12**	**57**	**-4-3-3**
12	**13**	**56**	**-21-2**
13	**14**	**60**	**3-3-2**
14	15	37	32-4
15	16	27	-12-3
17	**18**	**60**	**1-11**
19	20	35	-3-1-2
20	**21**	**57**	**-344**
22	23	51	-2-3-3
23	24	37	-1-10
25	**26**	**58**	**-2-43**
26	27	50	430
27	28	50	-3-3-4
28	**29**	**55**	**-3-2-3**
30	**31**	**57**	**2-3-3**
31	**32**	**62**	**22-1**
33	34	54	1-1-1
35	39	22	-401
36	37	46	2-3-2
37	38	53	-4-2-3
39	**40**	**58**	**342**
39	41	51	4-23
40	43	45	-44-3
42	43	52	-132
44	**45**	**60**	**-2-32**
45	**46**	**60**	**-1-1-1**
46	**47**	**58**	**323**
47	48	49	32-3
47	**50**	**59**	**-34-2**
48	49	39	-1-22
51	52	39	01-1
52	**53**	**60**	**-2-12**
53	54	48	-414
55	**56**	**57**	**-3-4-3**
57	**58**	**59**	**-11-1**
58	**59**	**57**	**1-33**

Table 4.14 The orientation/angle pairs for polyhedral particles specified in Fig. 4.28 (A2-3).

Particles		Angle [°]	Indices
No 1	No 2	±1	(Axis)
1	**2**	**55**	**223**
2	3	49	-1-24
4	**5**	**56**	**112**
7	**8**	**55**	**221**
7	9	48	312
10	**11**	**57**	**111**
11	**12**	**56**	**221**
12	13	17	134
14	15	40	331
14	16	50	142
17	**18**	**56**	**443**
18	**19**	**57**	**121**
6	**20**	**55**	**221**
20	**21**	**55**	**332**
21	**22**	**57**	**343**
22	23	40	141

Table 4.15 The orientation/angle pairs for polyhedral particles specified in Fig 4.29 (A2-4).

Particles		Angle [°]	Indices
No 1	No 2	±1	(Axis)
1	2	49	-1-32
2	3	50	1-34
4	5	39	01-1
5	6	41	31-4
6	4	42	-414
7	8	38	-101
11	12	17	-23-4
10	11	51	-1-12
9	12	45	-11-4
14	15	40	214
13	14	45	1-23
16	**17**	**54**	**-1-34**
19	20	43	14-1
22	**23**	**57**	**334**

Table 4.16 The orientation/angle pairs for polyhedral particles specified in Fig 4.30 (A2-5).

Particles		Angle [°]	Indices
No 1	No 2	±1	(Axis)
2	**1**	**56**	**-4-3-4**
4	3	52	-1-2-1
5	**6**	**58**	**334**
7	**8**	**60**	**1-11**
9	**10**	**60**	**221**
11	**12**	**60**	**1-1-1**
13	**14**	**57**	**011**
15	**16**	**55**	**-2-2-3**
16	**17**	**55**	**-313**
17	18	50	-111
18	**19**	**61**	**-21-2**
20	**21**	**56**	**-34-4**

Table 4.17 The orientation/angle pairs for polyhedral particles specified in Fig. 4.31 (A2-6).

Particles		Angle [°]	Indices
No 1	No 2	±1	(Axis)
1	2	50	-4-30
2	3	42	-401
3	4	45	-1-3-3
5	6	54	-110
6	7	53	-110
7	**8**	**59**	**334**
8	9	53	1-2-2
9	**10**	**61**	**-3-2-2**
11	**12**	**57**	**3-44**
13	**14**	**58**	**-111**
15	16	52	3-13

Table 4.18 The orientation/angle pairs for polyhedral particles specified in Fig 4.32 (A2-7).

Particles		Angle [°]	Indices
No 1	No 2	±1	(Axis)
1	**2**	**54**	**-3-44**
3	**4**	**60**	**-11-1**
5	6	22	-1-10
6	**7**	**60**	**21-2**

Table 4.19. The orientation/angle pairs for polyhedral particles specified in Fig. 4.35 (S1-1).

Particles		Angle [°]	Indices
No 1	No 2	±1	(Axis)
3	4	52	23-3
4	**5**	**62**	**2-12**
5	6	18	-34-4
5	7	43	210
8	**9**	**60**	**-33-2**
10	**11**	**59**	**-33-4**
12	**13**	**58**	**43-4**
14	**15**	**59**	**1-1-1**
16	17	37	034
18	**19**	**58**	**-344**
20	**21**	**57**	**-334**
22	**23**	**61**	**-1-2-2**
23	**24**	**60**	**-32-3**
24	**25**	**60**	**-3-4-4**
25	26	46	-22-1
27	**28**	**59**	**-1-11**
28	**29**	**60**	**443**
30	**31**	**59**	**-111**
31	**32**	**59**	**-11-1**

Table 4.20 The orientation/angle pairs for polyhedral particles specified in Fig 4.36 (S1-2).

Particles		Angle [°]	Indices
No 1	No 2	±1	(Axis)
1	**2**	**56**	**-43-3**
2	**3**	**57**	**-1-2-2**
4	5	53	1-3-2
3	6	44	-14-1
7	8	52	-1-11
8	**9**	**60**	**2-3-2**
10	11	40	1-1-3
11	**12**	**62**	**-1-2-2**
12	13	52	-1-2-1
14	15	51	-213
16	**15**	**58**	**-3-32**
17	**18**	**62**	**-21-2**
18	**19**	**58**	**233**
17	20	52	111
20	**21**	**57**	**12-2**
21	**22**	**59**	**-434**
23	**24**	**58**	**3-2-3**
25	26	50	-2-14
26	**27**	**58**	**-11-1**
26	28	50	12-4
26	**29**	**61**	**212**
28	29	55	-44-3
29	**30**	**56**	**22-1**
31	32	37	14-2
32	**33**	**57**	**-221**
33	34	55	314
34	35	51	1-1-1
35	36	38	-2-23
36	**37**	**60**	**-44-3**
38	37	52	-34-4
39	40	38	-4-1-2
41	**42**	**59**	**-11-1**
43	**44**	**57**	**-111**
44	45	51	11-1
45	**46**	**59**	**-1-11**
46	**47**	**59**	**-1-11**
47	**48**	**60**	**1-1-1**
49	**50**	**60**	**3-3-2**
50	**51**	**60**	**-4-33**
52	53	51	413
54	**55**	**60**	**-334**
56	**57**	**60**	**1-11**
57	**58**	**60**	**32-3**
58	**59**	**60**	**32-3**
60	**61**	**60**	**4-33**

Table 4.21 The orientation/angle pairs for polyhedral particles specified in Fig 4.37 (S1-3).

Particles		Angle [°]	Indices
No 1	No 2	±1	(Axis)
1	2	54	22-1
2	**3**	**59**	**-111**
2	**4**	**59**	**-4-3-3**
5	6	38	011
6	**7**	**60**	**1-1-1**
8	**9**	**59**	**-111**
10	**11**	**60**	**-334**
11	**12**	**59**	**-1-11**
11	**13**	**60**	**111**
11	**14**	**57**	**344**
15	**16**	**55**	**231**
16	**17**	**55**	**331**
18	**19**	**58**	**-1-1-1**
19	**20**	**60**	**-3-2-2**
21	**22**	**60**	**4-3-4**
23	24	46	-221
25	26	54	111

Table 4.22 The orientation/angle pairs for polyhedral particles specified in Fig 4.38 (S2).

Particles		Angle [°]	Indices
No 1	No 2	±1	(Axis)
1	**2**	**56**	**2-33**
2	**3**	**60**	**-1-1-1**
3	**4**	**57**	**-1-11**
5	6	28	40-1
6	7	57	10-1
7	8	58	-33-4
8	9	22	-3-3-1
8	**10**	**57**	**-2-3-4**
10	11	54	13-3
11	**12**	**59**	**-2-1-2**
10	13	54	13-3
13	**14**	**54**	**2-33**
14	**15**	**59**	**-1-1-1**
14	**16**	**56**	**3-2-2**
16	17	51	-4-23
17	18	50	-3-42
19	**20**	**60**	**-111**
21	**22**	**61**	**33-2**
23	24	57	-23-4
25	**26**	**55**	**111**
27	28	38	-101
27	**31**	**56**	**1-1-1**
28	29	36	-1-41
29	30	56	4-3-4
31	**32**	**59**	**3-32**
31	33	53	-3-13
33	**34**	**55**	**-43-4**
34	35	37	-430
36	37	35	-4-10
37	38	38	-1-2-1
38	39	38	-20-3
40	41	46	2-12
41	42	22	1-10
43	**44**	**59**	**-3-44**
44	**45**	**58**	**-1-1-1**
46	**47**	**57**	**-334**
48	49	52	3-32
50	**51**	**59**	**3-44**

Table 4.23 The orientation/angle pairs for polyhedral particles specified in Fig 4.39 (S5).

Particles		Angle [°]	Indices
No 1	No 2	±1	(Axis)
1	**2**	**58**	**-1-11**
2	**3**	**60**	**1-11**
3	**4**	**59**	**1-1-1**
5	6	41	24-1
6	**7**	**59**	**-10-1**
7	8	45	302
7-2	8	61	2-21
9	**10**	**56**	**-3-23**
10	11	47	0-1-3
10	12	37	-2-10
11	12	25	3-4-4
13	14	49	1-3-1
14	**15**	**56**	**3-3-4**
15	16	34	2-30
16	**17**	**60**	**-111**
18	**19**	**57**	**221**
20	**21**	**58**	**-21-2**
22	**23**	**60**	**3-43**
24	25	34	-1-41
26	**27**	**62**	**1-22**
28	29	41	4-34
29	30	55	-223
30	31	28	-110
32	**33**	**56**	**4-43**
35	**34**	**57**	**-4-33**
37	**36**	**59**	**313**
39	**40**	**55**	**2-12**
41	38	52	-2-21
44	**42**	**56**	**-4-34**
44	43	53	-1-10
45	**46**	**58**	**-221**
48	47	53	312
48	**49**	**59**	**34-4**
49	**50**	**60**	**3-2-3**
50	**51**	**56**	**-3-3-1**
52	53	54	432
53	54	27	4-30
55	**56**	**59**	**-2-21**
56	**57**	**57**	**1-11**
57	58	53	3-32
59	60	30	230

Table 4.24 N_A of primary silicon for EBSD samples (Table 4.10) for all particles in the selected area and for only interconnected particles (The values are averages for 18 different areas of a 10mm×10mm EBSD sample).

Casting Condition	Sample	N_A (/mm^2) (total particles)	N_A (/mm^2) (connected pairs)	Connected/Total particles (%)
Sand mould, Bottom cast/ no P	**C3**	24±7	7±3	29±8
Sand mould, Bottom cast/ 0.015 wt% P	**A2**	38±17	13±7	32±7
Steel mould, Chamber cast/ no P	**S1**	44±10	10±3	20±5
Steel mould, Chamber cast/ no P	**S2**	62±9	16±3	26±6
	Average , Uninoculated, chamber cast			**23±4**
Steel mould, Chamber cast/ 0.02 wt% P	**S5**	51±15	14±6	26±7

Table 5.1 Required data used in Perepezko nucleation model for the nucleation of primary silicon in solidification of hypereutectic Al-Si.

Parameter	Symbol	Value	Reference
The Surface-Dependent Model			
S/L interfacial energy	σ_{SL}	0.344 J/m^2	Evans et al 1991
Atomic jump distance for attachment of Si from the melt	a	3×10^{-10} m	Smithells 1983
Activation enthalpy for diffusion of Si in liquid Al-Si	Q	25740 J/mol	Petrescu 1970
Diffusivity in the melt	D_L	2.08×10^{-7} exp (-25740/8.314T) m^2/s	Petrescu 1970
Number of surface atoms of the nucleation site per unit volume of melt	N_0	10^{20} m^{-3}	Liang et al 1995
The Volume-Dependent Model			
S/L interfacial energy	σ_{SL}	0.3524 J/m^2	Gündüz and Hunt 1985
Base levels of nucleants	N_v^0	10^{13} m^{-3}	Gremaud et al 1996
Nucleant potency parameter	β	0.0590 K^{-1}	Gremaud et al 1996
Nucleant particle area	A_P	3.14×10^{-16} m^2	Gremaud et al 1996
Zeldovich factor	Z	0.0198	Gremaud et al 1996

Boltzmann's constant (k): 1.3806×10^{-23} J/atomK.

In order to calculate the liquidus temperature (T_L), the following equation can be used. This equation is based on the experimental data given by Murray and McAlister (1984), which has been approximated (Liang et al 1995) by polynominal functions for T_L:

$$T_L = T_{EU} + 14.93(C-C_{EU}) - 9.28\times10^{-2}(C-C_{EU})^2 + 3.59\times10^{-4}(C-C_{EU})^3$$

where T_L: liquidus temperature (°C); T_{EU}: equilibrium eutectic temperature, 571°C; C, alloy composition (at%) and C_{EU}: equilibrium eutectic composition, 12.2 at.% Si.

Table 5.2 Al-Si thermodynamic model parameters, J/mol, T in K (Murray and McAlister 1984).

${}^0G_{Al}^{fcc} = -10792 + 11.56T$	$A^L = -10695.4 - 1.823T$
${}^0G_{Si}^{fcc} = 12.12T$	$B^L = -4275.5 + 3.044T$
${}^0G_{Si}^{dia} = -50600 + 30.00T$	$C^L = 670.7 - 0.460T$
${}^0G_{Al}^{dia} = 30.00T$	$A^{fcc} = -200 - 7.594T$
${}^0G_{Al}^{L} = 0$	$A^{dia} = 89138 - 31.445T$
${}^0G_{Si}^{L} = 0$	

To calculate Gibbs free energy per unit volume for formation of solid Si from liquid Al-Si (ΔG_V), Murray and McAlister (1984) applied the following equation introduced by them for the Al-Si system and a parallel tangent construction gave the free energy change:

$$G^l = {}^0G_{Al}(1-x) + {}^0G_{Si}X + RT[x\ln X + (1-X)\ln(1-X)] + X(1-X)[A^l + B^l(1-2X) + C^l(1-6X+6X^2)]$$

where X is the mole fraction of silicon and A, B, and C are interaction parameters that are linearly dependant on temperature.

Table 5.3 The corrected contact angles ($\theta_1$and θ_2) (between primary silicon nucleus and the nucleant), using the surface-dependant and volume-dependant nucleation models, from the results of Liang at al (1995), and using ΔG_V (calculated using Murray and McAlister, 1984) in which ΔS_V varies with temperature.

ΔT (K)	32.2	34.2	34.8	36.3	38.5	41.4	43	45.4	46.7	50.5	51.1	64.9
θ_1 (deg)*	25.5	25.9	27	27.5	28	29.2	34	30.4	31.3	29.6	33	35.5
Corrected θ_1 (deg)	35.9	36.3	37.0	37.8	38.1	39.4	39.6	40.8	41.4	42.7	42.8	47.0
θ_2 (deg)	32.0	32.4	33.3	34.0	34.1	35.4	33.4	36.6	37.4	38.6	38.8	42.4

* From Liang et al 1995, T-independent ΔS_V.

Table 5.4 The calculated contact angles ($\theta_1$and θ_2) between primary silicon nucleus and the nucleant, using the surface-dependant and volume-dependant nucleation models, for different cooling conditions for Al-22 wt% Si and Al-32 wt% Si (the cooling conditions and the size of primary silicon have been taken from Ohmi et al, 1991, 1994, 1997.).

Al-22 wt% Si						
N_V (/mm^3)	T_dot (K/s)	T_f (K)	T_L (K)	ΔT (K)	θ_1 (deg)	θ_2 (deg)
13.8	10.6	963.5	981.2	17.7	30.5	27.2
42.2	50.6	961.7	981.2	19.5	30.9	27.4
42.2	50.7	959.1	978.8	19.7	32.1	28.5
416	255.9	864.4	981.2	116.8	61.9	56.9
195	93.7	920.1	981.2	61.1	46.3	41.7
195	95	918.8	978.8	60	46.7	42.1
219	193.3	889.5	981.2	91.7	55.4	50.4
Al-32 wt% Si						
N_V (/mm^3)	T_dot (K/s)	T_f (K)	T_L (K)	ΔT (K)	θ_1 (deg)	θ_2 (deg)
13.7	13.1	1086	1102	16	32.8	29.2
73.9	77.7	1043	1102	59	48.2	43.3
33.8	133	1040	1102	62	49.3	44.4
280	221	1010	1102	92	57.5	52.2

Table 5.5 The effect of multiplication of the number of primary silicon particles on contact angle between primary silicon nucleus and nucleant (θ_1) in the surface-dependant nucleation model.

Al-22 wt% Si					
N_V (/mm^3)	T_dot (K/s)	T_f (K)	T_L (K)	ΔT (K)	θ_1 (deg)
13.8	10.6	963.5	981.2	17.7	30.5
138					30.1
42.2	50.6	961.7	981.2	19.5	30.9
422					30.5
416	255.9	864.4	981.2	116.8	61.9
4160					60.9
195	93.7	920.1	981.2	61.1	46.3
1950					45.6
219	193.3	889.5	981.2	91.7	55.4
2190					54.5

Table 5.6 The calculated contact angles ($\theta_1$and θ_2) between primary silicon nucleus and the nucleant, using the surface-dependant and volume-dependant nucleation models, for different cooling conditions for an Al-19 wt% Si (the cooling conditions and the size of primary silicon have been taken from Kaneko et al 1979.).

N_V (/mm^3)	T_dot (K/s)	T_f (K)	T_L (K)	ΔT (K)	0_1 (deg)	0_2 (deg)
2.5	0.017	949	955	6	20.2	10.3
12.5	0.055	949	955	6	20.0	10.1
35	0.083	949	955	6	19.8	10.0
1250	1.67	949	955	6	19.2	9.5

Table 5.7 The calculated contact angles using Perepezko's surface-dependant model (casting conditions and quantitative measurements in Tables 4.1, 4.3, 4.5 and 4.6).

Sample	P level (wt%)	0_1 (deg)
C1	.....	23.5
C2	.....	24.0
C3	.....	24.8
C4	.....	24.3
		24.2±0.5
D3	.....	24.0
D5	.....	27.8
		25.9±2.7
S1	.....	28.3
S2	.....	24.0
S3	.....	23.2
		25.2±2.7
C5	0.02	26.9
C6	0.02	25.2
C7	0.02	23.7
C8	0.02	25.0
		25.2±1.3
D4	0.02	20.17
		20.17
S4	0.02	30.2
S5	0.02	35.2
S6	0.02	31.8
S13	0.02	23.0
S14	0.02	34.7
S15	0.02	24.5
		29.9±5.1
S7	0.04	25.6
S8	0.04	24.9
S9	0.04	24.3
		24.9±0.7
S10	0.08	24.6
S11	0.08	25.5
S12	0.08	25.4
		25.2±0.5

Table 5.8 The calculated contact angles using Perepezko's volume-dependant model (casting conditions and quantitative measurements in Tables 4.1, 4.3, 4.5 and 4.6).

Sample	P level (wt%)	0_2 (deg)
C1	.....	20.6
C2	.....	21.1
C3	.....	22.8
C4	.....	21.4
		21.5±0.9
D3	.....	21.2
D5	.....	24.6
		22.9±2.4
S1	.....	25.1
S2	.....	21.1
S3	.....	20.4
		22.2±2.5
C5	0.02	23.8
C6	0.02	22.2
C7	0.02	20.8
C8	0.02	22.0
		22.2±1.2
D4	0.02	17.6
		17.6
S4	0.02	26.8
S5	0.02	31.4
S6	0.02	28.2
S13	0.02	20.2
S14	0.02	31.0
S15	0.02	21.6
		26.5±4.7
S7	0.04	22.6
S8	0.04	21.7
S9	0.04	21.3
		21.9±0.7
S10	0.08	21.6
S11	0.08	22.5
S12	0.08	22.4
		22.2±0.5

Table 5.9 Summary of contact angles for the untreated, and P-inoculated ingots chamber cast into steel moulds. (θ_1: the contact angle calculated from the surface-dependant nucleation model and θ_2: the contact angle from the volume-dependant model.)

P addition level (wt%)	θ_1 (deg)	θ_2 (deg)
...	25.2±2.7	22.2±2.5
0.02	29.9±5.1	26.5±4.7
0.04	24.9±0.7	21.9±0.7
0.08	25.2±0.5	22.2±0.5

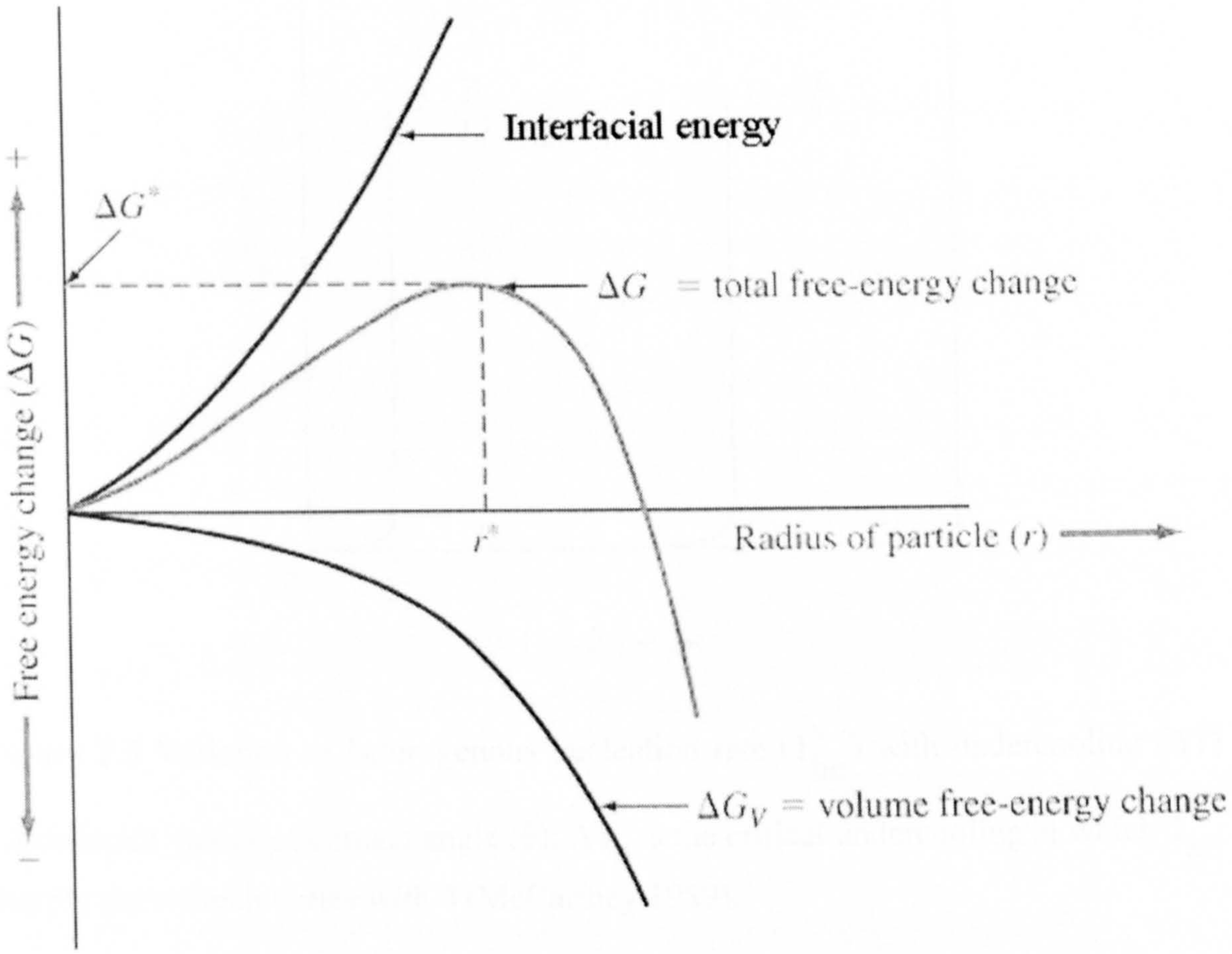

Figure 2.1 The free energy change associated with homogeneous nucleation (Chalmers 1964).

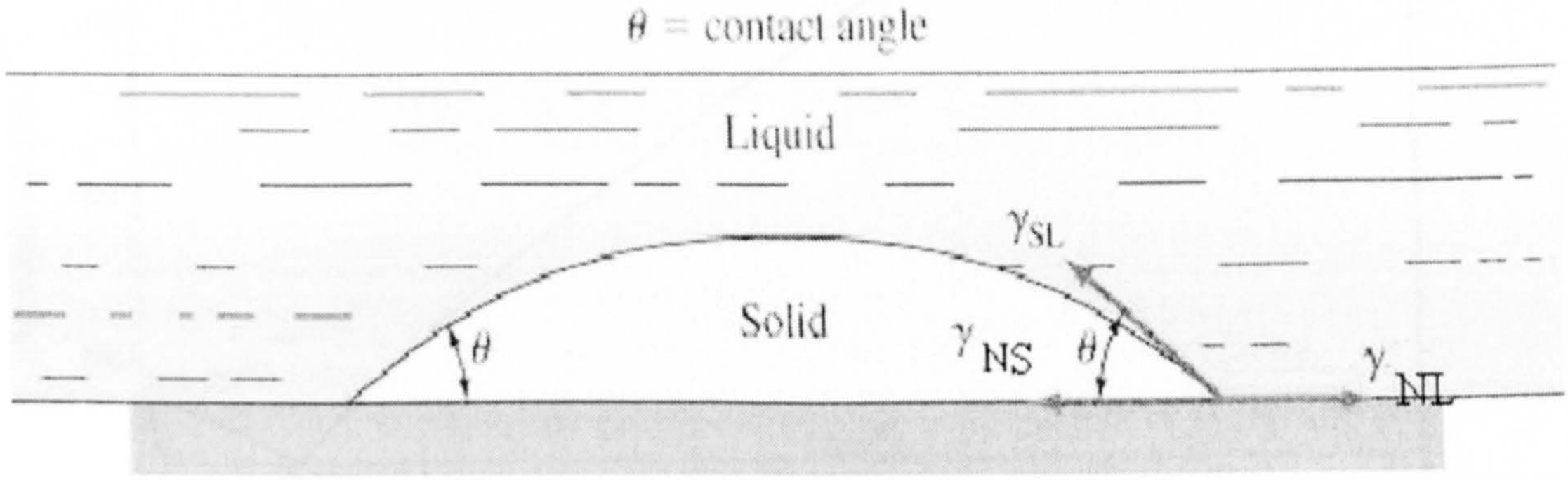

Figure 2.2 Heterogeneous nucleation of a spherical cap on a nucleating agent (Turnbull 1950 a).

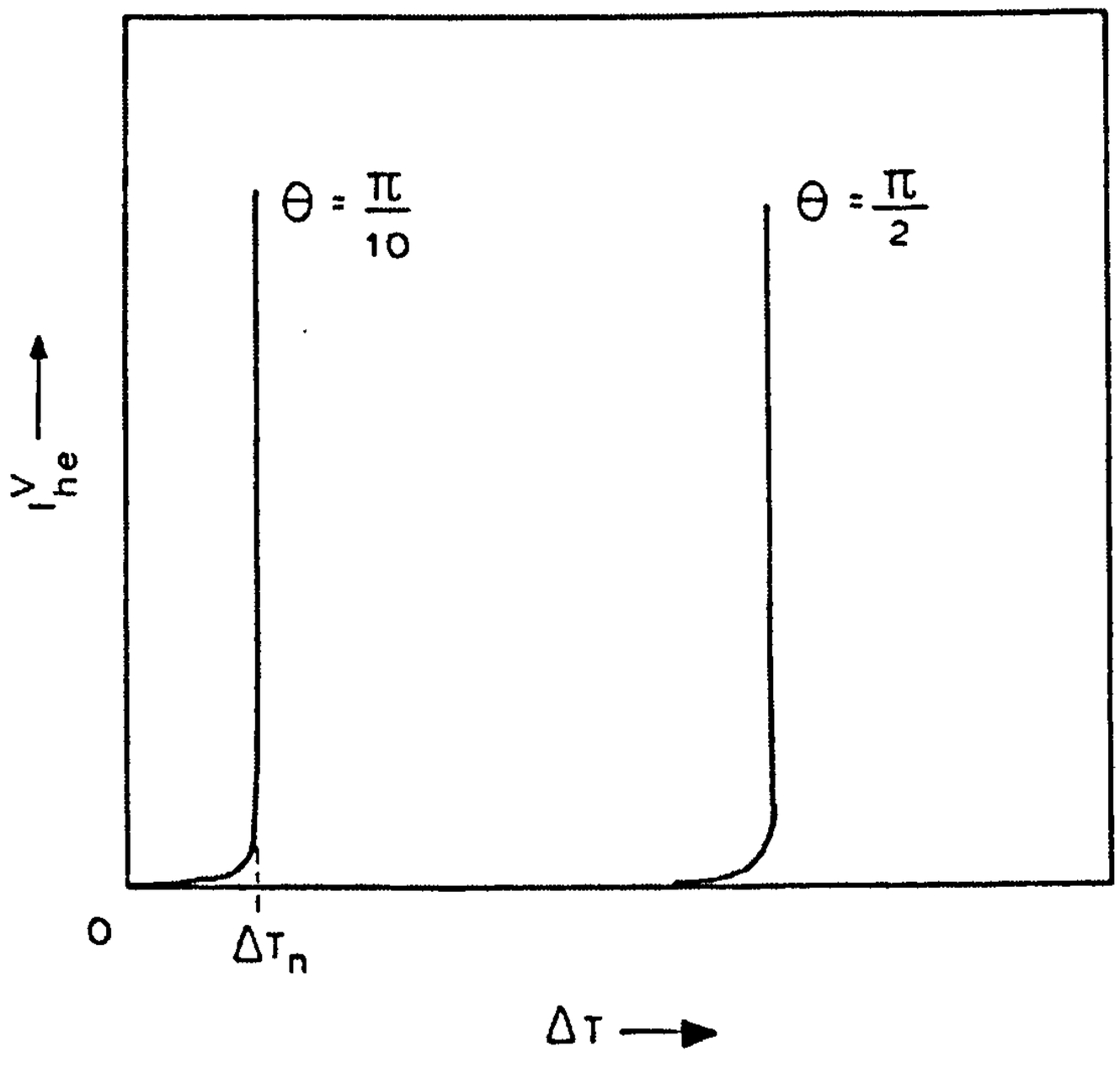

Figure 2.3 Variation of heterogenous nucleation rate (I^v_{he}) with undercooling (ΔT) for different values of contact angle (θ): ΔT_n is the critical undercooling at which I^v_{he} sharply rises which varies with θ (McCartney 1989).

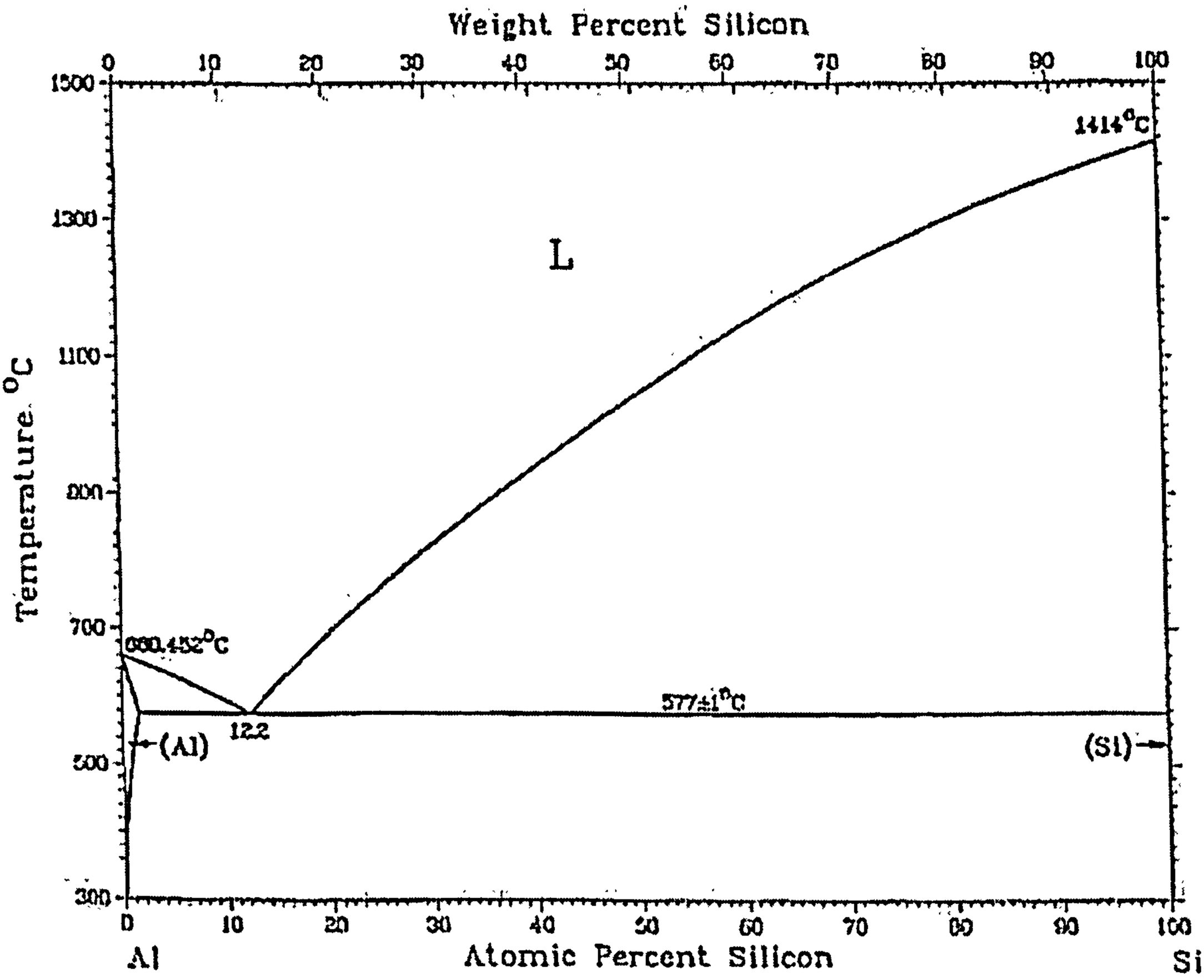

Figure 2.4 The assessed Al-Si binary phase diagram (Murray and McAlister 1984).

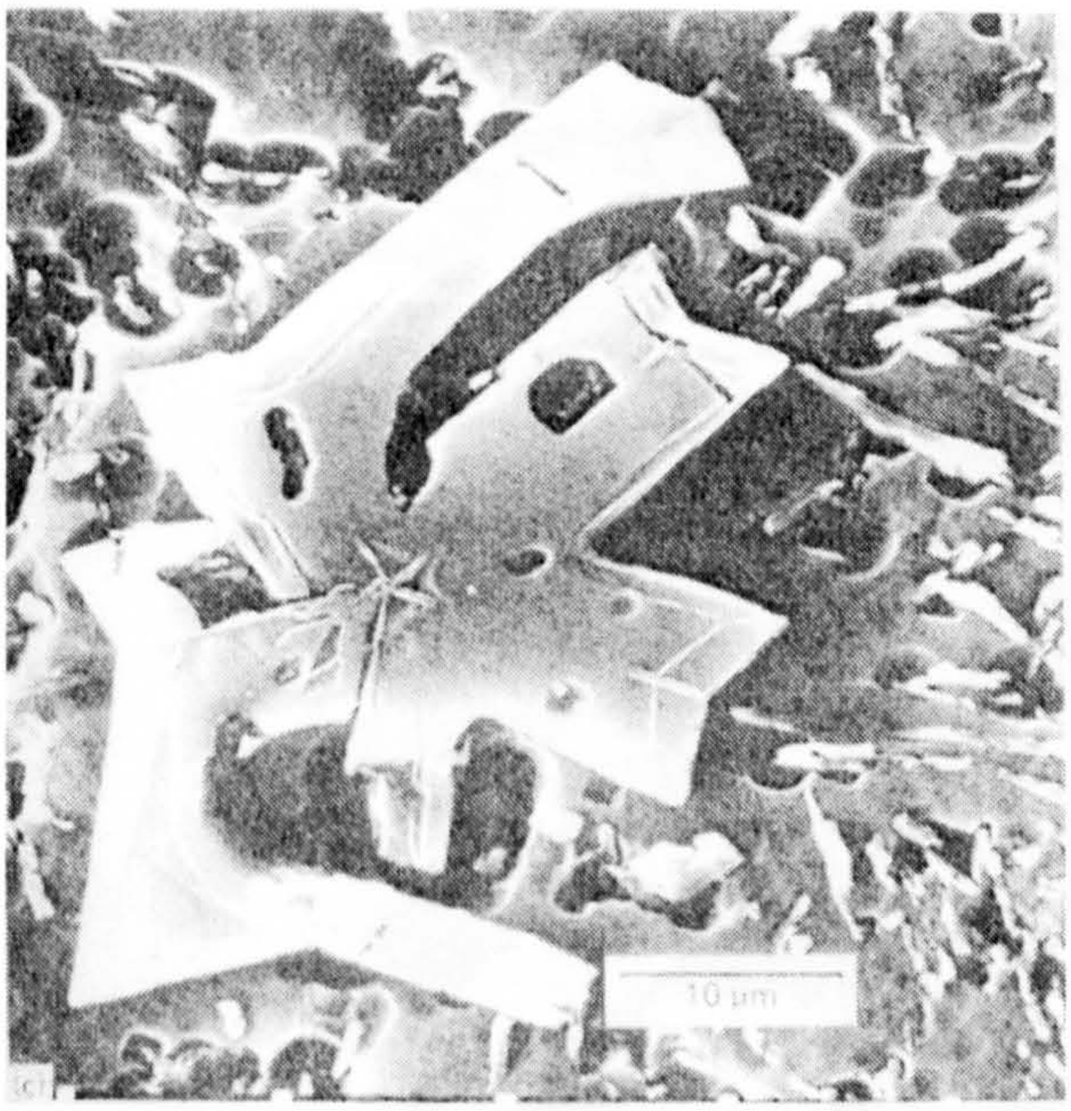

(a) Star-like

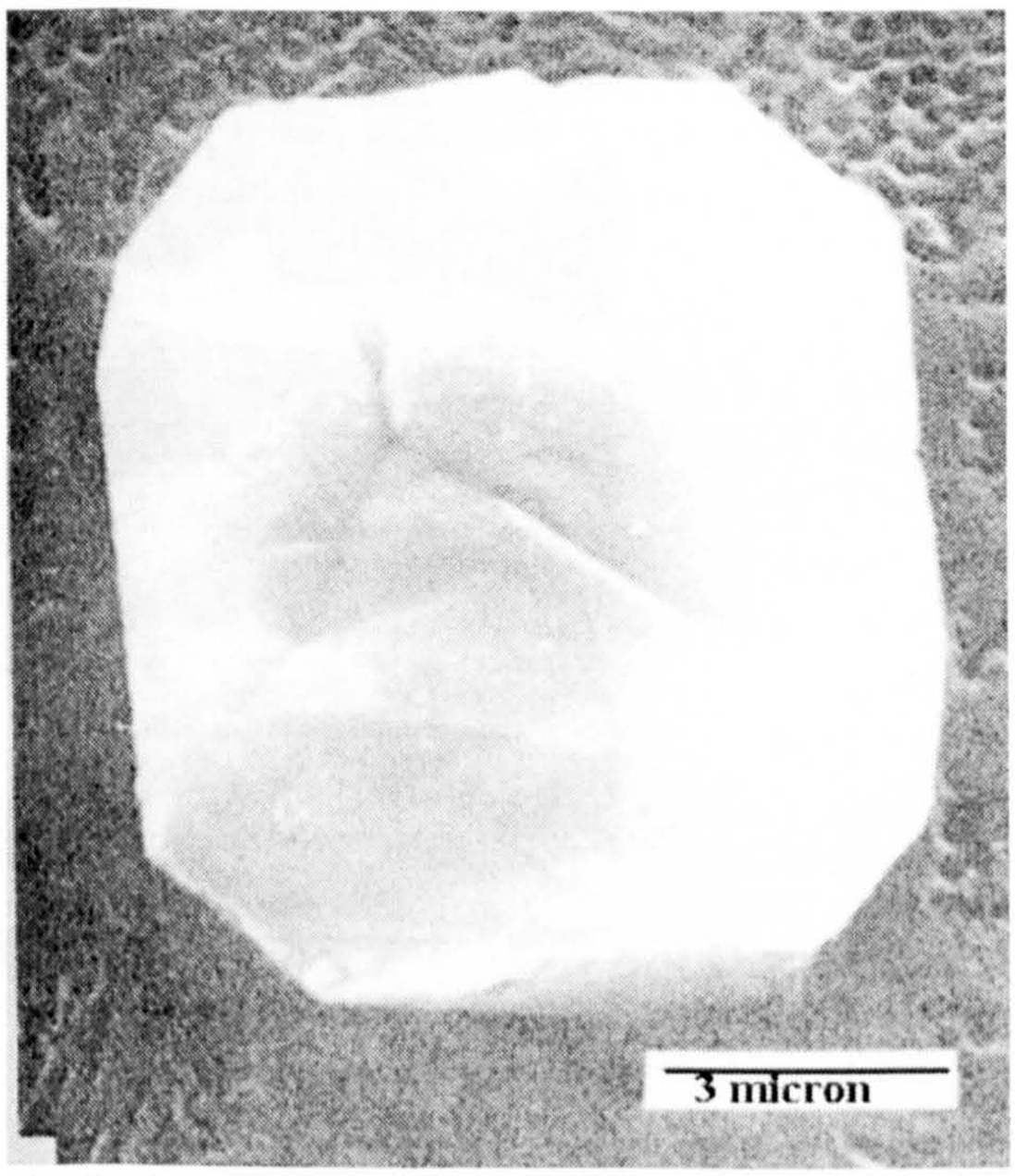

(b) Polyhedral

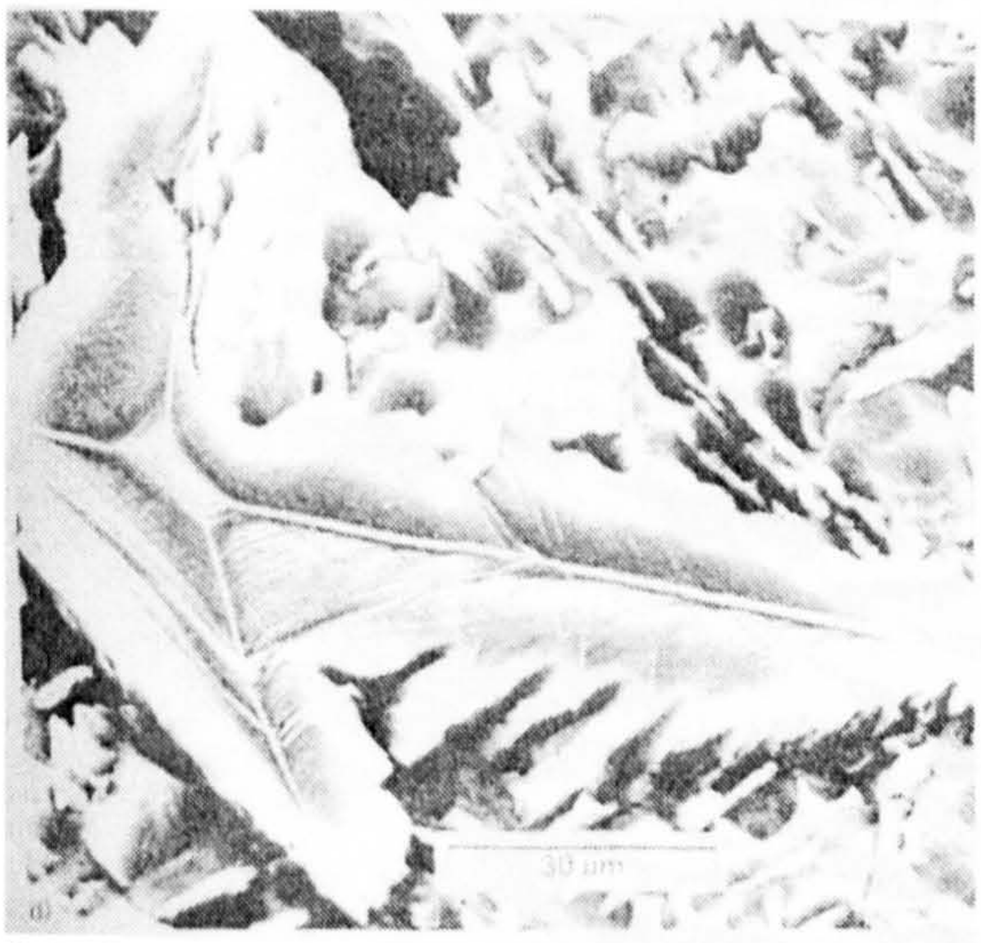

(c). Dendritic

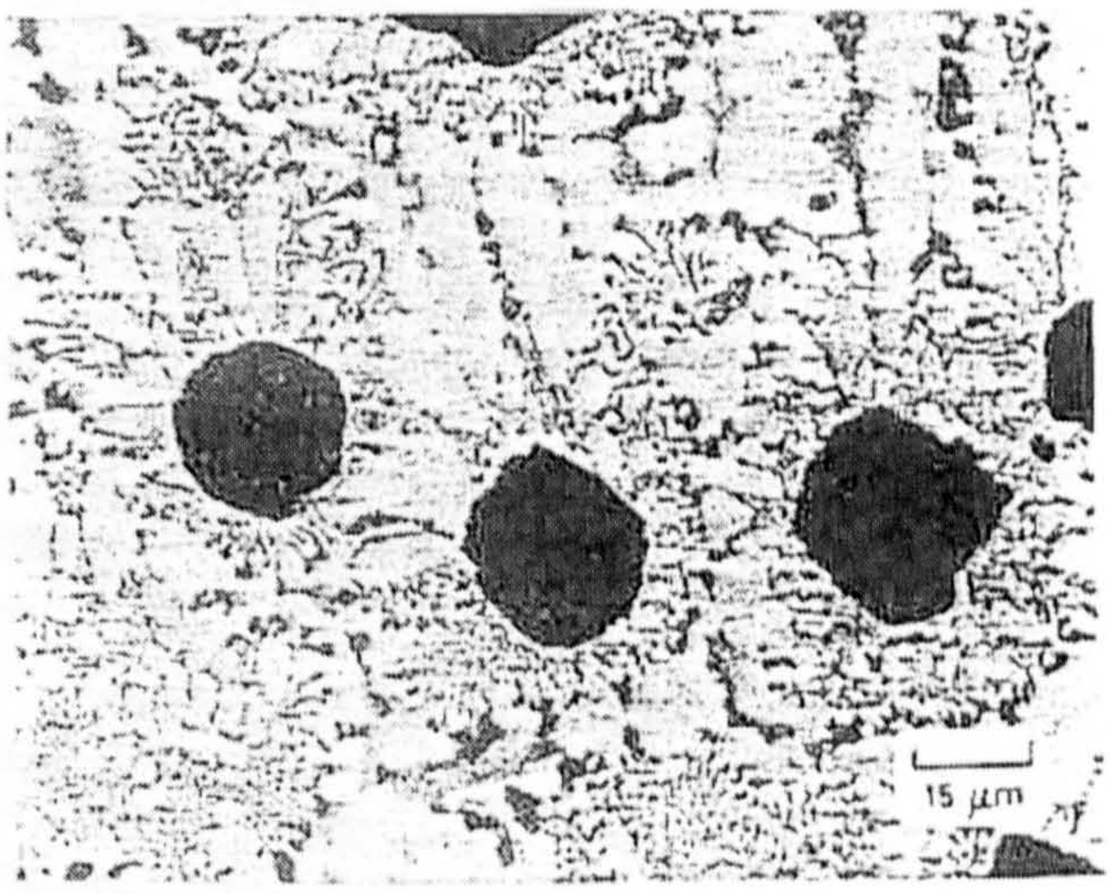

(d). Spheroidal

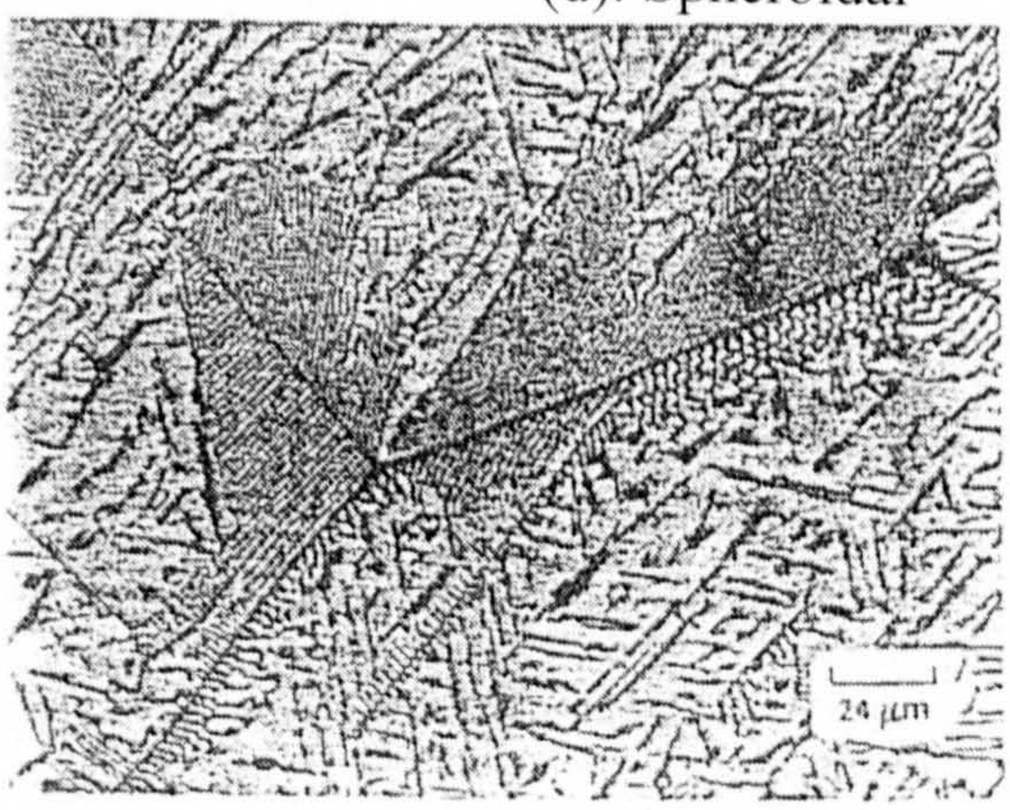

(e) Feathery

Figure 2.5 Primary silicon morphologies (Tenekedjiev and Gruzleski 1990).

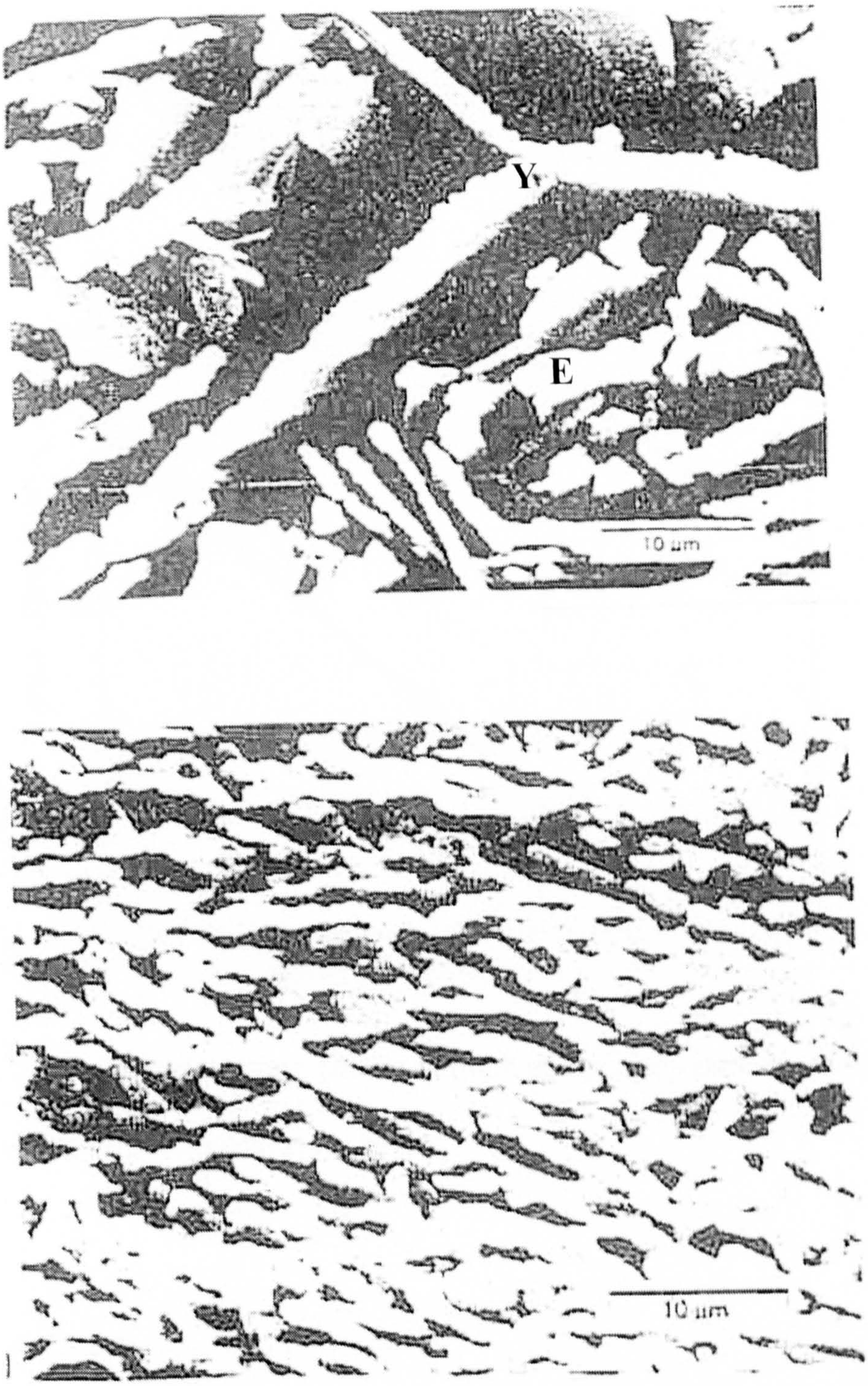

Figure 2.6 Eutectic silicon morphologies: (a) flake-like, (b) fibrous (Elliot 1984).

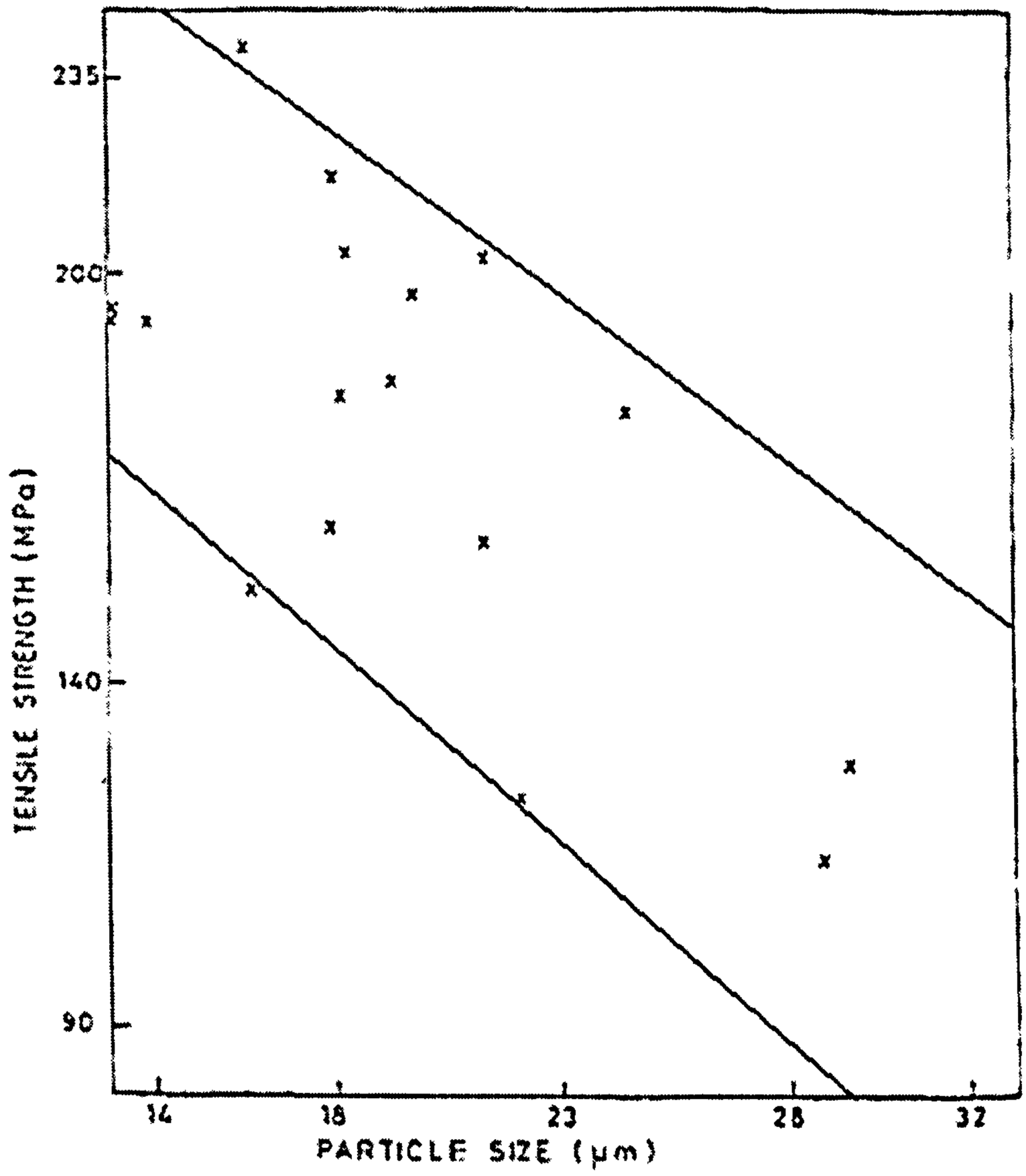

Figure 2.7 Relationship between tensile strength and primary particle size for Al-22 wt% Si (adapted from Mandal et al. 1991).

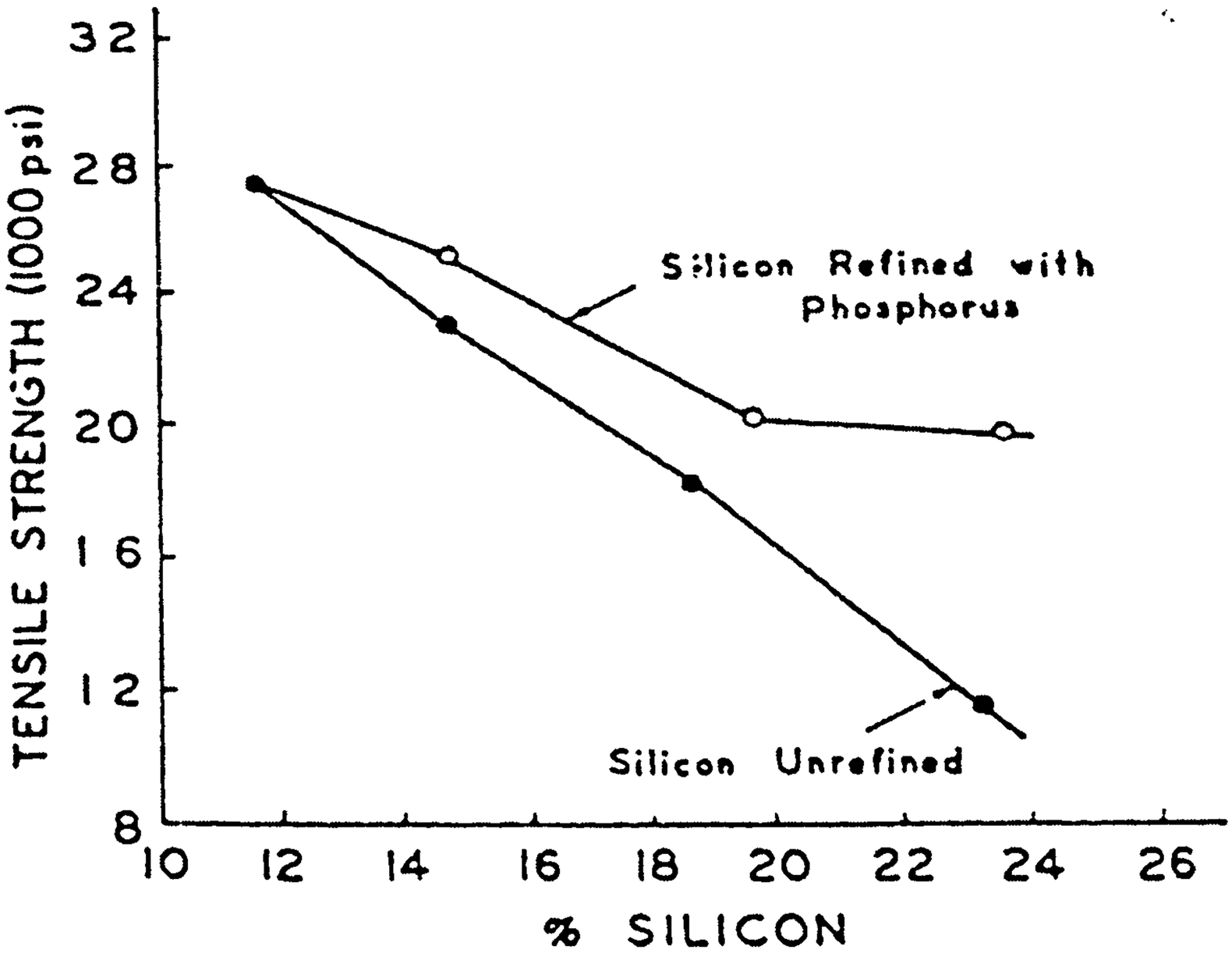

Figure 2.8 The variation in tensile strength of hypereutectic Al-Si alloys, both refined and unrefined, with silicon content (Tenekedjiev 1989).

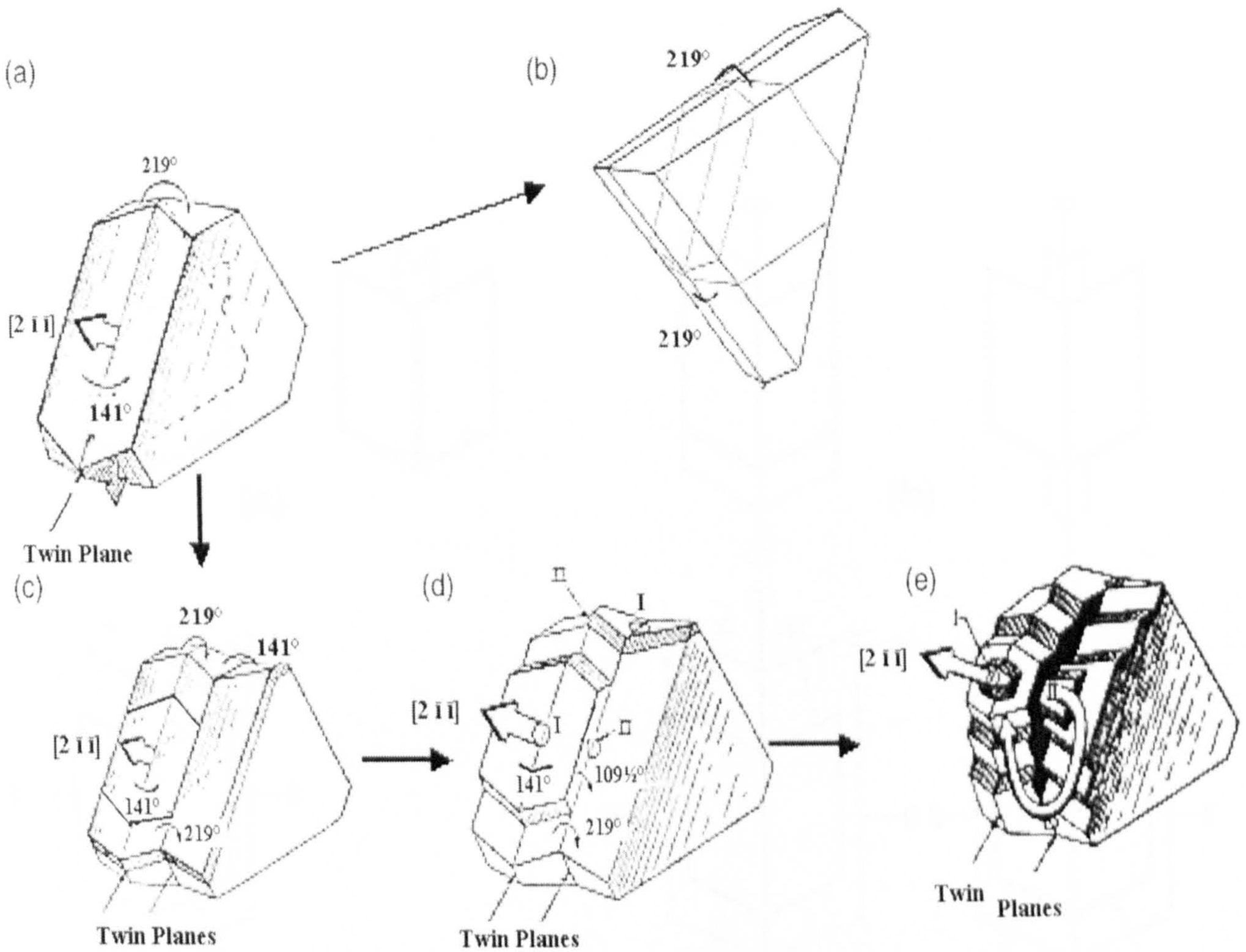

Figure 2.9 Illustrating the twin plane re-entrant edge mechanism schematically.

(a) crystal with a single twin, (b) closure of twins due to ridge formation,

(c) crystal with two twins, (d) creation of extra re-entrant corners I and II, (e) propagation of crystal due to re-entrant corners (Hamilton and Seidensticker 1960).

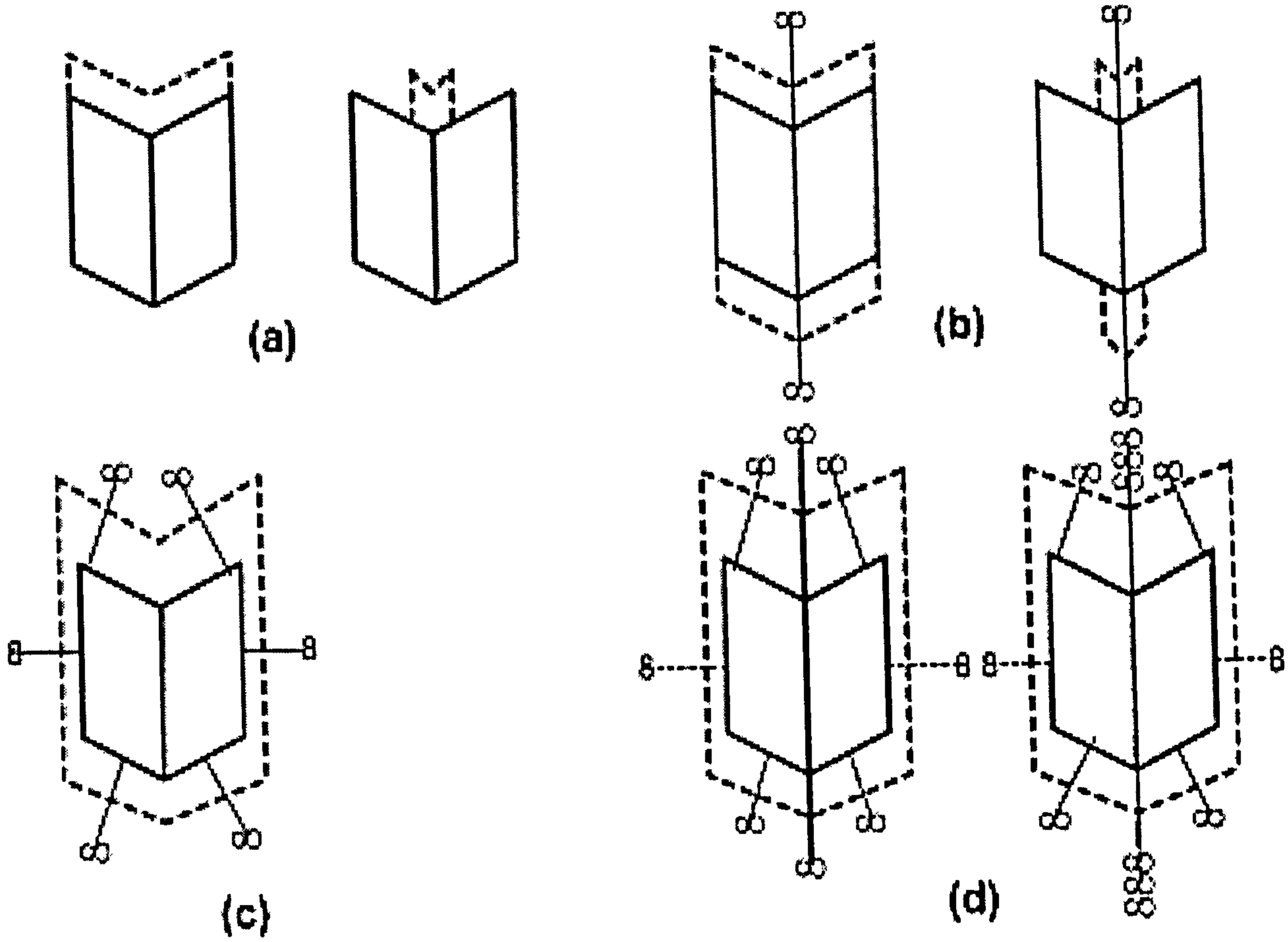

Figure 2.10 Hypothetical alignments of a screw dislocation and a re-entrant corner (Kitamura et al. 1979).

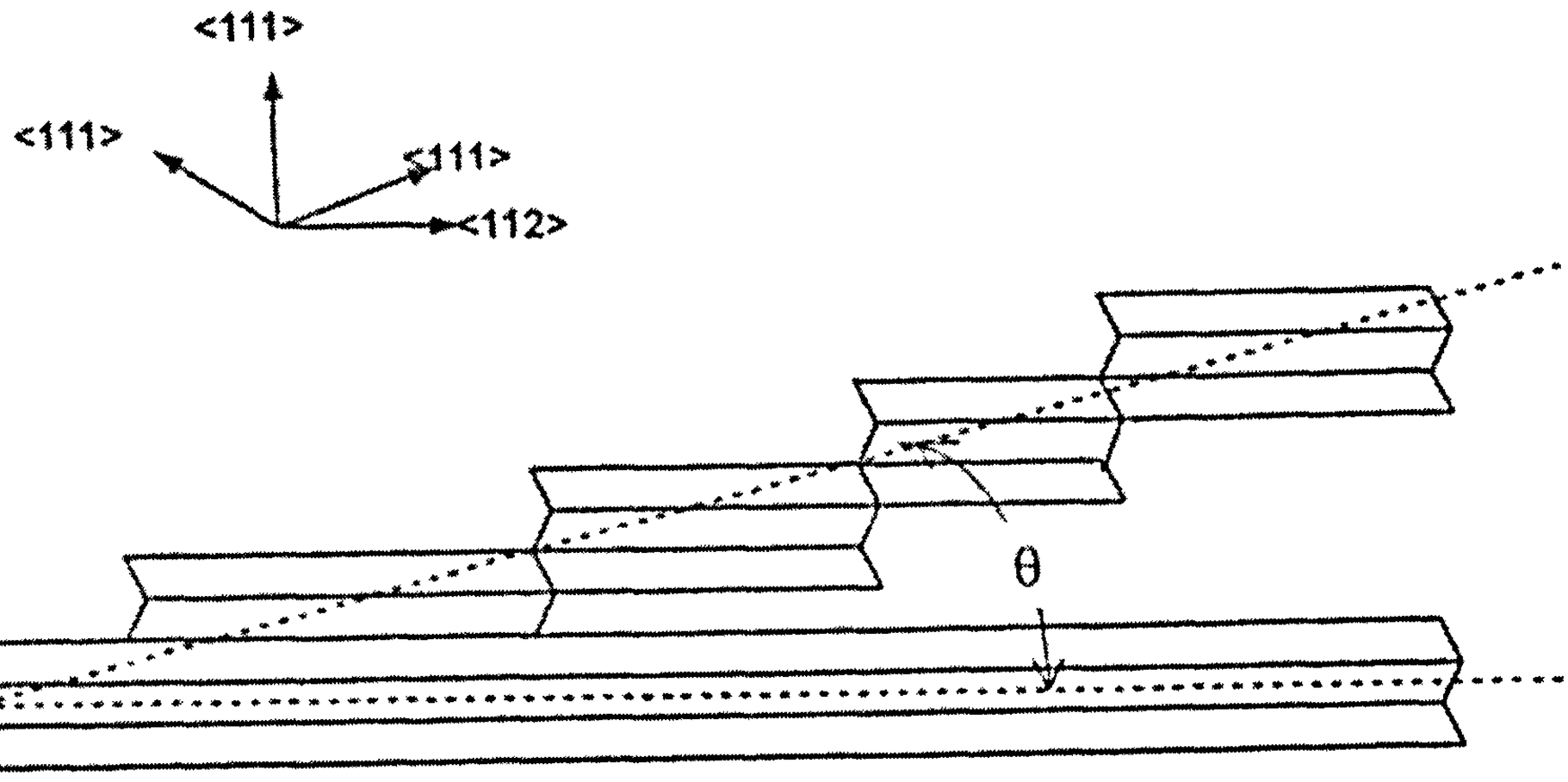

Figure 2.11 Representation of growth of flake silicon by displacement twinning (Shamsuzzoha and Hogan 1986).

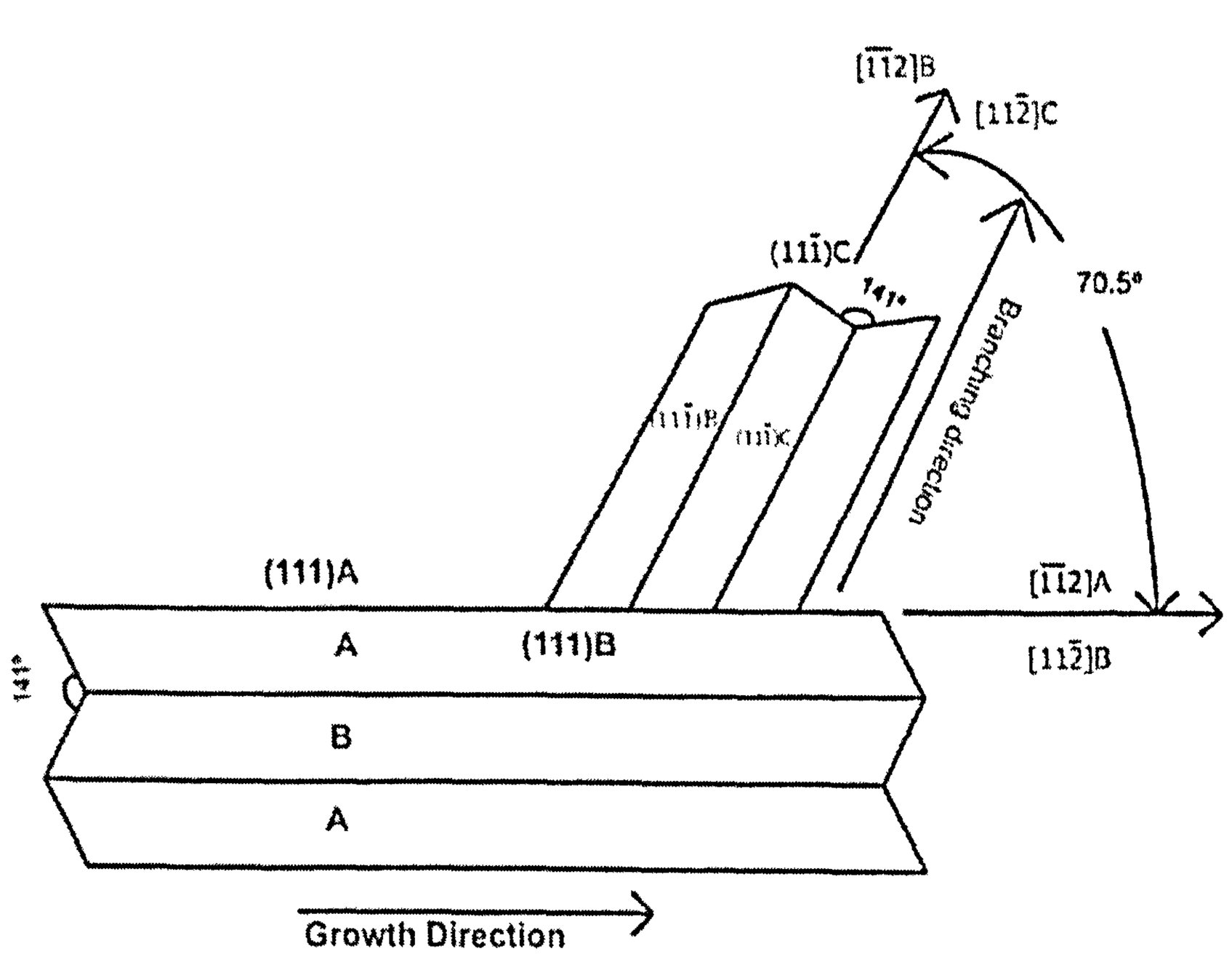

Figure 2.12 Representation of growth of flake silicon by multiple twinning (Shamsuzzoha and Hogan 1986).

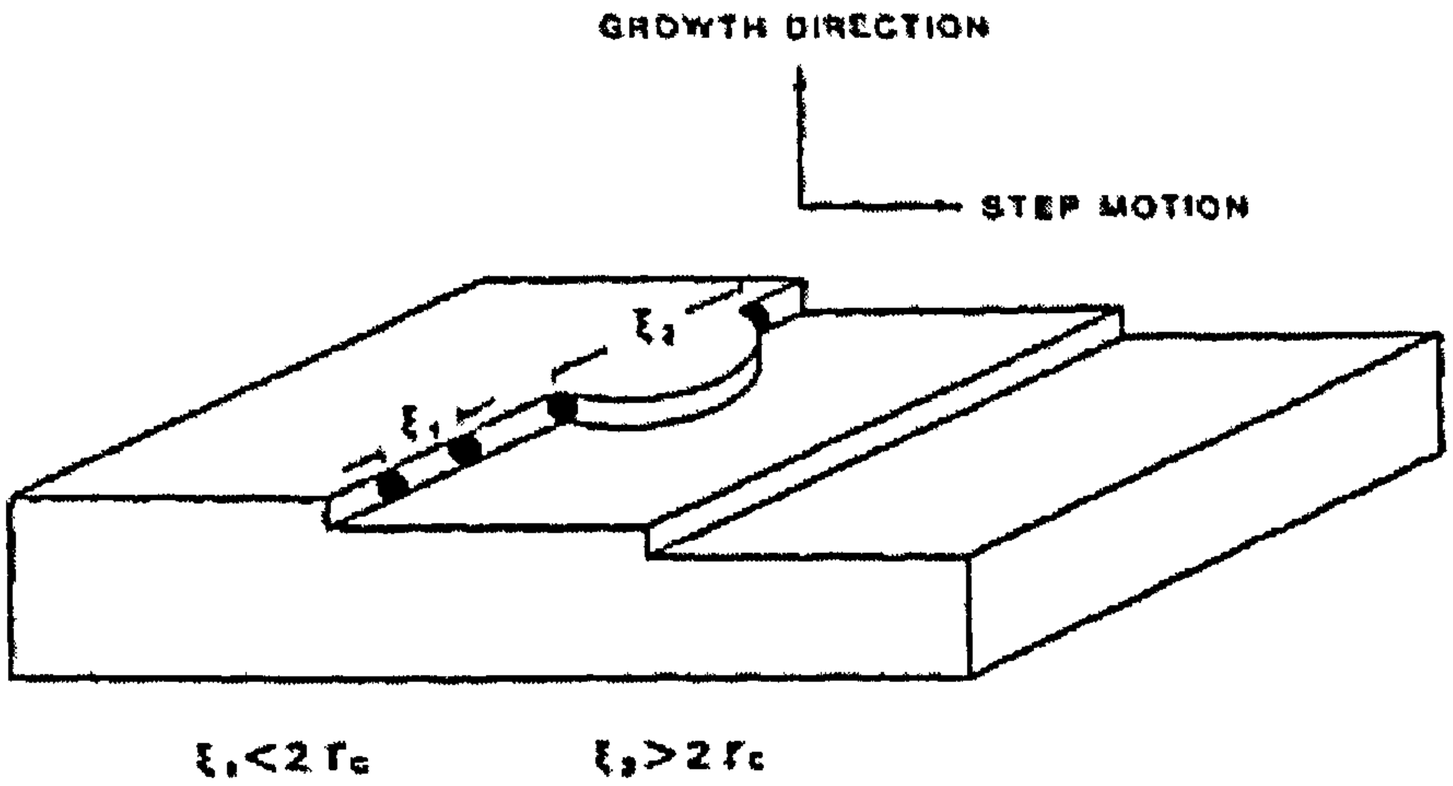

Figure 2.13 Representation of impurity atoms pinning the steps of a silicon crystal growing by the layer growth mechanism at the solid/liquid interface (Lu and Hellawell ,1987a).

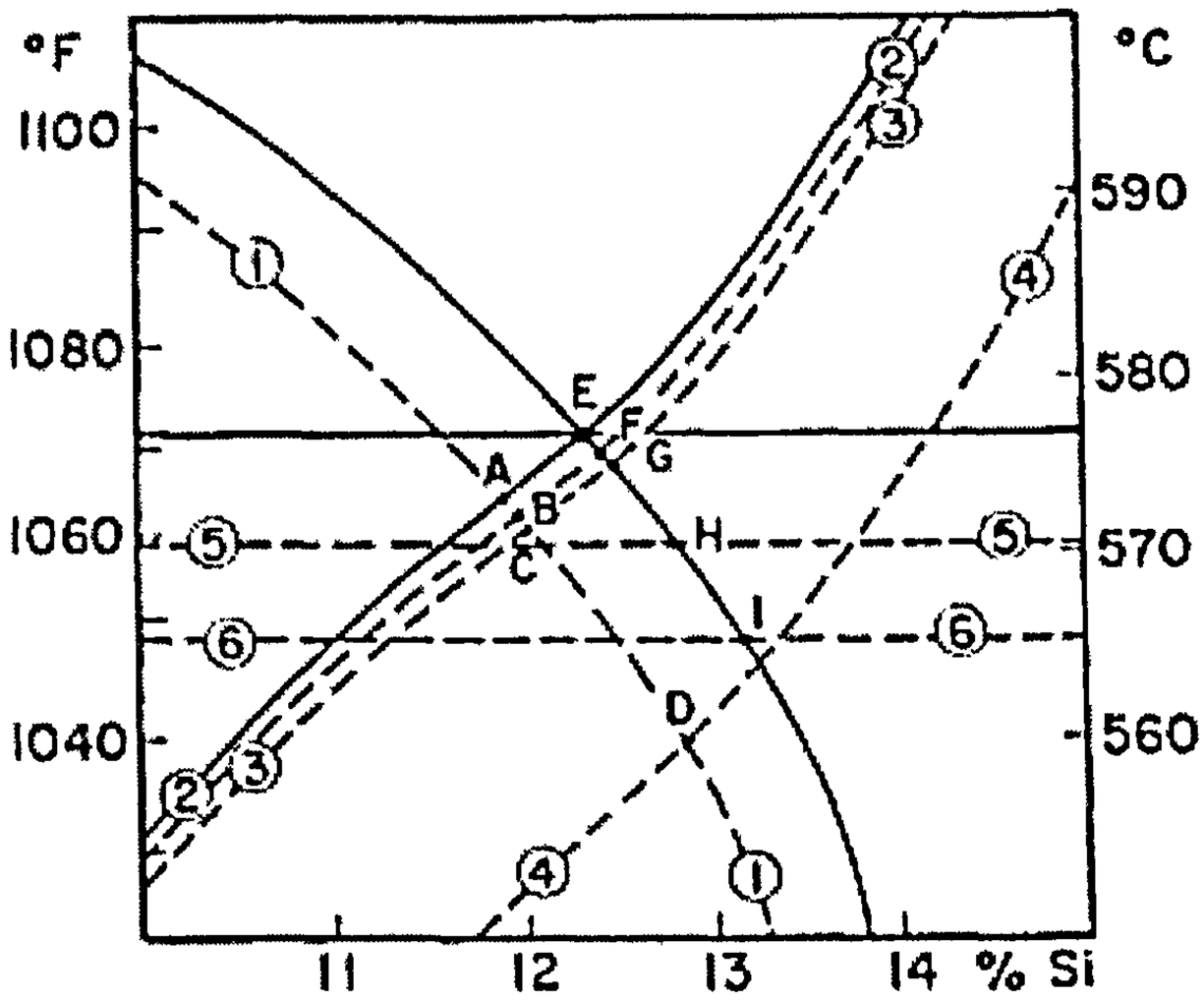

Figure 2.14 The Al–Si phase diagram with nucleation lines: (1) nucleation of aluminium by an unknown impurity, (2) nucleation of silicon by AlP, (3) nucleation of silicon by AlNaSi, (4) nucleation of silicon by an unknown impurity, (5) nucleation of silicon by aluminium, (6) nucleation of silicon by aluminium in the presence of sodium (Crosley and Mondolfo,1966).

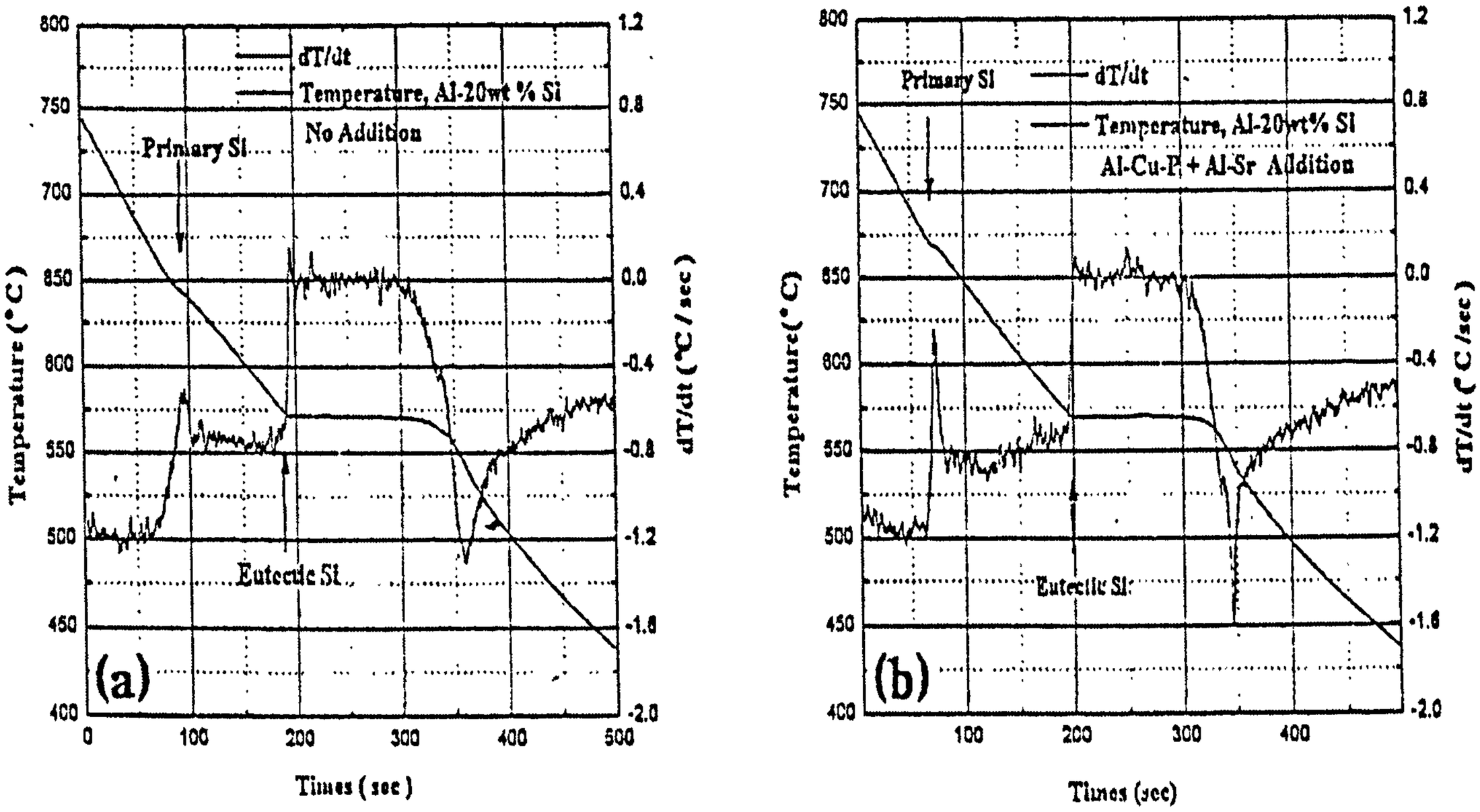

Figure 2.15 Cooling curves of Al-20 wt% Si and its derivatives, (a) No addition, (b) addition of 0.05 wt% Sr + Al-Cu-P (0.01 wt% P) (Park et al. 1995).

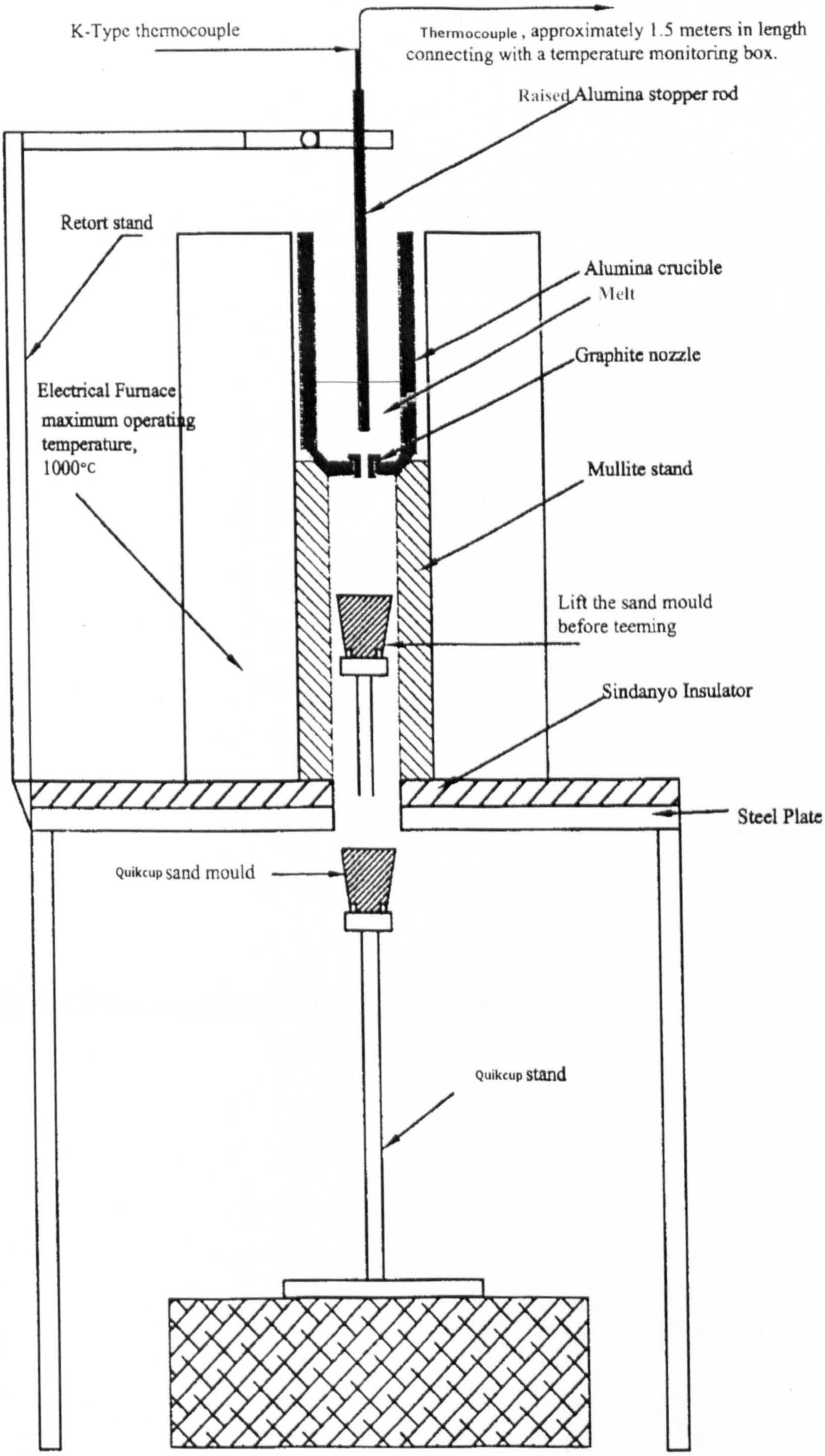

Figure 3.1 Bottom casting apparatus used in this study

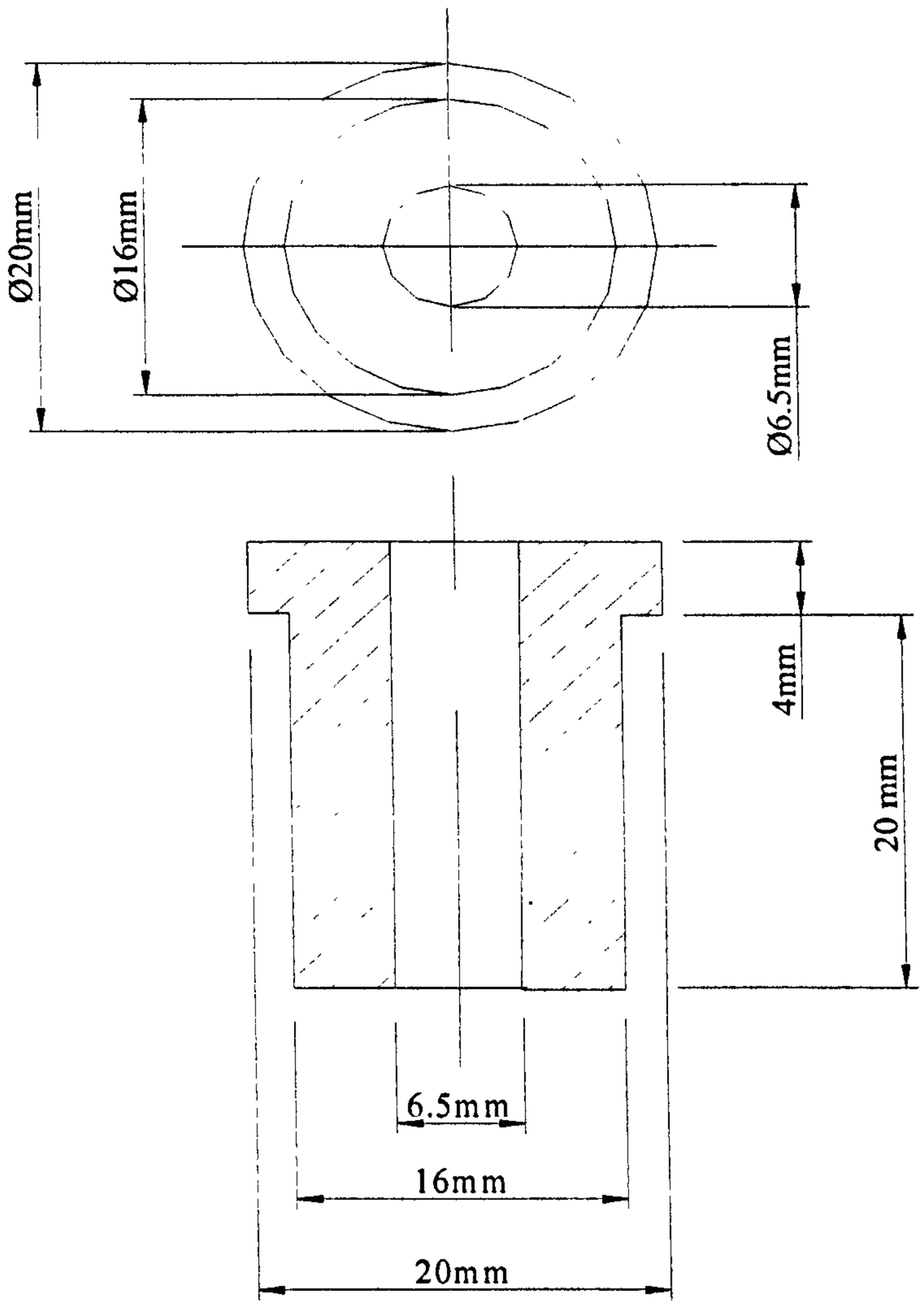

Figure 3.2 The dimensions of the graphite teeming nozzle used in this study

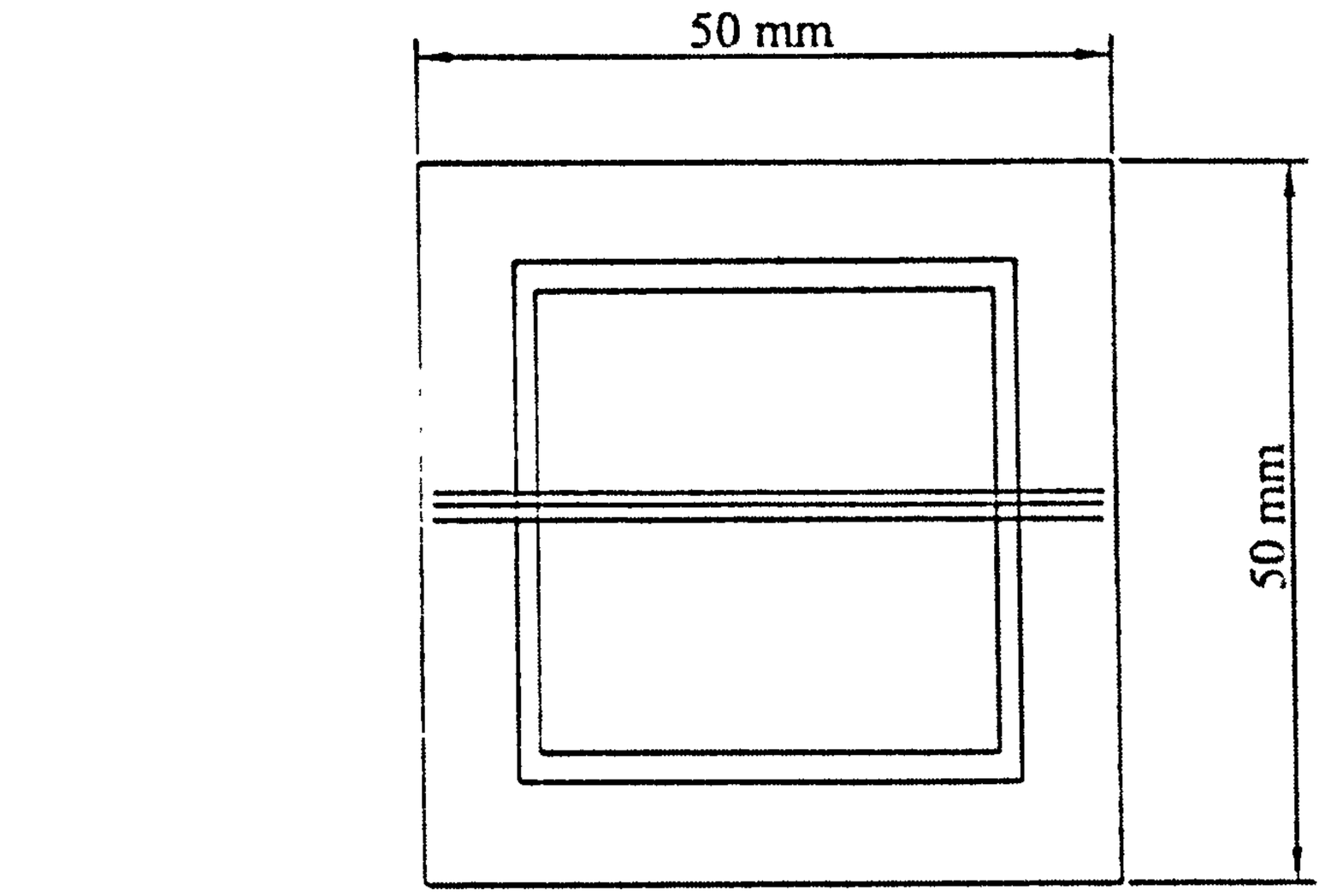

Top View

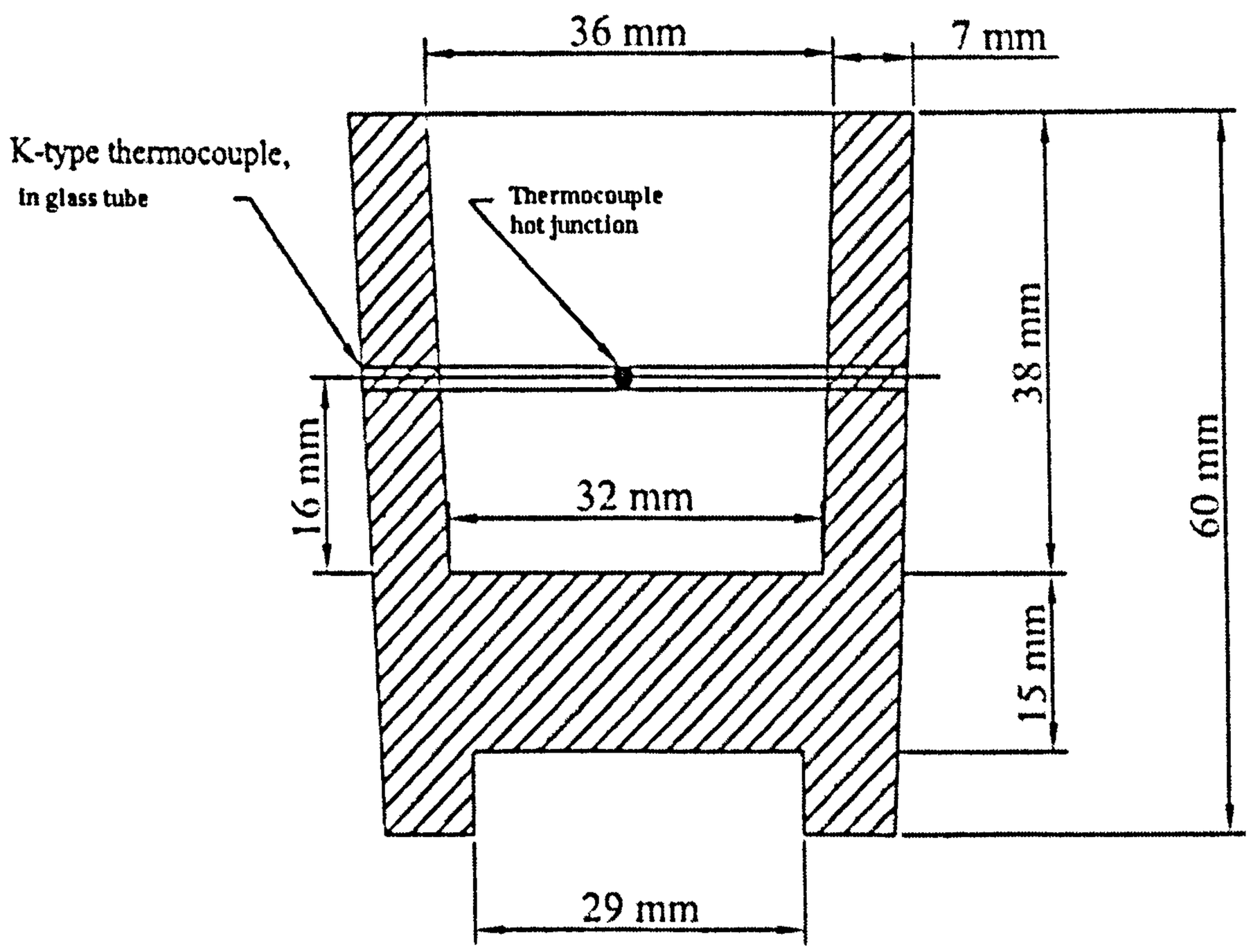

Front View

Figure 3.3 The dimensions of the Quikcup sand mould used in this study

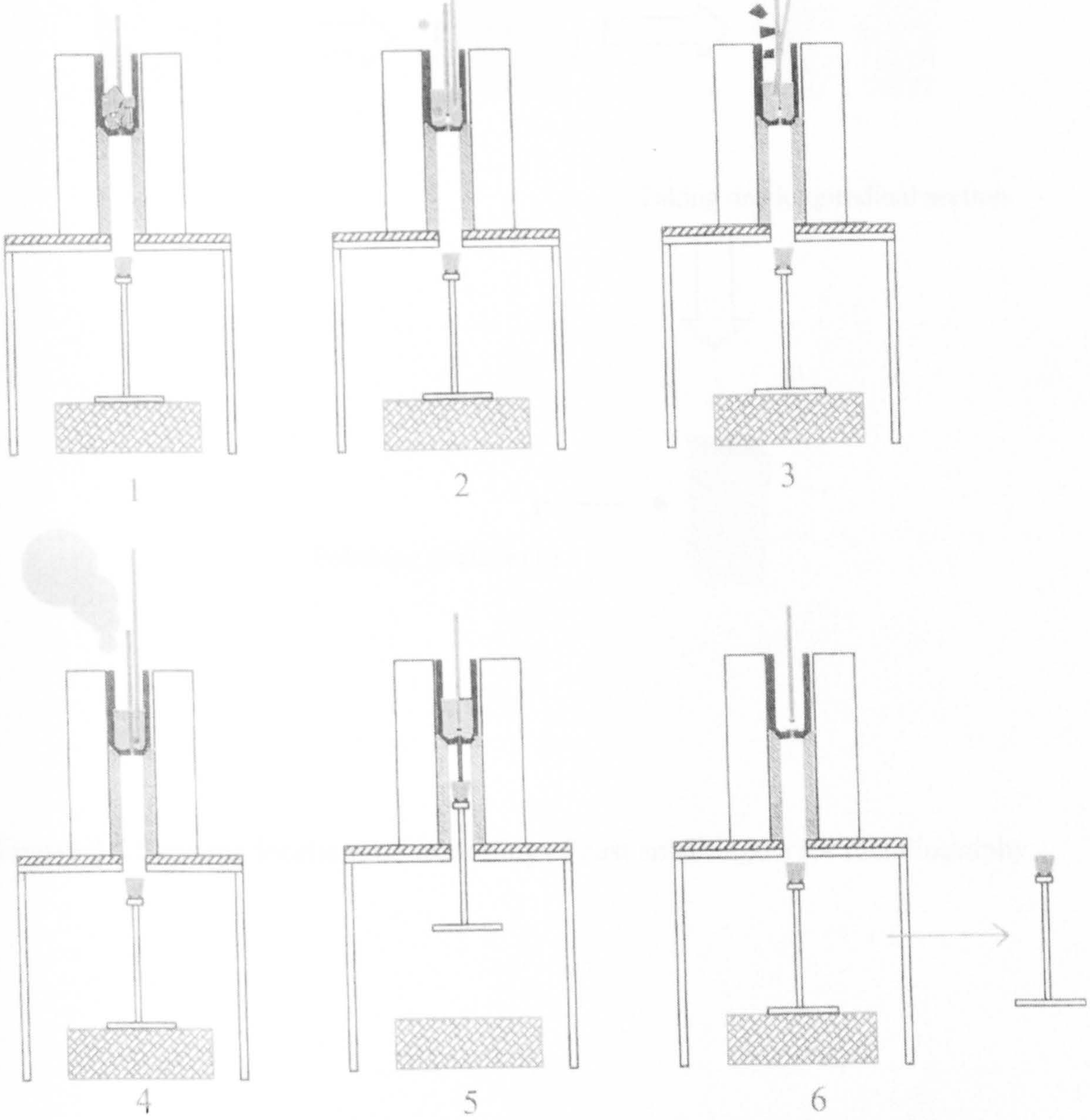

Figure 3.4 The procedure for bottom casting. (*1.* re-melting of the hypereutectic Al-Si, *2.* Adding phosphorus inoculant in Al foil, *3.* adding Al-Sr alloy, *4.* degassing with NITRAL tablets (supplied by FOSECO) , *5.* removing the stopper rod, *6.* removing the sand mould.)

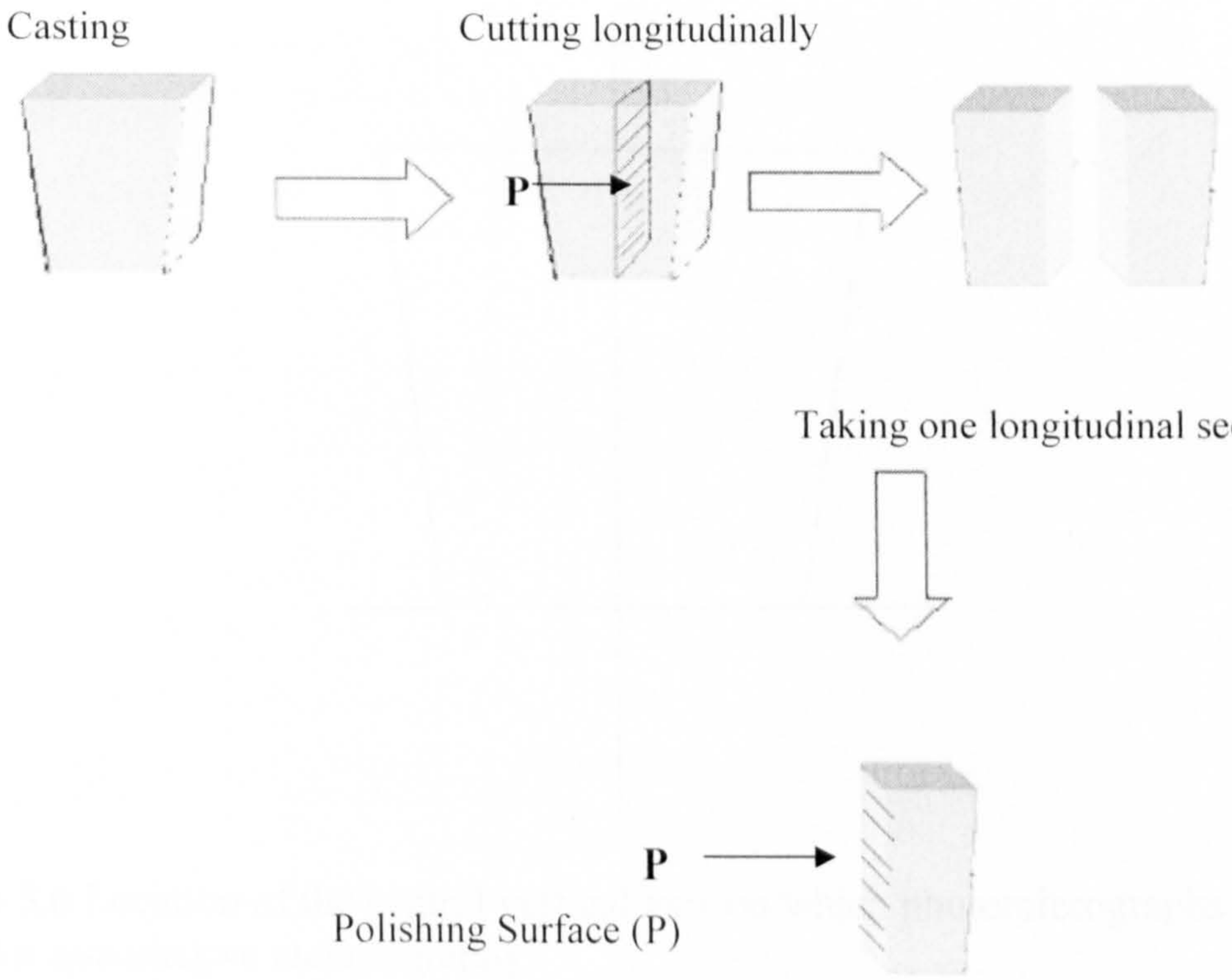

Figure 3.5 Showing locations of sectioning of cast small ingots for metallography

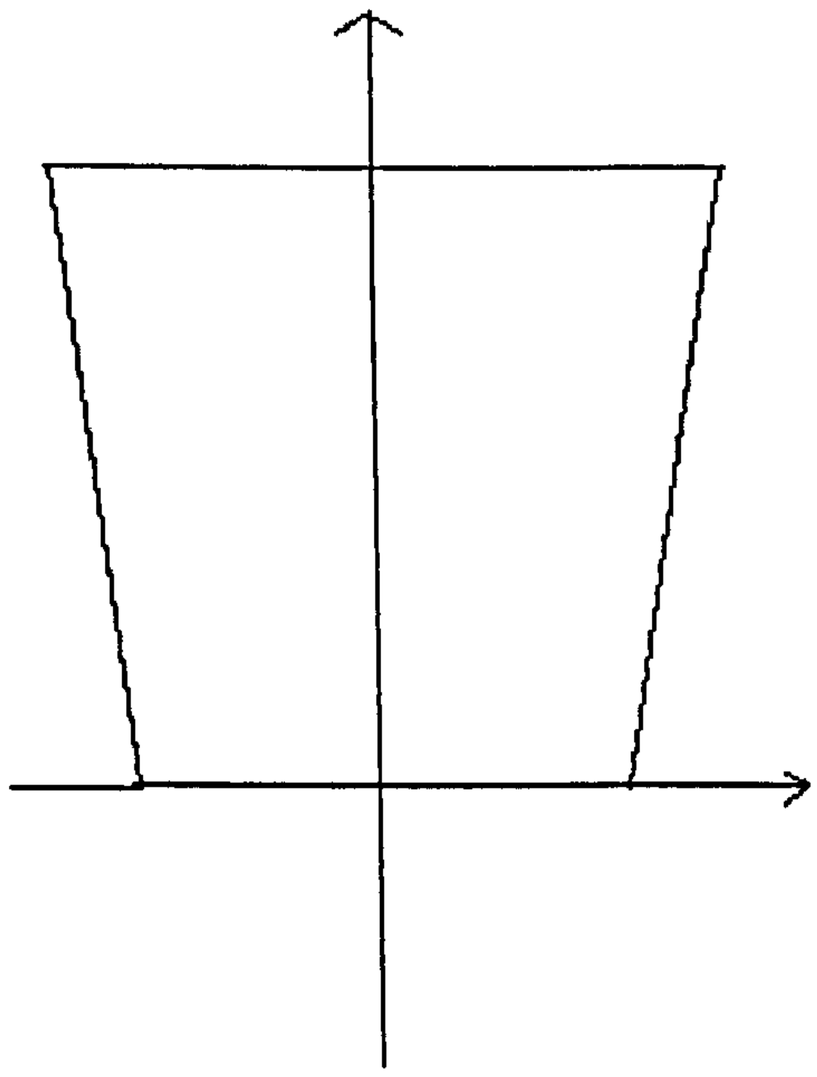

Figure 3.6 Location of the central vertical axis on which photomicrographs have been taken for quantitative metallography.

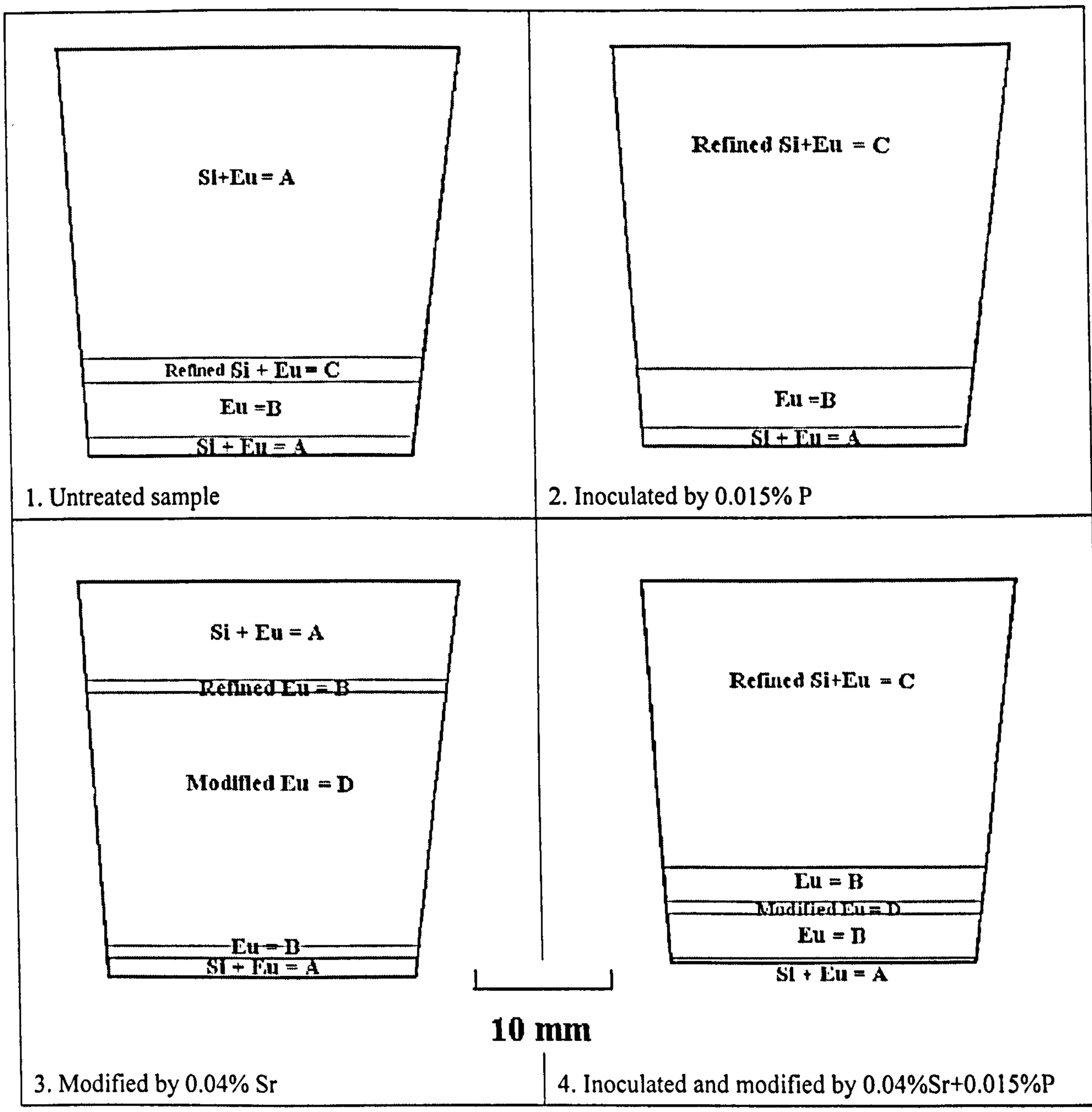

Fig 4.1 Distribution of phases in ingot: Si = Primary Si; Eu = Al-Si eutectic.

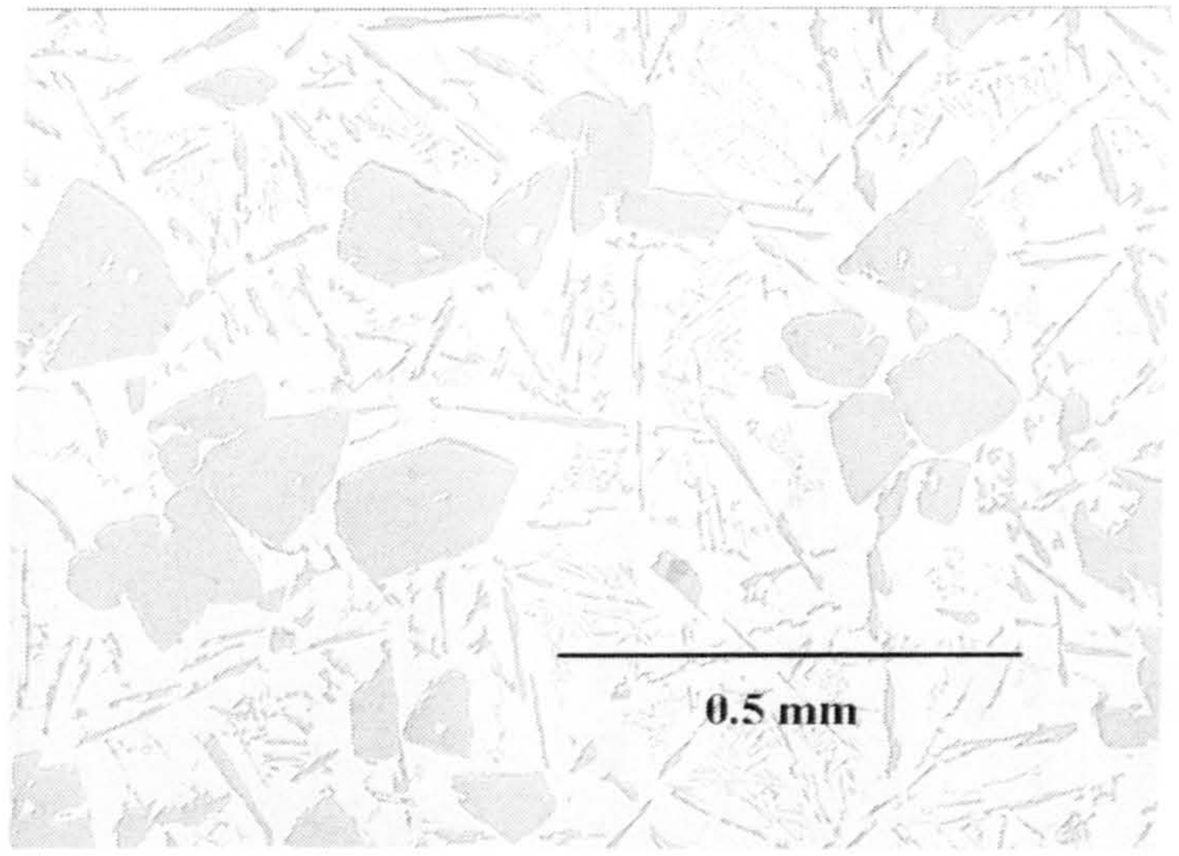

a: Large primary Si + coarse eutectic = A

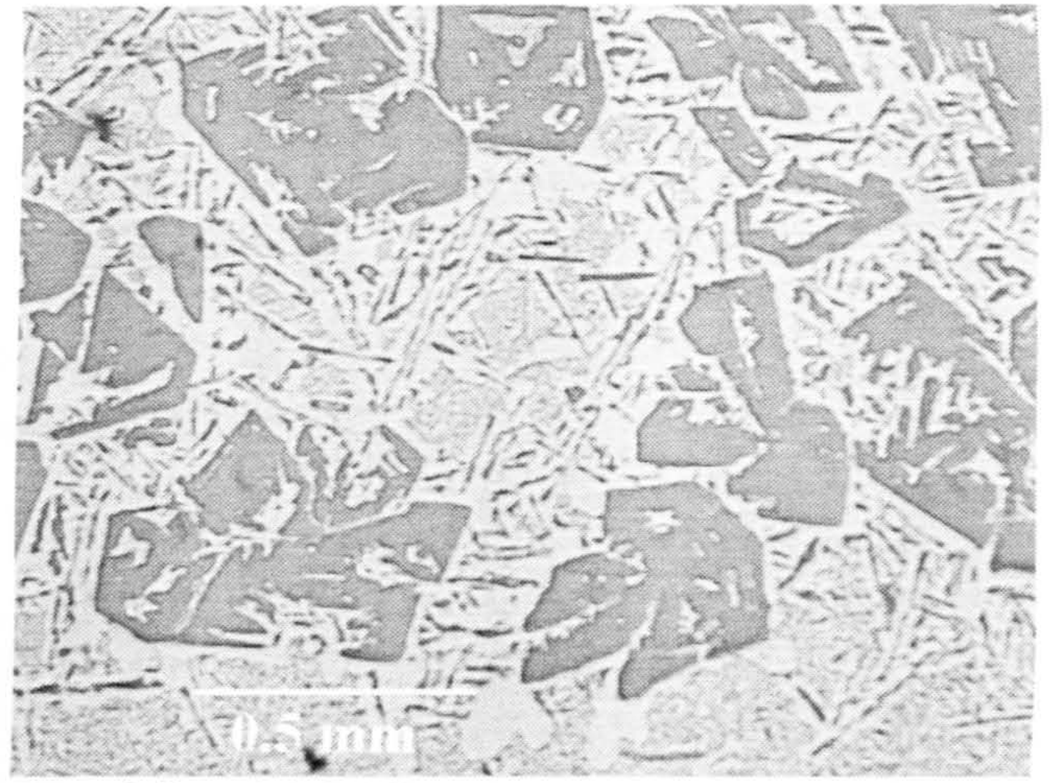

By adding 0.04%Sr

b: Branched primary Si + coarse eutectic

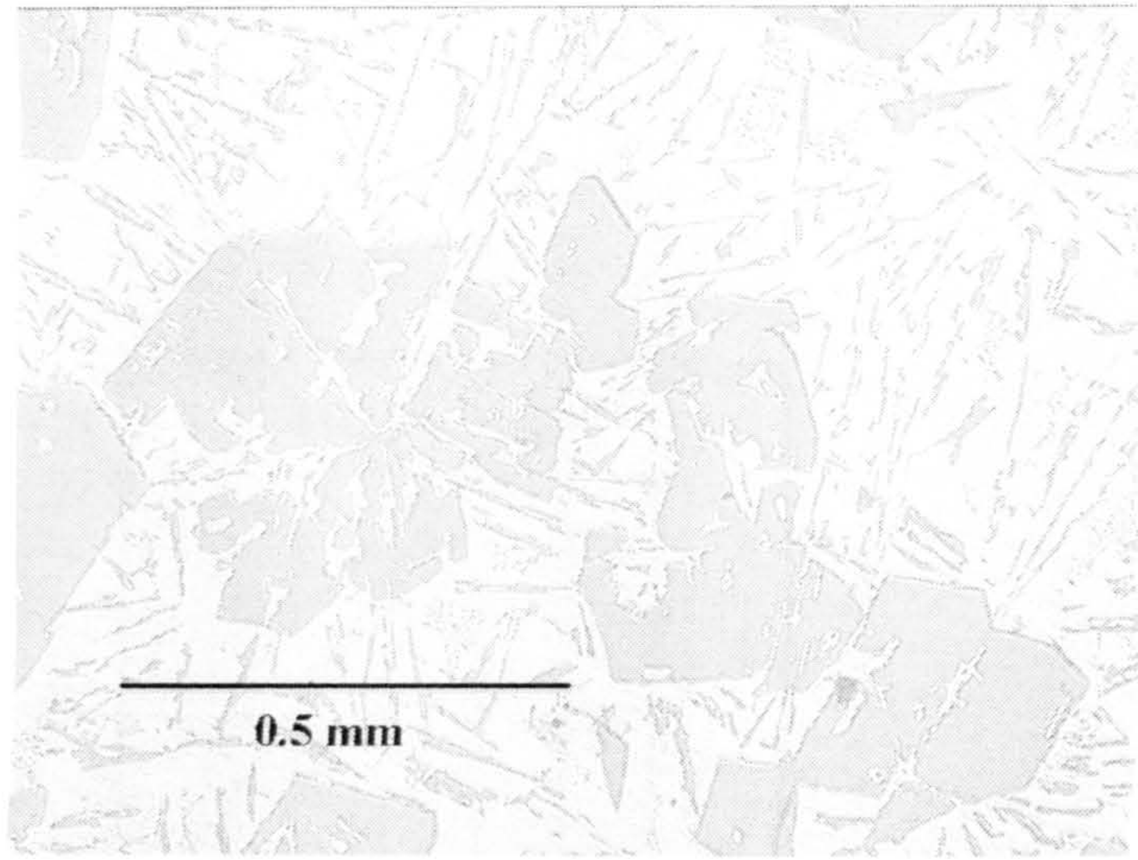

c: By adding 0.2%Sr, more branched primary Si

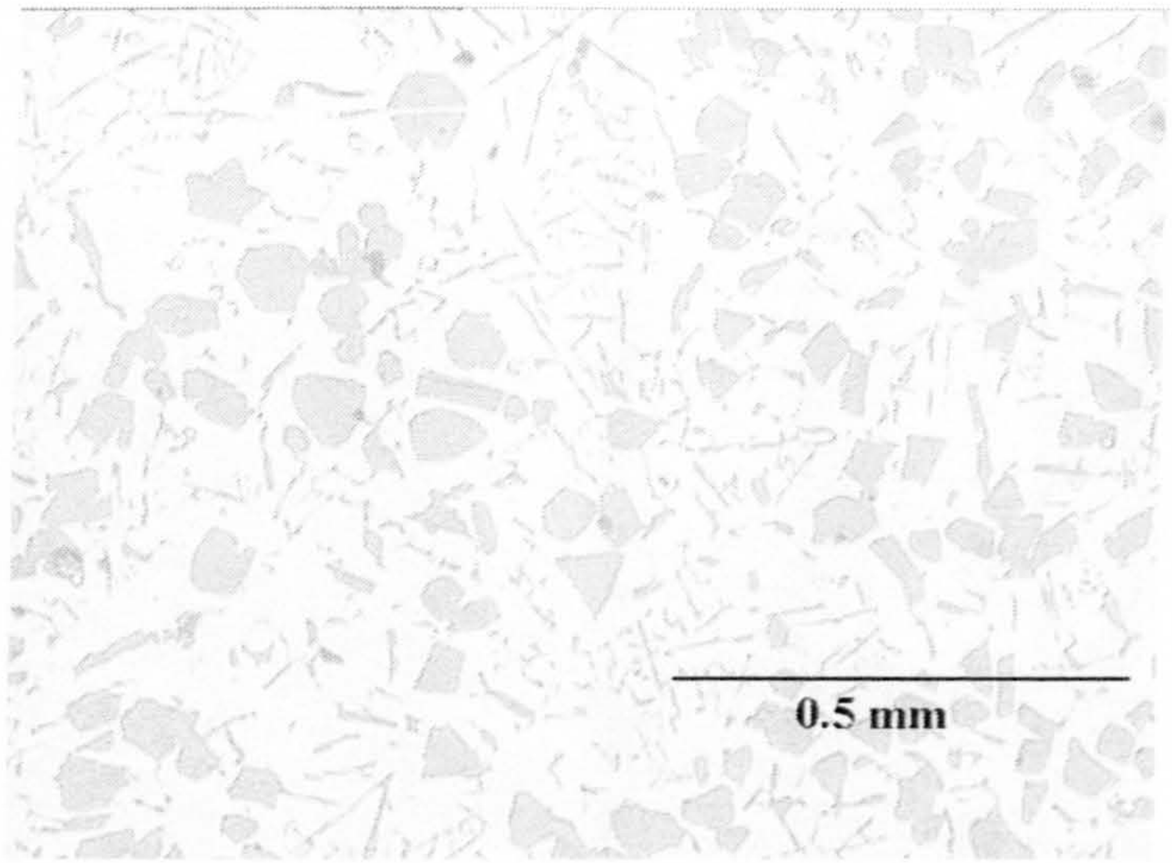

d: Refined primary Si + coarse eutectic = C

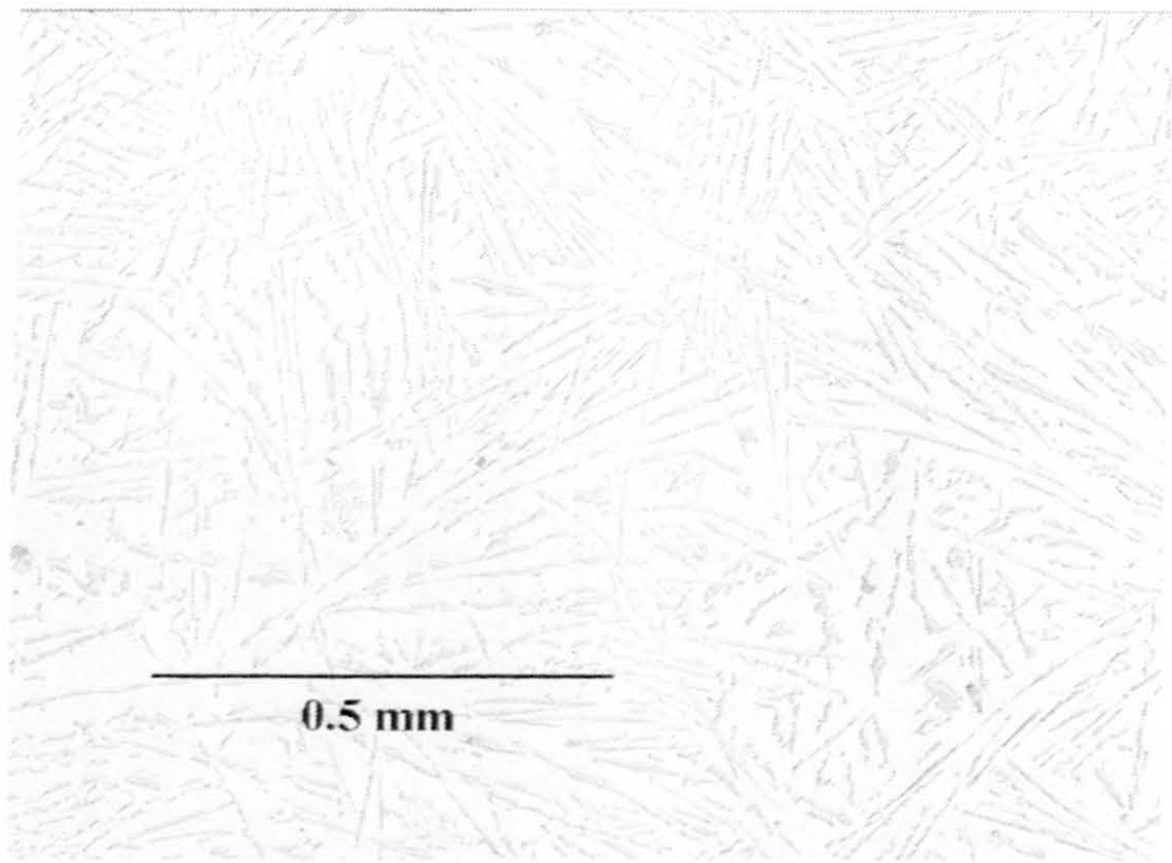

e: Coarse eutectic = B

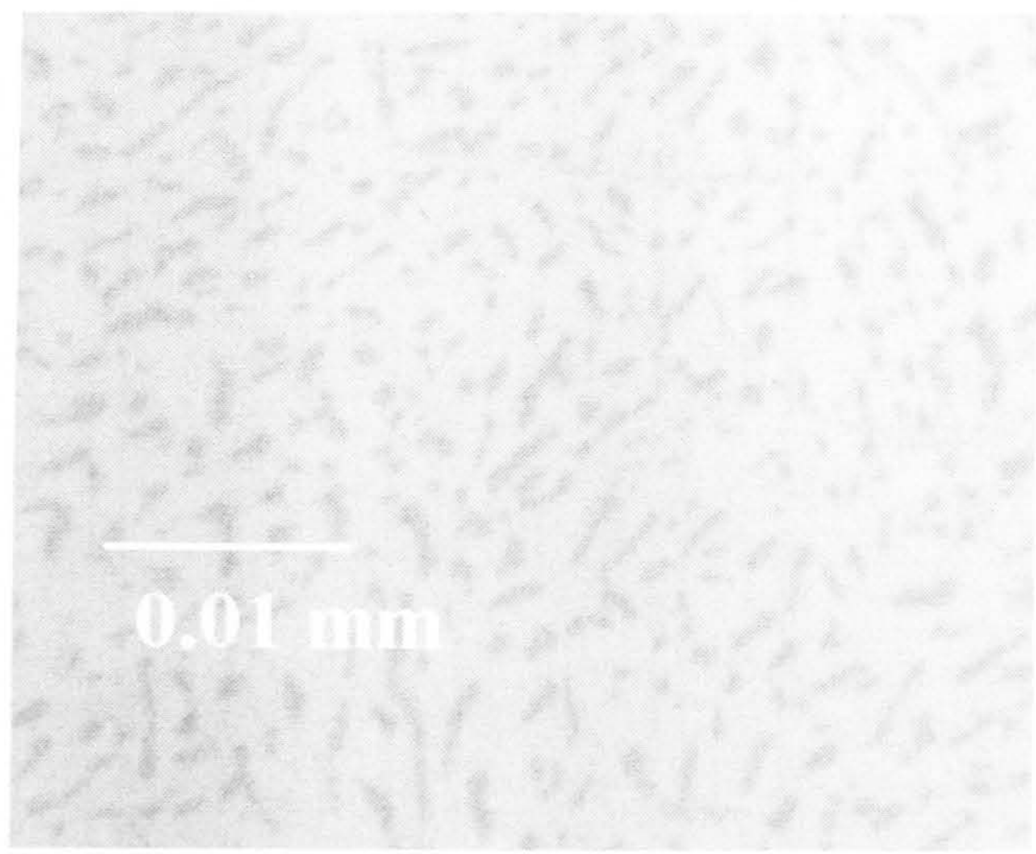

f: Modified eutectic = D

Figure 4.2 Typical microstructures (These photos are taken from the following samples, and have been chosen because they were the most representative of the mentioned morphologies, t.c. is the symbol for the position of thermocouple –both x & y directions- which was centred in the ingots).
a: C3, 4 mm above the t.c., b: B1: about 15 mm above the centre, c: C11, 17.5 mm above the t.c., d: C7, 10 mm below the t.c., e: C3, 17 mm below the t.c., f: C10, 10 mm below the t.c. (conditions are given in table 3.6).

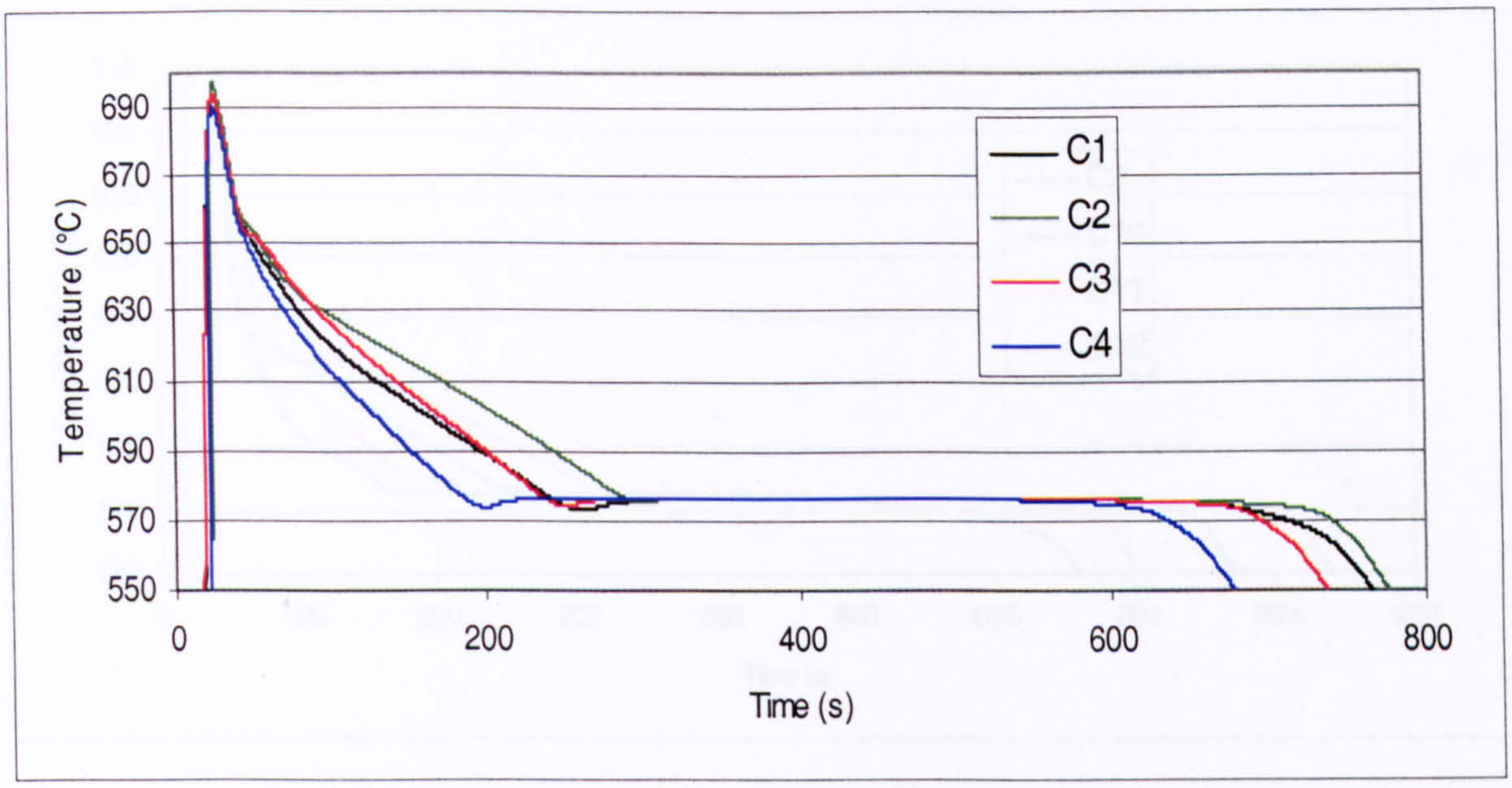

Figure 4.3 The cooling curves for uninoculated samples (Table 3.6).

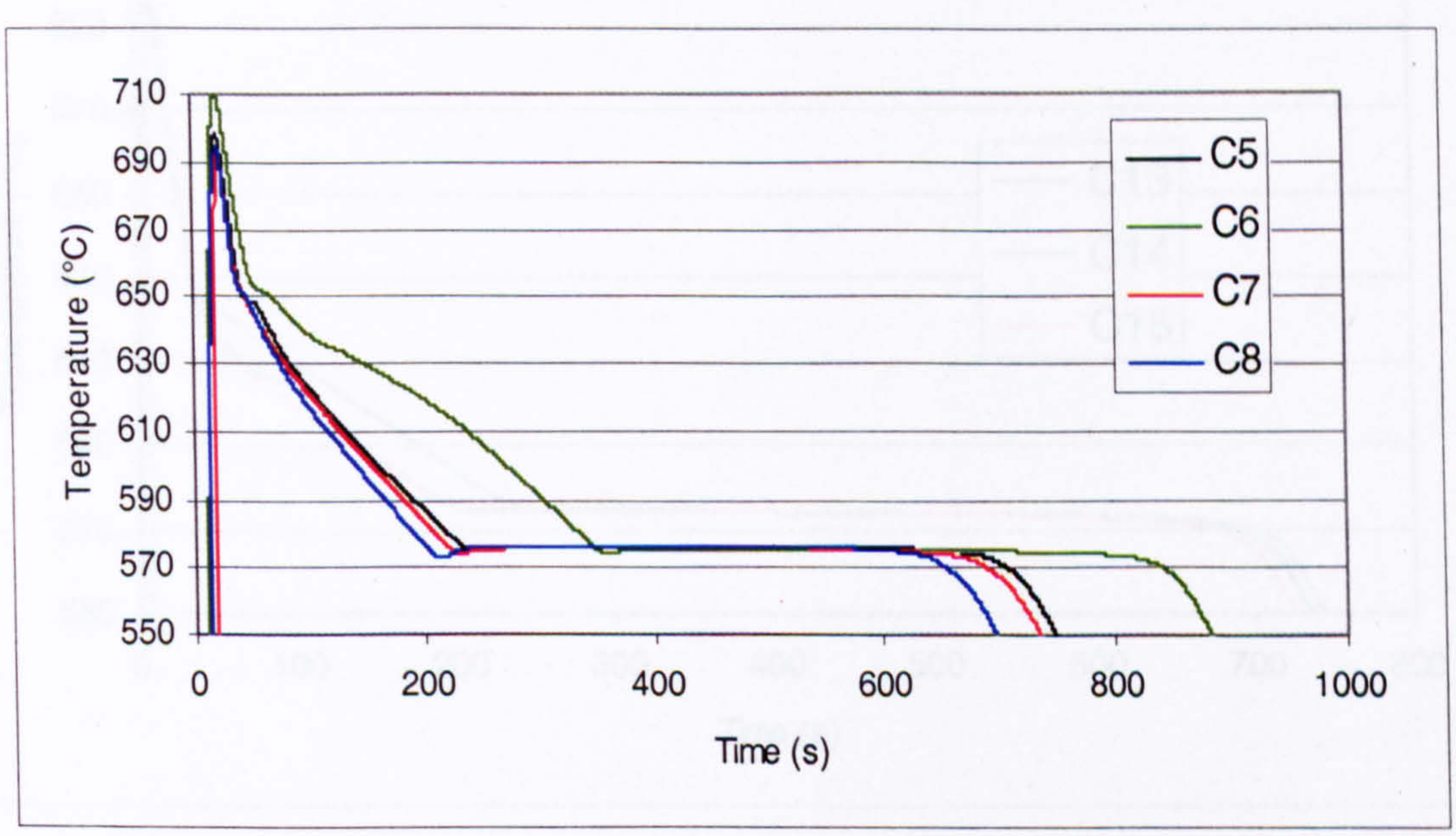

Figure 4.4 The cooling curves for samples inoculated by 0.02% P (Table 3.6).

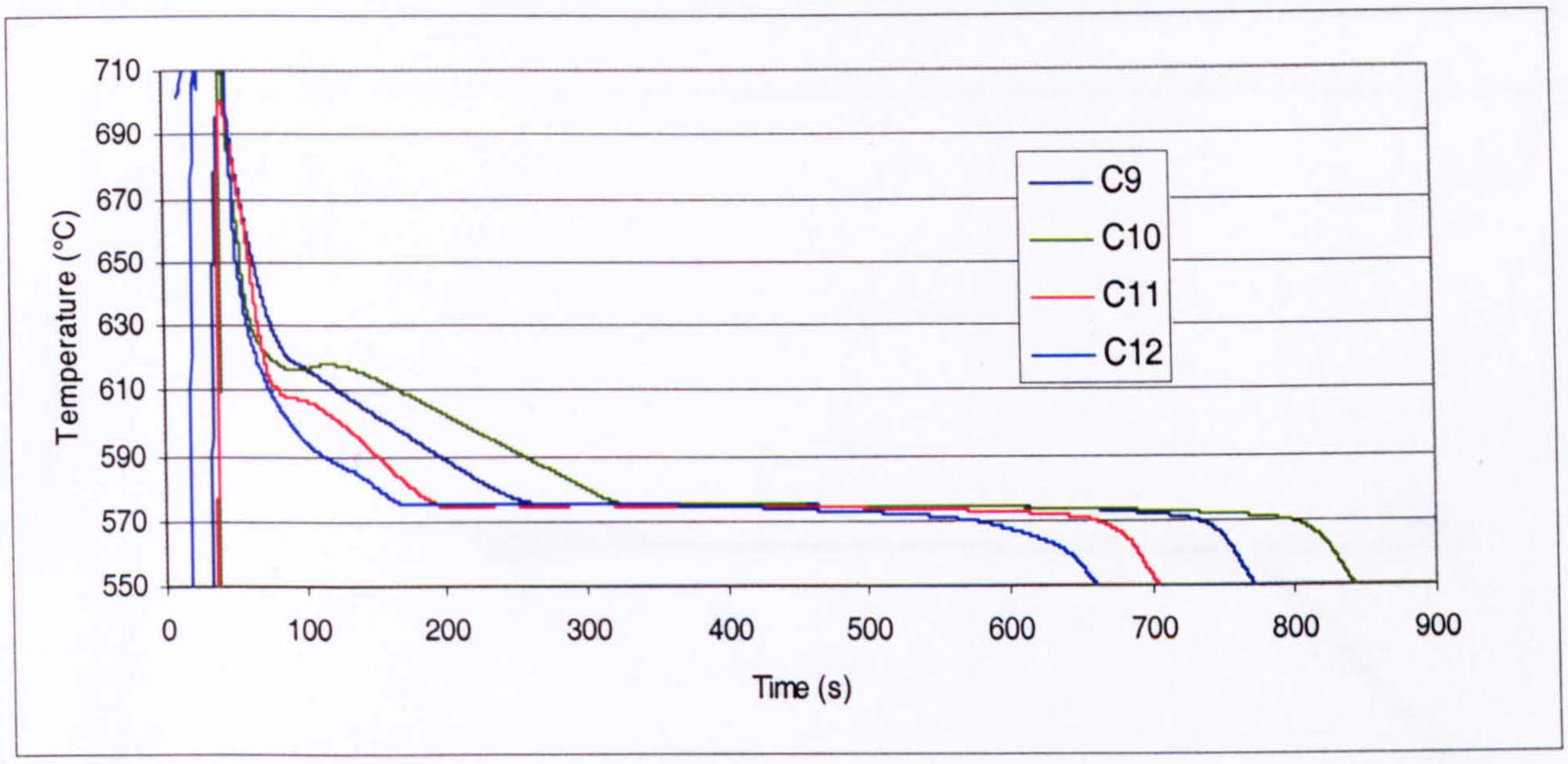

Figure 4.5 The cooling curves for samples modified by 0.2% Sr (Table 3.6).

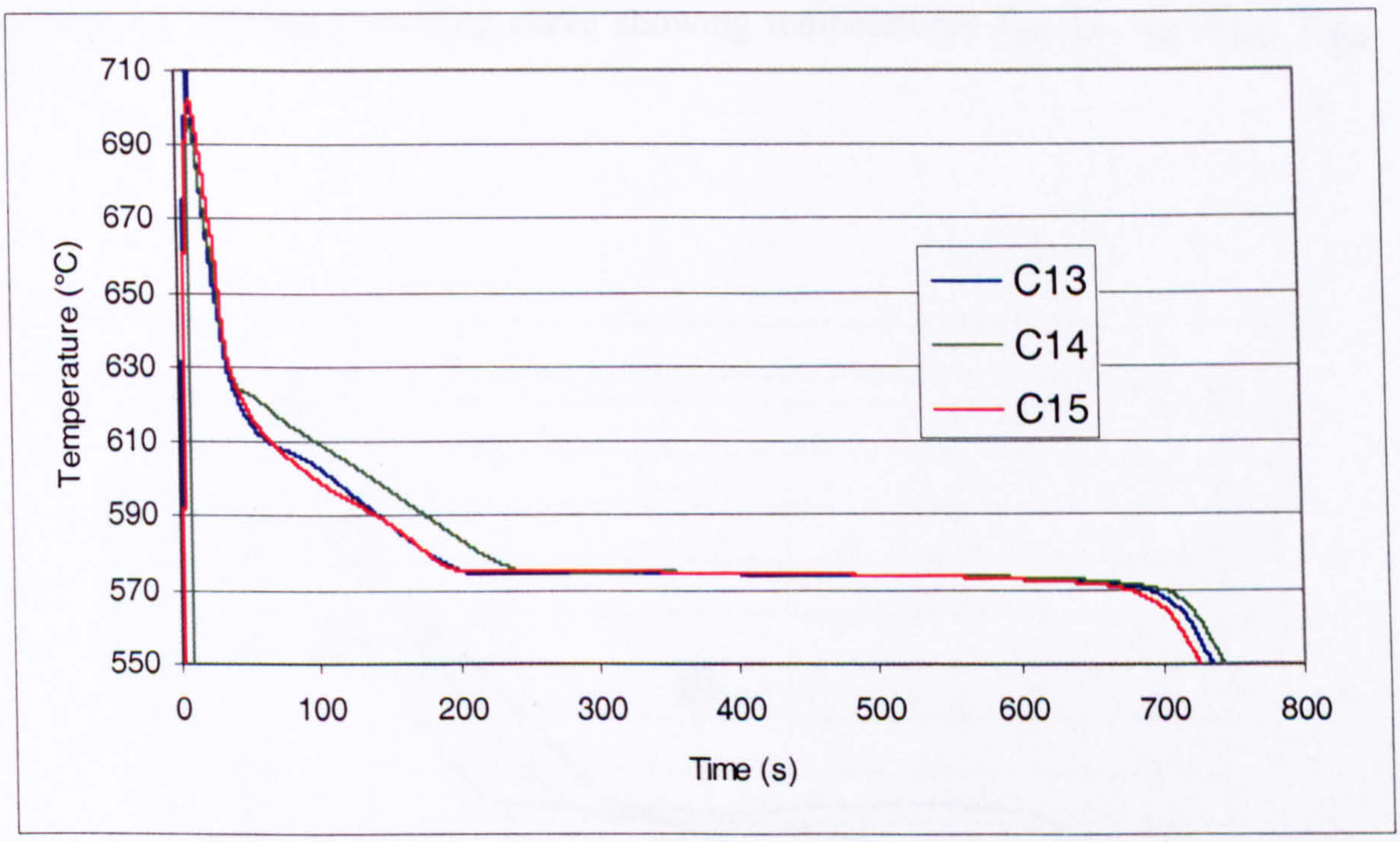

Figure 4.6 The cooling curves for samples simultaneously modified and refined by 0.2% Sr + 0.02% P (Table 3.6).

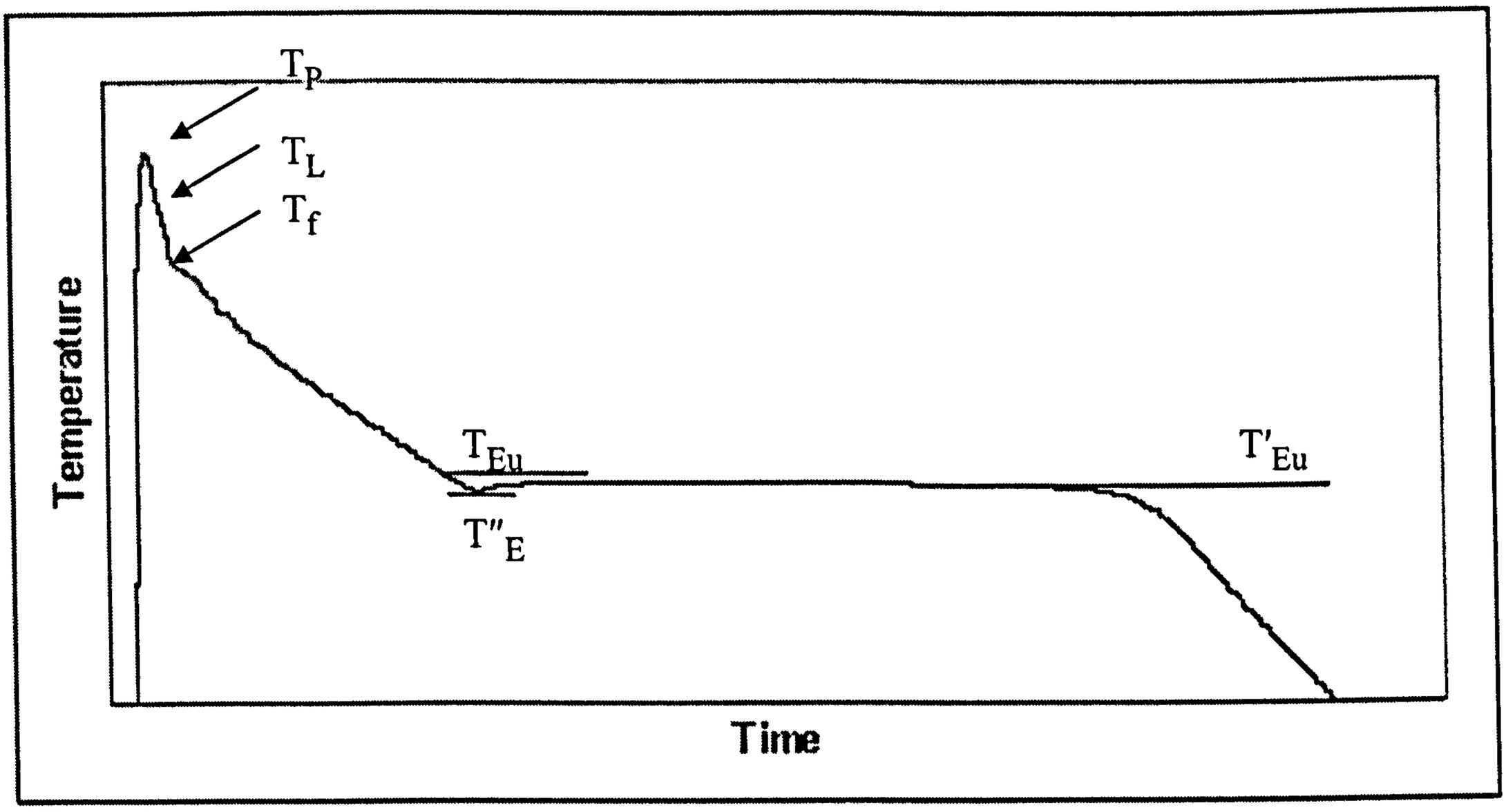

Figure 4.7.a Schematic cooling curve showing temperatures T_P, T_L, T_f, T_{Eu}, T'_{Eu} and T''_{Eu}.

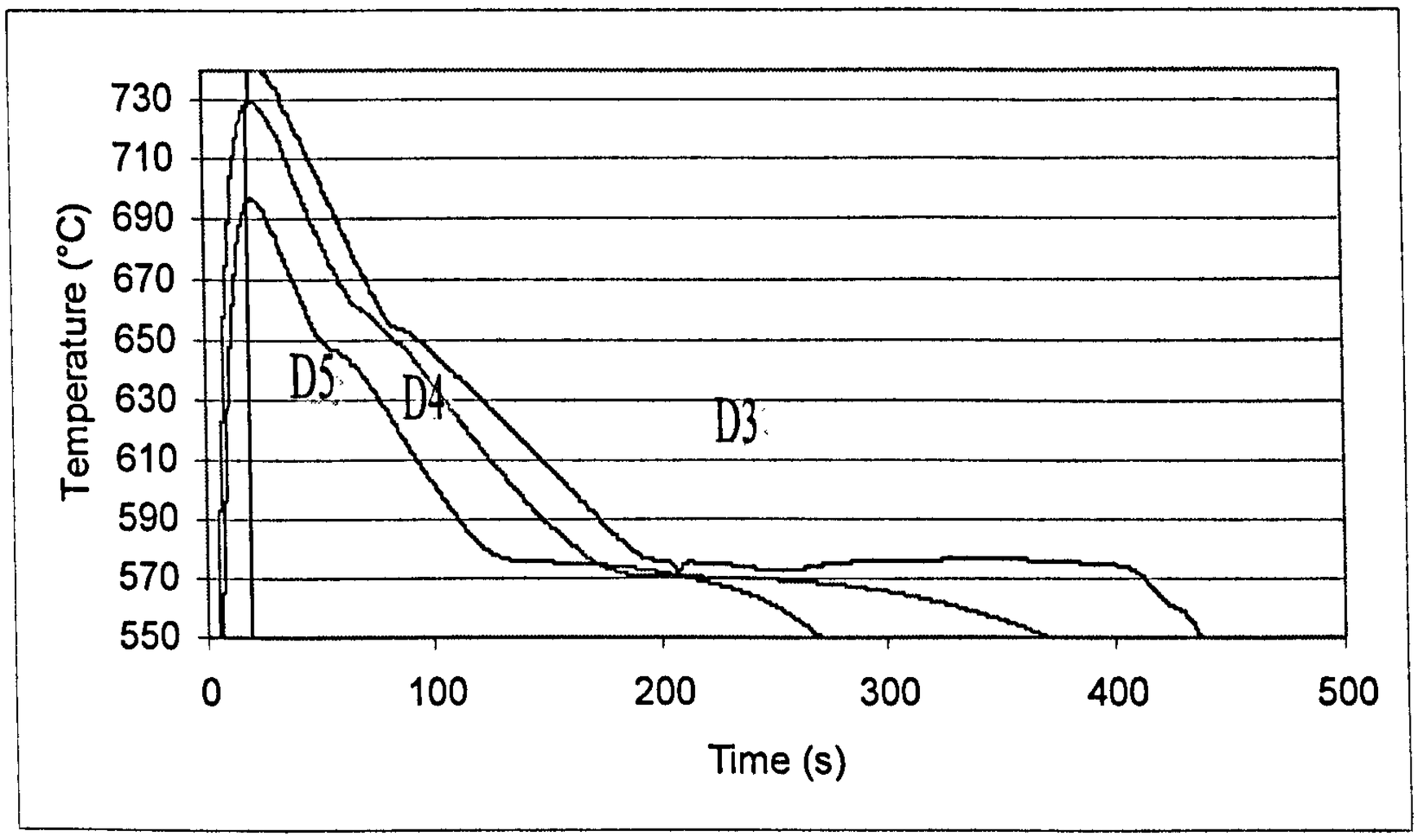

Figure 4.7 The cooling curves for untreated ingots remelted, inoculated with 0.02 wt% P and cast into alumina crucibles (Table 3.6).

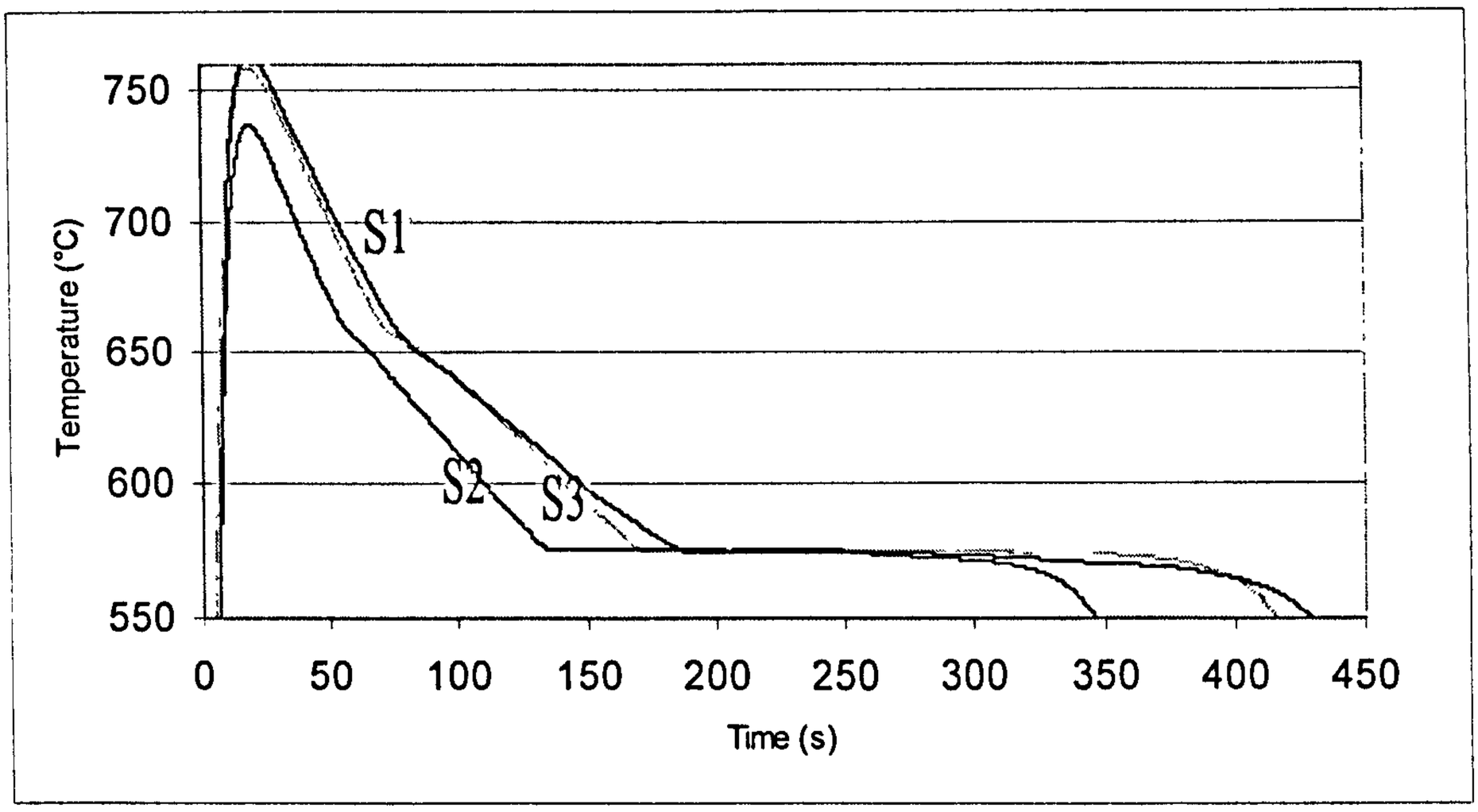

Figure 4.8 The cooling curves for ingots remelted, untreated and cast into stainless steel cups (Table 3.6).

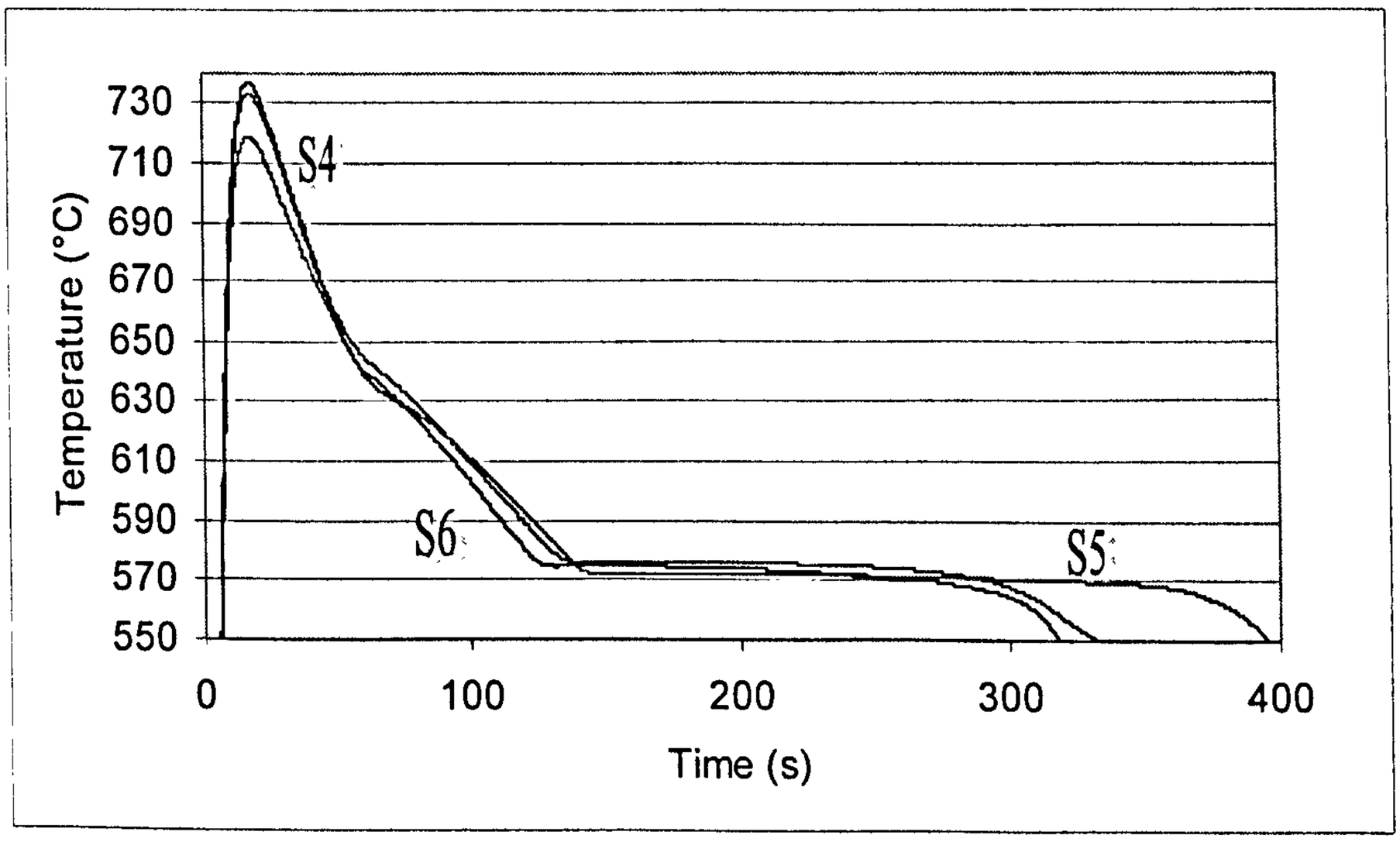

Figure 4.9 The cooling curves for ingots remelted, inoculated with 0.02 wt% P and cast into stainless steel cups (Table 3.6).

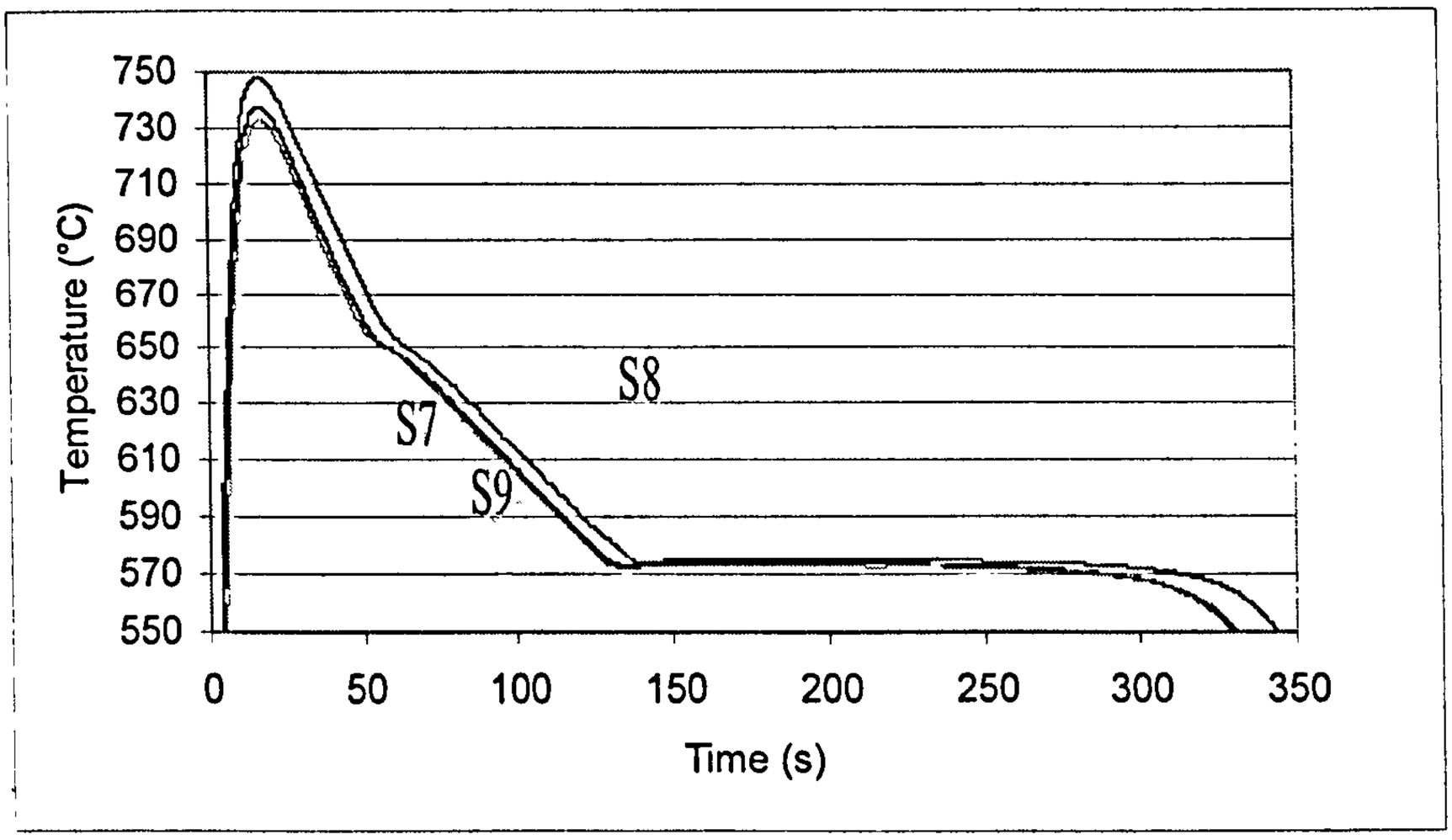

Figure 4.10 The cooling curves for ingots remelted. inoculated with 0.04 wt% P, and cast into stainless steel cups (Table 3.6).

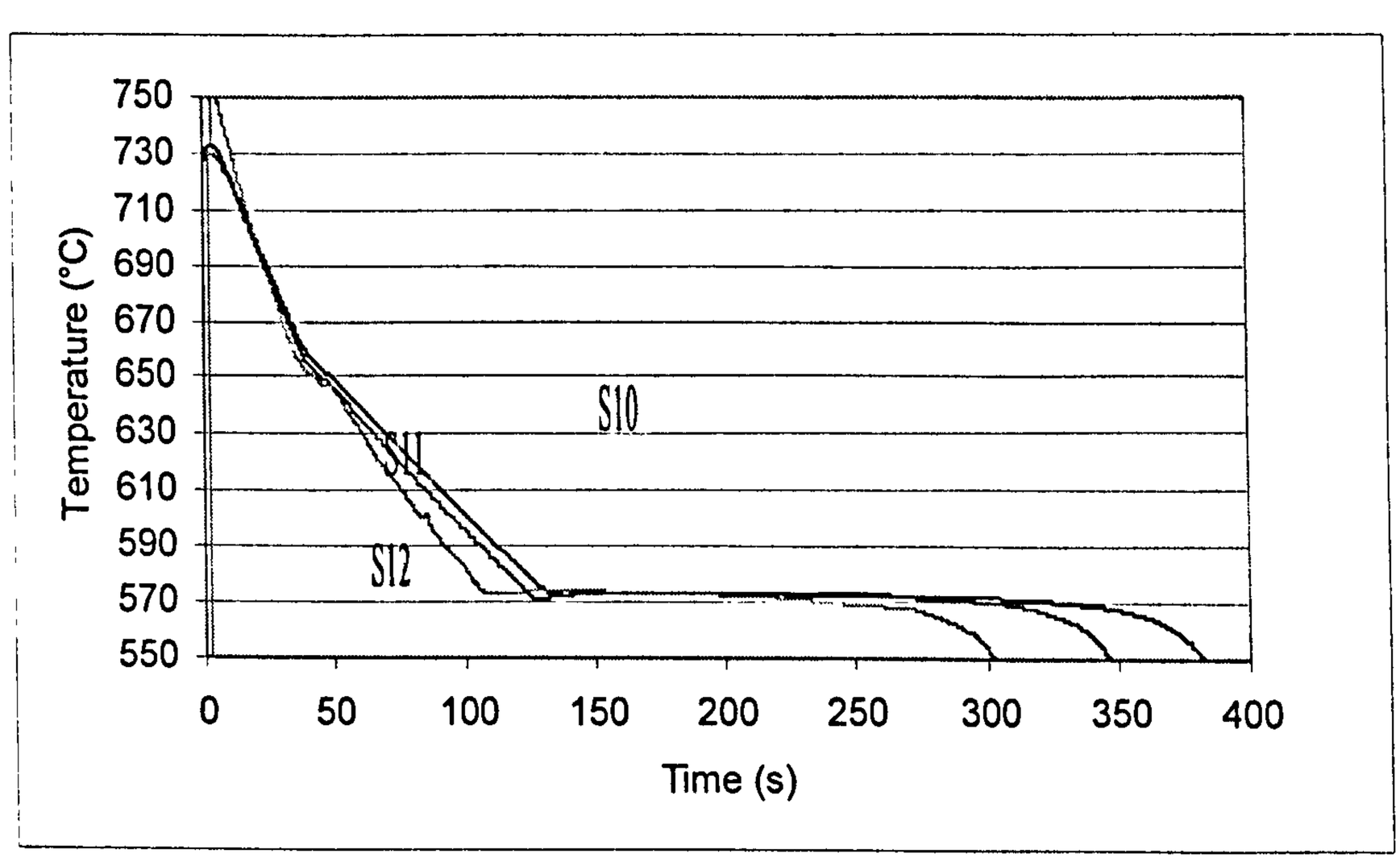

Figure 4.11 The cooling curves for ingots remelted, inoculated with 0.08 wt% P and cast into stainless steel cups (Table 3.6).

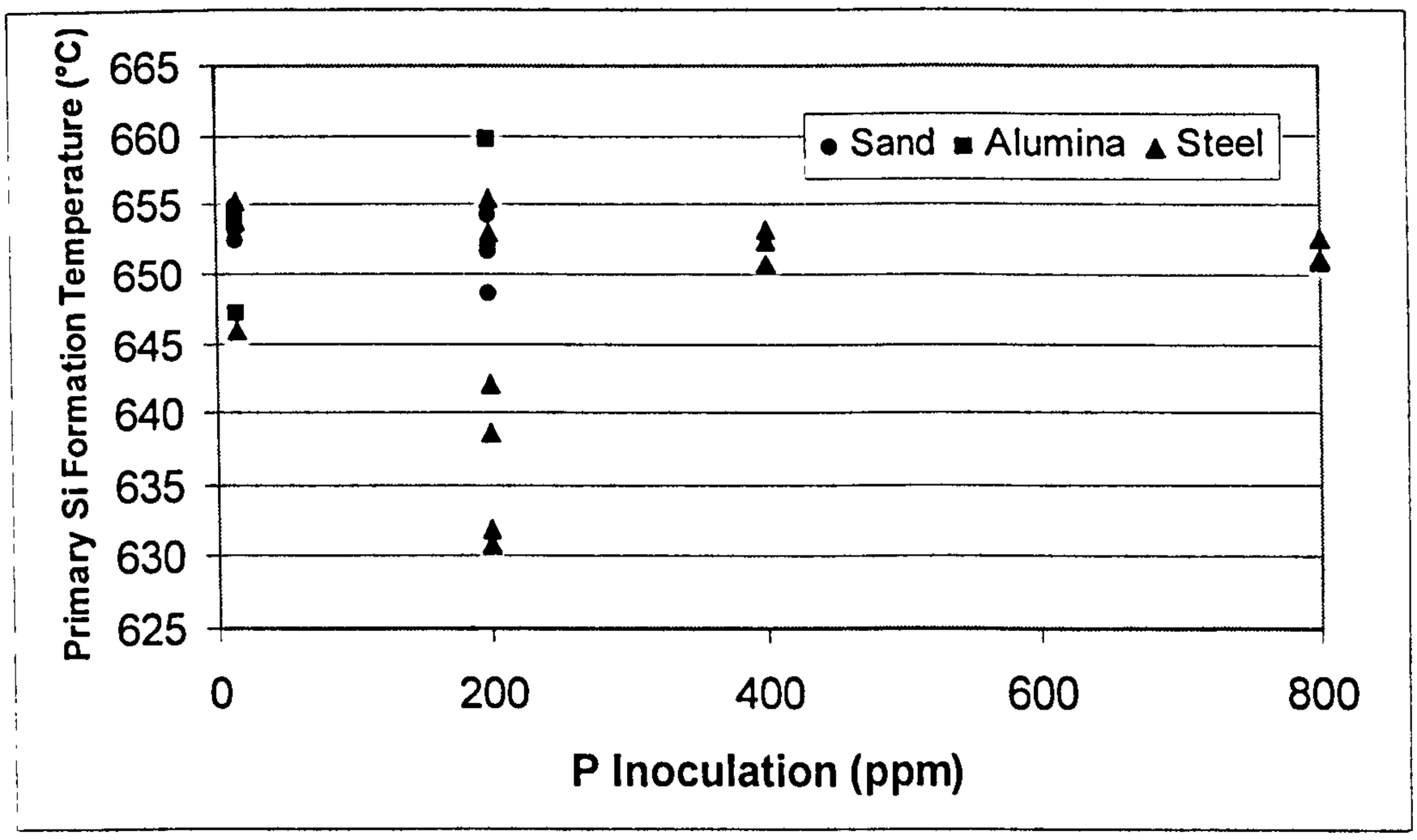

Figure 4.12a The effect of amount of P-inoculation on all formation temperatures of primary silicon phase for all cast ingots. (The uninoculated samples are considered as inoculated by 0.0014 wt% P as the supplied alloy already had traces of P, Table 3.1.)

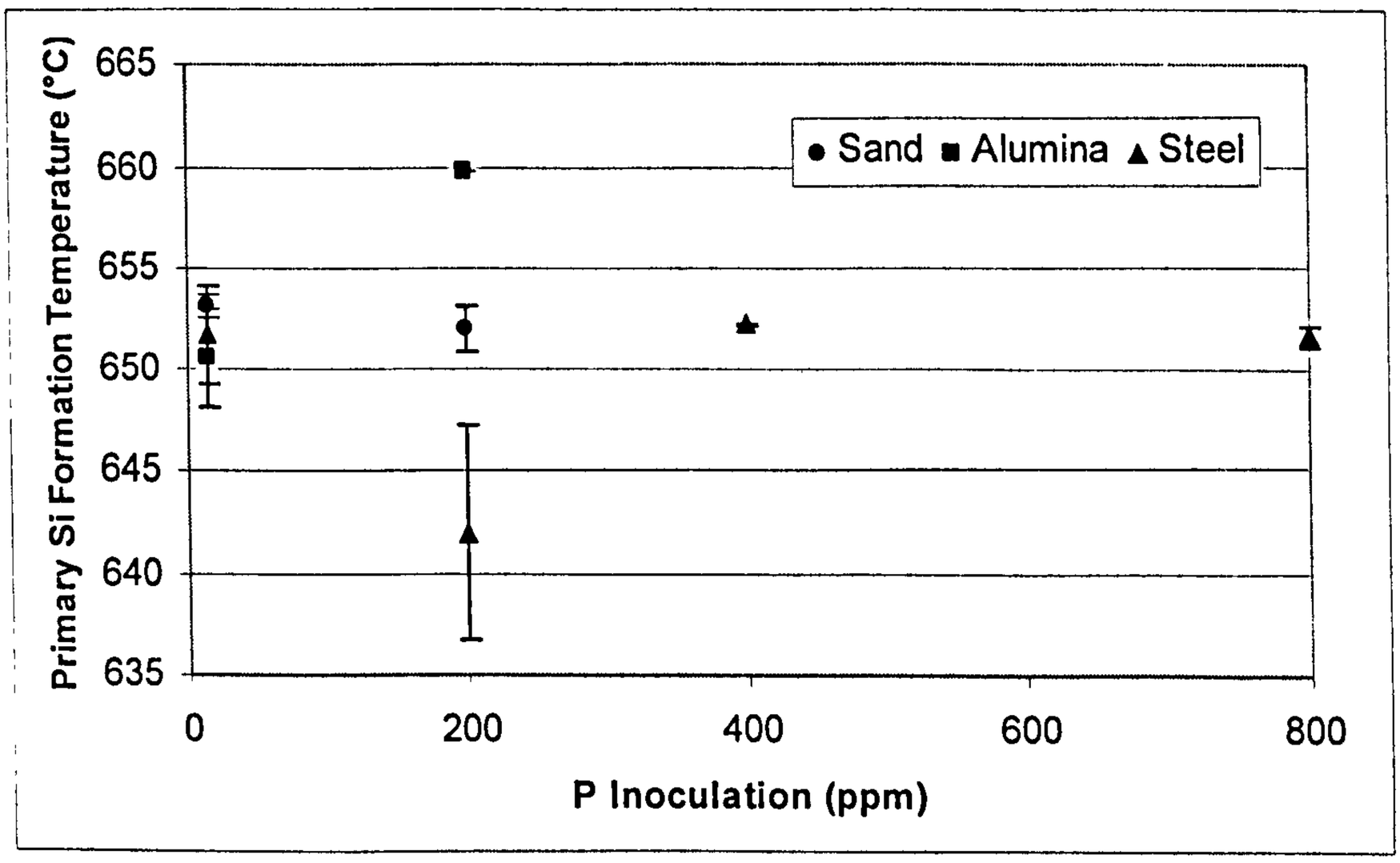

Figure 4.12b The effect of amount of P-inoculation on the formation temperature of primary silicon phase based on the separate average values for ingots, cast in sand, alumina and steel.

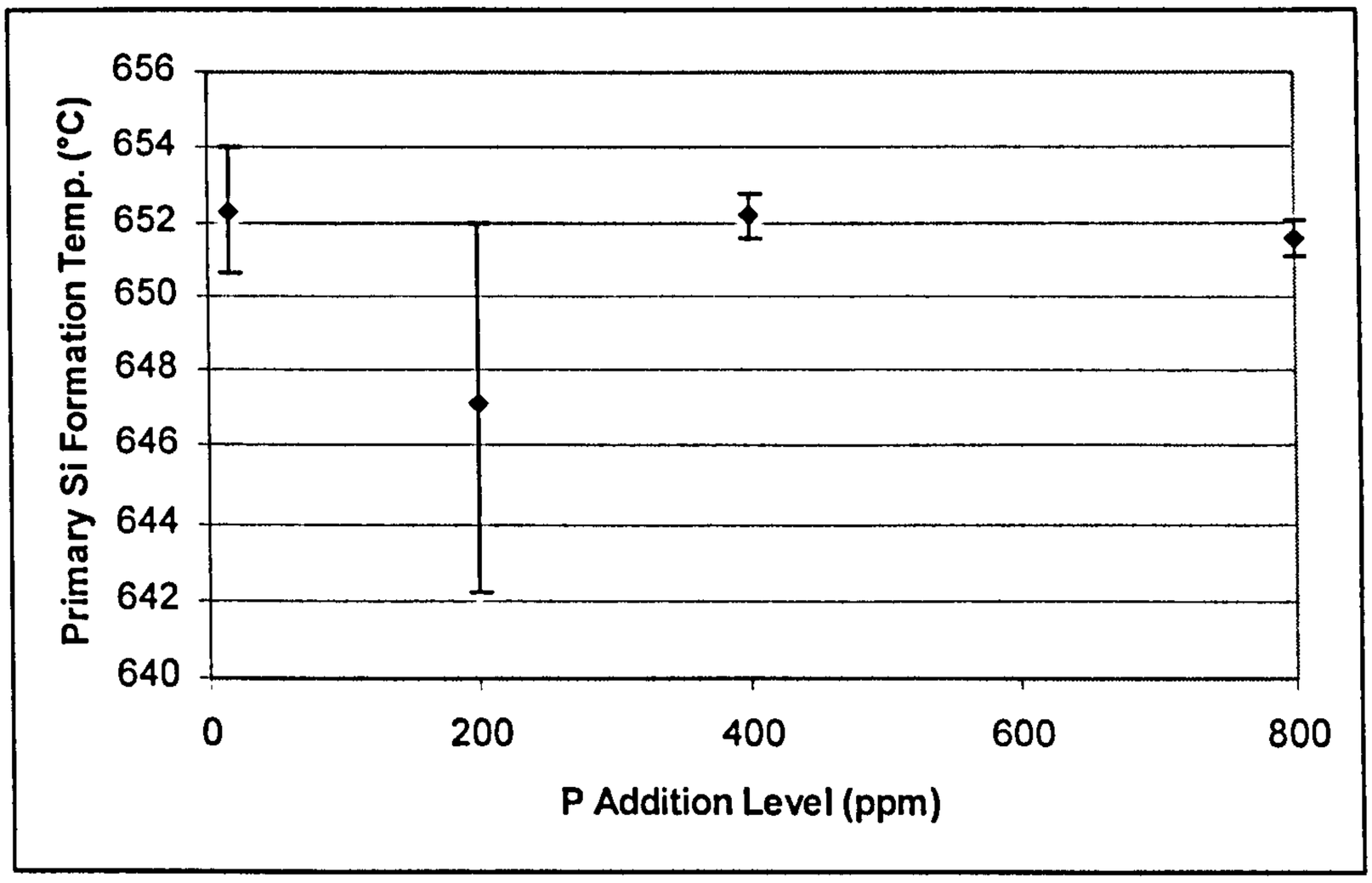

Figure 4.12c The effect of amount of P-inoculation on the formation temperature of primary silicon phase based on the overall average values for ingots cast in sand, alumina and steel moulds.

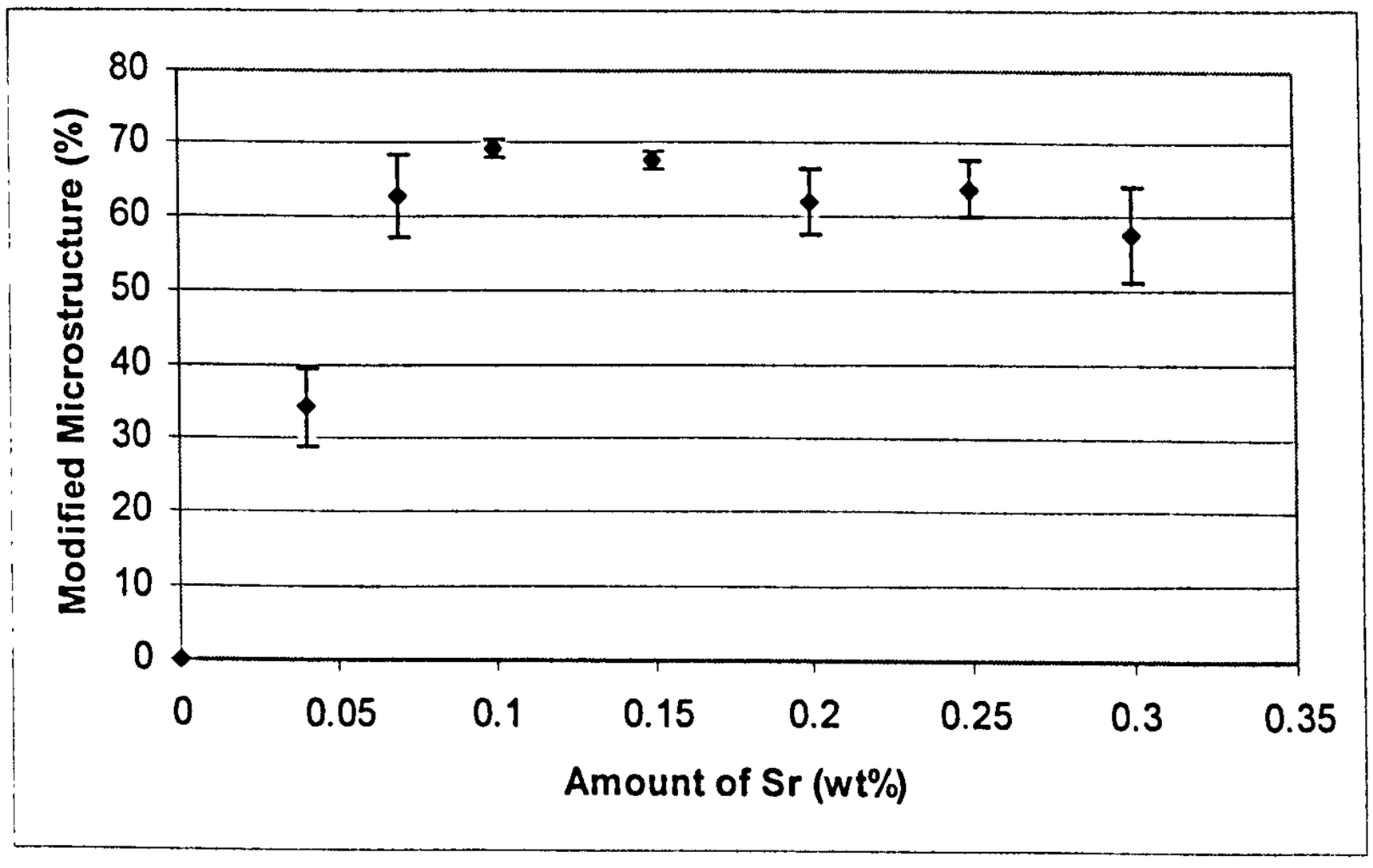

Figure 4.13 Showing the efficiency of modification of Al-18.6 wt% Si by different levels of strontium addition in a Quikcup sand mould, casting temperature 800°C.

No	Sample No.	Melt Temp. (°C)	Sr (wt%)	Microstructure features after heat treatment	Typical micrograph (before heat treatment)	Typical micrograph (after heat treatment)
1	B2	800	0.1	Eutectic fibres get bigger with a rounded tips	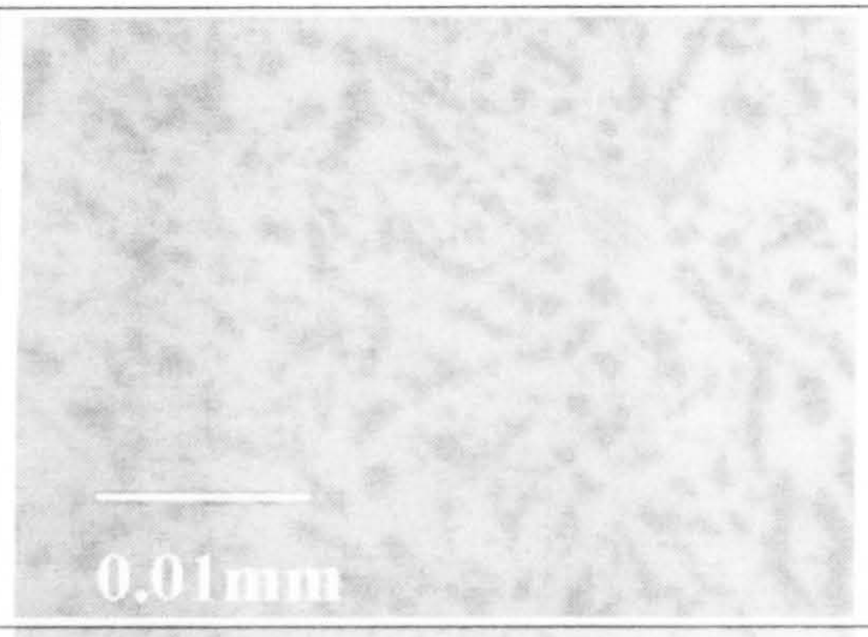	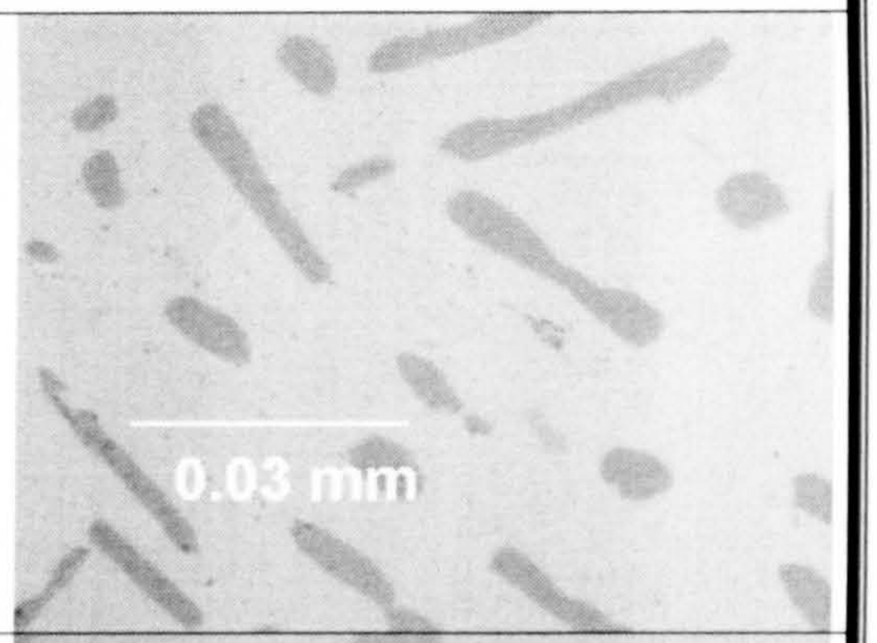
2	B3	800	0.15	Eutectic fibres get bigger & more rounded particles	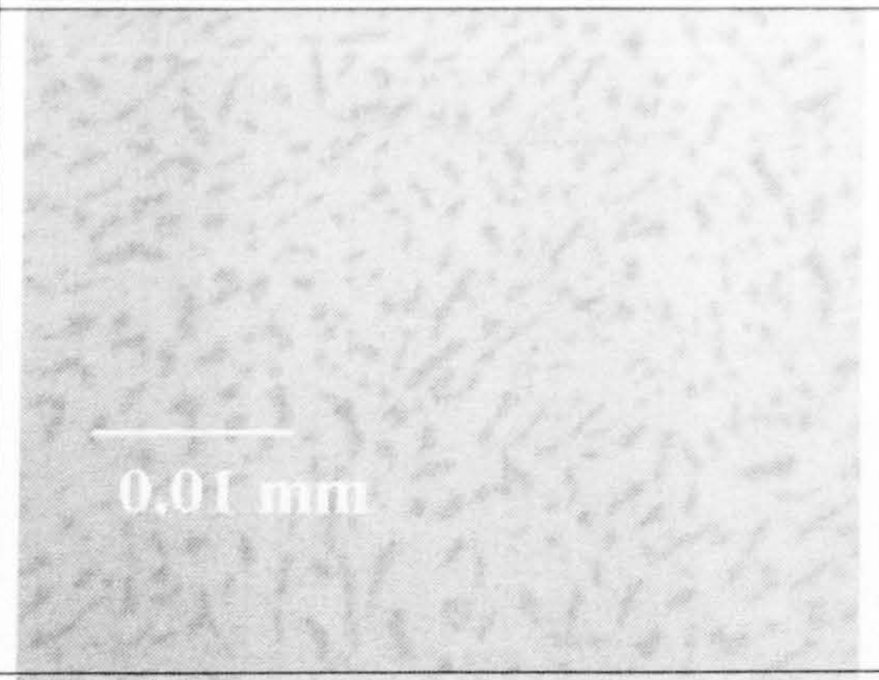	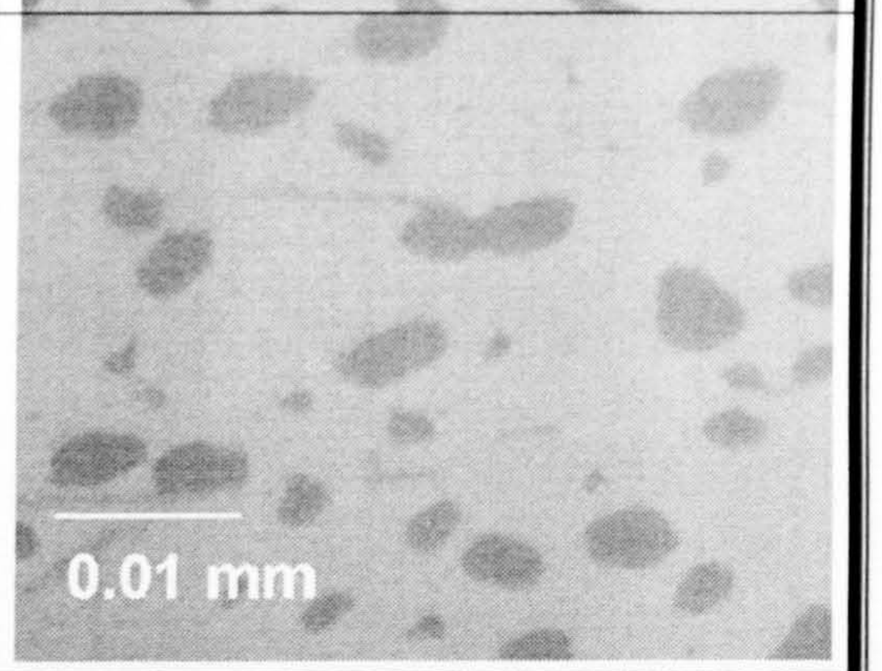
3	B4	800	0.2	Eutectic fibres get bigger & more rounded particles	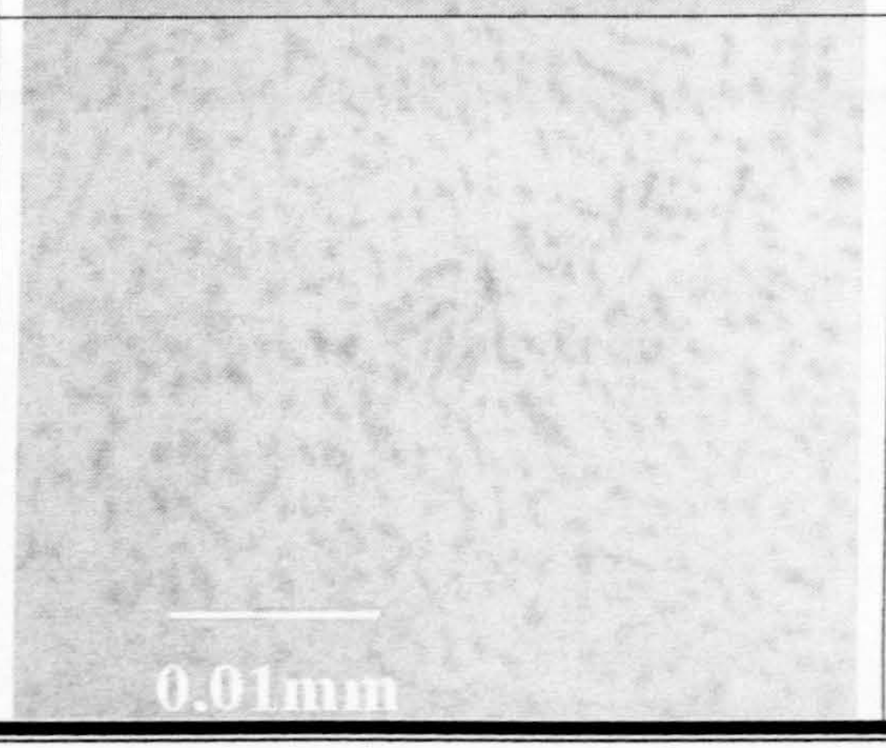	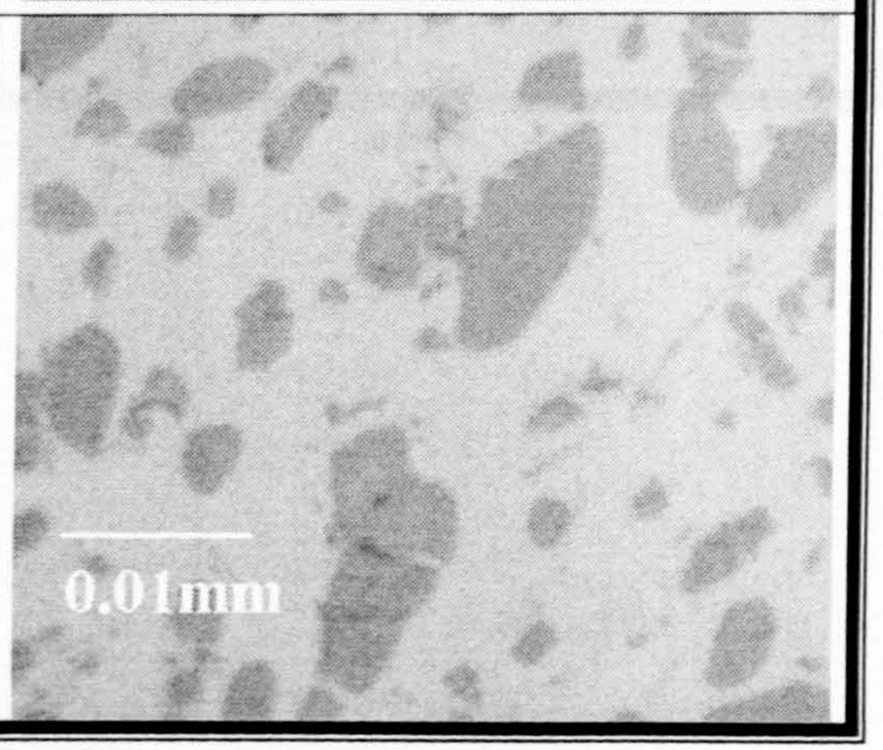

Figure 4.14 The tabulation of all heat-treated samples with their typical micrograph before and after heat treatment (Samples specified in Table 3.6).

No	Sample No.	Melt Temp. (°C)	Sr (wt%)	Microstructure features after heat treatment	Typical micrograph (before heat treatment)	Typical micrograph (after heat treatment)
4	B5	800	0.25	Eutectic fibres get bigger & more rounded particles		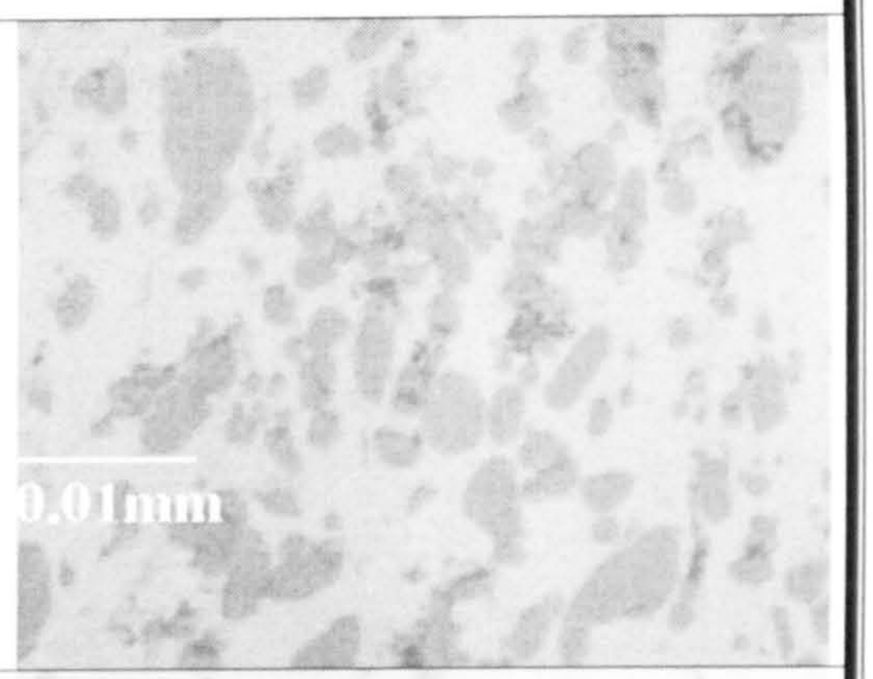
5	B6	800	0.3	Eutectic fibres get nodular	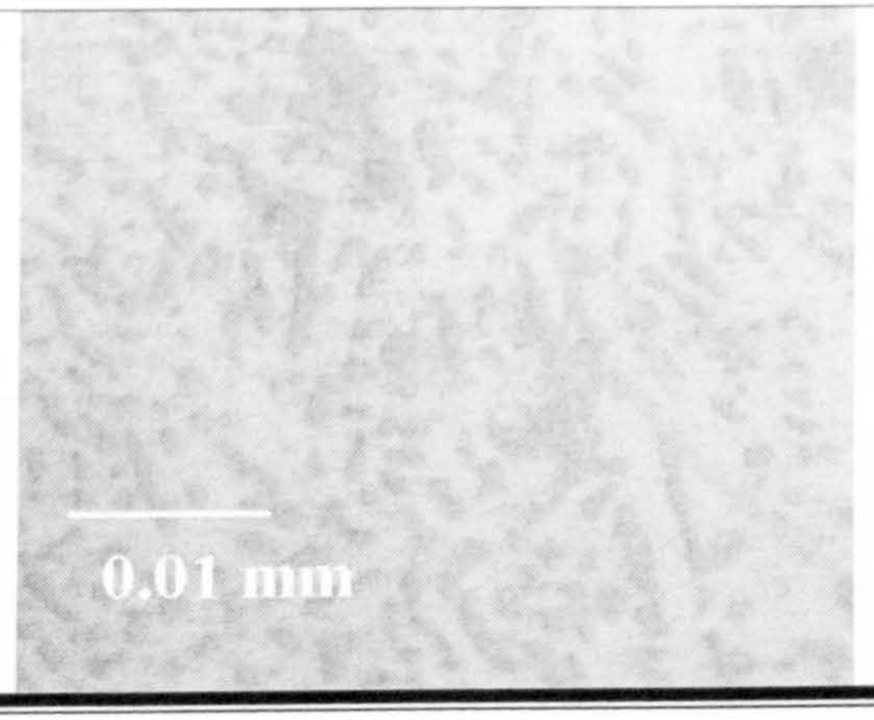	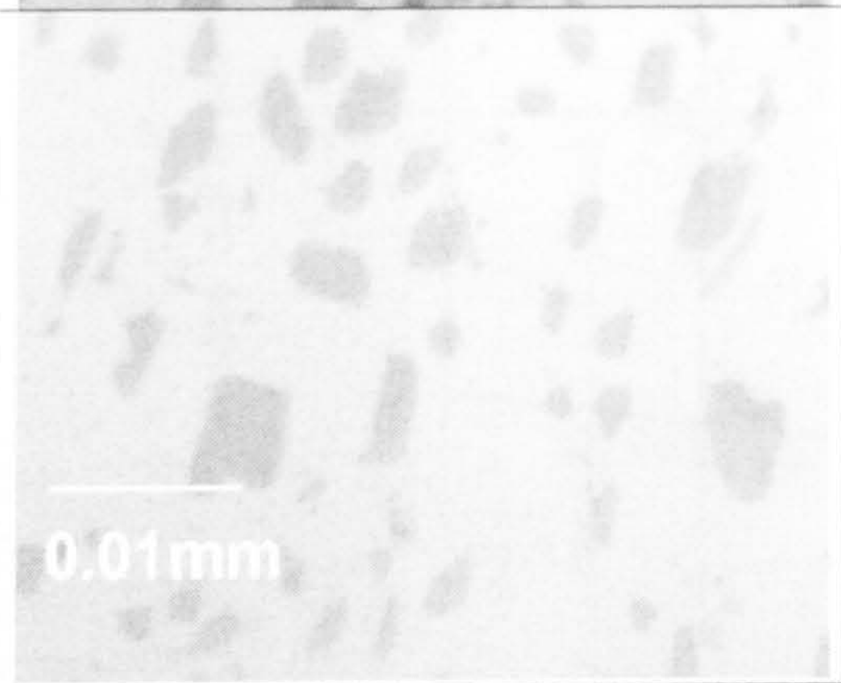

Figure 4.14, Continued

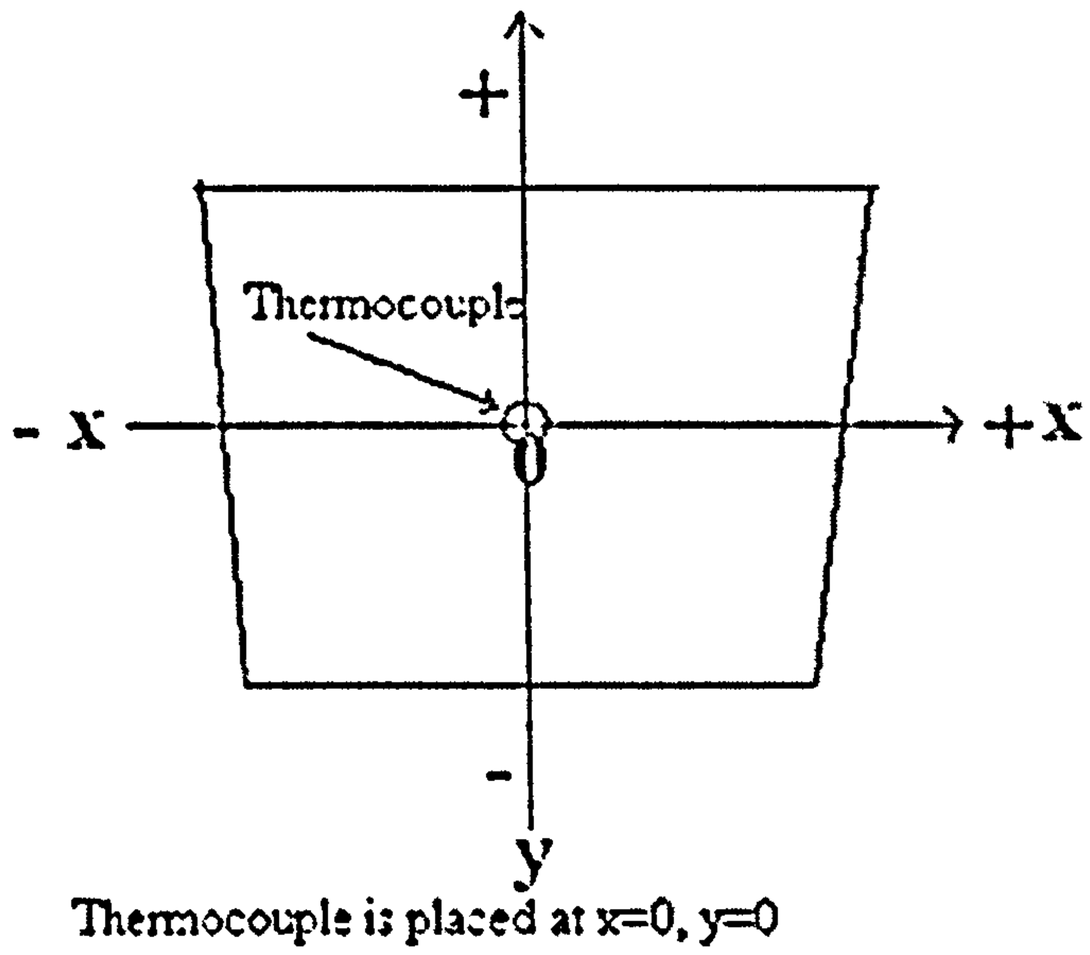

Figure 4.15 Location of the central vertical axis on which photomicrographs have been taken for morphological observations.

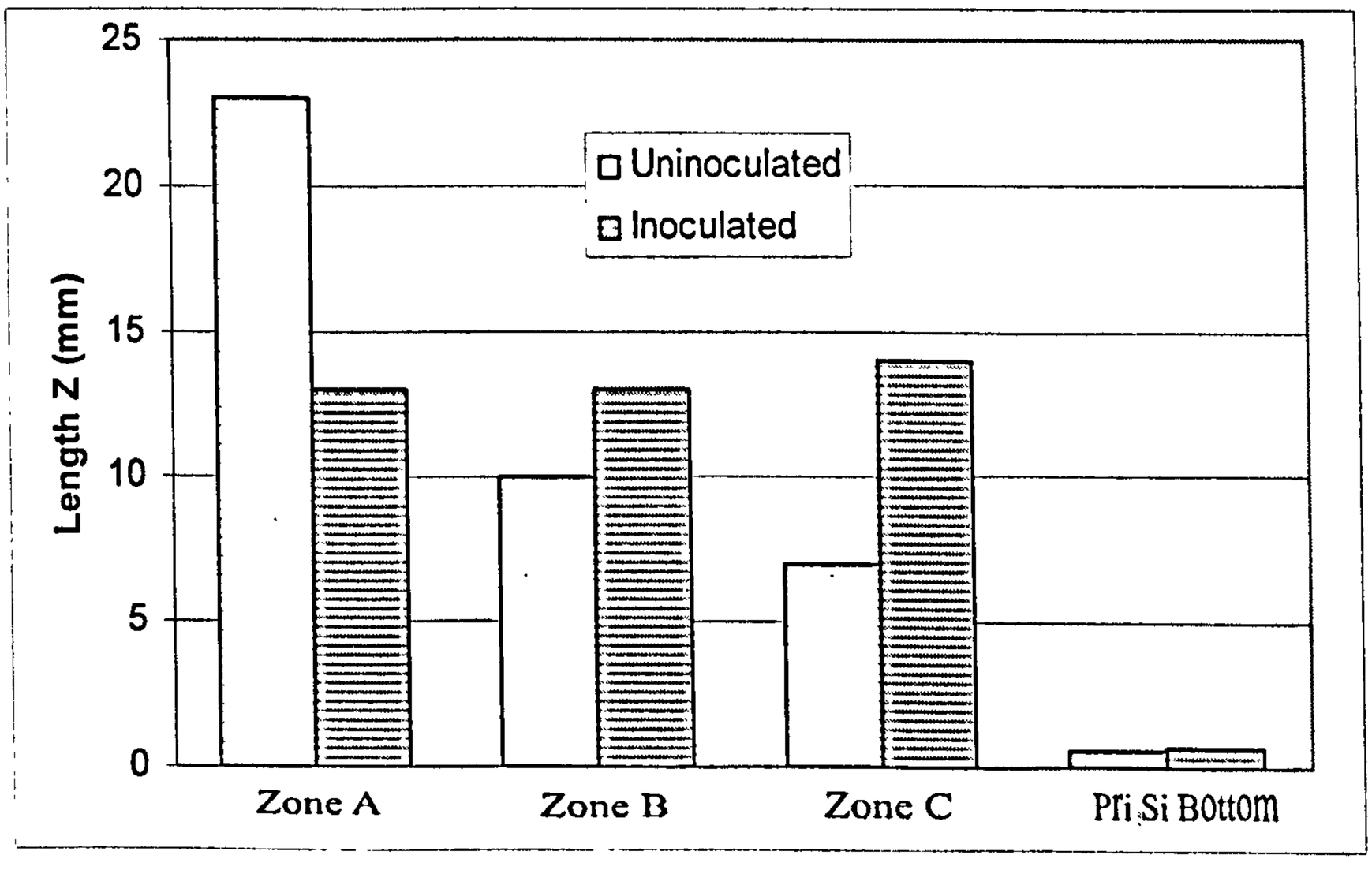

Figure 4.16 The effect of inoculation on the average length Z of morphological zones given in Tables 4.2.a and 4.2.b for bottom cast samples (C1-C8) (N_A for uninoculated = 30 ± 4 mm^{-2}, and for inoculated = 40 ± 7 mm^{-2}.)

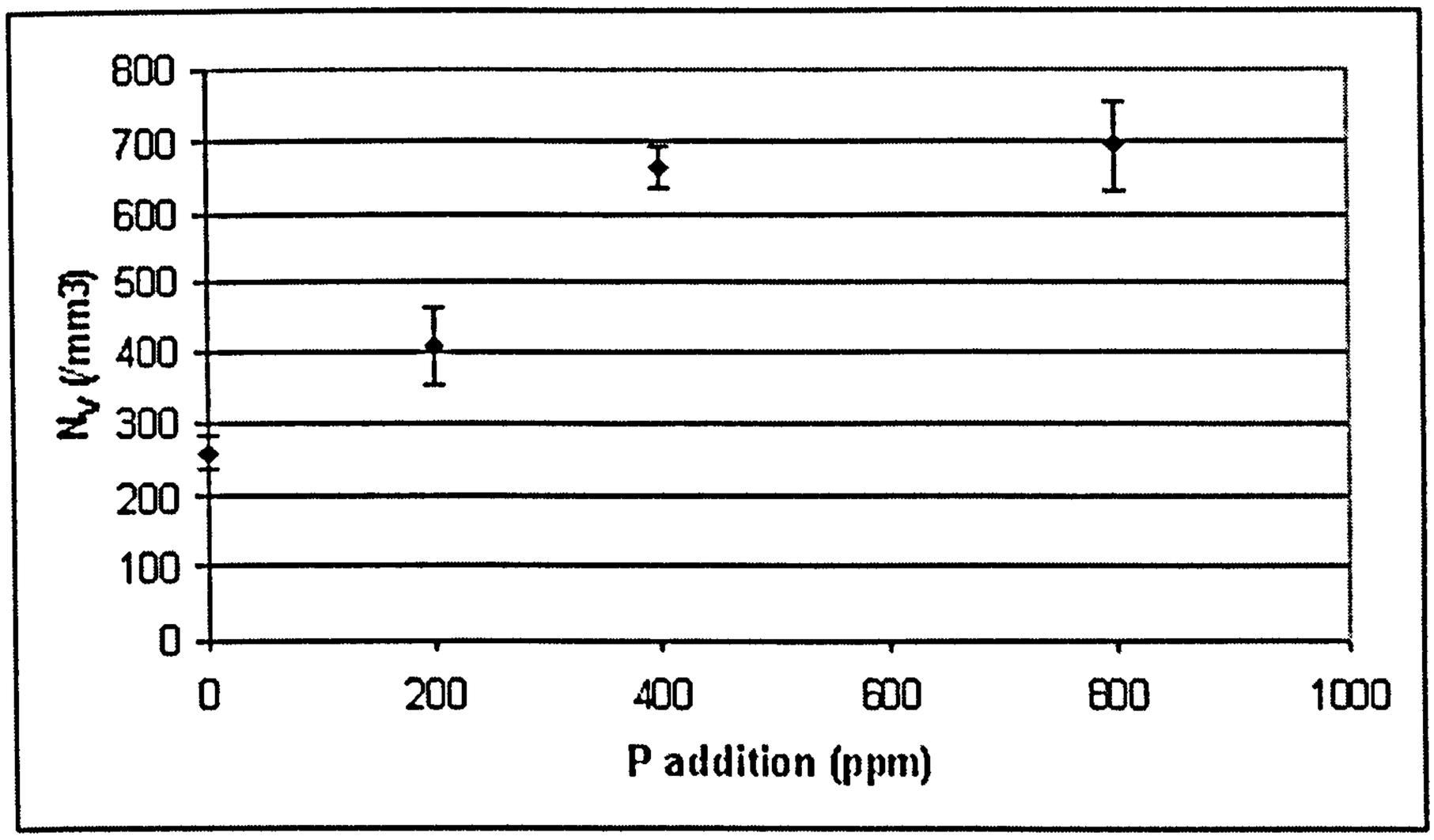

Figure 4.17 The effect of inoculation on the number of primary silicon particles per unit volume, average of all uninoculated and P-inoculated cast ingots. (The uninoculated samples are considered as inoculated by 0.0014 wt% P as the cast ingot already had that trace of phosphorus, Table 3.1.)

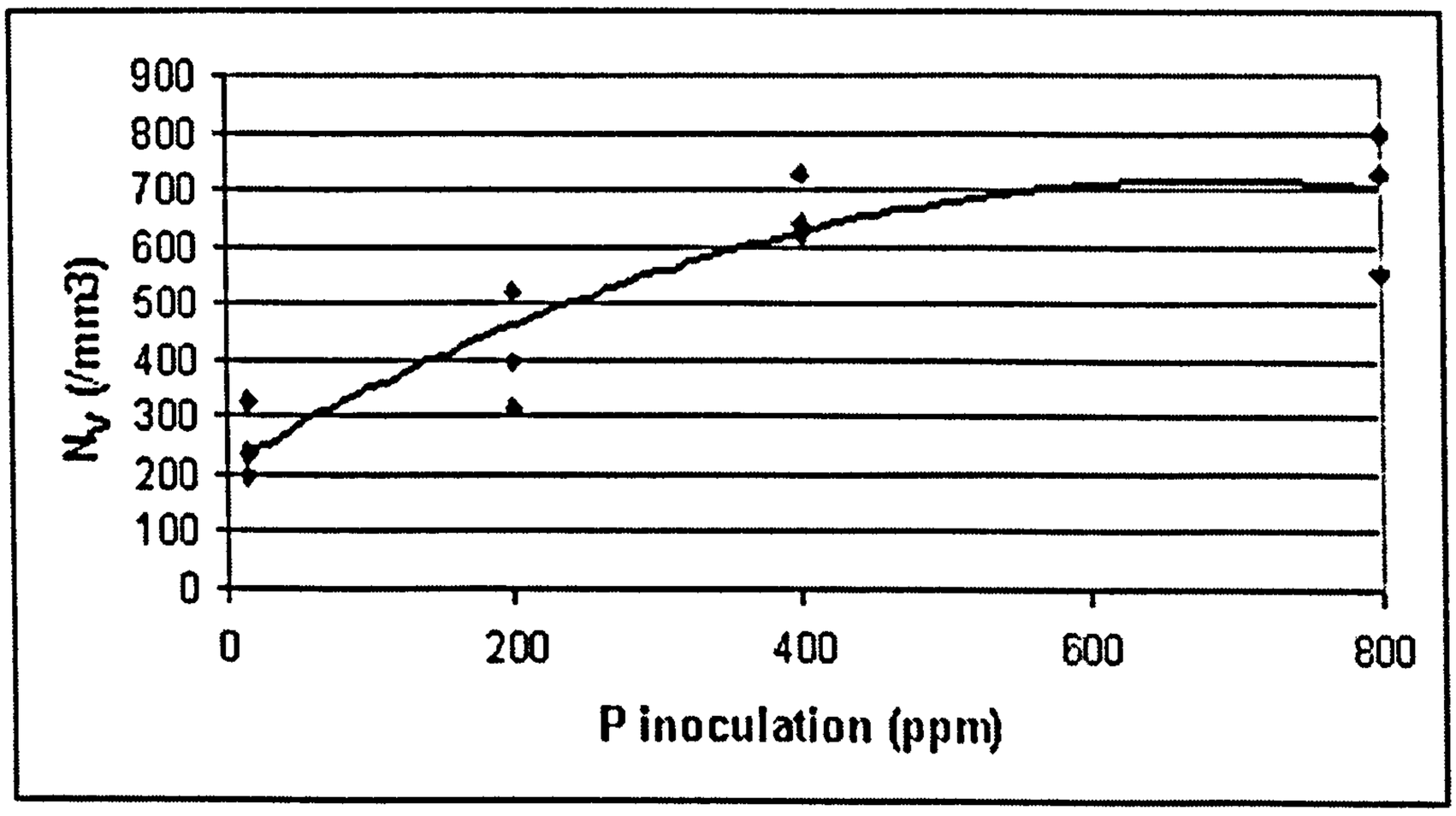

Figure 4.18 The effect of inoculation on the number of primary silicon particles per unit volume for uninoculated and P-inoculated steel cast ingots. (The uninoculated samples are considered as inoculated by 0.0014 wt% P as the cast ingot already had that trace of phosphorus, Table 3.1.)

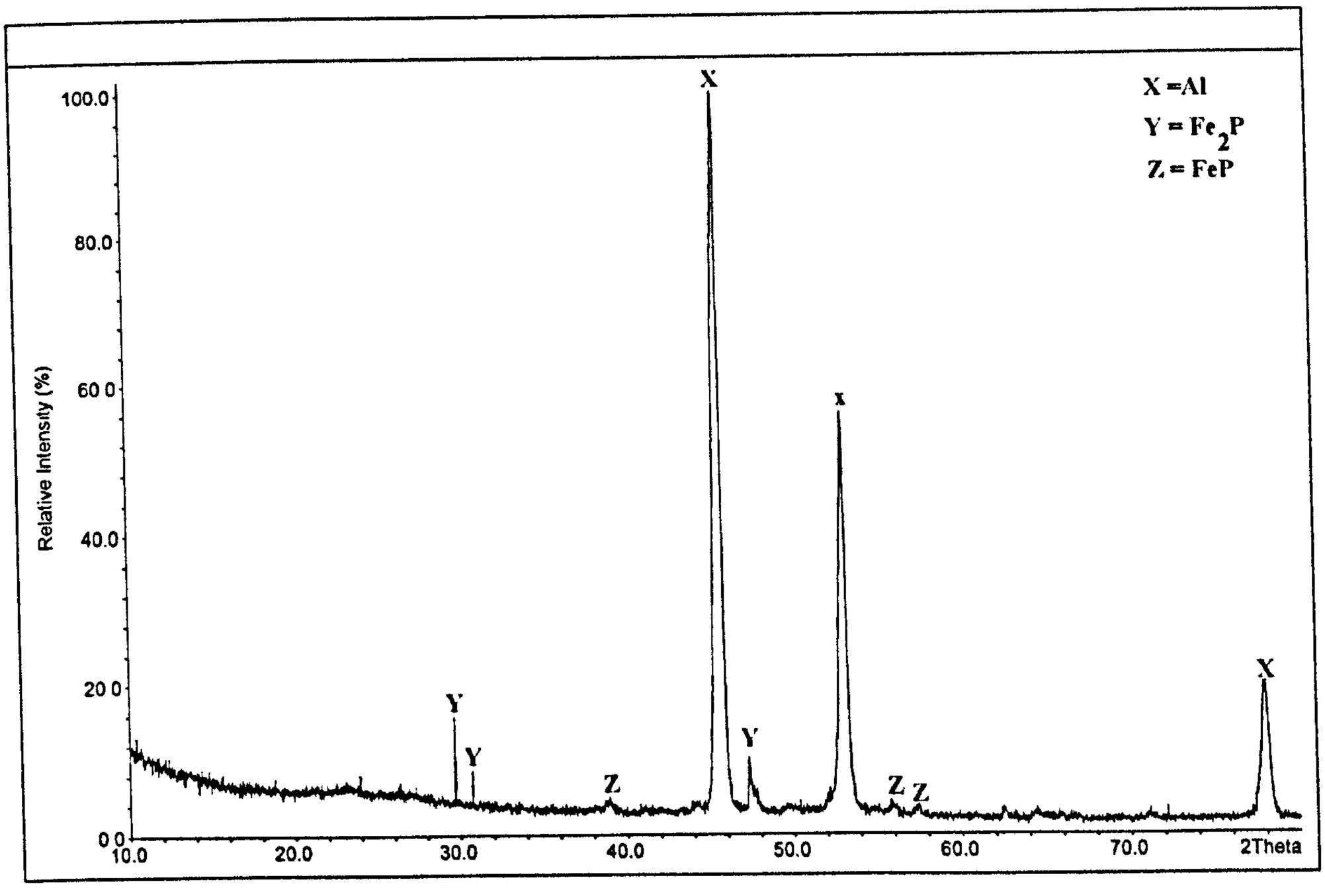

Figure 4.19 XRD trace of Al-Fe-P powder used as one of the phosphorus inoculants.

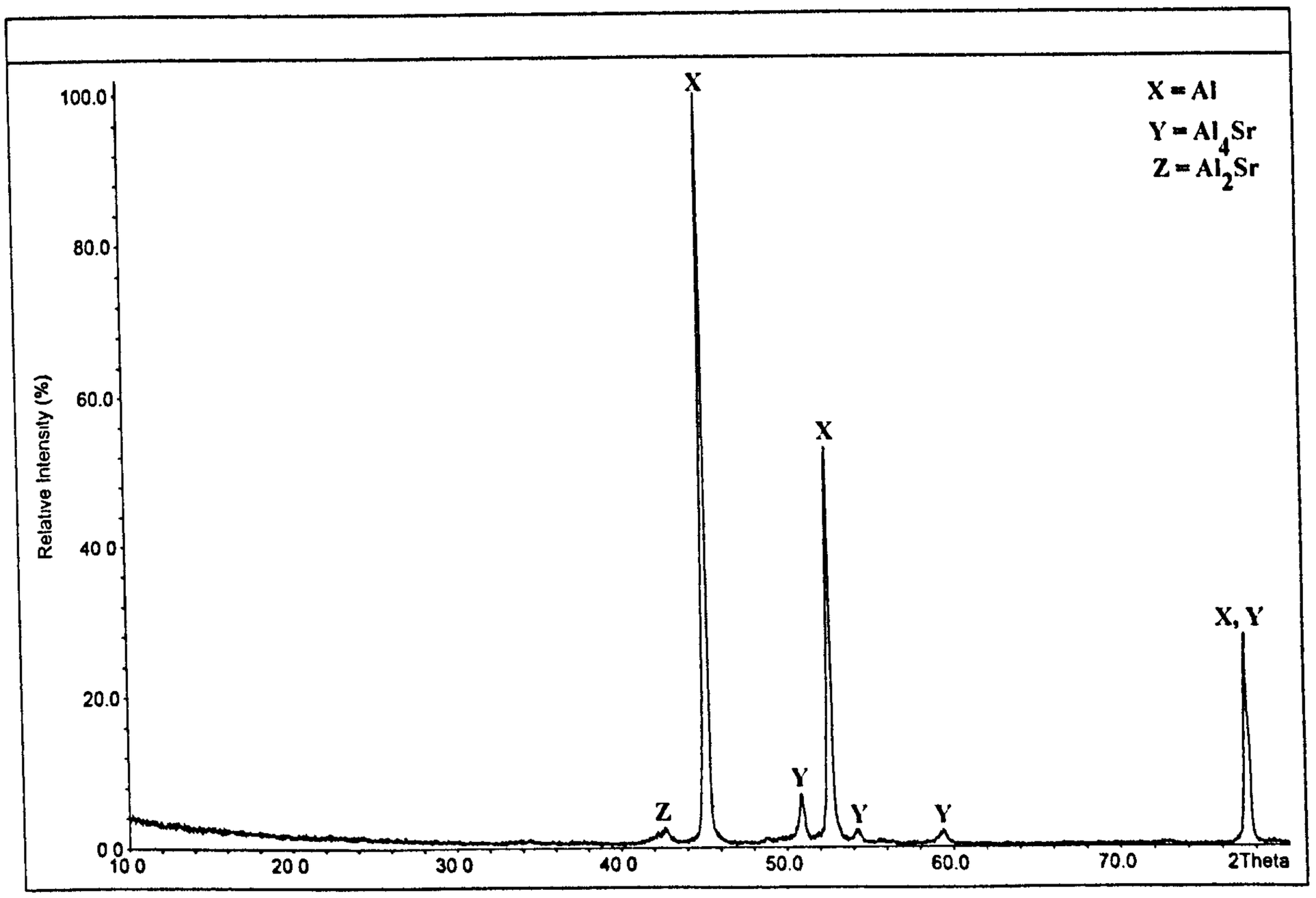

Figure 4.20 XRD trace of Al-Sr alloy used as eutectic silicon modifier.

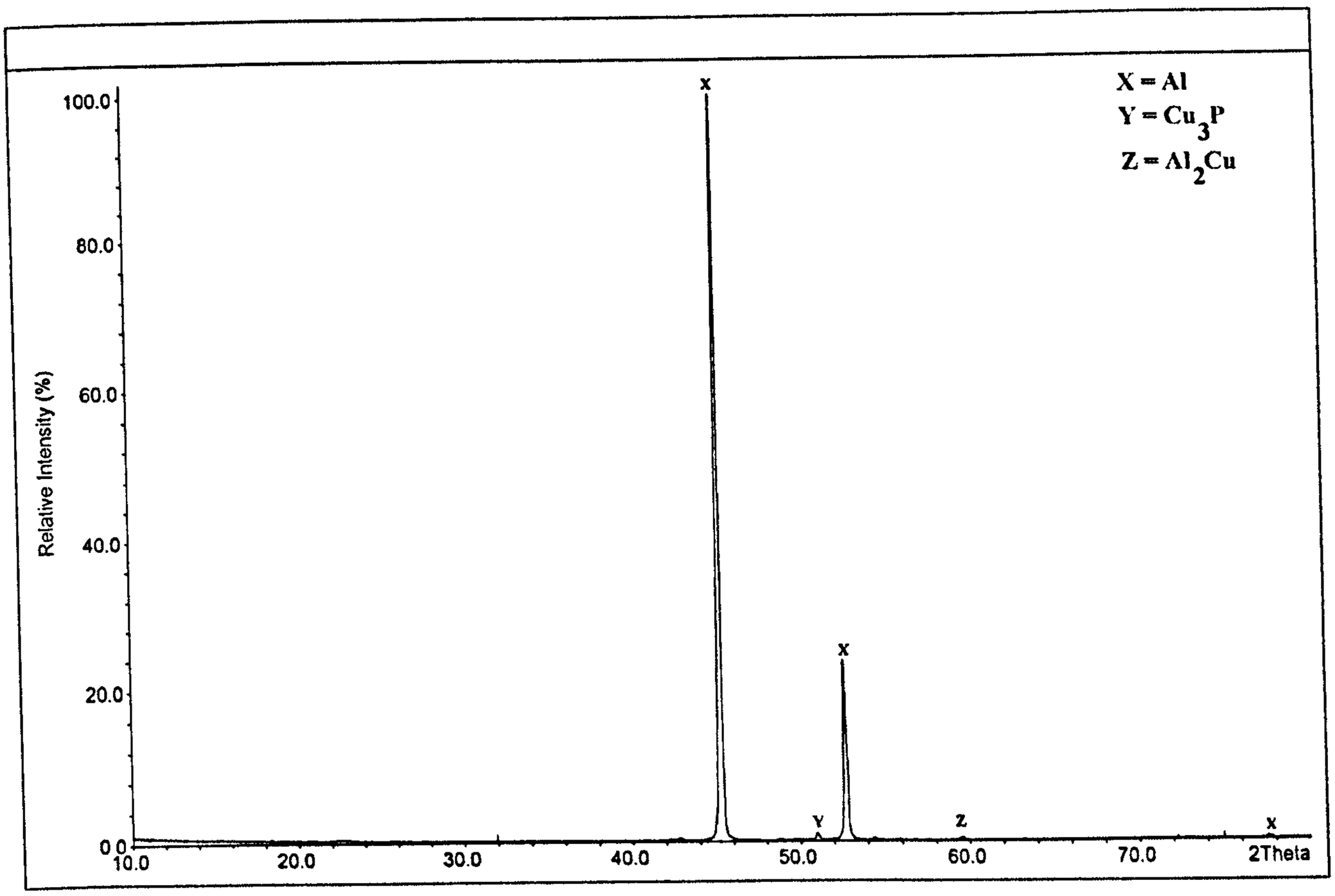

Figure 4.21 XRD trace of Al-Cu-P rod used as one of the phosphorus inoculants.

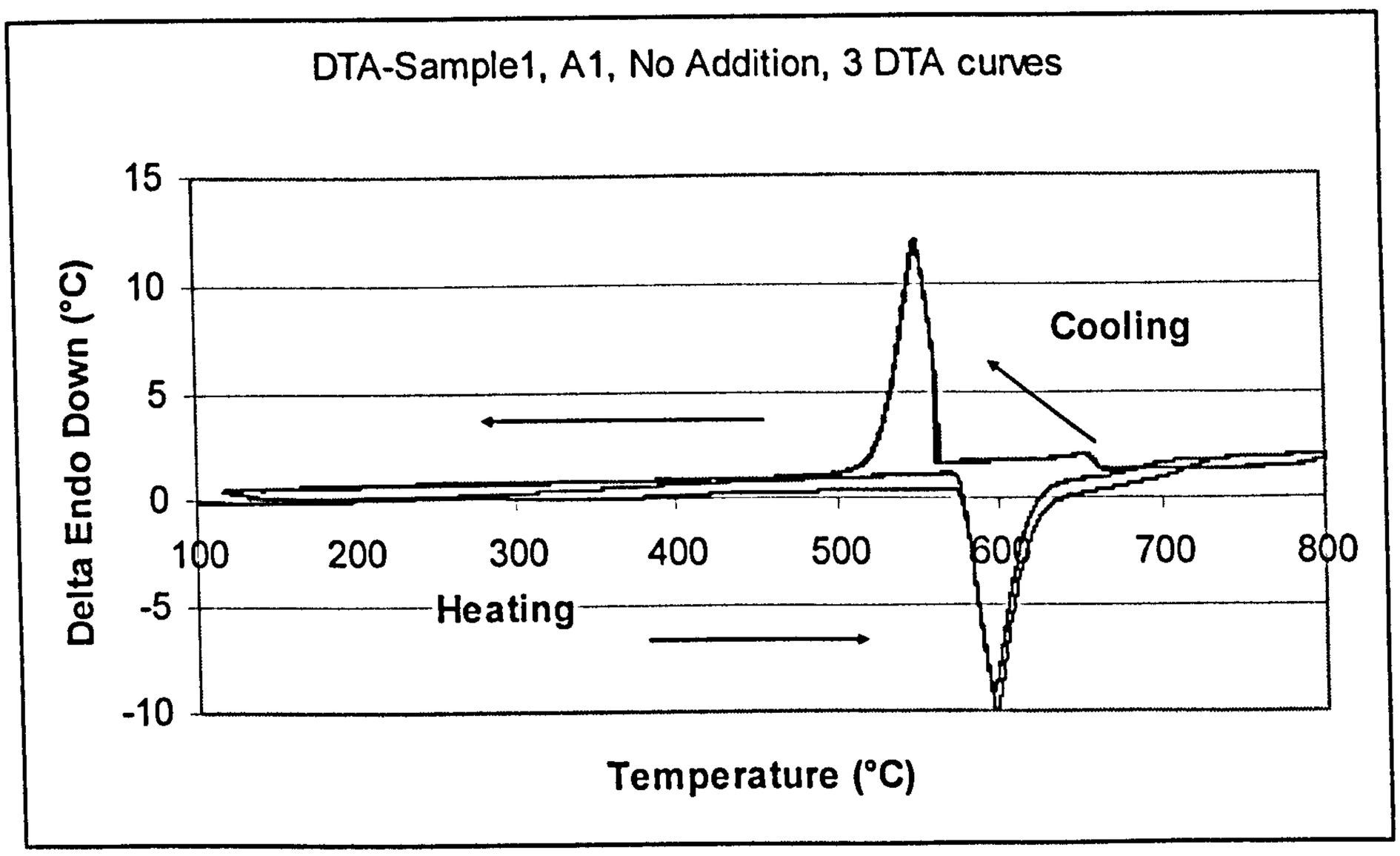

Figure 4.22 Three differential thermal analysis (DTA) curves performed on sample A1 (description in Table 3.6).

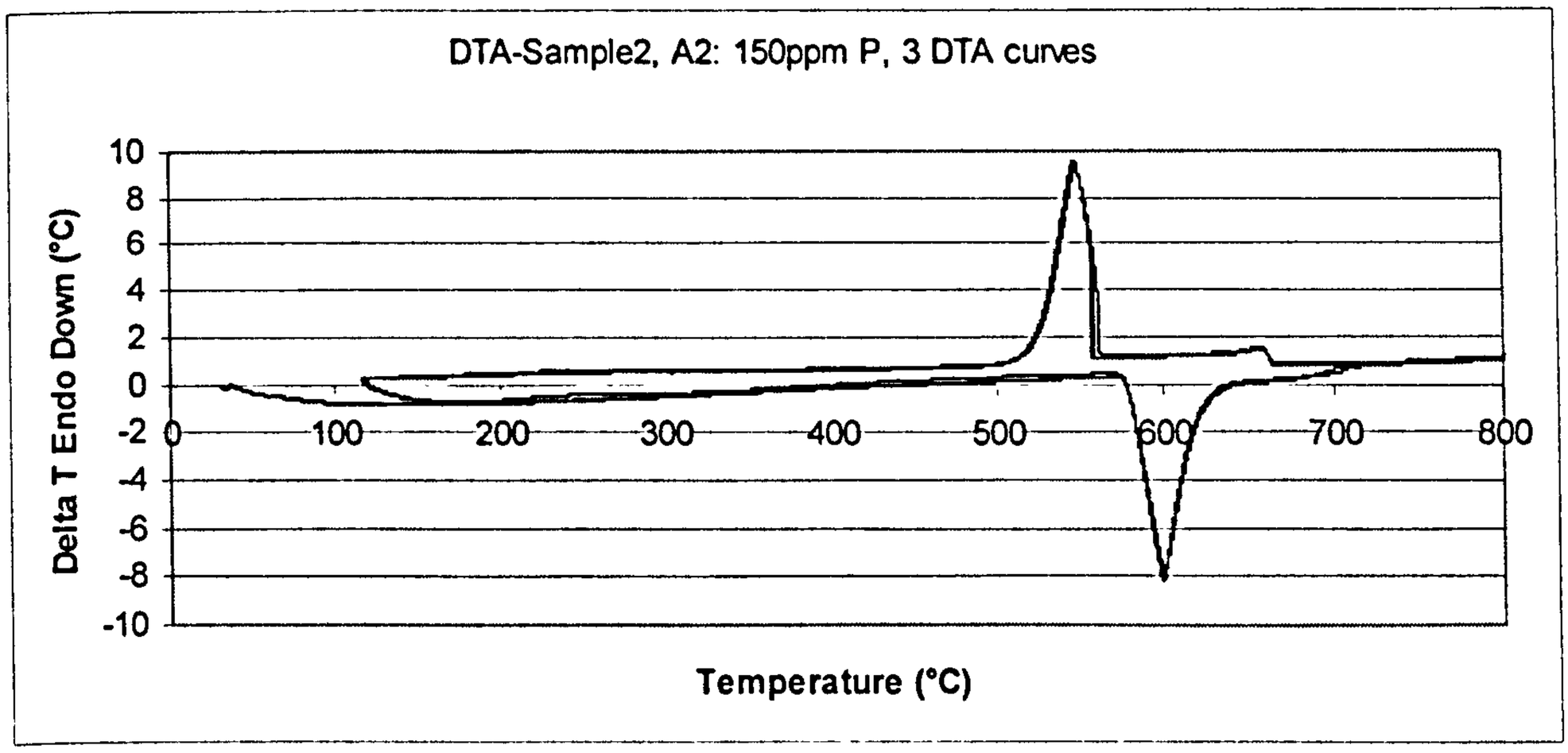

Figure 4.23 Three differential thermal analysis (DTA) curves performed on sample A2 (description in Table 3.6).

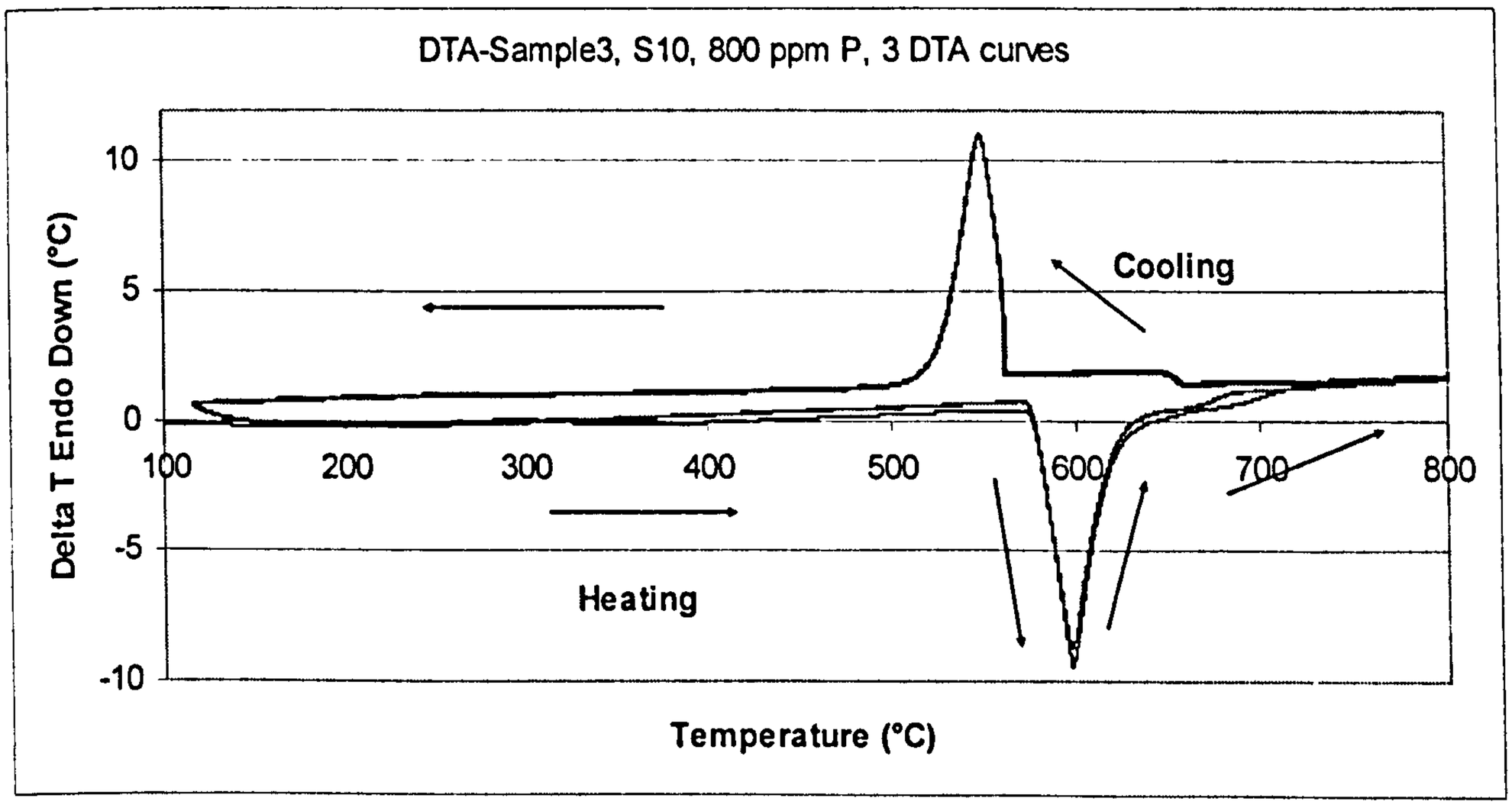

Figure 4.24 Three differential thermal analysis (DTA) curves performed on sample S10 (description in Table 3.6).

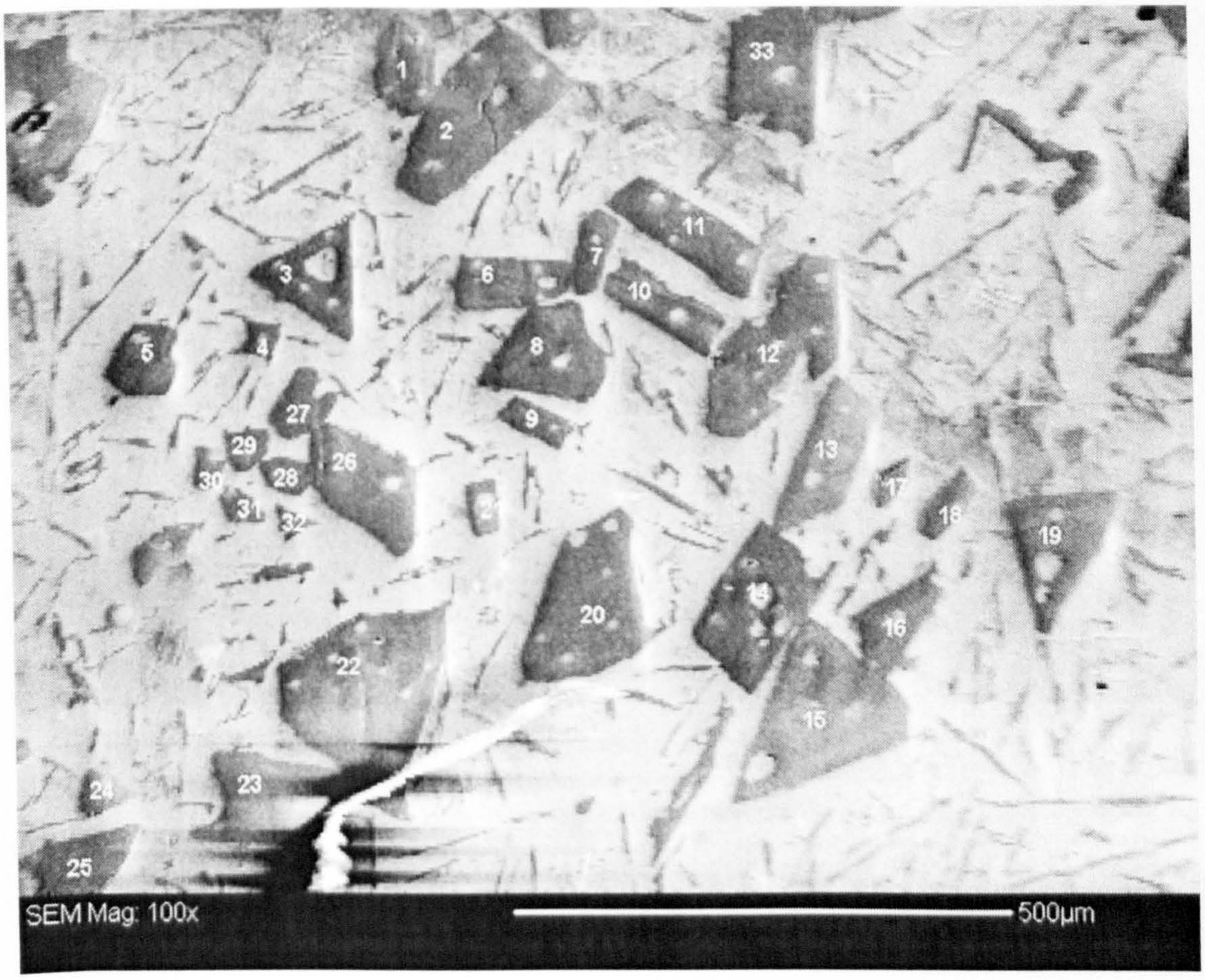

Figure 4.25 A randomly selected (but typical) part of the microstructure of Al-18.6 wt% Si uninoculated and bottom cast, used for EBSD (C3: cooling rate between T_f and T'_{Eu}: 0.35 K/s).

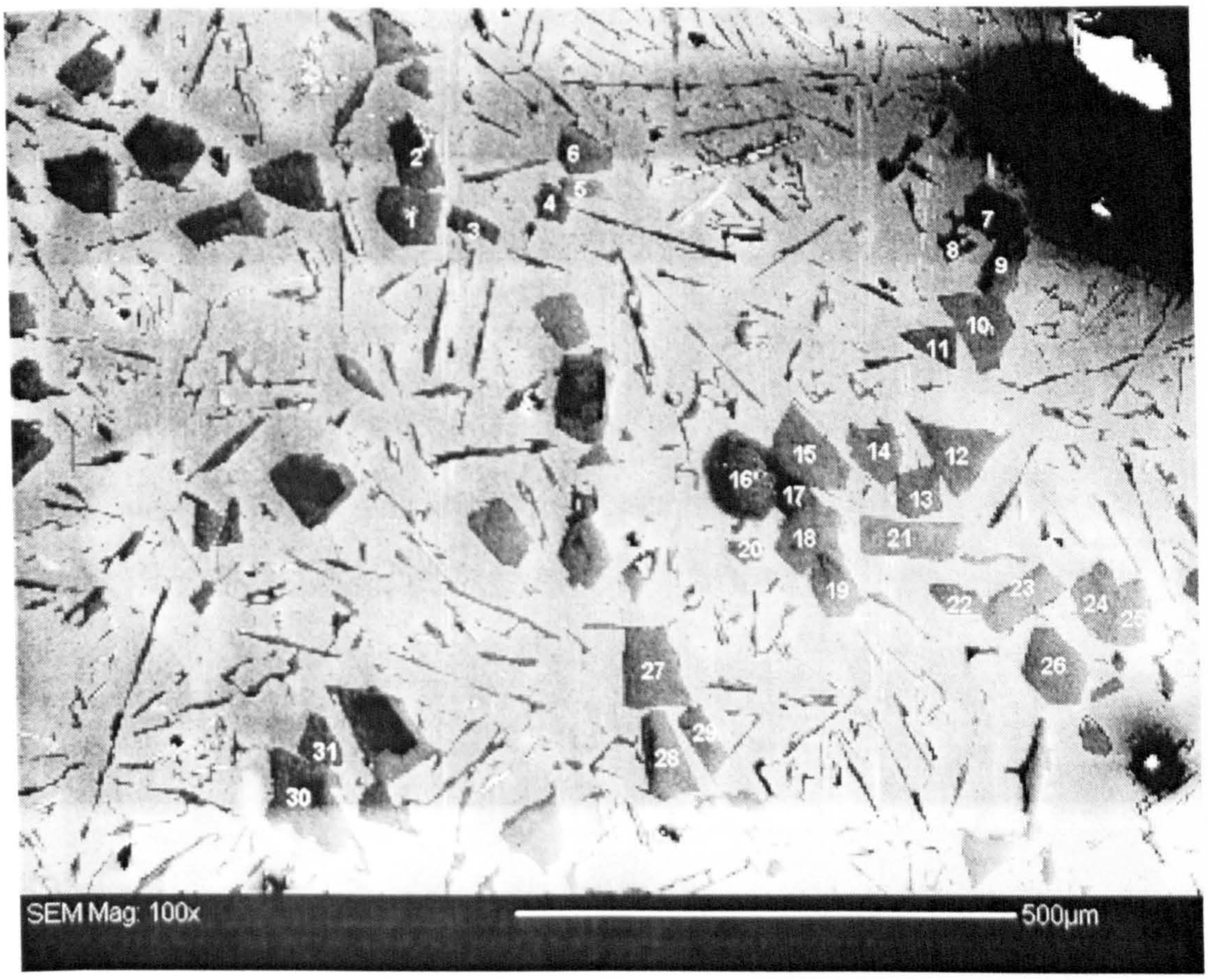

Figure 4.26 A randomly selected (but typical) part of the microstructure of Al-18.6 wt%Si inoculated with 150 ppm P and bottom cast (A2-1), used for EBSD (cooling rate between T_f and T'_{Eu}: 0.35 K/s).

Figure 4.27 Another randomly selected part of the microstructure of A2.

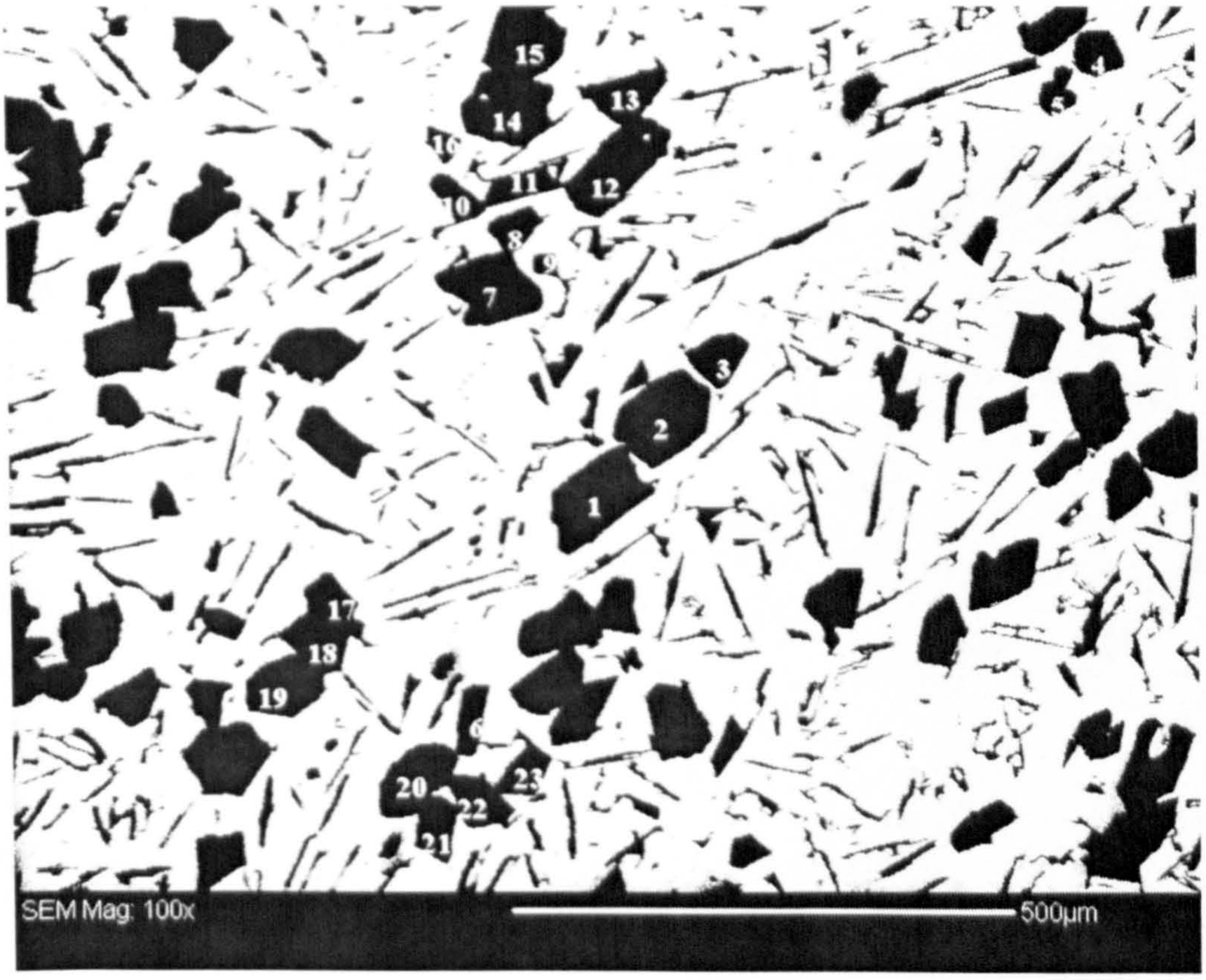

Figure 4.28 Another randomly selected part of the microstructure of A2.

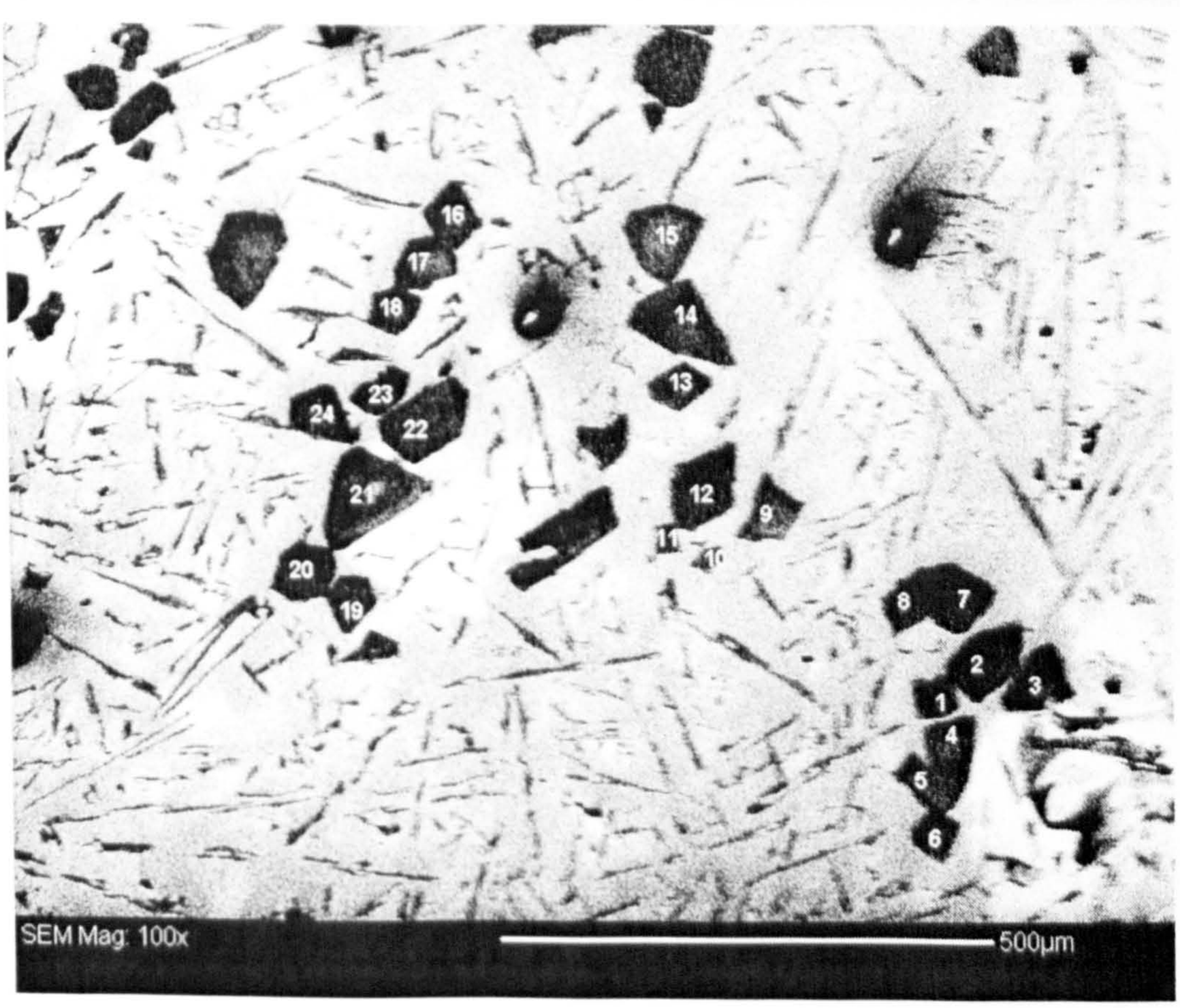

Figure 4.29 Another randomly selected part of the microstructure of A2.

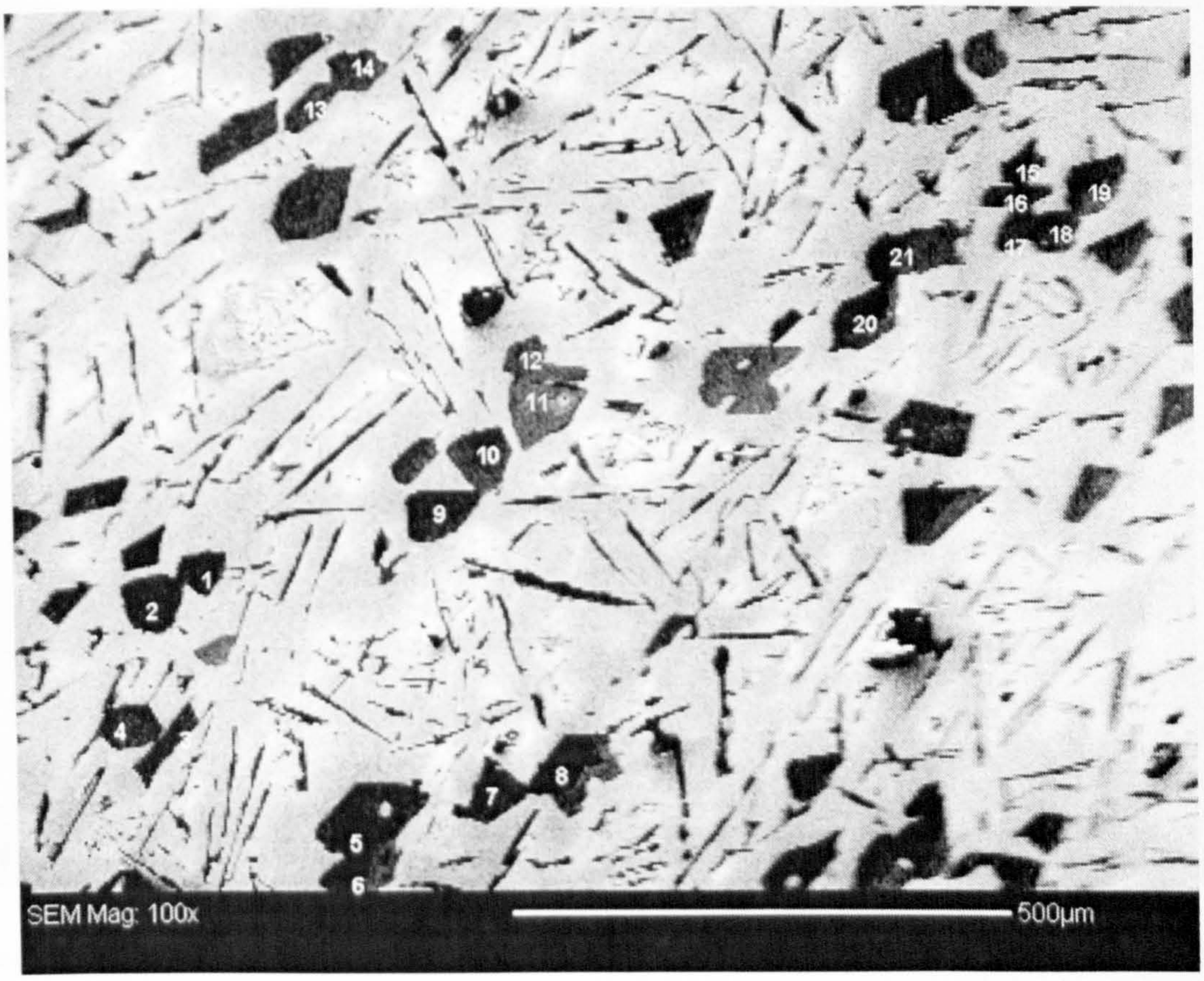

Figure 4.30 Another randomly selected part of the microstructure of A2.

Figure 4.31 A randomly selected (but typical) part of the microstructure of sample A2 (specified in Table 3.6) used for drawing pole figures of primary Si particles clusters.

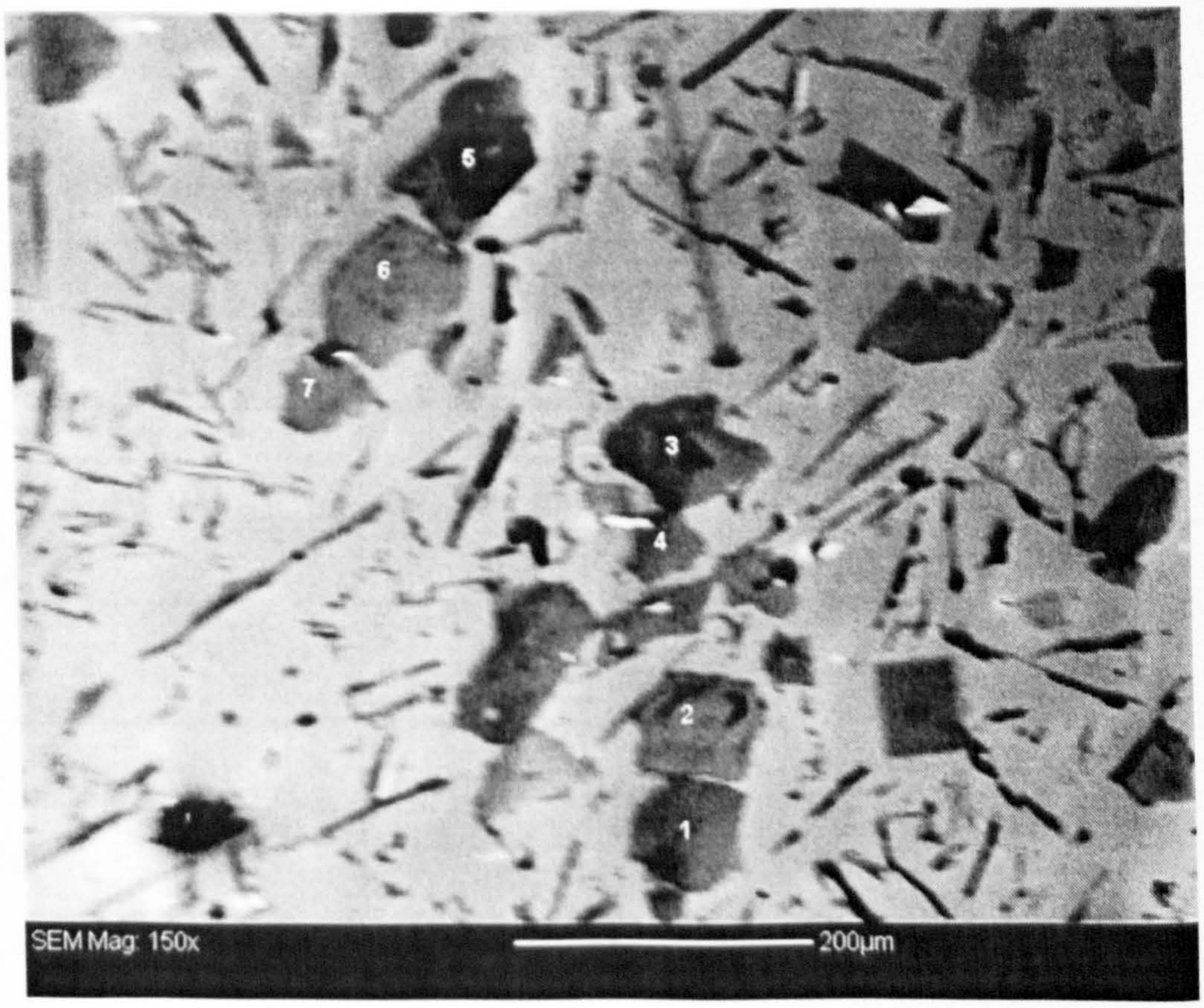

Figure 4.32 Another clusters in sample A2.

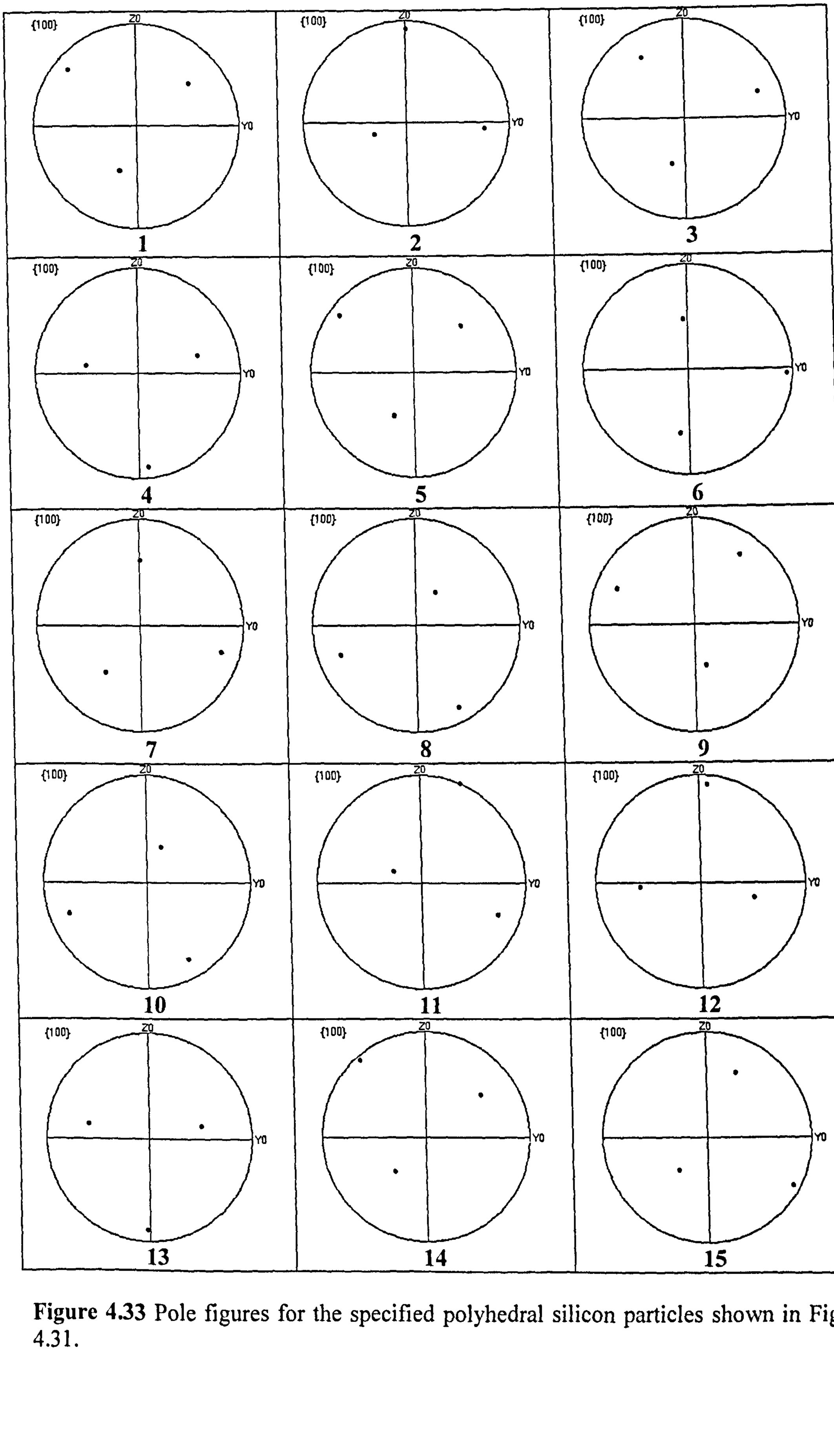

Figure 4.33 Pole figures for the specified polyhedral silicon particles shown in Fig. 4.31.

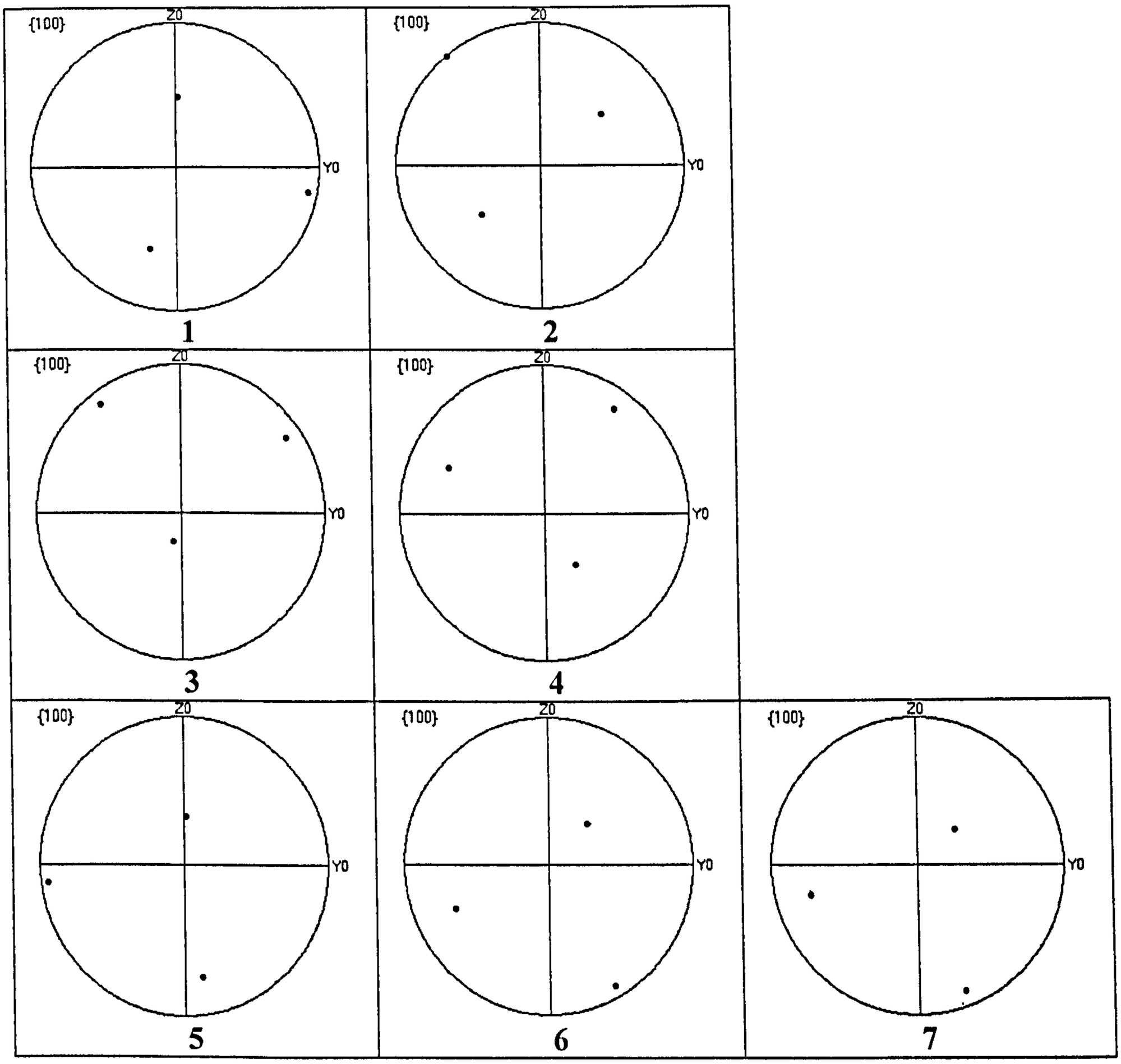

Figure 4.34 Pole figures for the specified polyhedral silicon particles shown in Fig. 4.32.

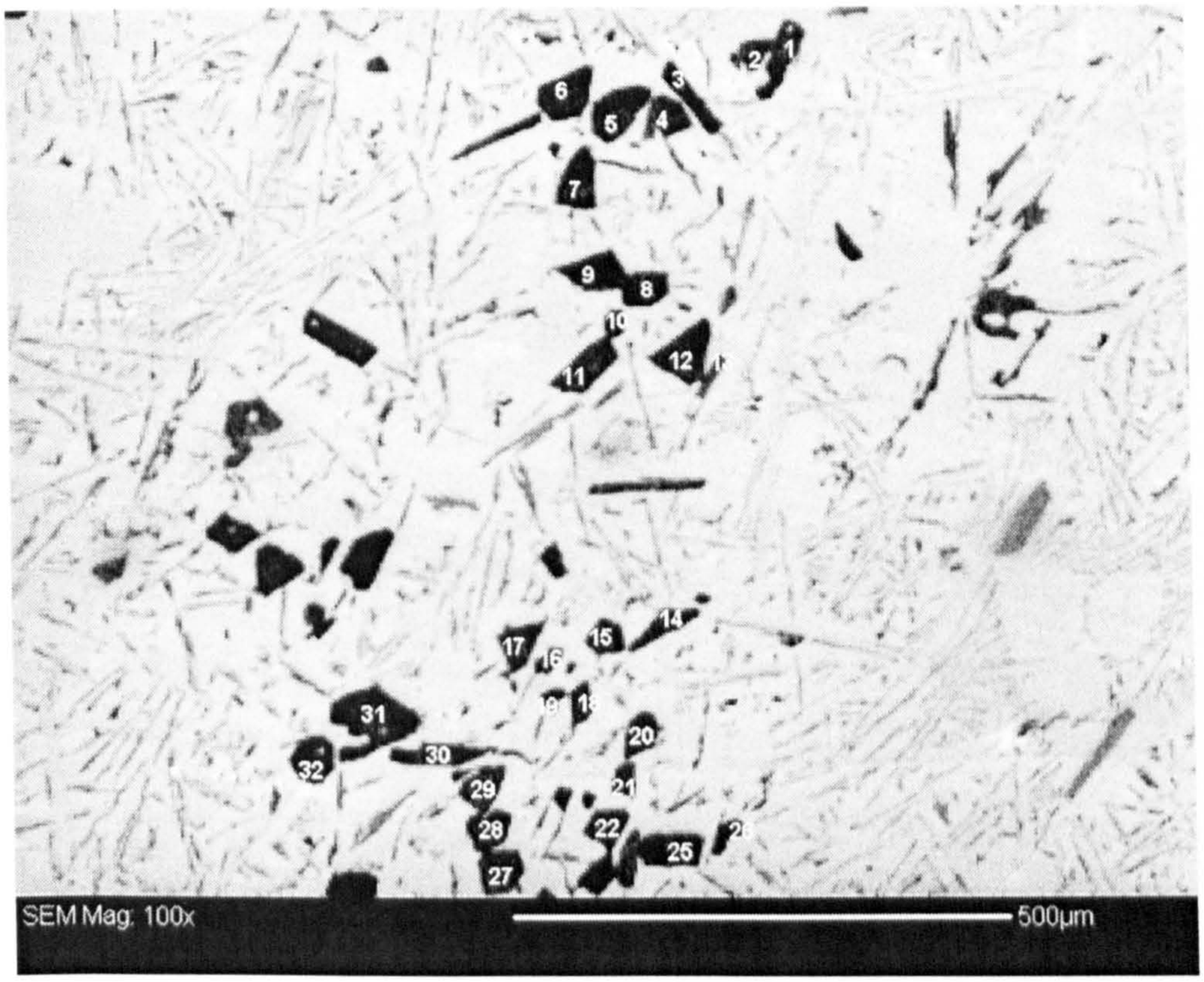

Figure 4.35 A randomly selected (but typical) part of the microstructure of Al-18.6 wt%Si uninoculated and chamber cast, used for EBSD (S1-1: cooling rate between T_f and T'_{Eu}: 0.77 K/s).

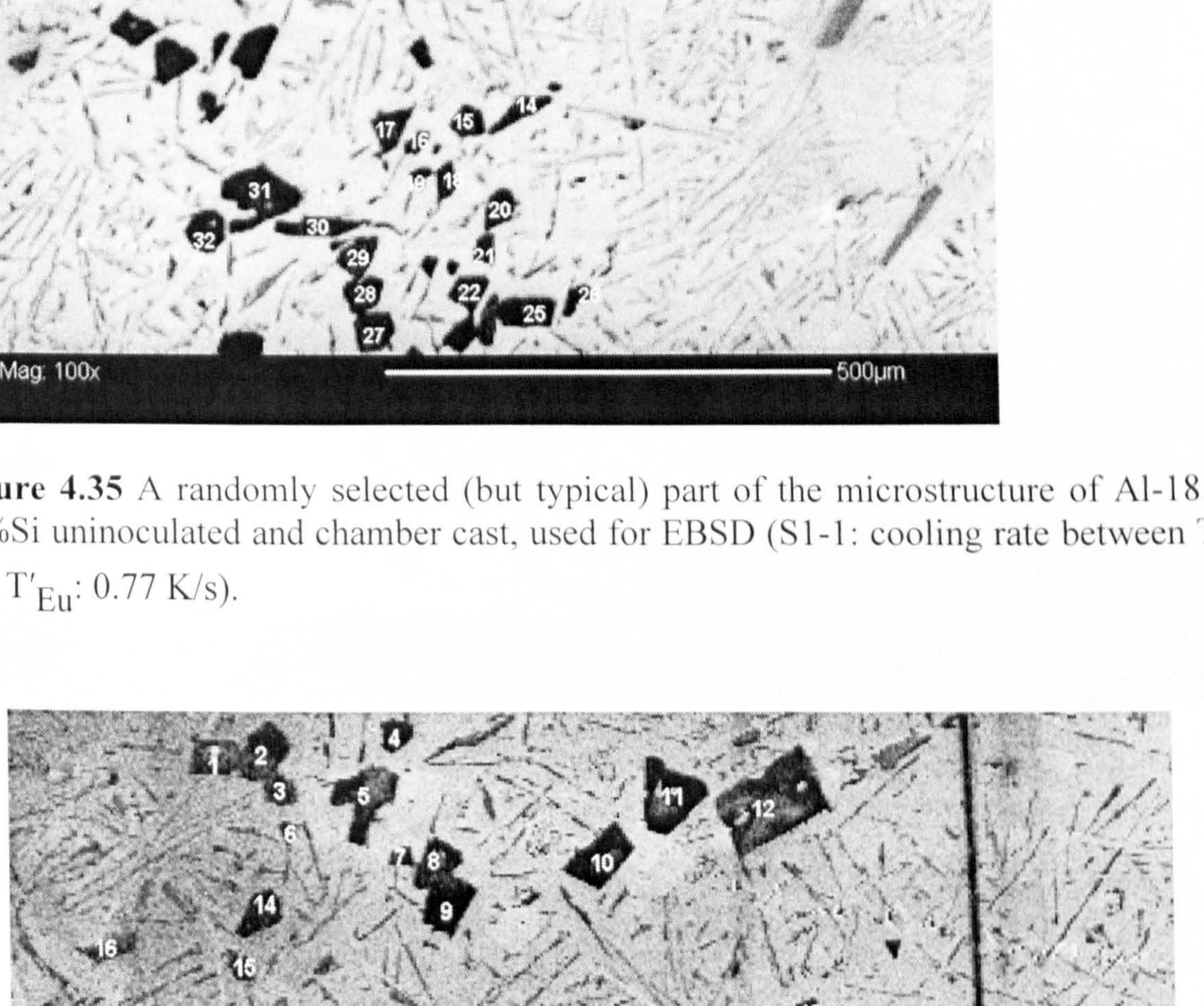

Figure 4.36 Another randomly selected part of the microstructure of S1.

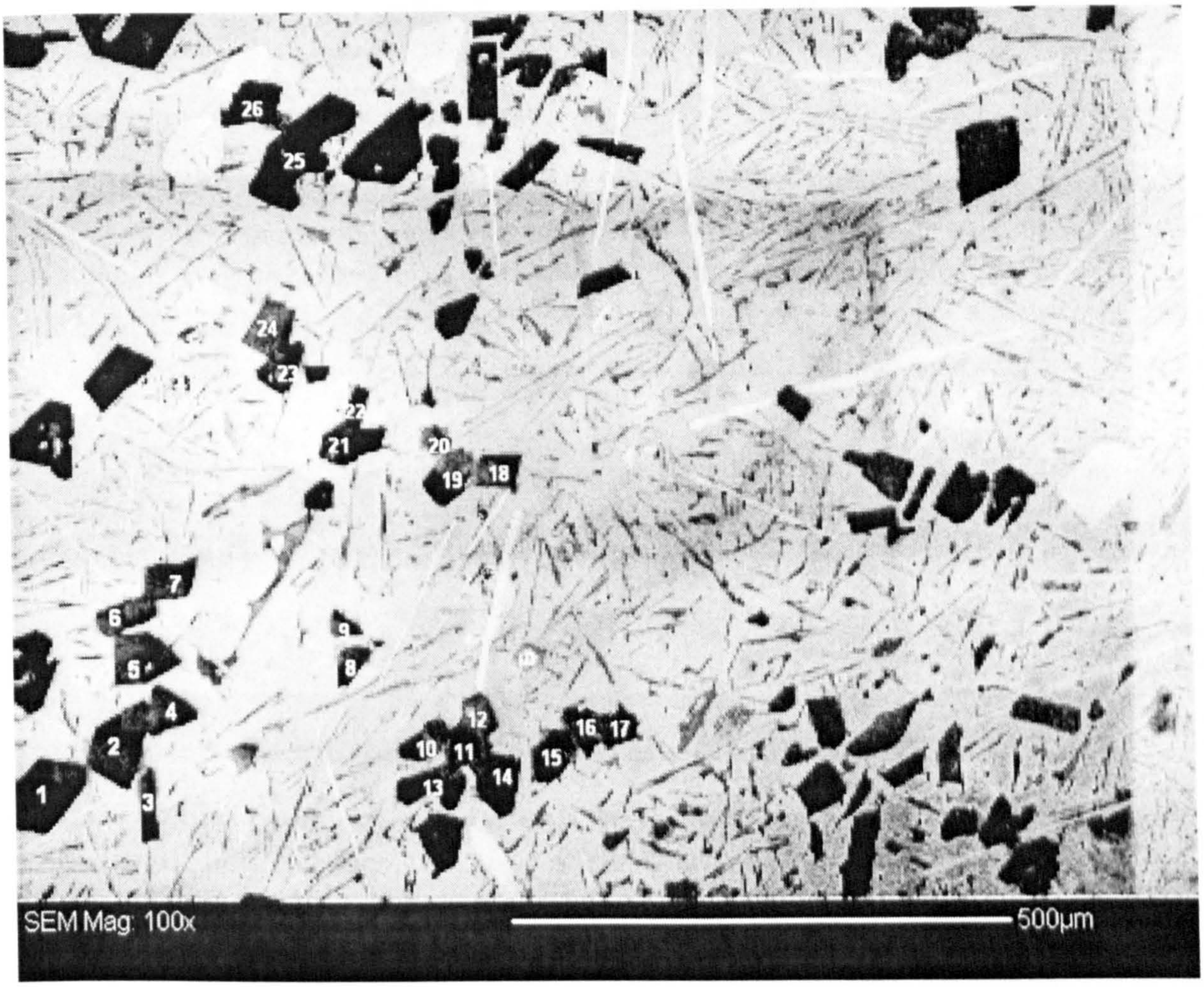

Figure 4.37 Another randomly selected part of the microstructure of S1.

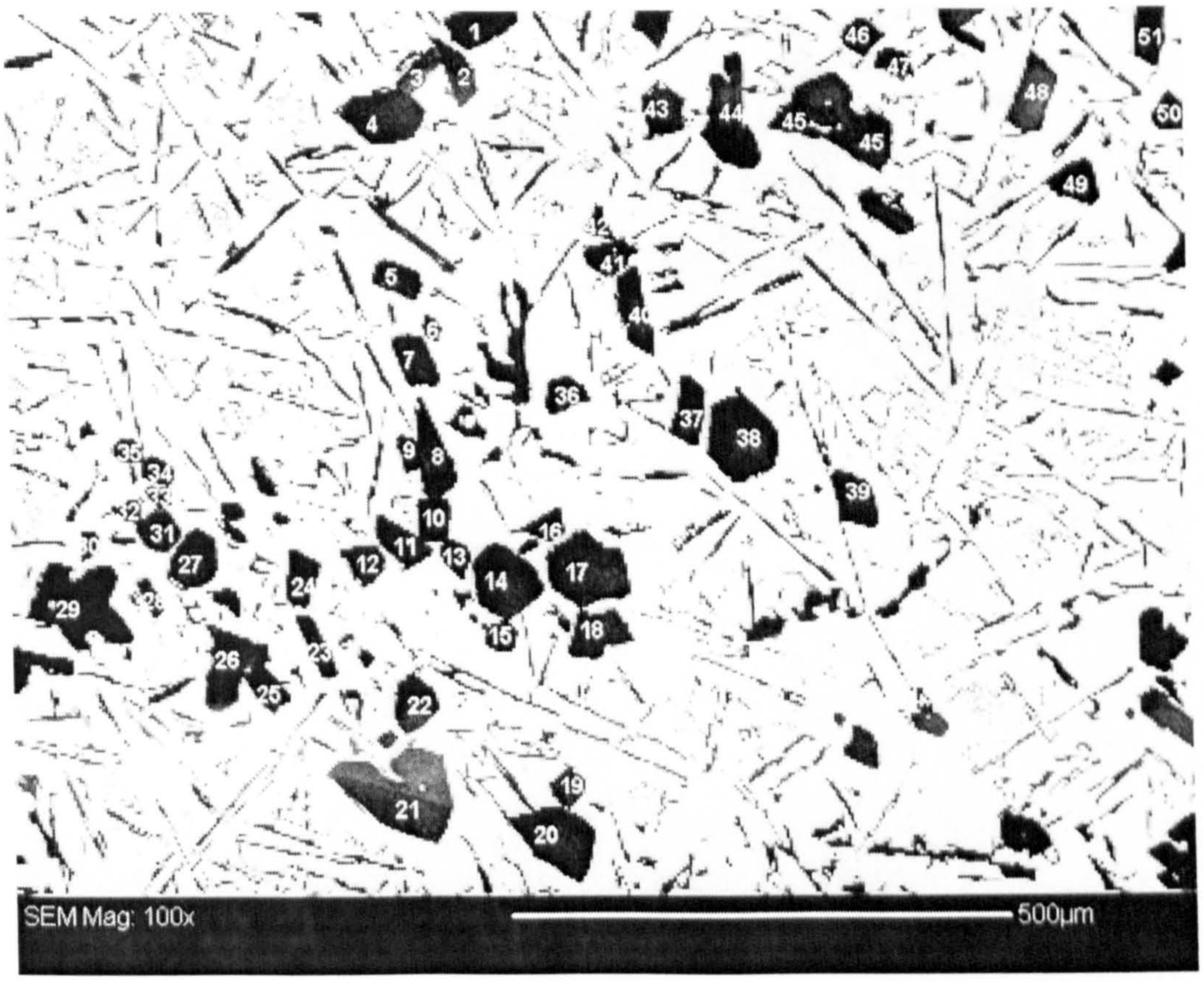

Figure 4.38 A randomly selected part of the microstructure of Al-18.6 wt% Si uninoculated and chamber cast, used for EBSD (S2: cooling rate between T_f and T'_{Eu}: 1.07 K/s).

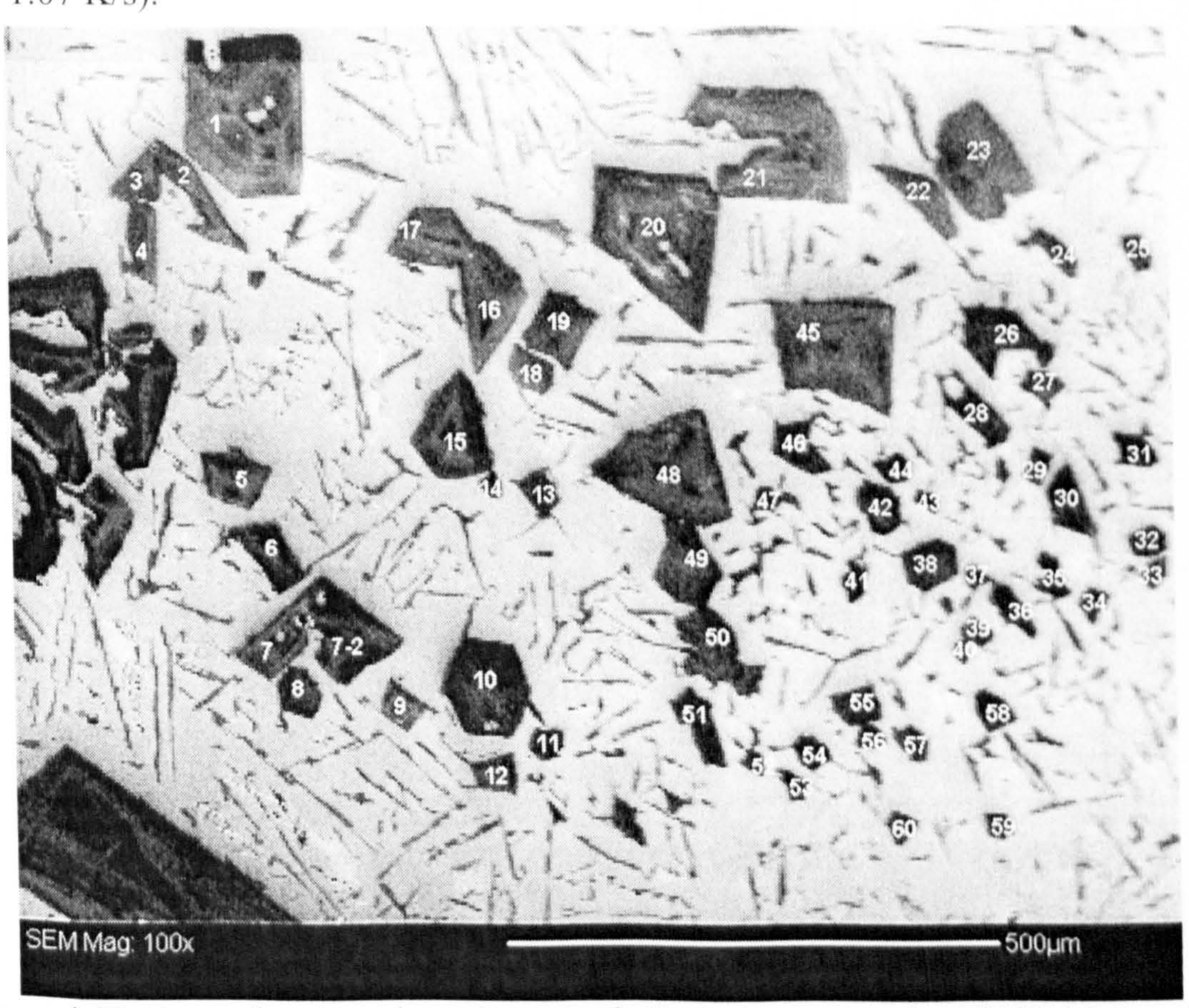

Figure 4.39 A randomly selected part of the microstructure of Al-18.6 wt% Si inoculated with 0.02 wt% P and bottom cast and chamber cast, used for EBSD (S5: cooling rate between T_f and T'_{Eu}: 1.0 K/s).

Figure 4.40-a A specific cluster of polyhedral silicon particles, shown in Fig. 4.38.

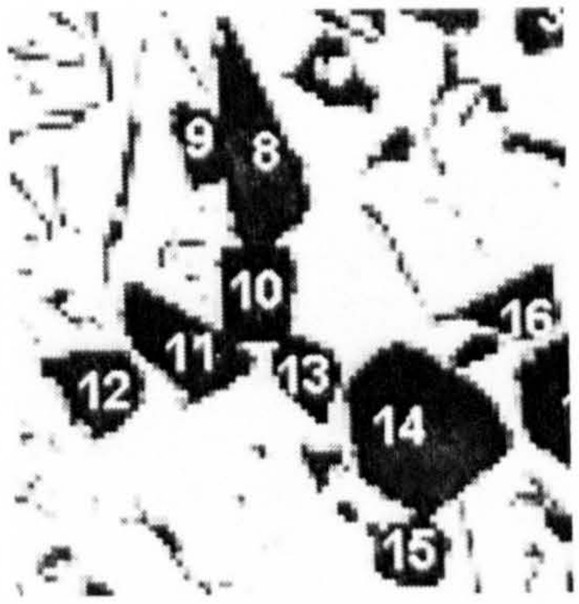

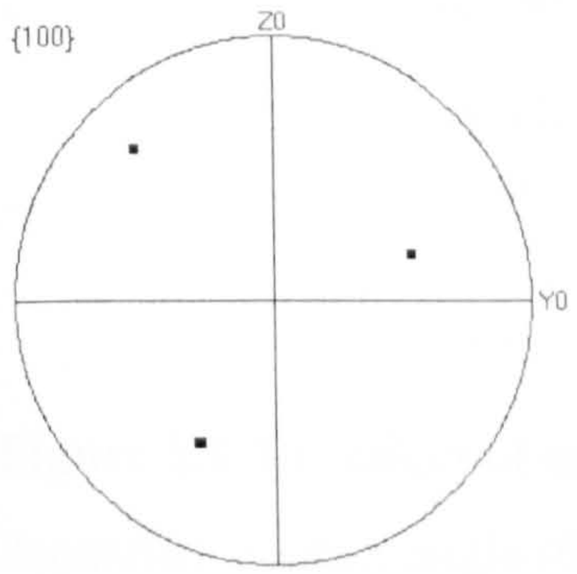

A. Particle No 8

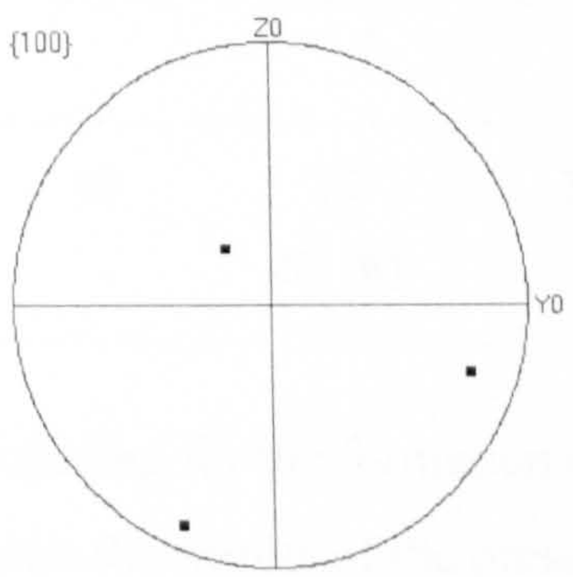

B. Particle No 9.

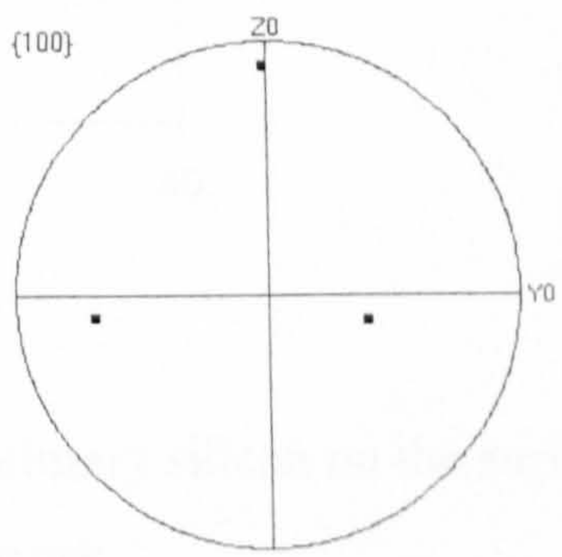

C. Particle No 10.

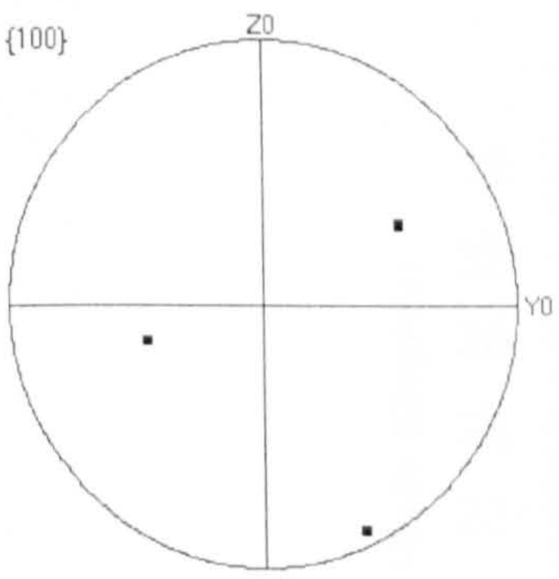

D. Particle No 11.

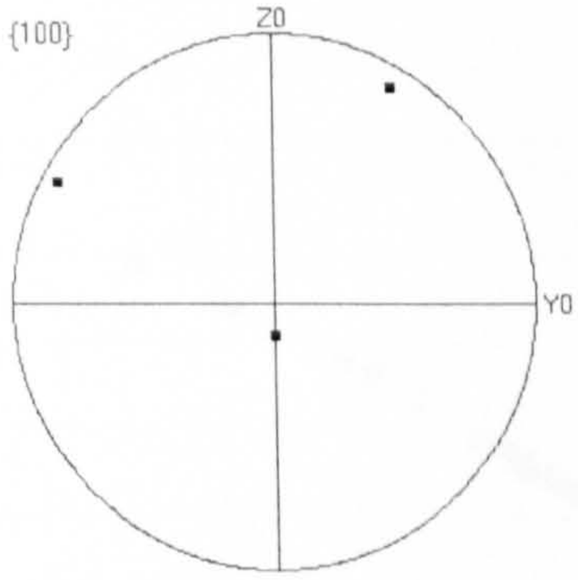

E. Particle No 12.

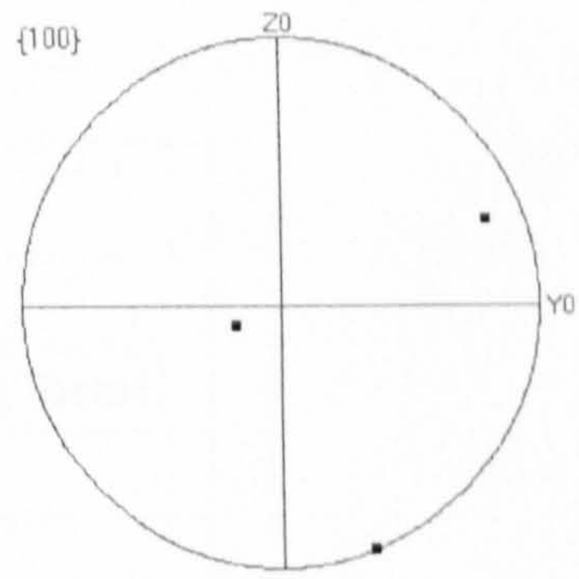

F. Particle No 13.

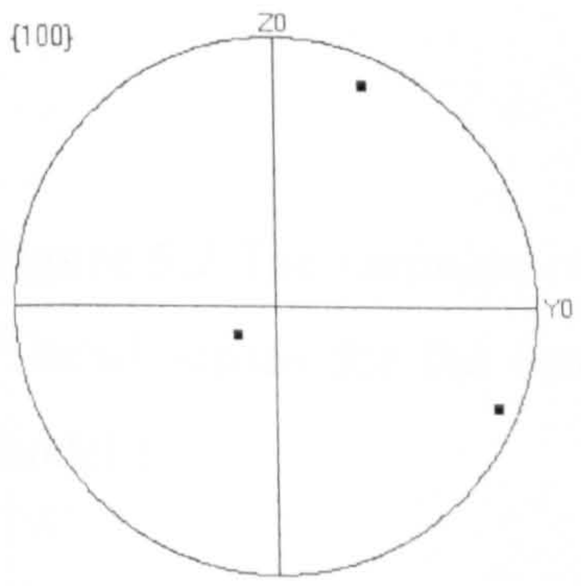

G. Particle No 14.

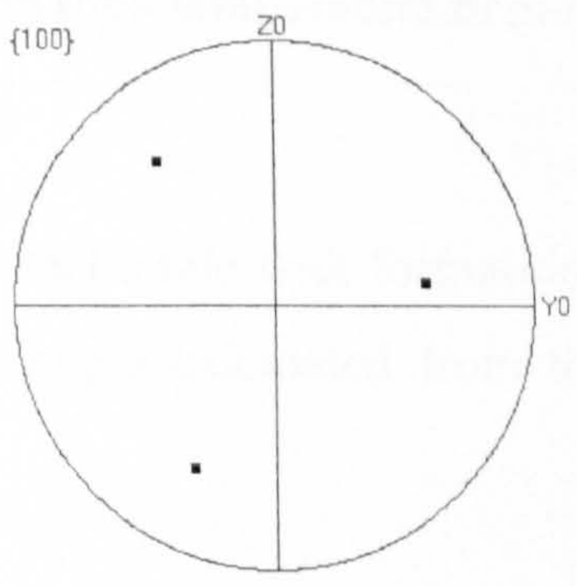

H. Particle No 15.

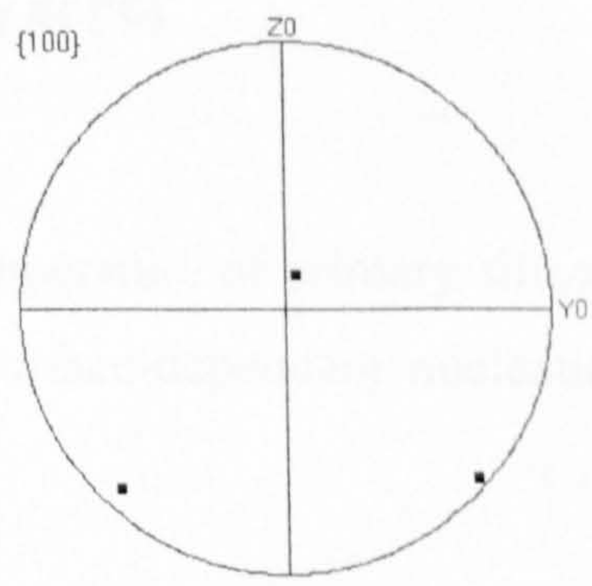

I. Particle No 16.

Figure 4.40-b shows pole figures drawn for 9 polyhedral primary silicon particles specified as Nos. 8-16 in Fig. 4.38 (uninoculated Al-18.6 wt% Si, chamber cast).

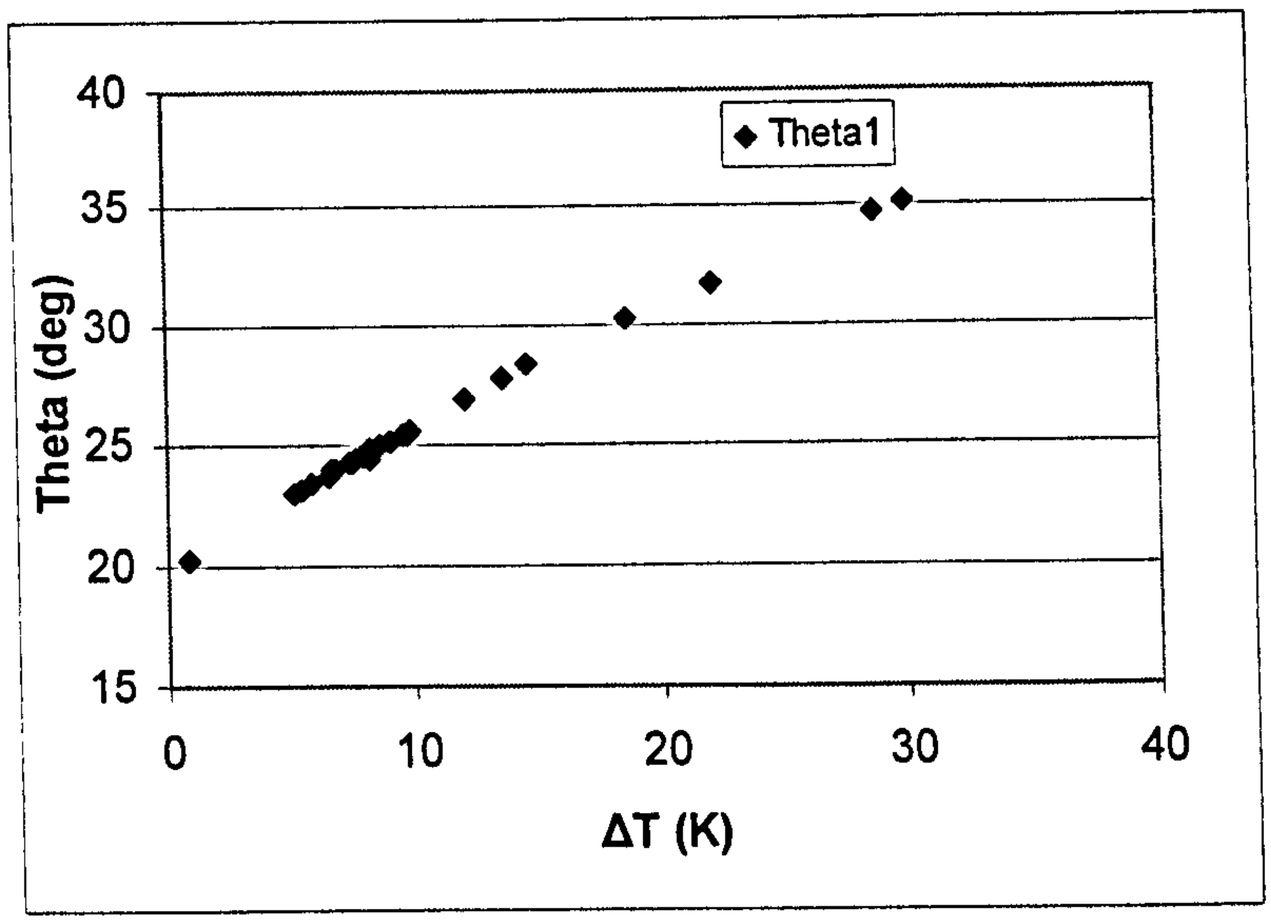

Figure 5.1 The effect of undercooling for the formation of primary silicon on the surface-dependant contact angle (θ_1) from the results of the present work.

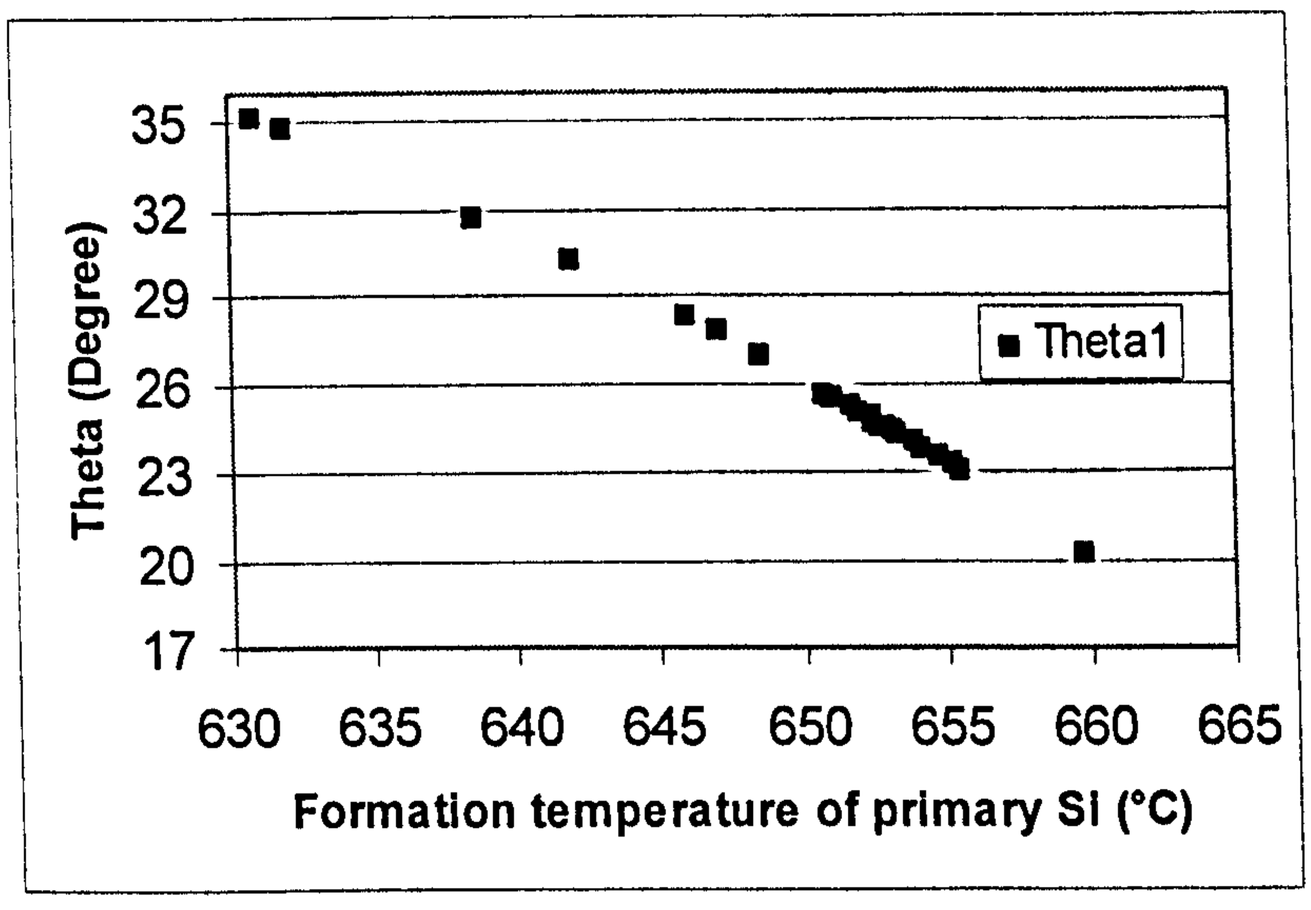

Figure 5.2 The variation of contact angle with formation temperature of primary silicon. (Theta1 stands for the contact angle calculated from the surface-dependant nucleation model.)

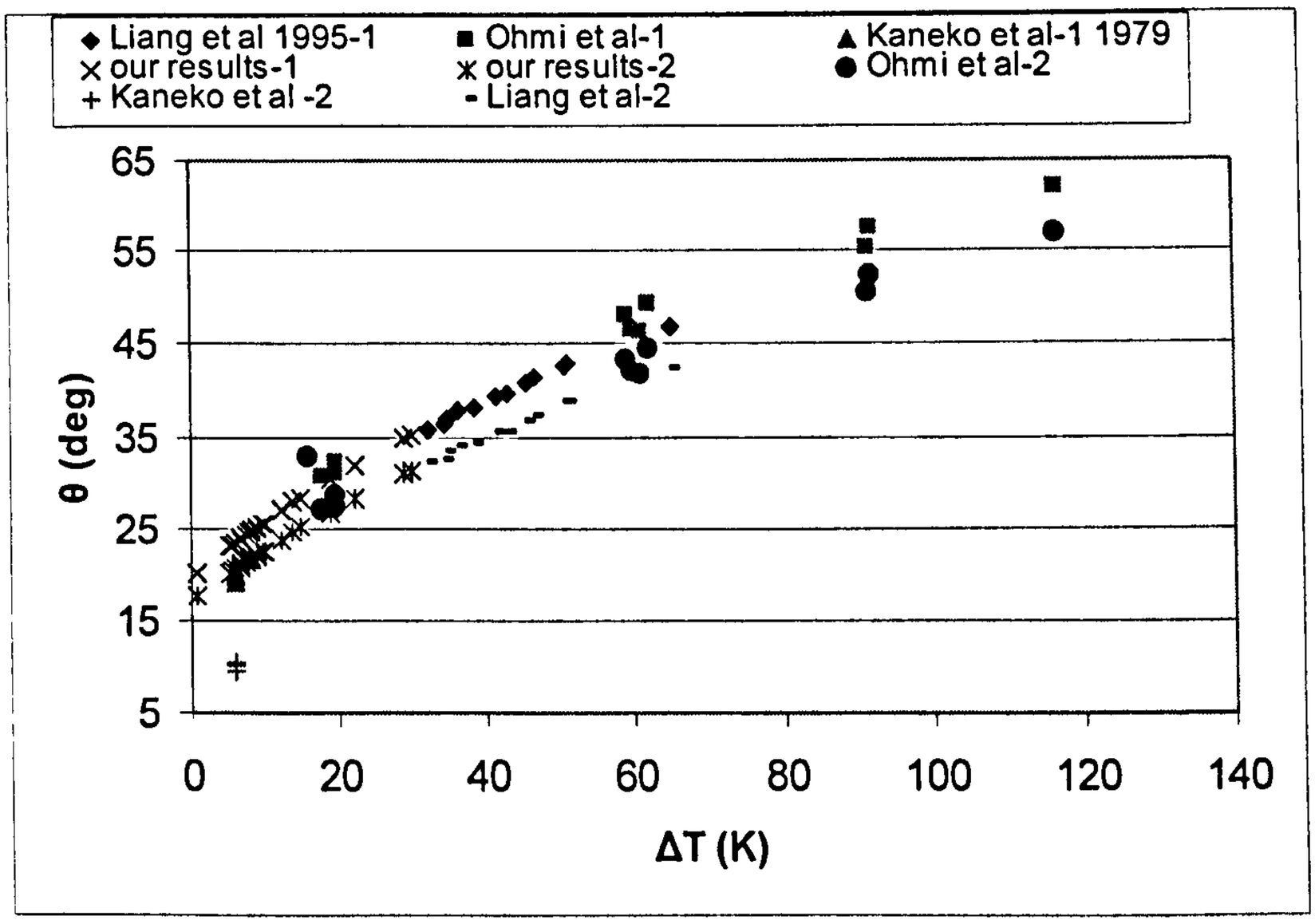

Figure 5.3 The change of contact angle with undercooling for the formation of primary silicon for our results and those of other workers. (There are two groups of results: one represents Theta1, the contact angle calculated from the surface-dependant nucleation model and the second represents Theta2, the contact angle from the volume-dependant model.). Liang et al (1995): Al-18.3 wt% Si, no P addition, $\dot{T}$: 0.6-18.9 K/s, Kaneko et al (1979): Al-19 wt% Si, 0.02 wt% P addition, $\dot{T}$: 0.017-1.67 K/s, Ohmi et al (1991, 1994): Al-32 wt% Si, Al-22 wt% Si, uninoculated, $\dot{T}$: 10.7-198 and 13.1-221 K/s, respectively.

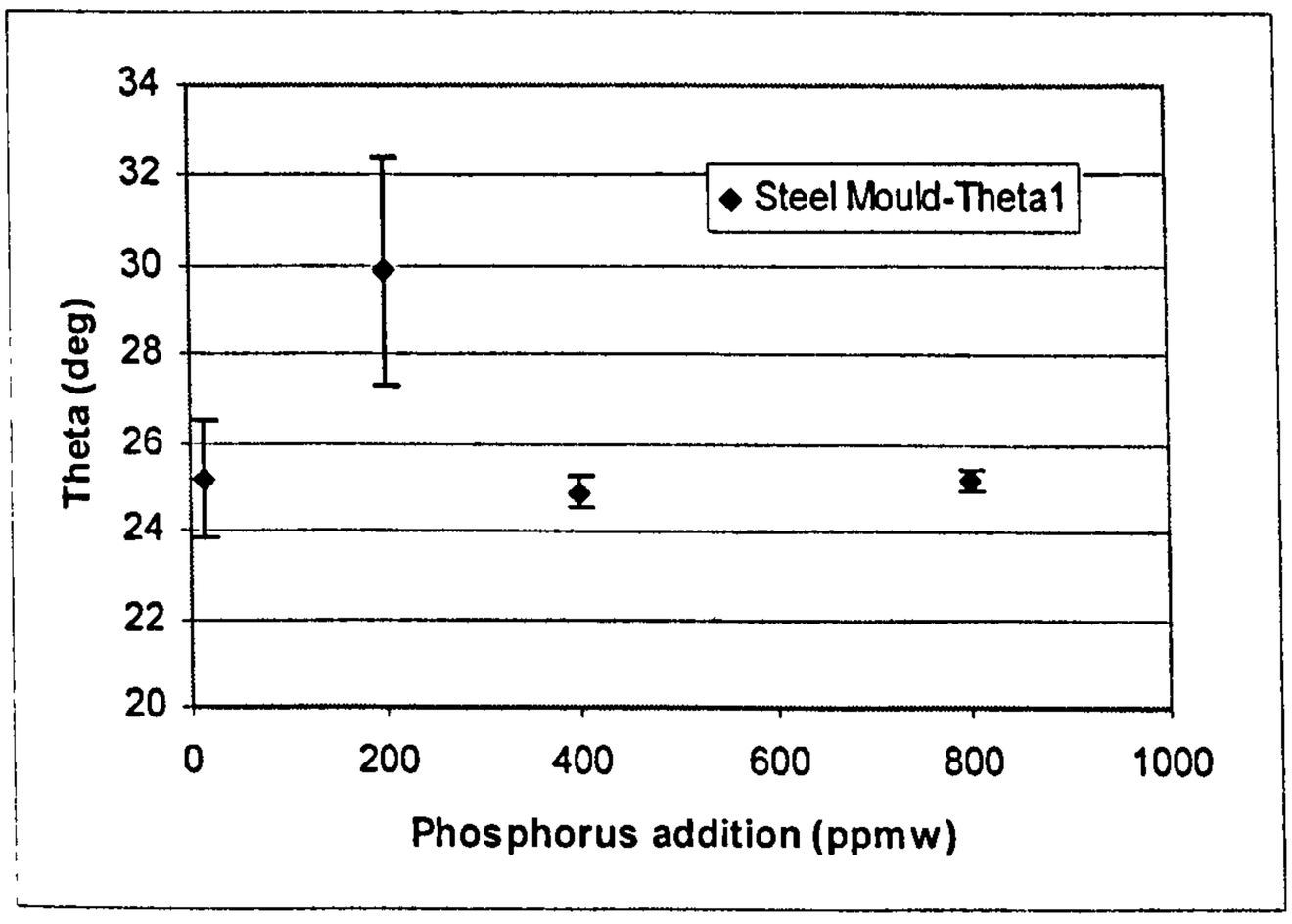

Figure 5.4 The effect of amount of phosphorus addition on the value of contact angle calculated via the surface-dependent model. (The uninoculated samples are considered as inoculated by 0.0014 wt% P as the cast ingot already had that trace of phosphorus.)

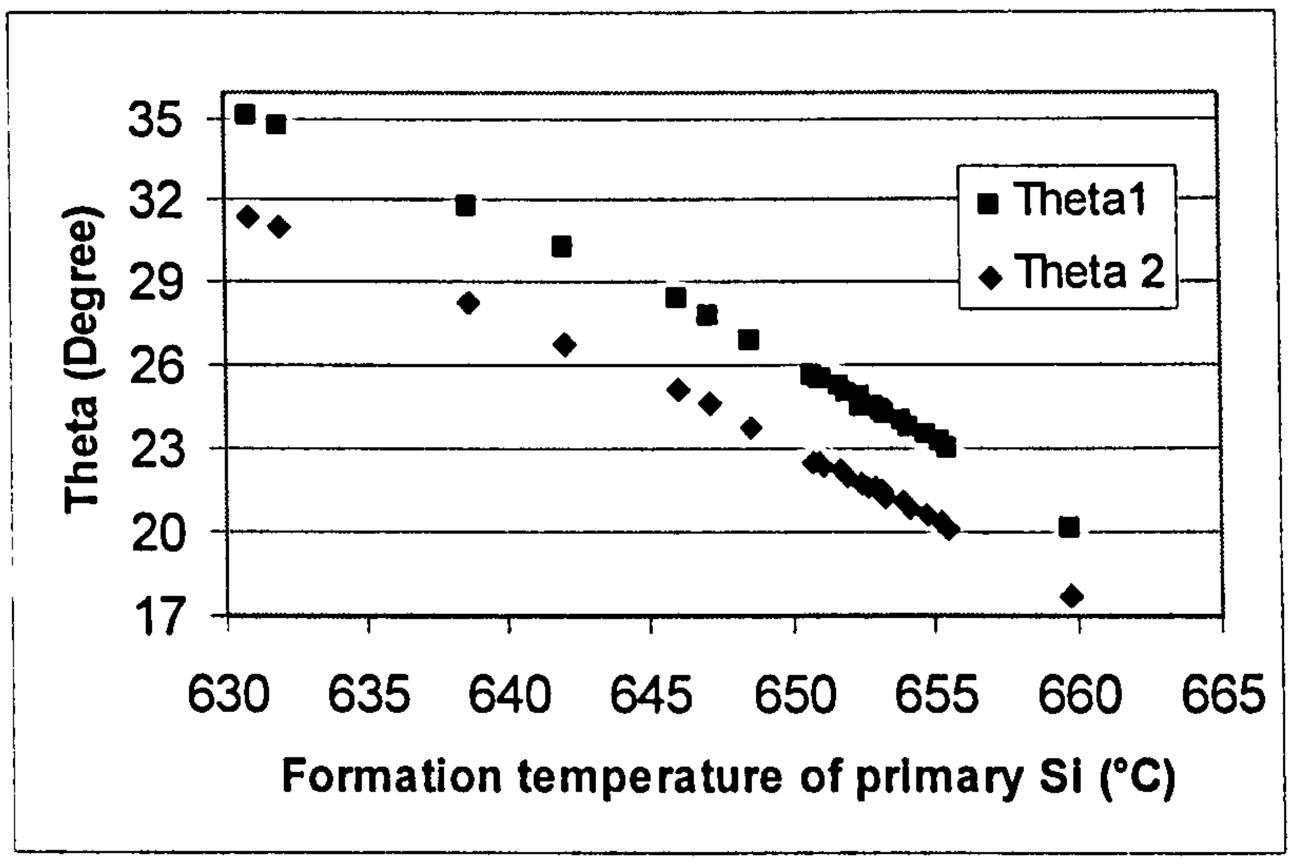

Figure 5.5 The variation of contact angle with formation temperature of primary silicon. (Theta1 stands for the contact angle calculated from the surface-dependant nucleation model and Theta2 represents the contact angle from the volume-dependant model.)

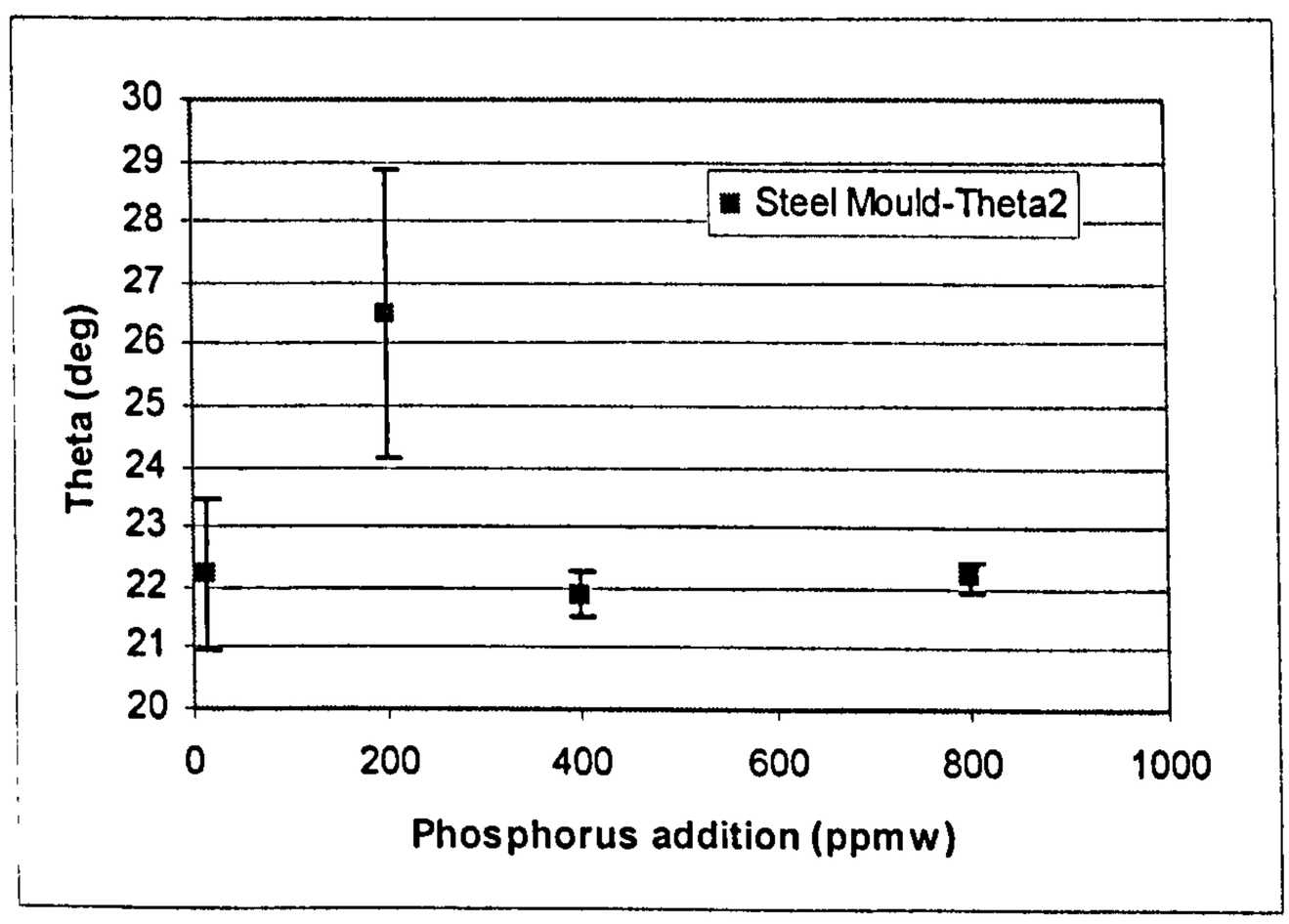

Figure 5.6 The effect of phosphorus addition on the value of contact angle calculated via the volume-dependent model. (The uninoculated samples are considered as inoculated by 0.0014 wt% P as the cast ingot already had that trace of phosphorus.)

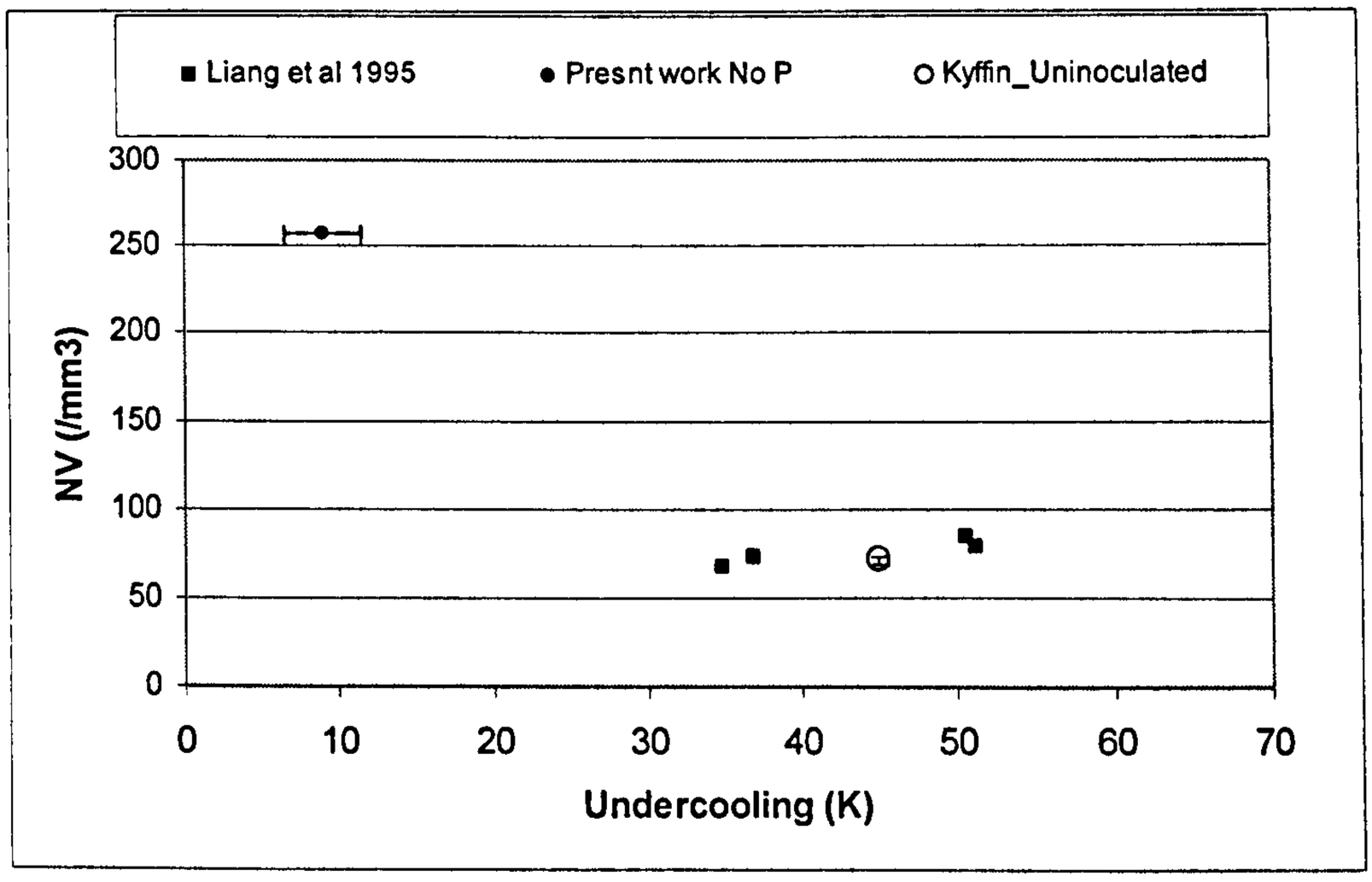

Figure 5.7.a The effect of undercooling on the number of primary silicon particles for different workers for uninoculated alloys. (Liang et al (1995): Al-18.3 wt% Si, $\dot{T}$: 1.0-2.0 K/s, Kyffin et al (2001): Al-20 wt% Si, $\dot{T}$: 1.1 K/s, the present work: Al-18.6 wt% Si: ingots chamber cast into steel mould, $\dot{T}_1$: 2.10 K/s.)

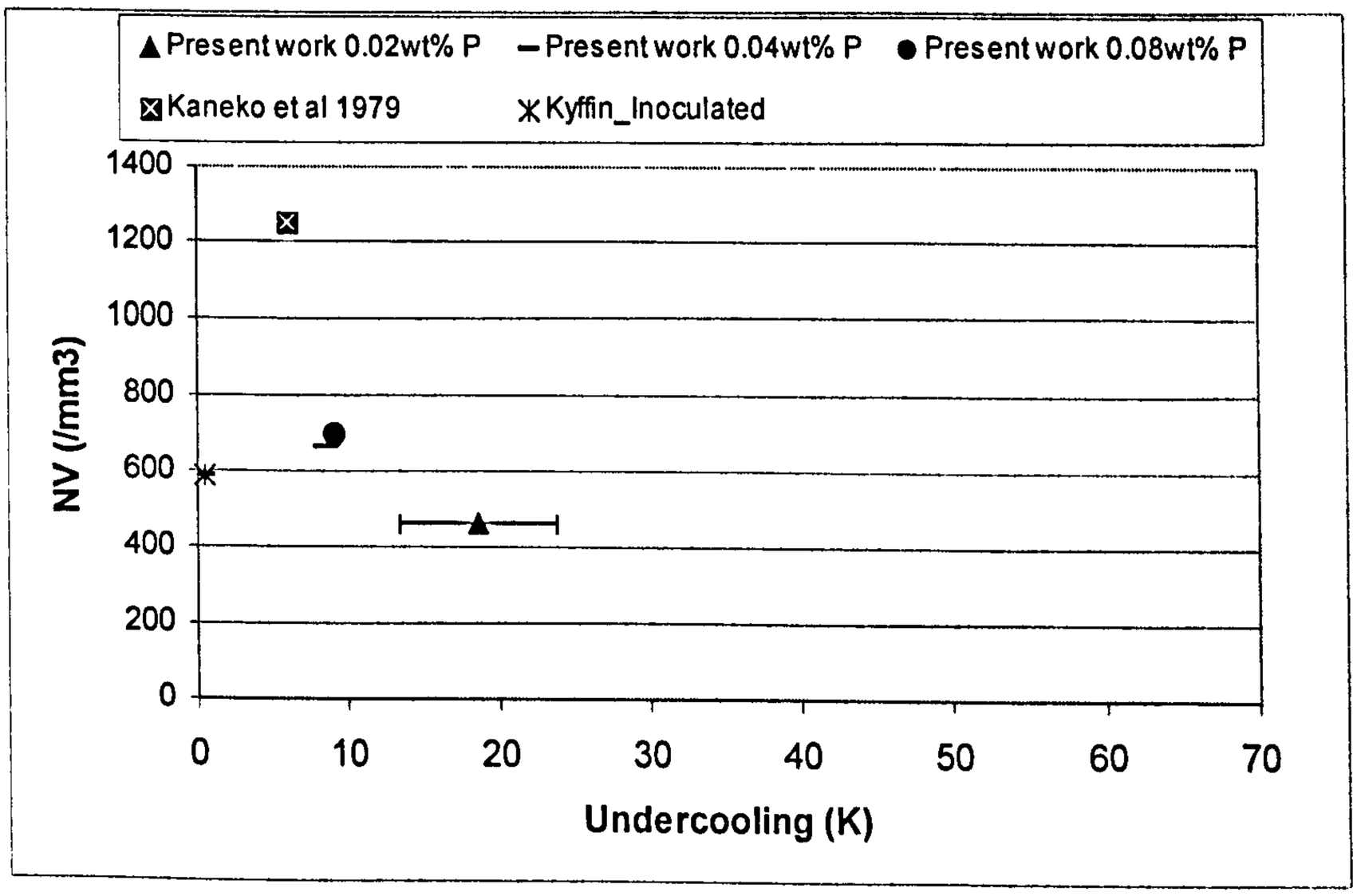

Figure 5.7.b The effect of undercooling on the number of primary silicon particles for different workers for P-inoculated alloys. (Kaneko et al (1979): Al-19 wt% Si, 0.02 wt% P addition, $\dot{T}$: 1.67K/s, Kyffin et al (2001): Al-20wt%Si, 0.01 wt% P, $\dot{T}$: 1.1 K/s, the present work: Al-18.6 wt% Si, 0.02, 0.04, 0.08 wt% P, ingots chamber cast into steel mould, with $\dot{T}_1$: 2.29, 2.54 and 2.57 K/s, respectively.)

JOURNAL OF MATERIALS SCIENCE

Effect of solidification cooling rate and phosphorus inoculation on number per unit volume of primary silicon particles in hypereutectic aluminium—silicon alloys

M. FARAJI, I. TODD, H. JONES
Department of Engineering Materials, University of Sheffield, Mappin Street, Sheffield, S1 3JD, UK

Published online: 5 October 2005

Collected data on derived number per unit volume $\bar{N}_V$ of primary silicon particles in hypereutectic Al-Si alloys show a power relationship with solidification cooling rate $\dot{T}$ of the form $\bar{N}_V = A\dot{T}^n$ where typically $n \sim 1$ and $A \simeq 130\ mm^{-3}\ (K/s)^{-1}$ in the absence of phosphorus and $A \simeq 720\ mm^{-3}\ (K/s)^{-1}$ in its prescence. Significantly lower apparent values of $\bar{N}_V$ from one set of results appear to stem from measurement of a mean long dimension rather than diameter of particle sections as well as lower measured undercoolings than in Bridgman experiments at similar $\dot{T}$.

Size refinement of primary silicon in hypereutectic Al-Si base alloys is a key requirement for meeting property targets [1–4] and can be achieved by inoculation with phosphorus, as is routinely applied in conventional foundry practice [5], or by increasing the cooling rate during solidification, which has been applied, for example, in the development of improved performance in alloys processed by spray forming [6], and other rapid solidification technologies [8]. Arnold and Prestley [9] showed micrographs indicating size refinement of primary silicon in Al-16 wt%Si with increase of solidification cooling rate $\dot{T}$ in the range 0.6 to 1.5 K/s, but the results were not quantified. Sulzer [10] reported refinement of primary silicon size from 27 ± 4 μm at 3 K/s to 15.5 ± 1.5 μm at 70 K/s for Al-20Si-1Cu-1Mg (wt%) base alloy with 0.16 wt% P addition. Kaneko *et al.* [11] determined average size and number per unit area of section $\bar{N}_A$ of primary silicon in Al-19 wt%Si-0.02 wt%P alloy over the range of $\dot{T}$ between 0.02 and 2 K/s, and obtained a linear relationship between logarithm of derived number of particles per unit volume $\bar{N}_V$ and log $\dot{T}$, with a slope of ~1.4. Moir and Jones [12] combined their own measurements of $\bar{N}_A$ versus solidification growth velocity V for two different temperature gradients G (Bridgman solidification and tungsten inert gas weld traversing) with measurements by Pierantoni *et al.* [13] for laser surface melt traversing to show a linear relationship between log $\bar{N}_A$ and log $(G\sqrt{V})$ with a slope of unity. Bayraktar *et al.* [14] combined all these results with additional Bridgman measurements to show $\lambda\ \dot{T}^{1/3} = 250\ \mu m\ (K/s)^{1/3}$ over the range $0.02 < \dot{T} < 10^6$ K/s where $\lambda = \bar{N}_A^{-1/2}$ is a measure of the primary silicon interparticle spacing. Mandal *et al.* [4] reported mean particle size $\bar{D}_A$ of primary silicon versus $\dot{T}$ in the range 15 to 31 K/s for Al-17, 22 and 27 wt%Si with 0.1 and 0.2 wt% P additions. Ohmi *et al.* [15, 16] reported $\bar{D}_A$ (*but see below*) of primary silicon and associated nucleation undercooling ΔT_m for Al-22 and 32 wt%Si for solidification cooling rates in the range 11 to 260 K/s, and showed particle size decreasing linearly with increase in undercooling and increasing with increased cooling rate (results show a reasonable fit with $\Delta T_m = A\dot{T}_{K/s}^n$ with $A = 3.5$ K $(K/s)^{-n}$ and $n = 0.6$). Liang *et al.* [17] measured $\bar{N}_A$ and $\bar{D}_A$ together with formation temperature T_f of primary silicon versus V and G in Bridgman in solidification of Al-18.3 wt%Si for comparison with model predictions for steady state heterogeneous nucleation of the primary silicon from the bulk melt. The experimental results show $N_v \propto \dot{T}^{1.2}$ and that nucleation undercooling increases from ~35 to ~52 K over the range $1 < \dot{T} < 20$ K/s, consistent with the model prediction for a nucleation contact angle θ increasing from 26 to 36 deg over the same range of $\dot{T}$. Most recently Kyffin *et al.* [18] reported the effect of phosphorus inoculation on $\bar{N}_A$ of primary silicon for the range $0.8 < \dot{T} < 16.5$ K/s for comparison with the results of Sulzer [10] for $3 < \dot{T} < 70$ K/s, Kaneko *et al.* [11] for $0.02 < \dot{T} < 2$ K/s and Mandal *et al.* [4] for $15 < \dot{T} < 30$ K/s.

The present purpose is to investigate the possible generality of the relationships between $\bar{N}_V$ and $\dot{T}$ obtained by Kaneko *et al.* [11], Ohmi *et al.* [15, 16] and Liang *et al.* [17]. The available experimental data are summarised in Table I and plotted in Fig. 1 as log $\bar{N}_V$ versus log $\dot{T}$. The results for phosphorus-free samples fall into two groups. Results from Bridgman solidification, TIG weld traversing and laser surface melt

0022-2461
DOI: 10.1007/s10853-005-3103-4

TABLE I Summary of data on $\bar{N}_V$ versus $\dot{T}$ for primary silicon in hypereutectic Al-Si alloys

Alloy composition wt%	Solidification technique	Range of cooling rate $\dot{T}$, K/s	Resulting $\bar{N}_V$ mm^{-3}	$\bar{N}_V/\dot{T}$, mm^{-3} $(K/s)^{-1}$	Reference
Al-16Si + 0 to 0.17P	Sand and chill casting	0.56 to 15.3	–	–	Arnold and Prestley 1961 [9]
Al-20Si-1 Cu-1Mg based + 0.16P	Chill casting	3 to 70	*4×10^3 to 2×10^4	730 ± 490	Sulzer 1961 [10]
Al-19Si – 0.02P	Cooled in a container	0.017 to 1.67	‡2.5 to 1250	390 ± 270	Kaneko *et al.* 1978 [11]
Al- 17.1, 18.2, 24.8, +30.7Si	TIG and Bridgman	7.7 to 3690	†740 to 7×10^5	140 ± 80	Moir and Jones 1991 [12]
Al-26Si	Laser surface melt traversing	1.6×10^4 to 10^6	†5×10^6 to 1.8×10^8	250 ± 100	Pierantoni *et al.* 1992 [13]
Al-18.4Si	Bridgman	0.9 to 15.5	†64 to 866	107 ± 39	Bayraktar *et al.* 1992 [14]
Al-17, 22, 27Si	Chill casting	16 to 31	*5×10^3 to 5×10^4	640 ± 560	Mandal *et al.* 1991 [4]
+0.1 or 0.2 P	–	–	–	780 ± 540	
Al-22 +32 Si	Crucible cooling, chill casting	10 to 220	*14 to 430	1.2 ± 0.5	Ohmi *et al.* 1991, 1994 [15, 16]
Al-18.3Si	Bridgman	1.0 to 18.9	†90 to 1260	77 ± 21	Liang *et al.* 1995 [17]
Al-20Si	Bridgman	0.8 to 16.5	†150 to 520	160 ± 40	Kyffin *et al.* 2001 [18]
Al-20Si + 0.1P	–	–	†1390 to 9270	840 ± 380	

Note: *$\bar{N}_V$ calculated from reported mean sectioned diameter $\bar{D}_A$ using $\bar{N}_V = \frac{4}{\pi}(\frac{2}{3})^{1/2} f/\bar{D}_A^3$ with f as volume fraction of primary silicon.
†$\bar{N}_V$ calculated from reported number $\bar{N}_A$ of primary silicon particles per unit area on sections using $\bar{N}_V = (\pi/6f)^{1/2}\bar{N}_A^{3/2}$.
‡$\bar{N}_V$ calculated by Kaneko *et al.* from $\bar{N}_A/\bar{D}_V$ with $\bar{D}_V = \pi\bar{D}_A/2$, where $\bar{D}_V$ is true mean volume diameter.

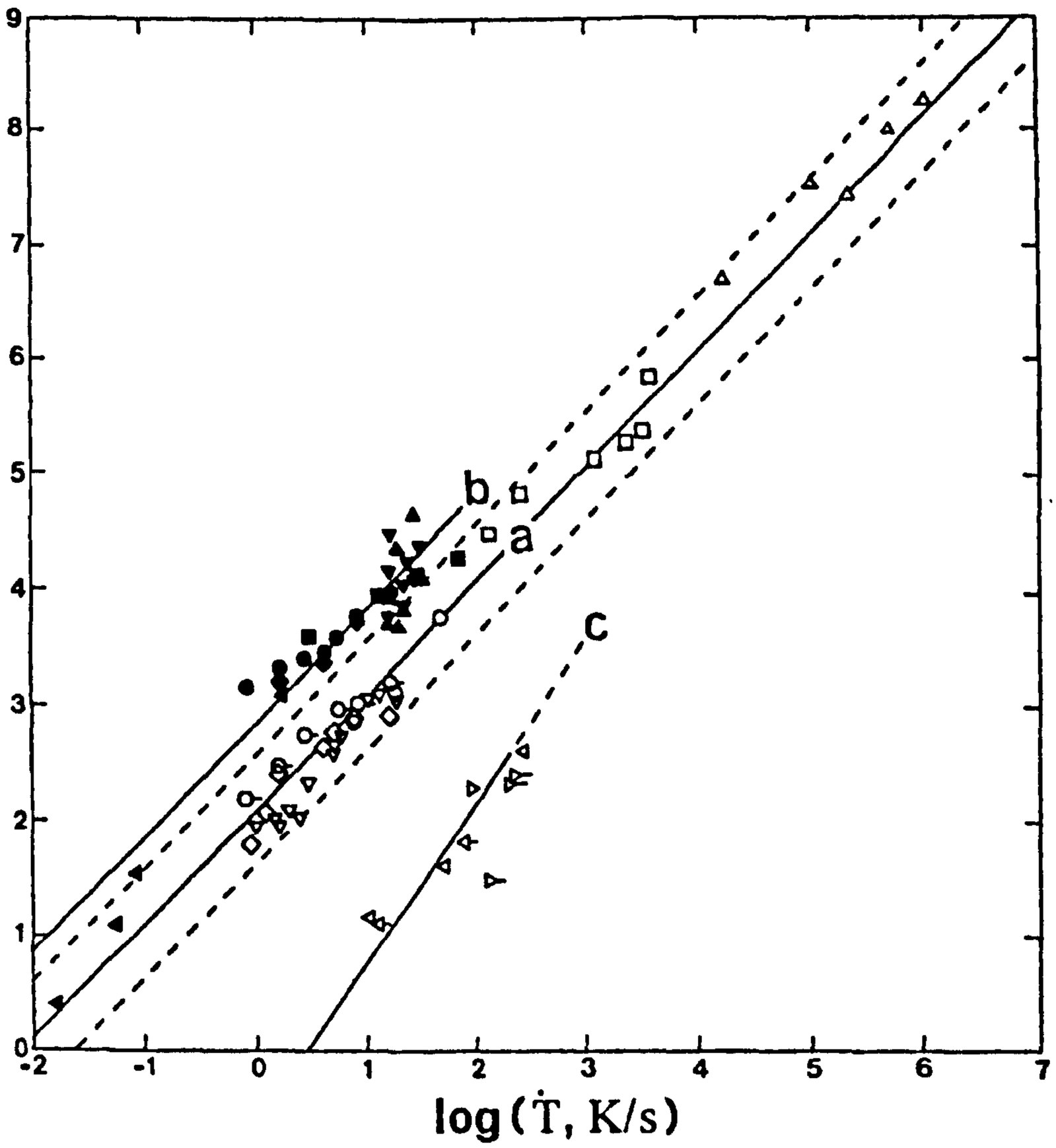

Figure 1 Mean number $\bar{N}_V$ of primary silicon particles per unit volume in hypereutectic Al-Si alloys versus solidification cooling rate $\dot{T}$. Key: Experimental data ■ Sulzer [10], ◄ Kaneko *et al.* [11],□ o Moir and Jones [12] TIG and Bridgman, Δ Pierantoni *et al.* [13], ◇ Bayraktar *et al.* [14], ▲∇Mandal *et al.* [4] 0.1 and 0.2 wt%P, ◄►Ohmi *et al.* [15, 16] crucible cooling and chill casting ▽Liang *et al.* [17], • • ♦ Kyffin *et al.* [18] 0.0P, 0.1P (Al-Fe-P) and 0.1P(Al-Cu-P). Filled points indicate inoculation with phosphorus. Further details of conditions are in Table I. Line a represents fit of the phosphorus-free data to Equation 1 with $n = 1$ and $A = 130$ mm^{-3} $(K/s)^{-1}$, with factor of 3 scatter band indicated. Line b represents fit of results with phosphorus present to Equation 1 with $n = 1$ and $A = 720$ mm^{-3} $(K/s)^{-1}$. Line c is the prediction of model B of Ohmi *et al.* [19] giving $n = 1.44$ and $A = 0.21$ mm^{-3} $(K/s)^{-1.44}$ in Equation 1

traversing show a good fit (within a factor of 3 in $\bar{N}_V$) with

$$\bar{N}_V = A\dot{T}^n \quad (1)$$

with $n = 1$ and $A = 130\ \text{mm}^{-3}\ (\text{K/s})^{-1}$. The results of Ohmi *et al.* [15, 16] for crucible cooling and chill casting, in contrast, show values of $\bar{N}_V$ some two orders of magnitude below the Bridgman and surface melting results. At least part of this discrepancy arises because it now appears that Ohmi *et al.* reported the mean long dimension of their primary silicon particles from sections rather than the mean diameter. Correction for this would move their data points in Fig. 1 closer to the other $\bar{N}_V$ measurements plotted there. Predictions of their nucleation model B [19] give $n = 1.44$ with $A = 0.21\ \text{mm}^{-3}\ (\text{K/s})^{-1.44}$ in Equation 1 at $\dot{T} < 200$ K/s in good accord with their measurements but exhibits plateaus in $\bar{N}_V$ at $\dot{T} > 200$ to 10^3 K/s depending on superheat. A further significant difference from the Bridgman results of Liang *et al.* was that Liang *et al.*'s associated measured nucleation undercoolings ΔT were relatively larger, e.g. 43 K at 13 K/s compared with 16 K at this cooling rate reported by Ohmi *et al.*, indicative of operation of heterogeneous nucleation at lower undercoolings in their work compared with the Bridgman studies. Fig. 1 also includes results for phosphorus inoculated samples (filled points). Except for the results of Kaneko *et al.* at 0.018 and 0.056 K/s, these lie mostly above the scatter band of the main body of results from phosphorus free samples, showing a fit of $\bar{N}_V$ within a factor of 3 of Equation 1 with $n = 1$ and $A = 720\ \text{mm}^{-3}\ (\text{K/s})^{-1}$, i.e. a factor of 5.5 higher $\bar{N}_v$.

In conclusion, collected data for number per unit volume $\bar{N}_V$ of primary silicon particles in hypereutectic Al-Si alloys, derived from measurements of number $\bar{N}_A$ per unit area or mean diameter $\bar{D}_A$ on sections, show a power relation with solidification cooling rate $\dot{T}$ of the form $\bar{N}_V = A\dot{T}^n$, where typically $n \sim 1$ and $A \simeq 130\ \text{mm}^{-3}\ (\text{K/s})^{-1}$ in the absence of inoculation with phosphorus and $A \simeq 720\ \text{mm}^{-3}\ (\text{K/s})^{-1}$ in the presence of phosphorus. The significantly lower values of $\bar{N}_V$ from the results of Ohmi *et al.* appear to be associated with measurement of mean long dimension rather than mean diameter of particle sections as well as nucleation at much lower measured undercoolings in their experiments compared with the undercoolings measured in the experiments of Liang *et al.*, which were associated with $\bar{N}_V$ values more typical of the majority of measurements.

Acknowledgements

This work forms part of an MPhil/PhD programme at the University of Sheffield by M F, financed by the Iranian Government

References

1. A. P. BATES, *Metallurgia* **61** (1960) 70.
2. J. L. JORSTAD, *Trans. Met. Soc. AIME* **242** (1968) 1217.
3. N. TENEKEDJIEV and J. E. GRUZLESKI, *Cast Metals* **3** (1990) 96.
4. P. MANDAL, A. SAHA and M. CHAKRABORTY, *AFS Trans.* **99** (1991) 643.
5. J. E. GRUZLESKI and B. M. CLOSSET, "The Treatment of Liquid Al-Si Alloys" (AFS, Des Plaines, Illinois, 1970) Ch. 7.
6. H. SANO, N. TOKIZANE, Y. OHKUBO and K. SIBUE, *Powder Met.* **36** (1993) 250.
7. P. STOCKER, F. RÜCKERT and K. HUMMERT, *MTZ Motortechnische, Z* **58** (1997) 502.
8. L. KATGERMAN and F. DOM, *Mater. Sci. Eng. A*, **375–377** (2004) 1212.
9. F. L. ARNOLD and J. S. PRESTLEY, *Trans. AFS* **69** (1961) 129.
10. J. SULZER, *Modern Castings* **39** (1961) 38.
11. J. KANEKO, M. SUGAMOTO and K. I. AKOI, *J. Jap. Inst. Met.* **20** (1979) 733.
12. S. A. MOIR and H. JONES, *J. Cryst. Growth* **113** (1991) 77.
13. M. PIERANTONI, M. GREMAUD, P. MAGNIN, D. STOLL and W. KURZ, *Acta Metall. Mater.* **40** (1992) 1637.
14. Y. BAYRAKTAR, D. LIANG, S. A. MOIR and H. JONES, *Mater. Lett.* **15** (1992) 314.
15. T. OHMI, Y. TANAKA and M. KUDOH, *Bull. Fac. Eng. Hokkaido Univ.* **156** (1991) 1.
16. T. OHMI, M. KUDOH, K. OHSASA, Y. ITOH, K. MATSUURA and K. ISHII, *J. Jap. Inst. Light Metals* **44** (1994) 91.
17. D. LIANG, Y. BAYRAKTAR and H. JONES, *Acta Metall. Mater.* **43** (1995) 579.
18. W. J. KYFFIN, W. M. RAINFORTH and H. JONES, *J. Mater. Sci.* **36** (2001) 2667.
19. T. OHMI, K. MATSUURA, M. KUDOH and Y. ITOH, *J. Jap. Inst. Light. Metals* **47** (1997) 71.

Received 31 March
and accepted 21 April 2005

Materials Science Forum Vols. 519-521 (2006) pp 1741-1746
online at http://www.scientific.net

The effect of casting variables on the structure of hypereutectic Al-Si alloys

M. Faraji, I. Todd, H. Jones,

Dept. of Engineering Materials, University of Sheffield, Mappin Street, Sheffield, S1 3JD, UK
mtp03mf@sheffield.ac.uk, I.Todd@sheffield.ac.uk, H.Jones@sheffield.ac.uk

Keywords: Hypereutectic Al-Si, Inoculation, Modification, EBSD

Abstract. The effect of size refinement of primary silicon and modification of eutectic silicon, separately and simultaneously, on microstructure of hypereutectic Al-20wt%Si has been investigated under different casting conditions. Results showed that number per unit volume of primary silicon particles was doubled by inoculation with 0.02% phosphorus in the alloy with 0.0015% phosphorus already in it, whereas 70% of a small ingot (40×35 mm) became modified eutectic, and the formation of primary silicon was suppressed, on adding 0.1% strontium. Simultaneous addition of phosphorus and strontium still refined the primary silicon but did not modify the eutectic. Addition of strontium alone caused roughening of the primary silicon, exemplified by increased undercooling registered on the cooling curve. Also crystallographic relationships between polyhedral primary silicon particles have been investigated by Electron Back Scattered Diffraction (EBSD).

Introduction

The mechanical and physical properties of hypereutectic Al-Si alloys are strongly dependent on the morphology of the silicon phase [1]. The coarse primary silicon can be refined by inoculation with phosphorus [2] or by increasing solidification cooling rate [3]. The coarse plate-like eutectic silicon is modified into a fibrous structure by adding Sr/Na [4] or increased cooling rate [2]. Simultaneous full size refinement of primary silicon and modification of eutectic silicon is not possible by adding P and Sr together because of chemical reaction between these additives [5]. Electron Back Scatter Diffraction (EBSD) has been used recently to determine crystallographic relationships between neighbouring eutectic Si particles in Al-Si alloys before and after adding Sr [6,7]. In the present work, firstly, the effects on primary and eutectic silicons, of using P and/Sr separately and simultaneously, have been studied. Secondly, the crystallographic relationships between neighbouring primary silicon particles have been determined using EBSD.

Experimental

Al-20Si-0.35Fe-0.02Cu-0.0015P (wt %) supplied by Norton Aluminium Products was used as the melt, with Al-6.75Fe-4.91P (wt %) supplied by KB Alloys as primary silicon refiner and Al-5.93wt%Sr supplied by LSM Ltd as eutectic Si modifier. The Al-Si alloy (150g) was melted in a stoppered alumina crucible positioned in a resistance heated vertical tube furnace. The melt temperature was 800°C. After allowing 15 min contact time for each addition the treated melt was cast into a Quik-Cup sand mould placed below the melting crucible by withdrawing the stopper rod. The dimensions of the mould cavity were 40mm×35mm with a built-in silica sheathed thermocouple on the central axis of the mould. An alternative casting method was also used to reduce the effect of turbulence during casting. A stainless steel cup (bore: 30mm, height: 30mm) with a cold charge of metal (30 g) with a ceramic-fibre lid (thickness: 13mm) was put into a chamber furnace which was set to 800°C. Inoculation of the melt was done outside the furnace by plunging 200ppm P wrapped with aluminium foil into the melt. After 15 min in the furnace it was taken out and placed onto a copper block (thickness: 35mm, diameter: 75mm). The six conditions studied are specified in Table 1. Metallographic characterisation of the ingots was done by

longitudinal sectioning, grinding and polishing. Measurements of the numbers of particles per unit area (N_A) were made with an Olympus VANTOX-T microscope connected to an Iiyama computer with an image grabber and KsRun 3 image analysis software. For each value of N_A, 15 micrographs were point counted by hand to give an average N_A. Two different ingots from conditions A2 and A6 were prepared for study in a JEOL SEM (JSM 6400) equipped with Oxford Instruments EBSD and HKL Channel 5 software. The metallographic preparation involved finishing with a colloidal silica suspension for about two and a half hours.

Results and Discussion

Table 2 shows N_A and derived N_V for primary silicon for five of the conditions (A1, A3, A4, A5 and A6) specified in Table 1. This indicates that 0.02% P increased N_V by a factor of ~2, while 0.2%Sr and 0.2%Sr+0.02%P decreased its value by 20 times in the bottom casting process. Efficiency of the eutectic modification of as-cast ingots was assessed on the basis of percentage of the well-modified microstructure from micrographs. Addition of Sr alone (A4) resulted in an increasing area of the ingot in which primary Si was suppressed and the eutectic was fully modified. Fig. 1 shows that this effect reached a maximum at 0.01% Sr addition. The addition of Sr depressed the primary silicon formation temperature (Fig. 2) as well as decreasing the frequency of nucleation of primary silicon (Table 2) and caused roughening of the internal surfaces of the primary silicon (Fig. 3) compared to the unmodified alloy (Fig4). Simultaneous addition of 0.015%P and 0.04%Sr refined some of the primary silicon but the eutectic modifying effect of Sr was limited to a very small part of the ingot (less than 2% of a 43×35 mm ingot). However, on increasing this addition of modifier to 0.2% Sr with 0.015%P, primary silicon refinement disappeared while modification of the eutectic was complete. This elimination of the refining effect of P on primary Si on addition of Sr along with P has been attributed to the formation of a new compound Sr_3P_2 as a result of decomposition of AlP as a consequence of adding Sr [8,9]. Figs 5 and 6 show polyhedral primary silicons produced with (A2) and without (A6) inoculation. Tables 3 and 4 represent the orientation/angle pairs for silicon particles specified in Figs 5 and 6. Rotation of 60° around <111> axis is characteristic of twinning for silicon particles [11]. Tables 3 and 4 show this specific twinning relationship between interconnected or neighbouring polyhedral silicon particles in both inoculated and uninoculated ingots. It can be concluded that particles showing this twin relationship result from branching in a twin direction. Based on Tables 3 and 4, 52% of pairs in the inoculated sample and 73% in the uninoculated sample show this twin relationship (near to 60° rotation around <111> axis) which confirms earlier claims without using EBSD that twinning is an important branching mechanism for silicon [12]. However, based on microstructural observations during EBSD, more connected polyhedral primary silicon particles were found in the inoculated sample (A2) than in the uninoculated sample (A6). It is notable that both unmodified and Sr-modified eutectic silicons also exhibit 60° rotations about <111> [11] characteristic of twinning.

Conclusions

1. The number per unit volume of primary silicon particles was doubled by inoculation with 0.02% P in Al-20%Si alloy for the conditions studied.
2. Addition of 0.1% Sr eliminated formation of primary silicon in favour of modified eutectic in 70% of a small ingot.
3. Simultaneous addition of 0.015% phosphorus and 0.04% strontium refined most of the primary silicon but did not modify the eutectic.

4. Based on morphological observations, addition of Sr alone caused roughening of the primary Si, exemplified by increased undercooling on the cooling curve.

5. Between two connected primary Si particles, the outermost layers of each Si particle are often related by a 60° rotation around axis <111>.

This work was part of a PhD research programme for M.F. at the University of Sheffield, supported by Iranian government.

References

[1] N. Tenekedjiev and J.E. Gruzleski: Cast Metals, 3 (2), (1990), p. 96-105.

[2] J.E. Gruzleski and B.M. Closset: *The Treatment of Liquid Al-Si Alloys*, (AFS, Illinois 1990).

[3] L. Katgerman and F. Dom: Mater. Sci. Eng. A, Vol. 357-377 (2004), 1212-1216.

[4] A. Hellawell: Progress in Mater. Sci. Vol. 15 (1), (1970).

[5] L.F. Mondolfo: J. Austral. Met. 10 (1965), p. 169.

[6] K. Nogita, S.D. McDonald and A.K. Dahle: Philosophical Magazine 84 (17) (2004), p. 1683-96.

[7] K. Nogita and A.K. Dahle: Mater. Trans. 42 (2001), p. 207-214.

[8] J. Cissé, G.F. Bolling and H.W. Kerr: Met. Trans. B Vol. 68 (1975), p. 195-97.

[9] J.Y. Park, J.S. Lee and H.Y. Ra: (3rd Asian Foundry Cong. Nov. 1995, Edited by Z.H. Lee, C.P. Hong, M.H. Kim, The Korean Foundrymen's Society) p. 167-74.

[10] J.W. Martin: *Worked Examples in the Strength of Metals and Alloys*, (The Institution of Metallurgists, UK 1983).

[11] G. Heiberg and L. Arnberg: J. Light Metals 1 (2001), p. 43-49.

[12] S.Z. Lu and A. Hellawell: Metall. Trans. A 18A (1987), p. 1721-1733.

Table 1. The six conditions investigated (melt at 800°C).

Samples	A1	A2	A3	A4/1-7	A5	A6
Additives	None	0.015%P	0.02% P	0.04-0.2%Sr	0 04/0 2%Sr+0 015/0 02%P	None
Casting method	Bottom casting into sand mould					Chamber casting

Table 2. N_A and N_V of primary silicon for five of the studied conditions.

Samples	A1	A3	A4 (0.2%Sr)	A5 (0.2%Sr+0.02%P)	A6
N_A/mm-2	28*	40**	3.8**	3.7†	30†
N_V/mm-3	230	380	10.1	10.8	260
STD (N_V)	70	100	2.3	2.3	70

* average for 5 ingots, ** average for 4 ingots and † average for 3 ingots.

N_V was calculated from N_A using $\overline{N_V} = \left(\frac{\Pi}{6f}\right)^{1/2} \overline{N_A}^{3/2}$. [10]

Table 3. The orientation/angle pairs for polyhedral particles specified in Fig. 5.

No 1	No 2	Angle [°]	Indices
Si1	**Si2**	**59.53**	**-3-44**
Si1	Si3	43.89	-3-2-3
Si4	**Si5**	**59.72**	**-1-11**
Si5	Si6	31.09	-4-2-3
Si8	**Si7**	**59.89**	**11-1**
Si7	**Si9**	**59.50**	**11-1**
Si9	**Si10**	**59.88**	**11-1**
Si10	*Si11*	*37*	*011*
Si12	Si13	34.76	102
Mapping for No12, 13 was not clear enough, so the offset was too much.			
Si13	**Si14**	**59.55**	**-111**
Si14	Si15	30.48	-130
Si15	**Si16**	**53.90**	**-4-3-3**
Si16	**Si17**	**54.19**	**-4-3-3**
Si17	**Si18**	**55.20**	**-4-33**
Si18	**Si19**	**58.45**	**334**
Si18	Si20	43.38	4-41
Si18	Si20	28.36	01-3
Si13	Si21	37.79	-1-43
Si22	Si23	42.92	-2-31
Si23	Si26	39.45	40-1
Si24	**Si25**	**59.94**	**-1-1-1**
Si27	**Si28**	**59.60**	**-443**
Si28	**Si29**	**49.49**	**-3-2-2**
Si27	**Si29**	**55.31**	**-4-3-3**
Si30	Si31	52.01	-34-1

Table 4. The orientation/angle pairs for polyhedral particles specified in Fig 6.

No 1	No 2	Angle [°]	Indices
Si3	Si4	52.11	23-3
Si4	**Si5**	**61.81**	**2-12**
Si5	Si6	18.41	-34-4
Si5	Si7	43.34	210
Si8	**Si9**	**60.31**	**-33-2**
Si10	**Si11**	**59.22**	**-33-4**
Si12	**Si13**	**58.12**	**43-4**
Si14	**Si15**	**58.59**	**1-1-1**
Si16	Si17	36.60	034
Si18	**Si19**	**57.82**	**-344**
Si20	**Si21**	**57.26**	**-334**
Si22	**Si23**	**60.54**	**-1-2-2**
Si23	**Si24**	**59.82**	**-32-3**
Si24	**Si25**	**60.31**	**-3-4-4**
Si25	Si26	46.33	-22-1
Si27	**Si28**	**58.66**	**-1-11**
Si28	**Si29**	**59.8**	**443**
Si30	**Si31**	**59.29**	**-111**
Si31	**Si32**	**59.27**	**-11-1**

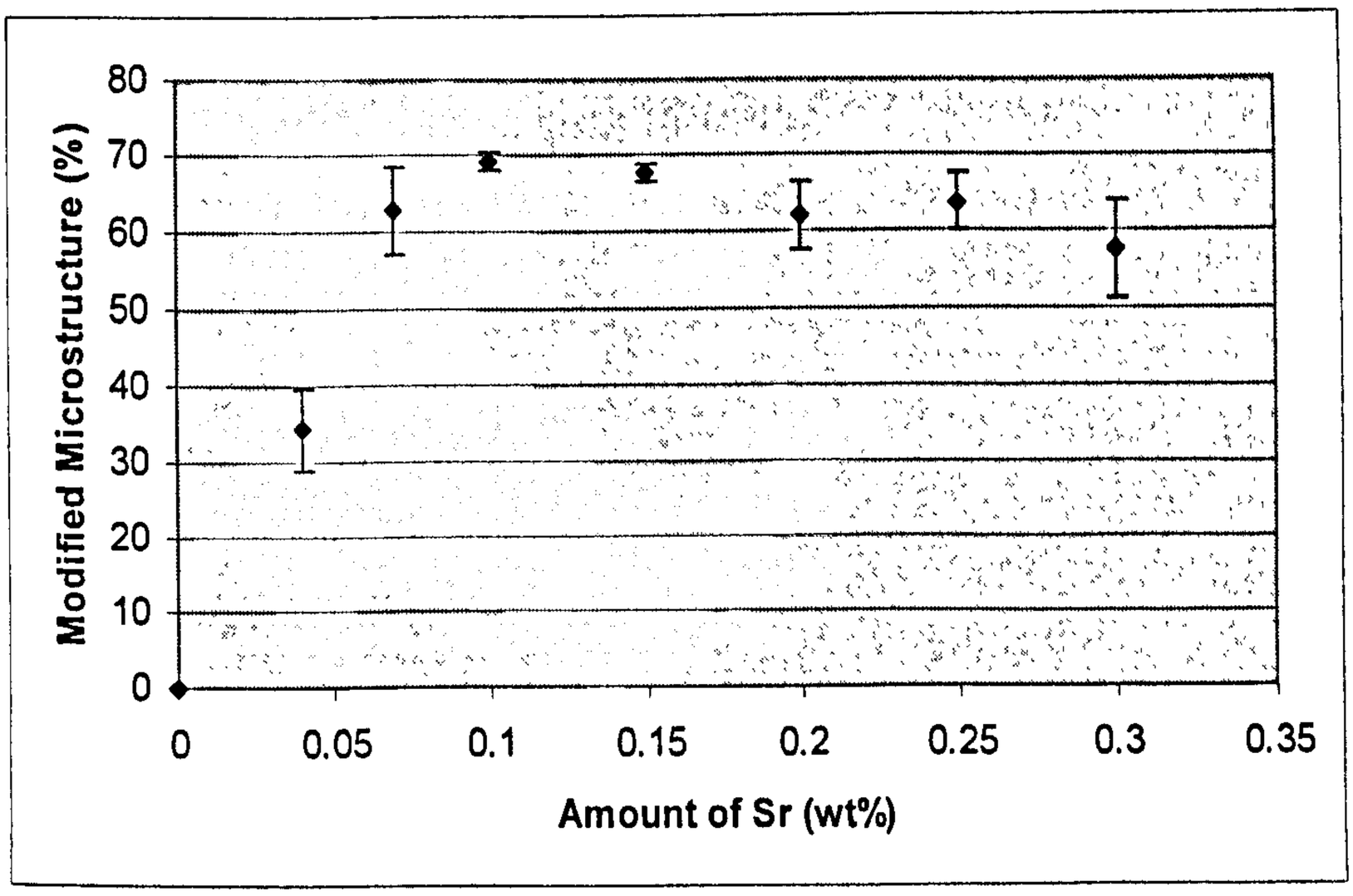

Fig. 1 Showing the efficiency of modification of Al-20wt%Si by different levels of Sr addition in a Quik-Cup sand mould, casting temperature 800°C (A4).

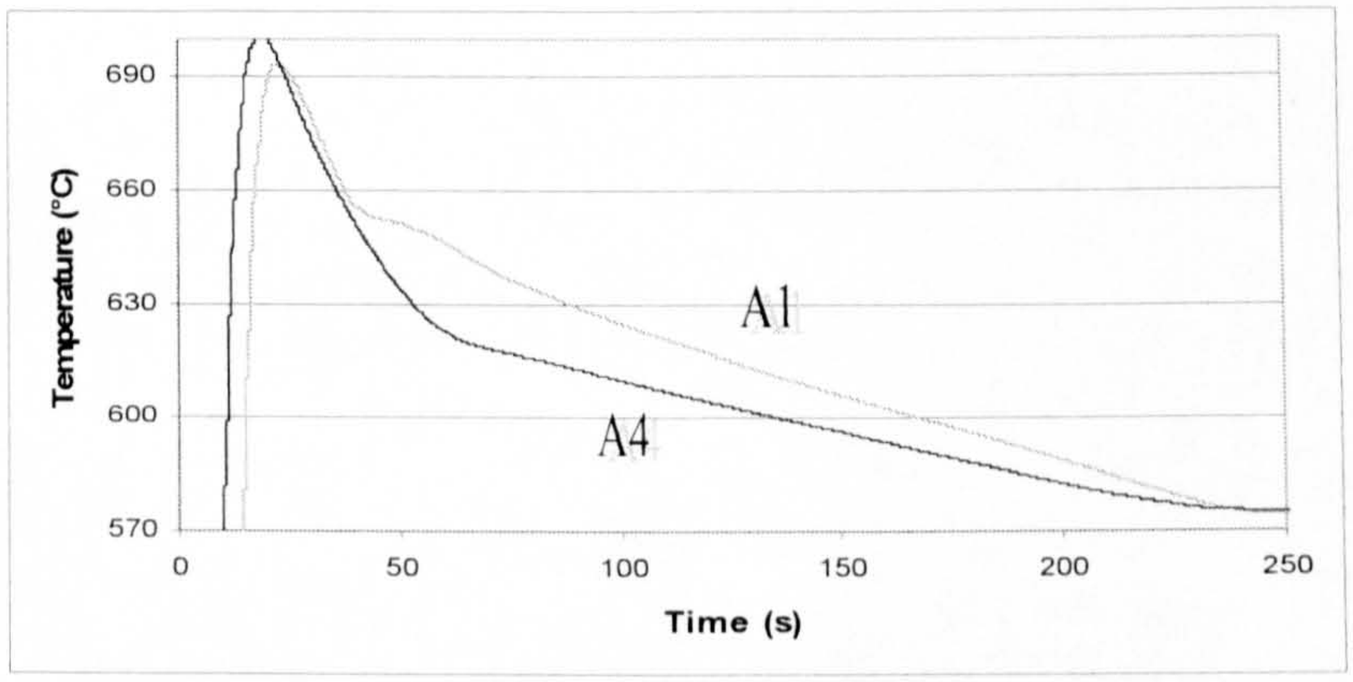

Fig. 2 The cooling curves for sample A1 (uninoculated) and condition A4 (0.2%Sr).

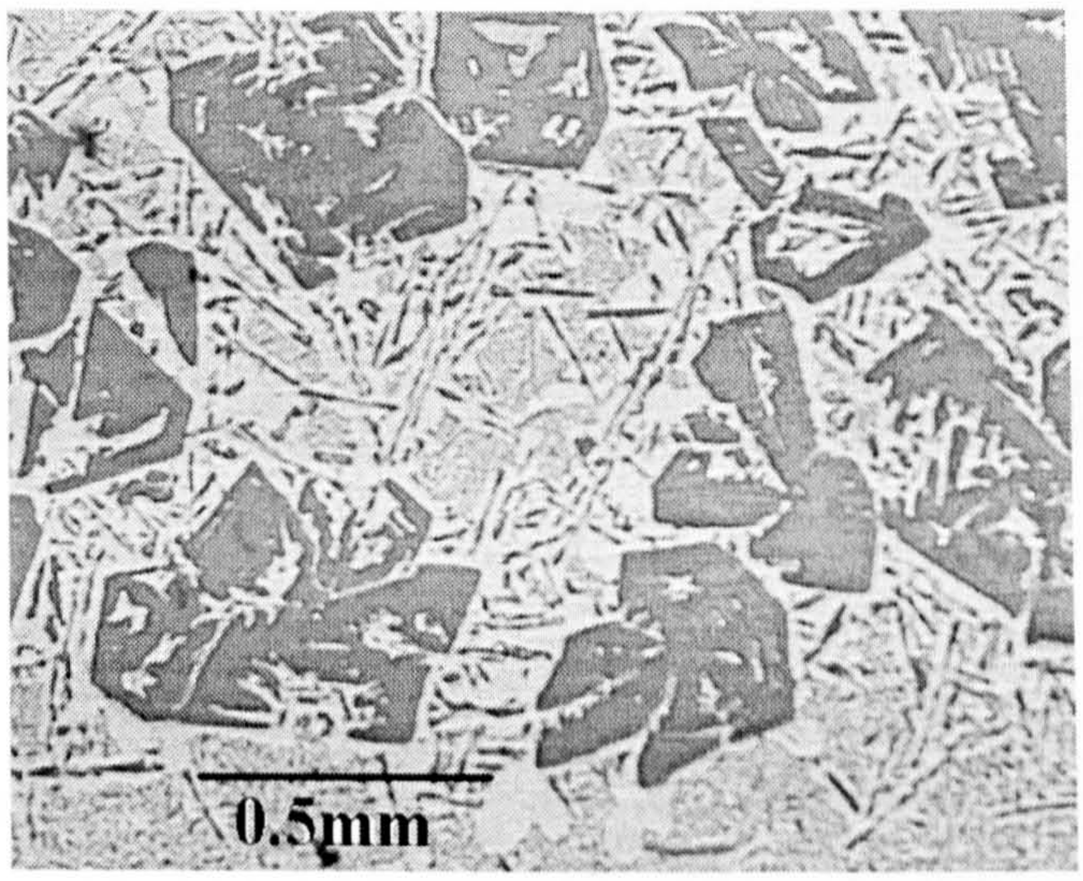

Fig. 3 Showing roughening of the internal surfaces of the primary Si in Al-20%Si produced by 0.04%Sr addition (A4).

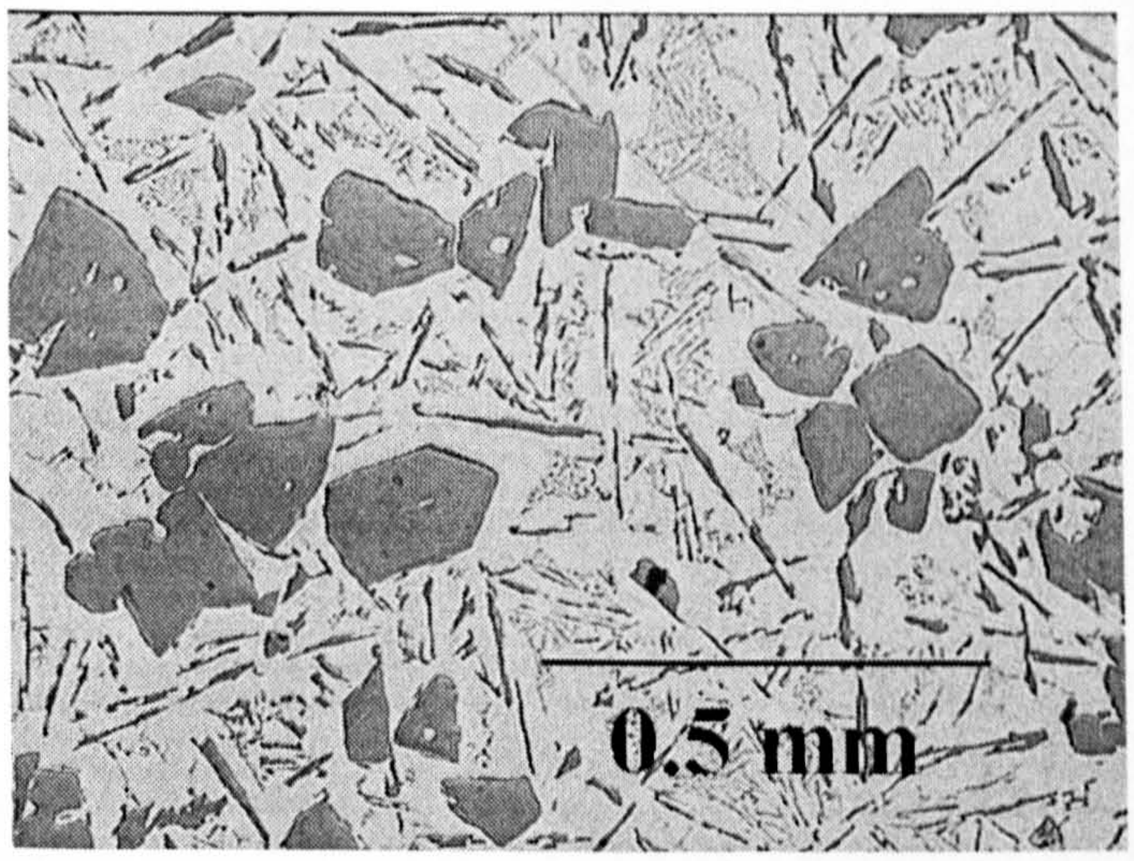

Fig. 4 Showing morphology of the primary Si without any roughening in Al-20%Si with no strontium addition (A1).

Fig. 5 A randomly selected (but typical) part of the microstructure of Al-20%Si inoculated with 150 ppm P and bottom cast, used for EBSD (A2).

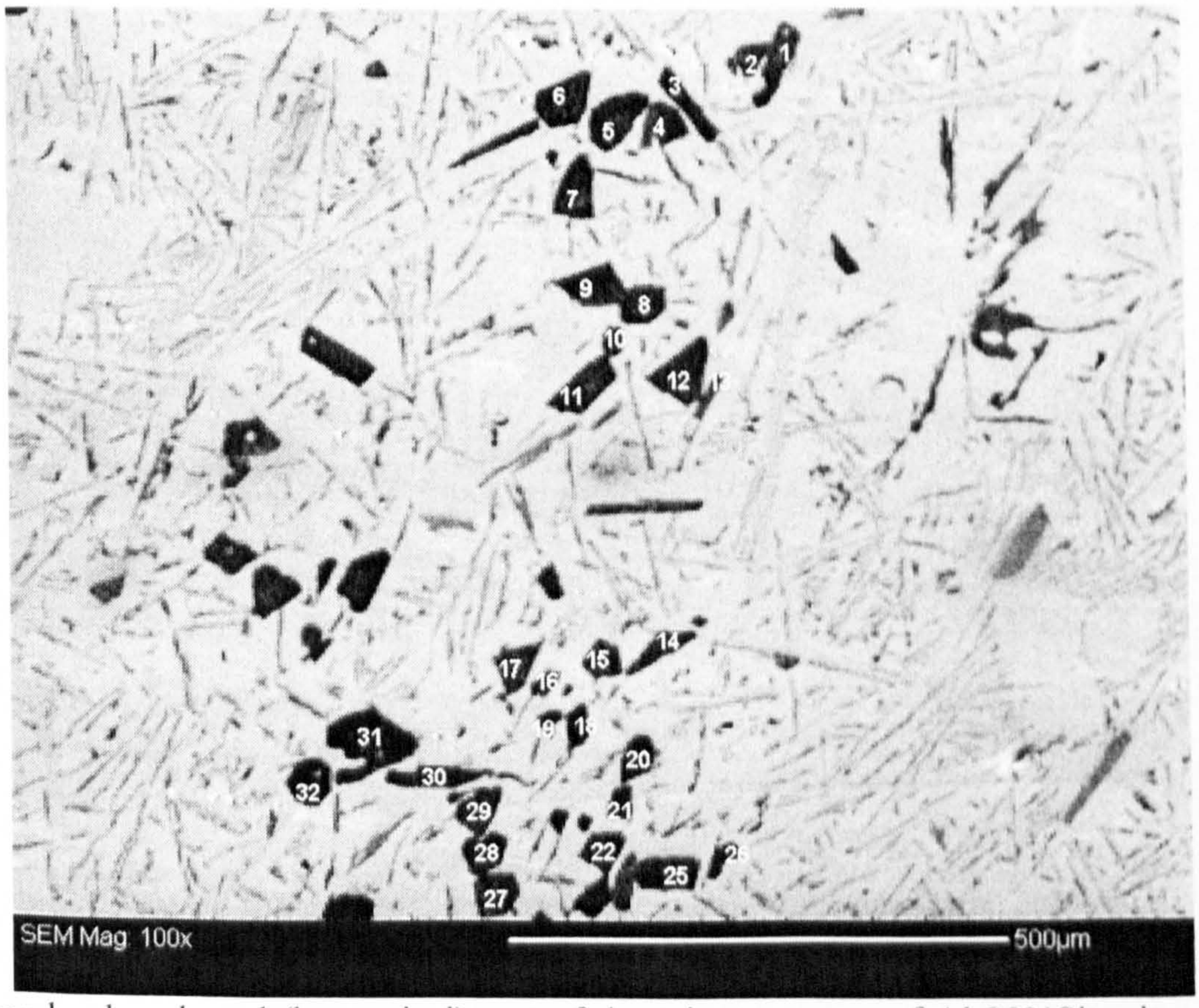

Fig. 6 A randomly selected (but typical) part of the microstructure of Al-20%Si uninoculated and chamber cast, used for EBSD (A6).